

# Crucial Role of Mitochondrial Mechanisms in the Antineoplastic Effects of Desethylamiodarone

**Fadi H. J. Ramadan**

Supervisor:

**Dr. Zita Bognar MD. Ph.D.**



**Ph.D. Thesis**

Interdisciplinary Doctoral School of Medicine

Leader of the program:

Prof. Dr. Ferenc Gallyas PhD, DSc.

Leader of the doctoral school:

Prof. Dr. Ferenc Gallyas, PhD, DSc.

**Department of Biochemistry and Medical Chemistry**

**Medical School**

**University of Pecs**

Pecs 2023



<b>1</b>	<b>Abbreviations .....</b>	<b>6</b>
<b>2</b>	<b>Introduction .....</b>	<b>8</b>
<b>2.1</b>	<b>Cancer.....</b>	<b>8</b>
2.1.1	Skin Cancer.....	9
2.1.2	Breast Cancer .....	11
<b>2.2</b>	<b>Cancer treatment.....</b>	<b>14</b>
2.2.1	Radiation Therapy.....	14
2.2.2	Surgery.....	14
2.2.3	Chemotherapy.....	14
2.2.4	Targeted and Immunotherapies.....	15
<b>2.3</b>	<b>Cancer Drug Resistance .....</b>	<b>15</b>
2.3.1	Intrinsic Resistance .....	15
2.3.2	Acquired Resistance.....	16
2.3.3	Mechanisms of Cancer Drug Resistance. ....	16
<b>2.4</b>	<b>Mitochondria .....</b>	<b>17</b>
2.4.1	An Overview .....	17
2.4.2	Mitochondria in Cancer .....	17
2.4.3	Targeting Mitochondria .....	18
2.4.4	Mitochondrial Apoptotic Pathways .....	18
2.4.5	Mitochondrial Dynamics .....	21
<b>2.5</b>	<b>Small Molecules in Therapy .....</b>	<b>22</b>
<b>2.6</b>	<b>Desethylamidarone (DEA).....</b>	<b>23</b>
<b>3</b>	<b>Objectives .....</b>	<b>24</b>
<b>3.1</b>	<b>Our aims: .....</b>	<b>24</b>
<b>4</b>	<b>Materials and Methods.....</b>	<b>25</b>
<b>4.1</b>	<b>Materials.....</b>	<b>25</b>
<b>4.2</b>	<b>Cell Culture.....</b>	<b>25</b>
<b>4.3</b>	<b>Cell Viability Assay .....</b>	<b>25</b>
<b>4.4</b>	<b>Colony formation assay .....</b>	<b>26</b>
<b>4.5</b>	<b>Annexin V &amp; Death Cell Assay .....</b>	<b>26</b>
<b>4.6</b>	<b>Cell Cycle Assay .....</b>	<b>26</b>
<b>4.7</b>	<b>Migration Assay.....</b>	<b>27</b>


<b>4.8</b>	<b>Measurement of Invasive Growth .....</b>	<b>27</b>
<b>4.9</b>	<b>Ethics .....</b>	<b>27</b>
<b>4.10</b>	<b>Mouse Pulmonary Metastasis Model .....</b>	<b>27</b>
<b>4.11</b>	<b>Subcellular Fractionation.....</b>	<b>28</b>
<b>4.12</b>	<b>Immunoblot Analysis .....</b>	<b>29</b>
<b>4.13</b>	<b><math>\Delta\Psi_m</math> Assay .....</b>	<b>29</b>
<b>4.14</b>	<b>. Analysis of Mitochondrial Network Dynamics .....</b>	<b>30</b>
4.14.1	Project 1 .....	30
4.14.2	Project 2 .....	30
<b>4.15</b>	<b>Bioenergetic Analysis .....</b>	<b>30</b>
<b>4.16</b>	<b>Determination of Cellular ROS Formation .....</b>	<b>31</b>
<b>4.17</b>	<b>Measurement of mPT .....</b>	<b>31</b>
<b>4.18</b>	<b>Statistical Analysis.....</b>	<b>32</b>
<b>5</b>	<b><i>Results and Discussion 1.0</i>.....</b>	<b>33</b>
<b>5.1</b>	<b>Results 1.0 .....</b>	<b>33</b>
5.1.1	Effect of DEA on the Viability of B16F10 Melanoma Cells.....	33
5.1.2	Effect of DEA on B16F10 Colony Formation.....	34
5.1.3	Effect of DEA on Apoptosis Activation in B16F10 cell .....	35
5.1.4	Effect of DEA on the Cell Cycle in B16F10 Cells .....	36
5.1.5	Effect of DEA on Outer Mitochondrial Membrane (OMM) Permeabilization .....	37
5.1.6	Effect of DEA on the $\Delta\Psi_m$ .....	39
5.1.7	Effect of DEA on Mitochondrial Fragmentation .....	41
5.1.8	Effect of DEA on the Energy Metabolism of B16F10 Melanoma Cells .....	42
5.1.9	Effect of DEA on Cellular Reactive Oxygen Species (ROS) Production .....	44
5.1.10	Effect of DEA on mPT in Intact B16F10 Melanoma Cells .....	45
5.1.11	Effect of DEA on Lung Metastasis Formation in an In-Vivo Model .....	46
<b>5.2</b>	<b>Discussion 1.0.....</b>	<b>48</b>

<b>6</b>	<b>Results and discussion 2.0.....</b>	<b>52</b>
<b>6.1</b>	<b>Results 2.0 .....</b>	<b>52</b>
6.1.1	DEA Induced Apoptotic Cell Death in BC Cell Lines .....	52
6.1.2	DEA Mitigated Invasive Growth of BC Cell Lines.....	53
6.1.3	DEA Differentially Modulated Regulators and Markers of the Cell Death Process in the BC Cell Lines.....	55
6.1.4	DEA Caused the Loss of Mitochondrial Membrane Potential ( $\Delta\Psi_m$ ).....	57
6.1.5	DEA Induced Mitochondrial Fragmentation in BC Cell Lines .....	58
6.1.6	DEA Impeded Mitochondrial Energy Production in the BC Cell Lines .....	60
6.1.7	COX-2 Inhibition Potentiated DEA's Anti-Neoplastic Effect in the TN BC Cell Line 62	
6.1.8	Effect of DEA on MCF-7 and 4T1 Colony Formation.....	63
<b>6.2</b>	<b>Discussion 2.0.....</b>	<b>64</b>
<b>7</b>	<b>Conclusions.....</b>	<b>67</b>
<b>8</b>	<b>References .....</b>	<b>69</b>
<b>9</b>	<b>List of Publication .....</b>	<b>75</b>
<b>9.1</b>	<b>First author publications connected to research topic: .....</b>	<b>75</b>
<b>9.2</b>	<b>Co-author publications connected to research topic: .....</b>	<b>75</b>
<b>9.3</b>	<b>Participation in Conferences .....</b>	<b>75</b>
9.3.1	Oral presentations (first-author):.....	75
9.3.2	Oral presentations (Co-author): .....	76
9.3.3	Poster presentation (first-author): .....	76
9.3.4	Poster presentation (Co-author):.....	76
<b>10</b>	<b>Acknowledgments .....</b>	<b>77</b>
<b>11</b>	<b>Appendix .....</b>	<b>78</b>



## 1 Abbreviations

○ AM	Amiodarone
○ DEA	Desethylamiodaron
○ BCL-2	B-Cell Lymphoma 2
○ BH3	BCL-2 Homology 3
○ AIF	Apoptotic Inducing Factor
○ ROS	Reactive Oxygen Species
○ Ca <sup>2</sup>	Calcium
○ Cyt c	Cytochrome C
○ NMSC	Non-Melanoma Skin Cancer
○ UV	Ultraviolet
○ BRAF	Serine/threonine-protein kinase
○ MAPK	Mitogen-Activated Protein Kinase
○ DTIC	Dacarbazine
○ TMZ	Temozolomide
○ PD-1	Programmed Cell Death Receptor Protein 1
○ PD-L1	Programmed Cell Death Receptor Protein 1 Ligand
○ BC	Breast Cancer
○ PR	Progesterone Receptor
○ ER	Estrogen Receptor
○ HR+	Hormone Receptor-Positive
○ TNBC	Triple Negative Breast Cancer
○ PI3KCA	Phosphatidylinositol-4,5-Bisphosphate 3-Kinase Catalytic Subunit Alpha
○ SMIs	Small Molecule Inhibitors
○ MAbs	Monoclonal Antibodies
○ COX-2	Cyclooxygenase-2
○ NFκB	Nuclear Factor κB
○ mtDNA	Mitochondrial DNA
○ OMM	Outer Mitochondrial Membrane
○ MOMP	Mitochondrial Outer Membrane Permeabilization
○ IMM	Inner Mitochondrial Membrane
○ ATP	Adenosine Triphosphate
○ OXPHOS	Oxidative Phosphorylation
○ NADPH	Nicotinamide Adenine Dinucleotide Phosphate
○ TKI	Tyrosine Kinase Inhibitor
○ FDA	US Food and Drug Administration
○ IMS	Mitochondrial Intermembrane Space
○ APAF1	Apoptotic Peptidase Activating Factor 1

- 
- SMAC Second Mitochondrial Activator of Caspases
  - XIAP X-Linked Inhibitor of Apoptosis
  - PARP-1 Poly (ADP-ribose) Polymerase-1
  - $\Delta\Psi_m$  Mitochondrial Membrane Potential
  - mPT Mitochondrial Permeability Transition
  - MFN1 Mitofusion-1
  - MFN2 Mitofusion-2
  - OPA1 Optic Atrophy-1
  - OMA1 OMA1 Zinc Metalloendopeptidase
  - DRP1 Dynamin-Related Protein 1
  - Fis1 Fission Protein 1
  - AKAP1 A-Kinase Anchoring Protein 1
  - R-123 Rhodamine 123
  - PBS Phosphate Buffer Saline
  - FBS Fetal Bovine Serum

## 2 Introduction

### 2.1 Cancer

Cancer, one of the major health problems in the world, is the second leading cause of death worldwide following cardiovascular diseases. Approximately 1.9 million new cases and 600,000 deaths were recorded by 2022 in the United States. In Hungary, more than 66,000 cases and over 32,000 deaths were recorded by 2020, however, 27.5 million new cases predicted by 2040 worldwide. Therefore, cancer is a serious health threat facing the humans. Unfortunately, cancer is a group of diseases where cells grow, change, and multiply out of control, at the tissue level, which makes it the major challenge for the specific diagnosis and treatment [1]–[4].

More than hundred types of tumors have been identified depending on the molecular and the anatomical composition of the tumor (**Table 1**) [2], [3]. In men, the most frequent types of cancer are prostate, lung, colon, urinary bladder, and melanoma cancer. In women, on the other hand, cancer prevalence is highest in breast, lung, colon, uterine corpus, and melanoma (**Fig. 1**) [3]. Different factors are involved in the initiation of cancers including, internal factors like hormones, genetics, and immune system conditions. Or/and external factors mainly known as carcinogens, which are a class of substances that affect DNA directly or indirectly such as, chemicals, asbestos, arsenic, radiations, tobacco, and others [3], [5]. In context of molecular biology, neoplasm is characterized by multi-genetic disorder starts by series of mutations affecting essential proteins, which are highly involved in the cell cycle. This in turn leads to uncontrolled cell growth and eventually metastasis. At this stage, tumor evades different organs where it is hard to control and can result in death [1]–[3], [5].

Based on Tissues	Based on Organs
<u>Carcinomas</u> : this cancer begins in the skin or in tissues that line or cover internal organs. There are different subtypes, including adenocarcinoma, basal cell carcinoma, squamous cell carcinoma and transitional cell carcinoma	Colorectal Cancer
<u>Sarcomas</u> : his cancer begins in the connective or supportive tissues such as bone, cartilage, fat, muscle or blood vessels	Lung Cancer
<u>Lymphomas</u> : these cancers begin in the cells of the immune system .	Liver Cancer
<u>Leukemia</u> : his is cancer of the white blood cells. It starts in the tissues that make blood cells such as the bone marrow.	Stomach Cancer
<u>Adenomas</u> : tumor that arise in the adrenal, pituitary gland, thyroid, and other glandular tissues.	Cervical Cancer
	Bladder Cancer
	Esophageal Cancer

**Table 1.** Classifications of cancer types based on the anatomy [3]



Generally, cancer is a static disease, it evolves overtime gaining multiple mutations to keep it alive. Those mutations include constant activation of oncogenes that are responsible for cell division and growth, or else, the deactivation of tumor suppressor genes leading to uncontrolled cell division. Additionally, cancer cell circumvents negative cell proliferation pathways, mainly apoptosis.

Through history, cancer therapies are being developed, and treatment decision is taken considering cancer type, location, size of the tumor, and the stage. Usually, the first therapy is chemotherapy or surgery, radiation, targeted, and/or immunotherapy [2], [3]. Additionally, among the new therapeutic approaches, targeted and immunological therapies are more effective since the target proteins are identified. Withal, cancer drug resistance is still increasing.

### 2.1.1 Skin Cancer

Skin is the organ that separates between the body and the environment. Human skin is made up from 3 main layers: the epidermis, dermis, and hypodermis [6]. Epidermis, the outermost layer, consists of different cell types including melanocytes and keratinocytes. Defect in those cell types can lead to different dermatologic diseases including skin cancer. Nearly half of all cancer patients in the United States were diagnosed with skin cancer, which makes it one of the most common types of cancer. Two main types of skin (neoplasm) cancer: melanoma and non-melanoma skin cancer (NMSC) [6], [7].

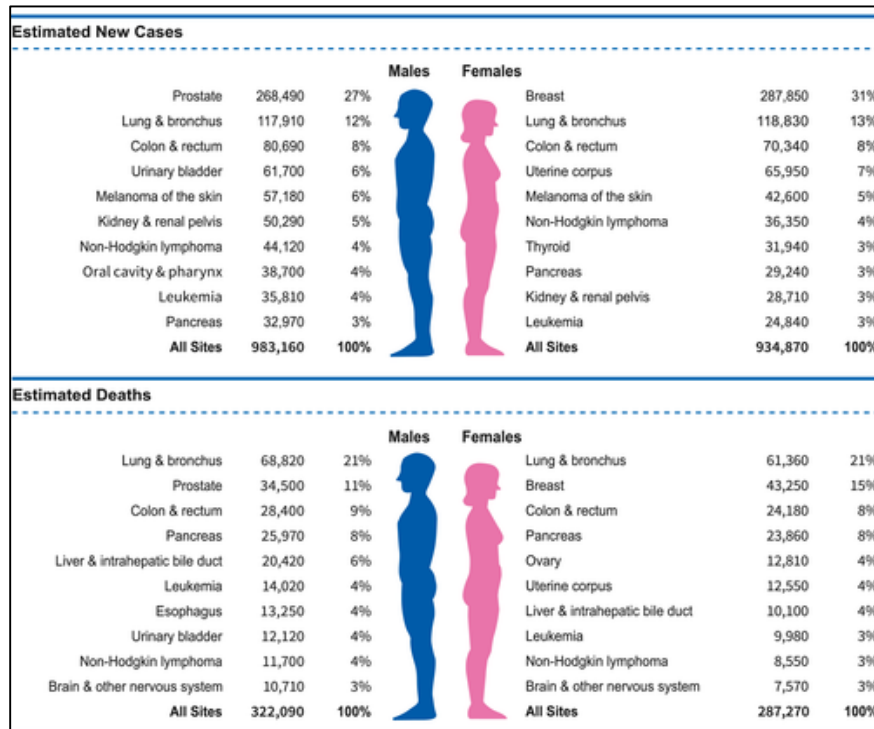



Figure 1: Cancer statistics 2022 [3].



### 2.1.1.1 Non-Melanoma Skin Cancer (NMSC)


NMSC is the keratinocyte cells' originated skin cancer, almost 2-3 million new cases are reported yearly worldwide, which makes it one of the most diagnosed malignancies with 95% representation of all skin cancer cases. Two main subtypes of NMSC basal cell carcinoma (BCC) which is the most common type of NMSC accounts for 80-85% of all NMSC. BCC arises from the basal membrane of epidermis, and in most cases, it develops in head/neck regions, however, BCC is rarely metastasized [6], [8]. On the other hand, Squamous cell carcinoma (SCC), is more dangerous, tissue invasive, and fatal than BCC. Yet, it represents 15-20% of all NMSC. SCC originates from the epidermal keratinocytes. Unfortunately, SCC is one of the highly mutated tumors with 95% of SCC cases have P53 mutated gene [6], [8].

Clinically, NMSCs are treated by various options, more commonly by surgery through a radical excision that goes along with the hypodermis depth. However, if the radical excision is not applicable then other treatment options are available including cryotherapy, diathermia, and radiotherapy, among others [8].

### 2.1.1.2 Melanoma Skin Cancer

Melanoma is the skin tumor of melanocytes, nearly 132,000 new cases yearly and it accounts for 4% of all skin cancer. However, 75% of total skin cancer deaths are caused by melanoma, which makes it the most lethal form of skin cancer, and one of the top six most common cancer-related mortality worldwide. Metastatic melanoma, the most severe form of melanoma, has a very poor prognosis with 15.1% five-year survival rate. The main causes of melanoma are, sun (ultraviolet (UV)) exposure or/and genetic mutation inheritance, which accounts for 5-12% of all melanoma cases [6], [9], [10].

Melanocytes, the least abundant cells in the epidermis, are responsible for melanin production through keratinocyte's activation in response to UV radiation preventing DNA damage which ultimately protects the development of melanoma skin neoplasm [6], [9]. Normally, UV radiation stimulates the production of  $\alpha$ -melanocyte stimulating hormone ( $\alpha$ -MSH) by keratinocytes, that binds to melanocortin 1 receptor (MC1R) on melanocytes to activate melanin synthesis. Melanin then shields and protect the nuclei from the mutagenic effects of UV radiation. Moreover, the coloration of the skin, eyes and the hair depend on melanin synthesis, which is mainly controlled by MC1R activity that is defined by its gene polymorphisms. Accordingly, fully functional MC1R lead to the black/brown eumelanin production, and so, the darker eumelanin the more functional MC1R the better UV protection. By contrast, less functional MC1R, produces the red/yellow pheomelanin, thus, the lighter pheomelanin the less MC1R function, therefore, more DNA mutations due to UV damage [6], [9].



The most frequent mutated melanoma pathways are serine/threonine-protein kinase (BRAF), and mitogen-activated protein kinase (MAPK) pathway, which accounts for two third of melanoma mutations. More than 85% of BRAF mutations are BRAFV600E, which plays an important role in the activity of downstream MAPK signaling resulting in uncontrolled growth and proliferation. MAPK mutant pathways, however, play a major role in the development of resistance [8], [9].

Different chemotherapeutic agents are used as the first line therapy, mainly dacarbazine (DTIC), the most used drug, once metabolized in the body it generates active DNA-methylating carbenium ions. Temozolomide (TMZ), an alkylating agent, that needs no metabolic activation, induces single or double-strand DNA breaks, and inhibits DNA replication. As a targeted therapy, vemurafenib and dabrafenib are used as BRAF inhibitors. Likewise, the new immunological approaches with programmed cell death receptor protein 1 (PD-1) expressed by T-cells and its ligand (PD-L1) on malignant melanocytes, are also being used as a therapy by blocking PD-1 receptor by pembrolizumab or nivolumab. Nonetheless, metastatic melanoma is still highly resistant to those agents [6], [8]–[11].

### 2.1.2 Breast Cancer

Breast cancer (BC) refers to tumors initiated from breast tissue, usually from the lobules or the inner lining of milk ducts. Currently, BC is the most diagnosed cancer type among all cancer patients especially females. According to 2022 statistics in USA, BC is the 4<sup>th</sup> cause of cancer mortality worldwide in both genders, and the 2<sup>nd</sup> cause of cancer death among females (**Fig. 1**). BC accounts for more than 2.2 million new cases and approximately 685,000 new deaths [12]–[14]. Early-stage BC, which is limited to the breast or spread to the axillary lymph nodes, is curable. Whereas advanced BC, characterized by metastases and invading surrounding organs, is not curable, yet treatable in terms of symptoms control and life prolongation. Several risk factors might lead to BC including gender, smoking, radiations, genetic history, genetic mutations, age, chemicals, drugs among others [12], [15].

BC is a heterogeneous characterized disease on the molecular level, where different biomarkers are identified considering the histological characteristics. Therefore, BC is classified as hormone receptor-positive (progesterone receptor (PR) or estrogen receptor (ER)-positive) and triple negative breast cancer (ER, PR, and human epidermal growth factor receptor-2 (HER2)-negative) (**Fig. 2**) [12], [14], [16].

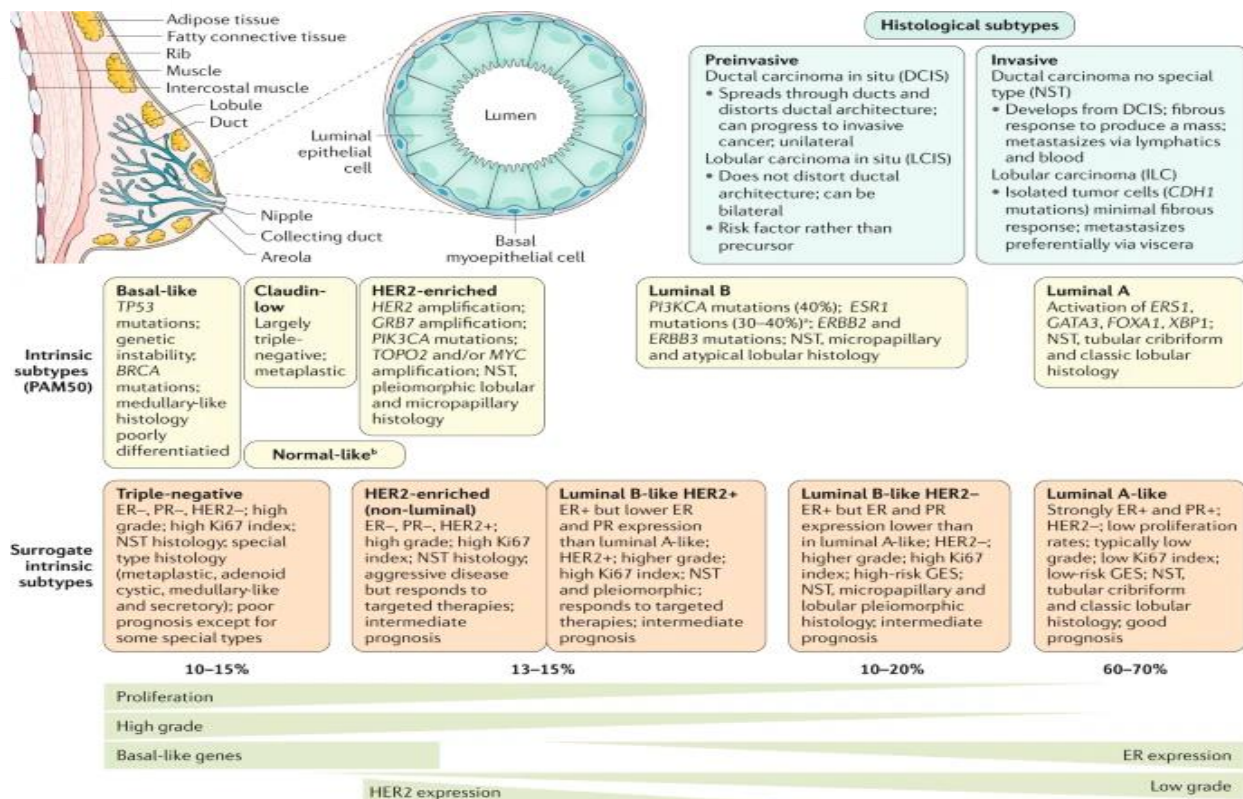


Figure 2: Breast cancer subtypes [12].

### 2.1.2.1 Hormone Receptor-Positive

Hormone receptor positive breast cancer (HR+ BC) represents nearly 65% of all breast cancer cases, 70-80% of them are ER-positive, of which 65% are also PR-positive. Unlike other types of neoplasms, HR+ BC prognosis for early stages is remarkably improved, which led to better effective treatments, and reduced death rate of advanced disease. Thus, HR+ BC death rates are falling quickly. Importantly, ER signaling plays an important role in ER+ BC therapy, where patient survival is improved. Accordingly, the most common therapy used is endocrine therapy by using fulvestrant (a selective ER degrader), tamoxifen (an ER inhibitor), or alpelisib (an  $\alpha$ -specific PI3K inhibitor) in case of phosphatidylinositol-4,5-bisphosphate 3-kinase catalytic subunit alpha (PI3KCA) mutation which represents 40% of HR+ BC [12], [17].

### 2.1.2.2 Triple Negative Breast Cancer

Triple negative BC (TNBC) on the other hand, ER, PR, and HER2 negative, is characterized with metastatic patterns and more aggressive with poorer prognosis compared to HR+ BC. TNBC represents about 15-25% of all BC cases and almost 5% of all cancer-related deaths. TNBC is a highly heterogeneous disease, where six different subgroups, and four transcriptional subtypes were identified (**Table 2**). Due to the various molecular phenotypes, endocrine and targeted therapies are not sensitive in TNBC. Thus, chemotherapy with taxane and anthracycline-based treatment is the mainstream of TNBC treatment. Additionally, monoclonal antibodies (MAbs) are being used in combination with chemotherapy including ladiratumumab, spartalizumab, and bevacizumab. Yet, the efficacy of chemotherapy is poor, and so TNBC is still one of the most resistant cancer types to drugs [12], [15], [18].

<b>TNBC subtypes</b>	<b>TNBC subgroups</b>
Basal 1 (BL1)	Immunomodulatory
Basal 2 (BL2)	Luminal androgen receptor expression
Mesenchymal	Mesenchymal stem-like
Luminal androgen receptor	Mesenchymal-like
	Basal-like
	Unstable

**Table 2:** TNBC subtypes and subgroups [15].



## 2.2 Cancer treatment

Recently, the main objective of cancer research and medical trials is to develop novel methods for cancer treatment, which comes after the extraordinary improvement towards understanding tumor developments and the molecular basis of the disease. Therefore, the choice of treatment and its progress depends on cancer type, location, size of the tumor, stage of progression, as well as the impact on non-tumor cells [2], [5], [19].

### 2.2.1 Radiation Therapy

Radiotherapy uses high-energy beams to destroy cancer cells by damaging their DNA. Radiations mostly effect quickly growing and dividing cells, therefore radiotherapy effects mainly tumor cells since they grow and proliferate faster than normal cells. Besides, this therapy can help reduce, remove, or control tumor growth at specific sites [5].


### 2.2.2 Surgery

Cancer surgery is a common treatment for different types of cancer, where the tumor mass is removed, if the tumor is found to be resectable. In most cases, the chance of cure after surgery is high, especially if the cancer is not metastasized to other site or organs in the body. Traditionally, surgery is being used to treat, however, it can be used to diagnose, relieve tumor's side effects, or prevent cancer in some cases [5], [19].

### 2.2.3 Chemotherapy

Chemotherapy is the most applied therapy after the diagnosis for cancer treatment before or after surgery. That was the case in the past and - in some countries - it is still the only option. Chemotherapy is the use of any anticancer (cytotoxic) drug (not specific). Usually, chemotherapeutics target cell's DNA and/or processes important for cell division to kill rapid dividing tumor cells, including rapid dividing normal cells (in the skin, epithelial cells of the hair and the intestine, red and white blood cells, and others). Different groups of chemotherapeutics where classified depending on the modes of action including alkylating agents, topoisomerases, microtubule targeting agents, antimetabolites, and antibiotics [5], [19]–[21]

The choice of drug depends on the type of cancer. Still, chemotherapy is the first line therapy for advanced tumor to slow down and inhibit the growth of tumor, shrink tumor size, and prolong the life of the patient, especially if the patient is diagnosed with a late stage. These combinations of drugs – chemotherapeutics - are given orally or usually intravenously so they circulate in the body and have a systemic effect reaching not only the tumor cells but also healthy cells. Unfortunately, these drugs have serious side effects including hair loss, loss of appetite, increased chance of infections, bleeding, nervous complications, and fatigue [5], [19]–[21]. Consequently, new therapies need to be developed to counter the side effects. It is also needed to increase the



specificity of the available therapeutic options. Thus, the current development and the use of MAbs or specific cell surface inhibitors are steps in that direction.

#### 2.2.4 Targeted and Immunotherapies

Targeted therapy is the use of antibodies, small molecule inhibitors (SMIs) or oral drugs that somehow specific and more precise to tumor cells and have limited effects to normal cells. Immunotherapy, on the other hand, is based on the use of patient's own natural defense system - immune system- to fight off cancer. Nowadays, the most important type of immunotherapy is the checkpoint inhibitory MAbs, where the target is the immune-modulating mechanisms which is used by the tumor cells to escape the immune system. For example, cytotoxic T-lymphocyte-associated antigen 4 (CTLA-4) and PD-1 with its ligand PDL-1. Accordingly, both therapies aim to treat and improve the overall survival of cancer patients [5], [21].

In fact, chemotherapeutic and targeted agents are used against cancer worldwide, nevertheless, no chemotherapy or targeted therapy is 100% effective since tumor cells evolve and gain resistance against the available drugs. At present, the evolution of monoclonal antibody or targeted therapy made the situation somewhat better mostly in developed countries. Yet, drug resistance to single-agent therapy, targeted and immunotherapies particularly, is still increasing [22].

### 2.3 Cancer Drug Resistance

Positive results and responses have been detected in cancer patients after treated with chemotherapy, targeted, or/and immunotherapy. Still, for the average cancer patient, these positive results were for a limited period of time only, and after a while these therapies become ineffective. For others, the therapy had no effect at all, tumor cells start to escape and resist therapy agents (cytotoxic drugs of chemotherapy and targeted therapy) by different mechanisms which are in general called drug resistance [22], [23]. Two major types of resistance are known: the intrinsic and the acquired resistance.

#### 2.3.1 Intrinsic Resistance

Intrinsic resistance, on the one hand, is the one that is already existed in cancer cells before therapy is started, like a mutation in certain genes. For instant, ceramide kinase (CERK) is a pro-apoptotic lipid kinase that controls ceramide in the cells. However, it is believed to have the opposite function in TNBC, a high expression of CERK was reported in TNBC cases where it plays a role in cell survival and mammary tumor recurrence. Moreover, it promotes tumor migration and invasion through PI3K pathway activation [24].



### 2.3.2 Acquired Resistance

Acquired, also called secondary resistance, on the other hand is the process in which tumor cells gain anti-drug resistance due to the prolonged treatment with anticancer agents [22], [23]. This is the case where cancer cells show a positive response to therapies in the first stages of treatment. Indeed, in many cases, most tumor cells are killed, yet not all and the remaining cells that acquired specific anti-drug resistance during therapies will proliferate and grow to form a tumor that is no longer sensitive to the treatment [22], [23], [25].

### 2.3.3 Mechanisms of Cancer Drug Resistance.


Gaining of secondary mutation is one of the various mechanisms that cancer develops to resist treatment. For example, vemurafenib is a melanoma targeted therapy agent that targets BRAF-V600E, reported cases showed acquired mutation in KRAS or/and MEK1 after vemurafenib treatment [22], [25]. Other mechanisms include alteration of drug targets, which can be done by different ways such as down-regulation of the gene responsible for the drug target, activation, or alteration of the signaling pathways of the target gene. For example, trastuzumab is a monoclonal antibody targets ERBB2 in ER+ BC, studies showed that BC trastuzumab-resistance increased through ERBB2 truncation, activation of another mutation like PI3KCA, or altering the signaling pathway of ERBB2 to ERBB3 or IGF1 [25].

Additionally, up-regulation of drug efflux pumps expression can also lead to multi-drug resistance. For example, a member of the ATP binding cassette drug transporter gene family, the ATP-binding cassette sub-family B member 1 (ABCB1) or P-glycoprotein (P-gp) belongs to multi-drug resistance protein 1 (MDR1) which is a xenobiotic efflux pump that can export drugs out of the cells. This protein is found to be overexpressed in drug resistant cancer cells. In addition, increased DNA damage repair by different pathways, like nucleotide excision repair pathway through excision repair cross-complementation group 1 protein (ERCC1) can cause chemotherapy resistance. Other pathways like mismatch repair, base excision repair, non-homologous end-joining, or homologous-recombination pathway can induce chemoresistance [23], [25].

#### 2.3.3.1 Inflammation-Related Cancer Drug Resistance

Immune system plays an important role in cancer treatment; however, inflammation can do completely the opposite through increasing tumor progression and drug resistance. Growing evidence have shown that chemotherapy-induced inflammation is one of the reasons for chemoresistance and metastasis in breast neoplasm. Hence, inflammation is considered as a key characteristic of cancer, especially chronic inflammation where the risk of malignancy is a typical sign. Indeed, cyclooxygenase-2 (COX-2) enzyme is one of the enzymes that leads to the transformation from acute to chronic inflammation upon treatment [26], [27].





COX-2 is a cyclooxygenases-member enzyme that metabolize arachidonic acid to prostaglandins including prostaglandin E2 (PGE2), which is an inflammation mediator. COX-2 overexpression has been reported in more than 40% of breast cancer, as well as skin, lung, bone, including other neoplasms. Accordingly, cancer progression is linked with the constitutive expression of COX-2 and PGE2, within the activation of different factors and pathways such as vascular endothelial growth factor (VEGF), PI3K/AKT pathway, MAPK, anti-apoptotic pathway, nuclear factor  $\kappa$ B (NF $\kappa$ B), and others, which in fact lead to increase tumor aggressiveness and cancer cell proliferation, angiogenesis, and therapy-resistance. Therefore, to overcome these complications; targeting COX-2 with celecoxib was suggested as a step in that direction [27], [28].

However, considering all mechanisms and factors for cancer drug resistance; apoptotic elusion plays a key role in cancer therapy resistance, since apoptotic evasion is one of the top hallmarks of neoplasm, especially intrinsic (mitochondrial) apoptosis.

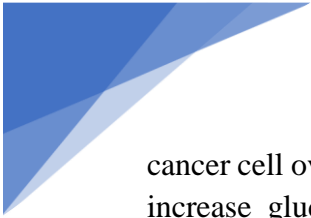
## **2.4 Mitochondria**

### **2.4.1 An Overview**

Mitochondria, known for centuries as the dynamic powerhouses of a cell, are considered one of the most important intercellular maternally inherited organelles of the cell. Since they have their own DNA called mitochondrial DNA (mtDNA), which provides them with the essential metabolic enzymes and proteins. Mitochondria are membrane-bound organelles that contain two major membranes, outer and inner membrane separated by intermembrane matrix. The outer mitochondrial membrane (OMM) contains protein-based pores for ions and large molecules passing. Whereas the inner membrane is more restricted compartment mainly for electron transport chain where adenosine triphosphate (ATP) is generated. In addition, mitochondrial matrix holds citric acid cycle that produces electrons for electron transport chain. To summarize, mitochondria are essential organelles for ATP production, metabolic signaling, redox homeostasis, as well as proliferation and apoptotic pathway control. However, metabolic alterations in mitochondria are linked with multiple diseases including cancer [29], [30].

### **2.4.2 Mitochondria in Cancer**

Naturally, cells undergo oxidative phosphorylation (OXPHOS) to produce ATP molecules [30]. Whereas tumor cells use high amount of glucose, so they switch from OXPHOS to glycolysis, in which a glucose molecule degraded into two pyruvate molecules [31]. Then pyruvate is reduced to lactate in the absence of oxygen via an anaerobic glycolysis to give two ATP molecules, this process is called Warburg effect. Here the question arises, why glycolysis but not OXPHOS, considering the 18-fold difference in ATP production by OXPHOS. Different possible explanations, first, ATP production through glycolysis is much faster than that of OXPHOS, so



cancer cell overexpress hexokinase-2, lactate dehydrogenase (LDHA), and glucose transporters to increase glucose uptake. Which leads to the second reason, the accumulation of glycolytic intermediates because of the high glycolytic flux, meet the demands of rapid proliferation as well as chemo-resistance. For example, the accumulation of glycolytic intermediates enhances pentose phosphate pathway (PPP), where nicotinamide adenine dinucleotide phosphate (NADPH) is produced for the maintenance of sufficient levels of reduced form of glutathione [29]–[31].

Of note, mitochondria control the intrinsic apoptosis which is one of the most important pathways in the cell, especially for cancer cell. Where pro-apoptotic and anti-apoptotic proteins are downregulated and upregulated, respectively. Yet, tumor cells are more sensitive to apoptosis than normal cells. Hence, targeting mitochondria have become the novel strategies for anti-cancer drugs [30], [31].

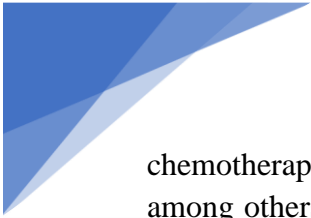
### 2.4.3 Targeting Mitochondria

Mitochondrial functions, such as bioenergetics, biosynthesis, and more importantly signaling pathways, are necessary for tumorigenesis. For that, targeting mitochondrial processes is the strategy nowadays for cancer treatment. Different mitochondrial compartments and contents are involved in the direct or indirect communication with other cell's organelles and compartments. Throughout anterograde, where the signal comes from the cytosol to mitochondria, while retrograde represents the signal produced by mitochondria and transduced to cytosol [29]. The latter mode, retrograde, is of a great interest for researchers since the pro-apoptotic signal proteins and factors are transported from mitochondria to other compartments in the cell.

The release of pro-apoptotic signal proteins from the mitochondria is mainly controlled by B-cell lymphoma 2 (BCL-2) family proteins. BCL2 gene discovery goes back to the chromosomal translocation at t(14;18) found in a patient's follicular lymphoma cells [32]. The family contains two groups of proteins, pro-and-anti-apoptotic proteins. On the one hand, Pro-apoptotic family contains pore-formers such as BCL-2-associated X protein (BAX), BCL-2 antagonist killer 1(BAK), and pro-apoptotic BCL-2 homology 3 (BH3)-only proteins including Bid and Bim among others. Overall, the activation of pro-apoptotic BCL-2 family triggers apoptosis. On the other hand, anti-apoptotic protein family BCL-2 and BCL-xl which are normally expressed to inhibit apoptosis activation [32] [33]

### 2.4.4 Mitochondrial Apoptotic Pathways

Apoptosis (programed cell death) is a highly regulated form of cell death to maintain a normal cell population, yet dysregulation in apoptotic pathways is carcinogenesis. Two main pathways of apoptosis: an intrinsic pathway, also called the mitochondrial apoptosis which involves different protein families including BCL-2, BH3-only proteins family, caspase-9, Akt, apoptotic inducing factor (AIF) and others. This type of apoptosis is induced by multiple signals such as DNA damage, loss of mitogens, increase reactive oxygen species (ROS) level,



chemotherapeutic agents, cytochrome C (Cyt c), and calcium ( $\text{Ca}^{2+}$ ) overload in mitochondria, among others. Intrinsic apoptosis depends mainly on OMM permeabilization which can lead to mitochondrial apoptotic death [29], [33]; therefore, we studied the effect of DEA on OMM integrity. When the OMM is intact, pro-apoptotic intermembrane proteins such as Cytochrome c (Cyt c) and AIF are retained in the mitochondria. Anti-apoptotic of the BCL-2 family form heterodimers with pro-apoptotic members, thereby inactivating them. When the BCL-2-associated agonist of cell death (Bad) is dephosphorylated, it binds to anti-apoptotic BCL-2 family members, releasing the pro-apoptotic ones, which in turn dimerize with each other, translocate to the OMM, and permeabilize it. This leads to a release of the pro-apoptotic intermembrane proteins, eventually resulting in apoptotic cell death [33], [34]. A major mechanism of protection against apoptosis is the phosphorylation of Bad by the cytoprotective kinase Akt. Opa1 is an IMM-associated large GTPase protein that is present in the mitochondria only [34], [35]. Stimuli leading to OMM permeabilization and Cyt c release results also in release of Opa1 to the cytosol.

Extrinsic pathway, on the other hand, involves cell surface death receptor FAS-associated death domain protein (FADD), or tumor necrosis factor (TNF) receptor members, by external signals like drugs, hormones, and/or pathogen effectors. Aiming to activate the downstream caspase-8 and bid protein. The latter protein can play a role in the crosstalk between the two apoptotic pathways. Accordingly, apoptosis of both pathways is initiated by the activation of down-stream of the executioner caspase-3 (**Fig. 3**) [33]

Accordingly, intrinsic apoptosis can be induced throughout two main pathways: caspase-dependent or/and caspase-independent apoptosis. In most cases, both pathways are initiated upon the activation of Bax/Bak by BH3-only family proteins mainly Bid or by self-activation. Normally, Bax is a monomer located in the cytosol, when activated by tBid, it oligomerizes and recruited to OMM. While Bak is already localized in the OMM as an inactive-complex form, it become active when it is released from the complex by tBid upon apoptosis. Therefore, truncation process of Bid is an important step for apoptotic pathways [33], [34].

Caspase-dependent mitochondrial-apoptosis is the pathway that mainly involves the initiator and the executioner caspases, caspase-9, 7, and caspase 3, respectively. This pathway is initiated by the permeabilization of the OMM (MOMP), which is induced by the activation of Bax/Bak by tBid and the inhibition of anti-apoptotic BCL-2/BCL-XL proteins. MOMP leads to the release of mitochondrial intermembrane space (IMS) proteins such as second mitochondrial activator of caspases (SMAC), Omi, AIF, and more importantly Cyt c. Accordingly, the release of SMAC and Omi to the cytosol counter-effect the activity X-linked inhibitor of apoptosis (XIAP), which is inhibiting caspases mainly caspase-9 and preventing it of forming apoptosome. The latter effect, apoptosome is a complex important for caspase-9 activation, it is formed by procaspase-9, Cyt c, and apoptotic peptidase activating factor 1 (APAF1). Once caspase-9 is activated; it cleaves and activates caspase-7, then cleaved caspase-7 cleaves caspase-3 which leads to apoptosis. Finally, Apoptotic body formation is the end-product of apoptosis (**Fig. 3**). Of note, cleaved caspase-3

translocates to the nucleus for poly (ADP-ribose) polymerase-1 (PARP-1)'s DNA damage-repair inhibition through cleaving PARP-1 [33], [34].

On the other hand, caspase-independent apoptotic pathway can be induced by two ways: First by IMS proteins release following MOMP, mainly AIF and endonuclease G (EndoG). AIF is the 2<sup>nd</sup> protein found to be released from mitochondria to the cytosol after being cleaved to become soluble protein. Then it translocates to nucleus where it leads to chromatin condensation and DNA fragmentation, the same goes for EndoG protein. Second way rely on mechanisms such as mitochondrial fragmentation as a result of mitochondrial dynamics dysfunction. Or mitochondrial matrix swelling due to mitochondrial permeability transition (mPT) pores opening. Nevertheless, both mechanisms can also play roles in caspase-dependent apoptosis. For example, mPTP is normally found closed in the IMM, increased Ca<sup>2</sup> concentration in mitochondria or/and oxidative stress lead to mPTP opening. Followed by loss of mitochondrial membrane potential ( $\Delta\Psi_m$ ), OMM rupture, mitochondrial matrix swelling. As well as IMS proteins release like AIF and EndoG which cause caspase-independent apoptosis, although Cyt c is also released by mPTP opening which is a key protein in caspase-dependent apoptosis. Of note, mPTP opening was reported to be one of the most important events of apoptosis, it was referred as the point-of-no-return [33], [34].

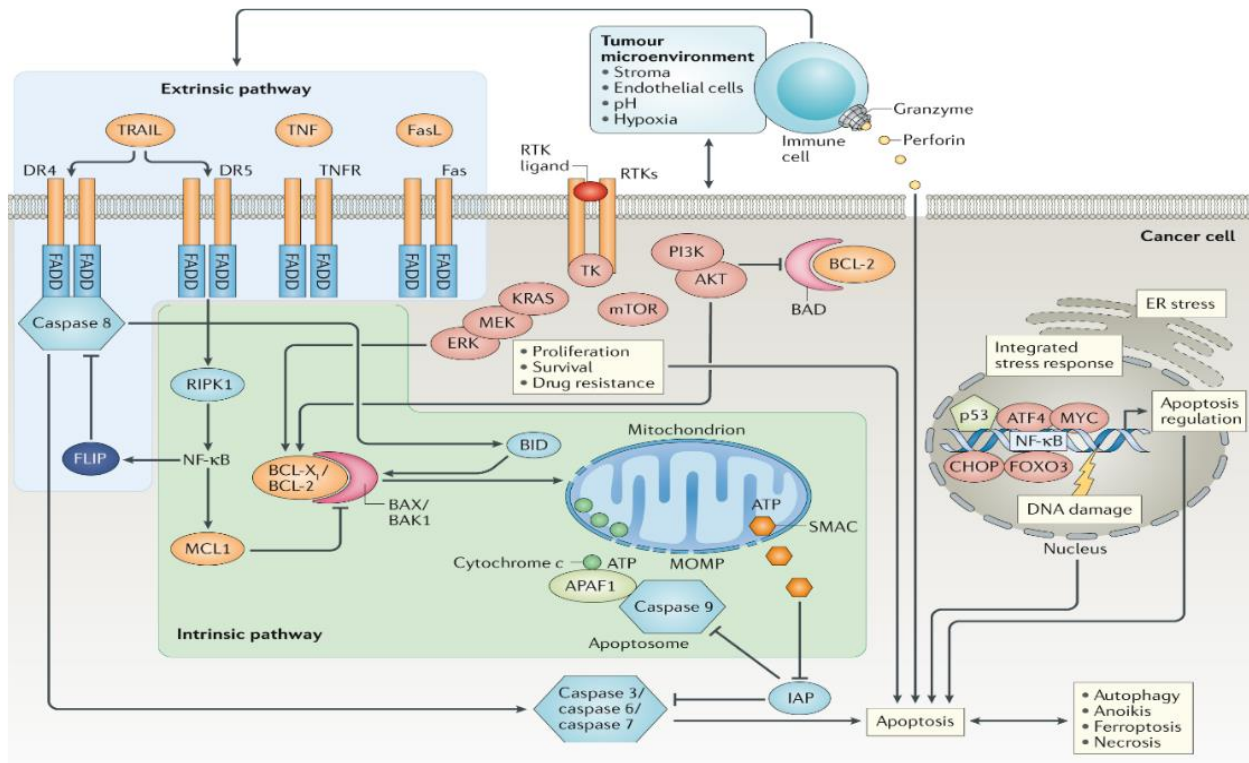


Figure 3: Apoptotic pathways [33].

## 2.4.5 Mitochondrial Dynamics

Mitochondria are highly dynamic organelles undergo continuous morphology changes to meet their cellular energy demands. The morphology -physiological- change processes are tightly controlled by mitochondrial fusion and fission to form long tubules or small units, respectively. Fusion, on the one hand, is important to keep the cell alive by increasing OXPHOS,  $\Delta\Psi_m$ , and keep cristae junction closed. More importantly, fusion allows for the complementation of damaged mtDNA as well as other contents like lipids and proteins. Mitochondrial fusion has two steps: fusion of the OMM by the interaction between mitofusion proteins (MFN1 and MFN2), and secondly the fusion of the IMM which is mediated by optic atrophy-1 (OPA1). Importantly, OPA1 has two isoforms, large OPA1 controls cristae junctions to keep them closed. However, following MOMP, shorter isoform of OPA1 indicates cleavage of OPA1 by OMA1 zinc Metalloendopeptidase (OMA1), which results in dysregulation and opening of cristae junctions. Not to mention, more than 80% of Cyt c, among other pro-apoptotic proteins, is stored in cristae junctions. Thus, during apoptosis, tBid-triggered Bax/Bak activation associates with mitochondrial fusion reduction, mainly through MFN2 inhibition and OPA1 cleavage. Therefore, MFN1,2 inhibition and OPA1 cleavage indicates loss of mitochondrial fusion which leads to IMS apoptotic proteins release and mitochondrial fragmentation which also could be called mitochondrial fission [34].

Fission, on the other hand, is the process where mitochondria split into parts mainly for cellular homeostasis maintenance by removing damaged mitochondria. In other words, fission play a key role in mitochondrial quality control. The process itself, is controlled by dynamin-related protein 1 (DRP1) and its receptors mitochondrial fission factors including mitochondrial fission protein 1 (Fis1) on the OMM [36], [37]. DRP1 is regulated by multiple proteins, mainly A-Kinase anchoring protein 1 (AKAP1), which is a scaffold protein that facilitates DRP1 phosphorylation at serine 637 by the interaction with cyclic adenosine 3'5'-monophosphate (cAMP)-dependent kinas A (PKA). This phosphorylation leads to the release of DRP1 from the OMM by inhibiting the oligomeric assembly of the protein, which eventually inhibits fission and induces mitochondrial elongation [38]. Nevertheless, during apoptosis, AKAP1 activity is inhibited and DRP1 is activated by the phosphorylation at serine 616 and/or serine 579, which indicate fission and fragmentation of mitochondria [36]–[38].

In the context of cancer, OPA1 is significantly overexpressed in many cancer types including TNBC. Indeed, as stated by previous studies [39], OPA1 regulates angiogenesis, which is essential for tumor growth, and lymphangiogenesis that is important for metastasis. So, deletion of OPA1 curtails tumor metastasis and growth. Accordingly, huge work was put in together for finding a novel drug to target OPA1 in neoplasm. In fact, a selective OPA1 inhibitor, N- (1,5-dimethyl-3-oxo-2-phenyl-2,3-dihydro-1H-pyrazol4-YL)-3-methyl-1-PH+ (MYLS22) was identified. Overall, MYLS22 is a first-in-class small molecule that target and inhibit OPA1, and trigger tumor growth inhibition [39].

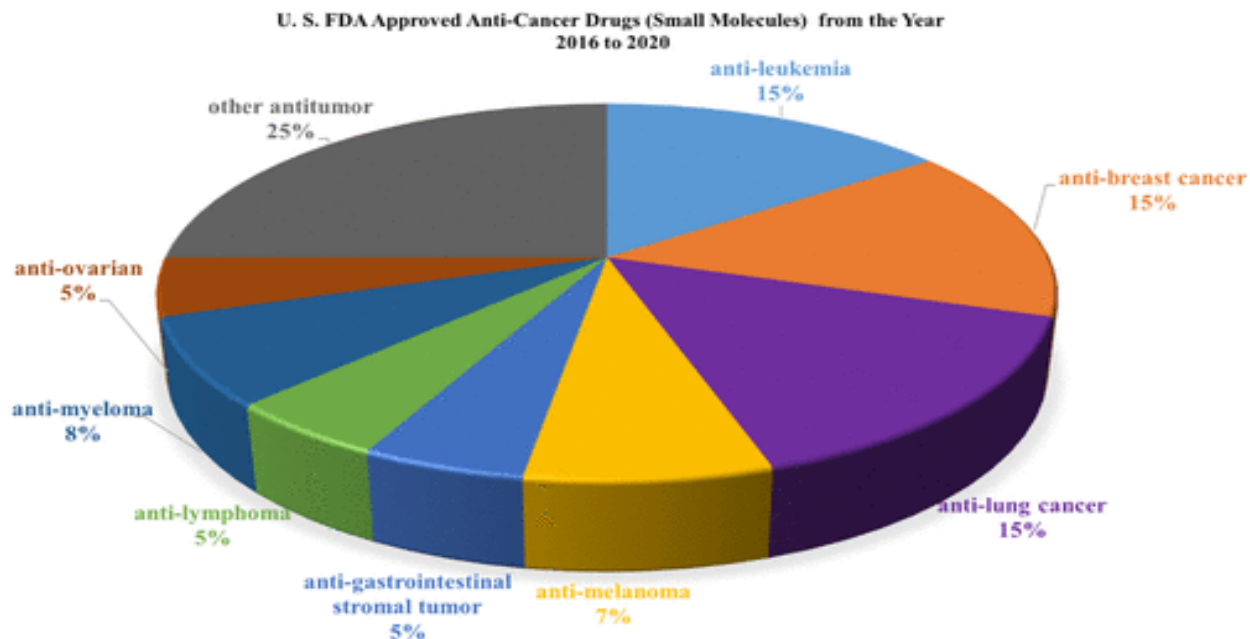


*Figure 4: FDA approved small anti-cancer molecules in the past five years [40].*

## 2.5 Small Molecules in Therapy

In 2001, tyrosine kinase inhibitor (TKI) was the first small molecule to be approved by the US Food and Drug Administration (FDA) [41]. At present, 42 small anti-cancer molecules have been approved by the FDA (**Fig. 4**) [40]. Thereby, small molecules are in a great interest and demand for cancer treatment, despite the huge use and challenges by macromolecules especially monoclonal antibodies. Due to the advantages of small molecules: costs, pharmacokinetic properties, drug storage and transportation, patient compliance, absorption method, and more importantly their mood of action which is signal transduction inhibition. Furthermore, cell membrane and blood brain barrier penetration of small molecules are easier than macromolecules, which are the limitation of antibodies use [40], [41].

## 2.6 Desethylamiodarone (DEA)

Nowadays, small-molecule targeted drugs are in a great interest, due to their effectiveness, cost, storage, transportation, and pharmacokinetic properties [41]. Thereby, mono-N-desethyl amiodarone (Desethylamiodarone-DEA), a small pharmacological active compound, is the major metabolite of the widely used antiarrhythmic drug, Amiodaron (AM) [36], [42]. AM, (2-butyl-3benzofuranyl 4-[2-(diethylamino)-ethoxy]-3,5-diiodophenyl-ketone hydrochloride), is an FDA approved class III antiarrhythmic drug for variety of cardiac diseases including ventricular and supraventricular arrhythmias. Usually, AM is given orally to patients with a recommended therapeutic range of  $<5.7 \mu\text{M}$ , where its half-life is in the range of 14-59 days. AM metabolism takes place in the liver and in the gut wall by an oxidase-dependent oxidative de-ethylation reaction catalyzed by cytochrome p450 3A family (CYP3A) to give DEA (Fig. 5) [42]–[44].

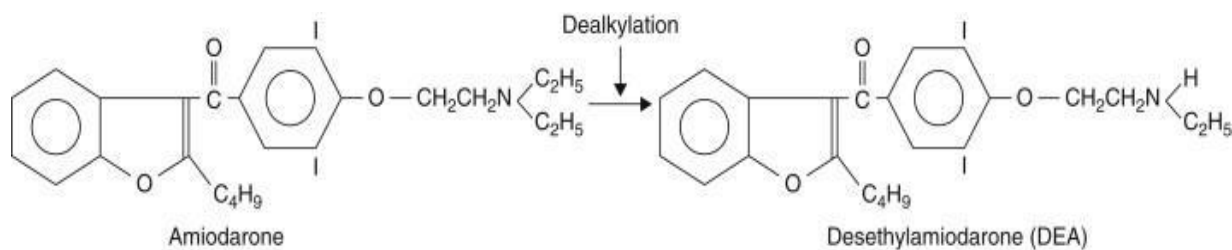


**Figure 5.** Structure of Amiodarone and Desethylamiodarone[45]

DEA has a similar electrophysiologic effects as AM, where both work on the prolongation of action potential duration by blocking  $\beta$ -adrenergic receptors, sodium, and L-type calcium channels. Both AM and DEA are strongly bound to plasma proteins, However, DEA-serum level is higher than that of AM-serum level during long-term AM treatment  $1.7\text{-}4.5 \mu\text{M}$  and  $1.6\text{-}5.3 \mu\text{M}$ , respectively, as its elimination half-life is approximately 40 days. Moreover, in the context of treatment, DEA compared to AM is more toxic *in-vitro*, where AM's activity triggers necrotic cell death, while DEA activates apoptotic pathways. Due to DEA's lipophilic structure; it is highly accumulated (higher than AM) in skin, liver, lungs, myocardium, thyroid gland, pancreas, but not in adipose tissue. Different toxic side-effects (hepatic, dermatologic, cardiac, pulmonary, thyroid, ocular, etc.) limit long-term AM therapy, due to the fact that DEA and AM are highly concentrated in the tissues after AM treatment, which can be hundred to more than thousand times higher than that of the plasma concentration [10], [36], [43]. Thereby, based on the toxic effects of DEA and tissue accumulation properties, its potentiality in cancer therapy was proposed [10], [36], [43], [46], [47].



### 3 Objectives

Throughout history, neoplasm used to be primarily a disease of the minority, however, recently has become a leading cause of morbidity and mortality in the majority of human populations. Consequently, cancer research and treatment trials are constantly growing to design, identify, and describe targets, mechanisms, and pathways of different tumor types aiming for treatment. Indeed, in the light of these information provided by enormous number of cancer research, we aim to imply a DEA on multiple neoplasm types. The thesis is structured into two parts, which are closely related since they deal with experimental data about skin and breast cancer treatment.

#### 3.1 Our aims:

- To establish DEA's potentiality in B16F10 metastatic melanoma cells including *in-vivo* lung metastasis formation, *in-vitro* cell viability, cell cycle arrest, apoptosis, Reactive Oxygen Species (ROS) formation, colony formation and mitochondrial processes, including mitochondrial respiratory chain, mitochondrial permeability transition (mPT), and mitochondrial membrane potential ( $\Delta\Psi_m$ ).
- To study and compare the *in-vitro* cellular and mitochondrial effects of DEA on different BC cells. Including cell death, cell migration, mitochondrial respiratory chain, mitochondrial dynamics and fragmentation, mitochondrial membrane potential ( $\Delta\Psi_m$ ). And possible TNBC DEA's resistance mechanism.





## 4 *Materials and Methods*

### 4.1 **Materials**

Protease inhibitor cocktail and all chemicals for cell culture were purchased from Sigma-Aldrich Kft (Budapest, Hungary). DEA was a gift from Professor Andras Varro (Department of Pharmacology and Pharmacotherapy, University of Szeged, Szeged, Hungary). The following primary antibodies were used: anti-Bad, anti-phospho-Bad (Ser136), anti-Akt, anti-phospho-Akt (Ser473), anti-AIF, anti-histonH1, anti-cytochrome C, anti-Opa1, anti-BCL-2, anti-Bax, anti-caspase 3 (clone H-277), anti-poly (ADP-ribose) polymerase 1 (PARP-1), anti-p53, anti-p21, anti-p27, anti-COX-2, anti-OPA1, anti-Mfn1, anti-Mfn2, anti-Drp1, anti-phospho-Drp1(Ser637), anti-Fis1, anti-AKAP, anti-cyclin dependent kinase (CDK)2, anti-cyclin D1 (1:500 dilution), anti-glyceraldehyde-3-phosphate dehydrogenase (GAPDH) (1:2000, clone 6C5), and anti-actin (1:2000). All the antibodies were purchased from Cell Signaling Technology (Beverly, MA, USA), but anti-GAPDH antibody was from EMD Millipore Bioscience (Darmstadt, Germany).

### 4.2 **Cell Culture**

B16F10 mouse metastatic melanoma, MCF-7 and 4T1 BC cell lines were obtained from the American Type Culture Collection (LGC Standards, Wesel, Germany). All cells were split twice a week for 4 months and maintained as monolayer adherent cultures under standard conditions (5% CO<sub>2</sub>, 37 °C) in RPMI 1640 media supplemented with 10% fetal bovine serum (FBS) and 1% penicillin–streptomycin mixture (Life Technologies, Darmstadt, Germany).

### 4.3 **Cell Viability Assay**

B16F10, MCF-7, and 4T1 cells were seeded in 96-well plates at a starting density of  $5 \times 10^3$  cells/well in quintuplicate (five replicate wells per sample) overnight. All the cells were treated with 0 to 15  $\mu$ M of DEA for 24 or 48 h. Then, the cells were rinsed with phosphate-buffered saline (PBS) and were fixed in 100  $\mu$ L of cold 10% trichloroacetic acid solution (TCA). Following 30 min incubation at 4 °C, the plates washed five times with distilled water, and then were dried overnight at room temperature. The cellular protein content in the wells was determined by sulforhodamine B (SRB) assay. Briefly, 70  $\mu$ L of 0.4% SRB (Sigma-Aldrich Co., Budapest, Hungary) prepared in 1% acetic acid were added to each well for 30 min at room temperature. Afterwards, the solution was discarded, and the plates were washed five times with 1% acetic acid and were dried at room temperature for a few hours. Then, 200  $\mu$ L of a 10 mM tris(hydroxymethyl)aminomethane base was added to each well, and the plates were agitated at room temperature on a plate shaker for 30 min to solubilize the bound SRB. Absorbance was measured at 560 and 600 nm in parallel with a GloMax®-Multi Instrument (Promega, Madison, WI, USA). Optical density (OD)600 was subtracted as a background from the OD560. The experiments were repeated five times.

#### **4.4 Colony formation assay**

B16F10, MCF-7, and 4T1 cells were plated at a starting density of 500 cells/well into 6-well plates. After culturing overnight, the cells were treated with different concentrations of DEA for 7 days. Then, the cells were washed with PBS and stained with 0.1% Coomassie Brilliant blue R 250 (Merck KGaA, Darmstadt, Germany) in 30% methanol and 10% acetic acid. Then, the colonies with diameter of > 0.5 mm were counted. The number of colonies was determined and normalized to the number of colonies in the controls using ImageJ software. All experiments were repeated three times.

#### **4.5 Annexin V & Death Cell Assay**

To detect live, early apoptotic, late apoptotic, and dead cells, Muse™ Annexin V & Dead Cell Assay (Luminex Corporation, Austin, TX, USA) was used. The assay utilizes annexin V to detect phosphatidylserine on the external membrane of apoptotic cells. The experiments were carried out according to the manufacturer's protocol. B16F10, MCF-7, and 4T1 cells at a starting density of 105 cells/well were seeded into 6-well plates and were treated for 24 hours with or without the indicated concentrations of DEA. After the treatment, the cells were harvested and were diluted in their medium. Afterwards, 100 µL of the Muse™ Annexin V & Dead Cell reagent was added to 100 µL of cell suspension ( $4 \times 10^4$  cells), which was followed by 20 minutes incubation in a dark room at room temperature. Five thousand single-cell events were measured per sample using a MUSE Cell Analyzer device. All experiments were repeated three times.

#### **4.6 Cell Cycle Assay**

B16F10 cells were seeded and treatment with the indicated DEA concentrations for 24 h. The cells then were collected by centrifugation at 300 x g for 5 minutes, washed with ice-cold PBS, fixed with 70% ethanol, stained with a premixed reagent composed of the nuclear DNA intercalating stain propidium iodide (PI) and RNase A in a proprietary formulation, and analyzed according to the manufacturer's protocol. PI discriminates cells at different stages of the cell cycle, based on differential DNA content in the presence of RNase to increase the specificity of DNA staining. The Muse Cell Cycle Software Module performs calculations automatically. All experiments were repeated three times.

## 4.7 Migration Assay

To assess cell motility, we used the wound-healing assay. MCF-7 and 4T1 cells were seeded into flat-bottom 6-well plates, and they were cultured to form a sub-confluent monolayer. Then, a wound was inflicted into the cell layer by using a sterile 200  $\mu$ L pipette tip, and the cells were treated with the indicated concentrations of DEA for up to 12 h. The wounds were imaged at 0, 6, and 12 h by an EVOS microscope (Thermo Scientific Hungary, Budapest, Hungary) at 4 $\times$  magnification. The distance differences were measured using ImageJ software. The experiment was repeated twice in duplicates.

## 4.8 Measurement of Invasive Growth

MCF7 and 4T1 cells were seeded at a starting density of  $9 \times 10^3$ /well and  $5 \times 10^3$ /well, respectively, in an electronic microtiter plate (E-Plate®) (ACEA Biosciences, San Diego, CA, USA). The cells were cultured for 24 h before they were treated with 0, 5, or 10  $\mu$ M DEA for 24 h, during which the impedance was measured every 5 min. The xCELLigence Real-Time Cell Analysis (RTCA) device (ACEA Biosciences, San Diego, CA, USA) was used according to the manufacturer's protocol. The instrument was placed in a humidified incubator at 37 °C and 5% CO<sub>2</sub>. These experiments were repeated twice running in three parallels.


## 4.9 Ethics

Animal experiments were conducted in strict accordance with the recommendations in the Guide for the Care and Use of Laboratory Animals of the National Institutes of Health. The experimental protocol was approved by the Animal Research Review Committee of the University of Pecs, Hungary (Permit number: BA02/2000-5/2017).

## 4.10 Mouse Pulmonary Metastasis Model

Six weeks old male C57BL/6 mice were bred and maintained at the Department of Biochemistry and Medical Chemistry, University of Pecs, Medical School. All animals were housed 3 or 4 per cage, under controlled laboratory conditions ( $22 \pm 1$  °C, 50 – 60% relative humidity and 12/12-hour light-dark cycles) with free access to water and standard rodent chow. Paper tunnels were used for environmental enrichment.

We used the pulmonary metastasis model that is widely used as an *in-vivo* test for assessing antitumor efficacy of medications [48]. B16F10 cells ( $5 \times 10^5$ /0.1 ml) were injected into the lateral tail vein of mice using 30G 1/2 needle and 1-ml syringe. There were no changes observed in motility or food intake in tumor bearing animals during the experiment. All animals were checked at least once daily for aspects of general health including activity, posture and fur grooming, body condition score was also assessed as previously described [49].



The mode of DEA administration and dosage were determined based on the study by DeWitt et al. [50]. Prior to the study, safety of DEA treatment was confirmed by administration of 25 mg/kg DEA to 5 mice for two weeks. Mice were randomly divided into 2 groups of 6 mice each. Each mouse was given a daily intraperitoneal injection of either 100  $\mu$ l 0.9% saline solution containing 10% ethanol as the vehicle control or 25 mg/kg DEA. Treatment was started one day after cell injection and was given every third day, lasted for consecutive 16 days after injection when the animals were weighed and sacrificed by cervical dislocation under isoflurane (AbbVie Ltd., Budapest, Hungary) anesthesia. The lungs were removed, rinsed in PBS, and weighed. The lung mass index was calculated as the ratio of lung weight to body weight. The harvested lungs were fixed in 4% formalin. Tumor nodules on the surfaces of the lungs were counted under a stereomicroscope. Then, the whole lung was embedded in optimum cutting temperature compound (Sakura Finetek, USA), sectioned (12  $\mu$ m thickness), and stained with hematoxylin and eosin. Histological observations were performed under a microscope (BX51, Olympus, Japan) by an expert blind to the experiment. Percentage of the total area occupied by tumor was measured using the Panoramic viewer 1.15.4 (3DHISTECH, Hungary).

#### **4.11 Subcellular Fractionation**

Three semi-confluent 10 cm plates of B16F10 cells were harvested, washed twice with PBS, and suspended in 1 mL of fractionation buffer (250 mM of sucrose, 20 mM of 2-[4-(2-hydroxyethyl) piperazin-1-yl] ethane sulfonic acid (HEPES), pH 7.4, 10 mM of KCl, 1.5 mM of MgCl<sub>2</sub>, 1 mM of ethylenediamine-tetraacetic acid (EDTA), 1 mM of ethyleneglycol-tetraacetic acid (EGTA), 1 mM of dithiothreitol (DTT), and proteinase inhibitor cocktail (Sigma, #P2714)). The cell lysate was manually homogenized in a Teflon–glass homogenizer, chilled on ice, and centrifuged for 7 min at 720 $\times$  g at 4 °C. The nuclear pellet was suspended in 700  $\mu$ L of fractionation buffer, re-homogenized, and centrifuged for 10 min at 600 $\times$  g. This procedure was repeated one more time, and the pellet was suspended in lysis buffer (10% glycerol, 25 mM of NaCl, 50 mM of NaF, 10 mM of Na-pyrophosphate, 2 nM of EGTA, 2 nM of DTT, 20 nM of p-nitrophenylphosphate, 25 mM of Tris-HCl, pH 7.4, 50 nM of beta-glycerophosphate, and 0.1% Triton X-100) to yield the nuclear fraction. The supernatant of the 7 min, 720 $\times$  g centrifugation step was subjected to centrifugation at 10,000 $\times$  g for 5 min at 4 °C. The supernatant and pellet of this step yielded the cytoplasmic and mitochondrial fractions, respectively; the latter was not used in this study.

## 4.12 Immunoblot Analysis

B16F10, MCF-7, and 4T1 cells were seeded in 10 cm plates at 106 cells/plate and treated with DEA as described above for the cell viability assay. The cells were harvested at intervals in chilled lysis buffer containing 0.5 mM of sodium-metavanadate, 1 mM of EDTA, and protease inhibitor cocktail (1:200). The cell lysates were boiled and subjected to 10% sodium dodecyl sulfate polyacrylamide gel electrophoresis before being transferred to nitrocellulose membranes. The membranes were blocked in 5% low-fat milk for 1.5 h at room temperature, and then exposed to primary antibodies at 4 °C overnight in blocking solution. Appropriate horseradish peroxidase–conjugated secondary antibodies were used at a dilution of 1:5000. Signals were visualized by using enhanced chemiluminescence and captured on X-ray film. The films were scanned, and the pixel densities of the bands were determined using the NIH ImageJ software. Alternatively, chemiluminescence was measured on an Azure 300 (Azure Biosystems) imaging system that digitized the bands' chemiluminescence intensities using its inbuilt software. For stripping and reprobing, the membranes were washed in stripping buffer (0.1 M glycine, 5 M MgCl<sub>2</sub>, pH 2.8) for 1 h at room temperature. After washing and blocking, the membranes were incubated with primary antibodies against non-phosphorylated or loading control proteins. These experiments were repeated three times.

## 4.13 $\Delta\Psi_m$ Assay

Changes in  $\Delta\Psi_m$  were assayed using the mitochondrial fluorescent dye JC-1 (Sigma-Aldrich) for B16F10, MCF-7, and 4T1 cells. The cells were seeded at a starting density of  $2.5 \times 10^4$  cells/well in 6-well plates containing coverslips and cultured at least overnight before the experiment. After subjecting the cells to different concentrations of DEA for 3 h, the coverslips were rinsed twice in PBS and placed upside down on top of a small chamber formed by a microscope slide filled with PBS supplemented with 10% FBS and 1  $\mu\text{g}/\text{mL}$  of JC-1 dye (Molecular Probes, Eugene, OR, USA). Images were taken with a Nikon microscope (Inverted Microscope Eclipse Ti-U Instruction, Auro-Science Ltd., Budapest, Hungary) equipped with a SPOT RT3 2Mp Monochrome camera including SPOT Advanced software, using a 20 $\times$  objective lens with epifluorescence illumination. After the cells were loaded with dye for 15 min, the same microscopic field was first imaged with a 490 nm bandpass excitation and > 590 nm (red) and < 546 nm (green) emission filters. Under these conditions, we did not observe considerable bleed-through between the red and green channels. The quantification of JC-1 fluorescence intensities in each sample was performed in 15 randomly chosen microscopic fields containing 20–30 cells using the MetaXpress image analyzer software (Molecular Devices LLC., San Jose, CA, USA). These experiments were repeated three times.

## 4.14 . Analysis of Mitochondrial Network Dynamics

### 4.14.1 Project 1


For confocal imaging, B16F10 cells were seeded onto 25 mm round glass coverslip medium at a starting density of  $2.5 \times 10^4$  cells/coverslip and cultured in antibiotic-free culture for 24 h. The transient transfection of B16F10 cells with mtRFP was performed using TransFectin Lipid Reagent (Bio-Rad, Hercules, CA, USA). On the following day, the cells were treated for 3 h, as indicated in the text; washed twice in PBS; and fixed in 4% formalin. Fluorescence was visualized on an Olympus FluoView 1000 (Olympus, Hamburg, Germany) confocal laser scanning microscope. For excitation, a multiline argon-ion laser at 488 nm and a green helium-neon laser at 543 nm were used (10  $\mu$ s/pixel) in the photon-counting and sequential mode. The field of interest was scanned in XYZ mode, scanning the total thickness of the cells with a 1.5  $\mu$ m layer distance and taking 1024  $\times$  1024-pixel images of each layer. Image analysis for mitochondrial fragmentation was performed by MetaXpress High-Content Image Acquisition and Analysis Software. The quantitative determination of mitochondrial fragmentation was as the following: we considered mitochondria shorter than 2  $\mu$ m to be fragmented and those longer than 5  $\mu$ m as filamentous. These experiments were repeated three times.

### 4.14.2 Project 2

MCF-7 and 4T1 cells were seeded in ultrathin-bottomed 96-well plates and were cultured overnight. The cells were treated as indicated in the figure legends, were rinsed twice in PBS, and were incubated in PBS containing 20 nM of MitoTracker Red for 30 min in a CO<sub>2</sub> incubator at 37 °C. Fluorescence images were taken via a 60 $\times$  Plan Apo Lambda objective of an ImageXpress Micro 4 High-Content Imaging System (Bioscience Ltd., Budapest, Hungary). Image analysis for mitochondrial fragmentation was performed by MetaXpress High-Content Image Acquisition and Analysis Software. Mitochondria shorter than 2  $\mu$ m were considered as fragmented, while those longer than 5  $\mu$ m were considered as filamentous. All experiments were performed in triplicates.

## 4.15 Bioenergetic Analysis

To determine the balance of oxidative vs. fermentative energy production in B16F10, MCF-7, and 4T1 cells, oxygen consumption rate (OCR) and extracellular acidification rate (ECAR) were measured using a Seahorse XFp Analyzer (Agilent, Santa Clara, CA, USA). Cells were seeded into XFp cell culture 8-well miniplates at a starting density of  $4 \times 10^4$  cell/well in duplicate and cultured under standard conditions overnight. Then, the cells were treated with different concentrations of DEA for 3 and 6 h. Prior to the measurement, the medium was replaced with Seahorse XF Assay Media (Agilent, Santa Clara, CA, USA) pH 7.4 supplemented with 10 mM of glucose, 2 mM of L-glutamine, and 1 mM of pyruvate. Mitochondrial stress test was performed using the following inhibitors at the indicated final concentrations: 1  $\mu$ M of oligomycin, 1  $\mu$ M of carbonyl cyanide 4-(trifluoromethoxy) phenylhydrazone (FCCP), and 1  $\mu$ M of rotenone–



antimycin A. In each experiment, two wells without cells were running to assess the non-cellular oxygen consumption, which was subtracted from the corresponding OCR value. The OCR and ECAR data were normalized to the mg protein content using the Micro BCA Protein Assay kit (Thermo Fisher Scientific, Waltham, MA, USA) for the measurement of protein concentrations. No other data correction was applied. These experiments were repeated three times.

#### **4.16 Determination of Cellular ROS Formation**

B16F10 cells were seeded as described above for the viability assay and treated with 5 or 10  $\mu\text{M}$  of DEA or 5  $\mu\text{M}$  of taxol (positive control [51]). The cellular ROS levels were determined based on the formation of N-acetyl-8-dodecyl-resorufin and 6-carboxy-2',7'-dichlorofluorescein from their nonfluorescent reduced counterparts, N-acetyl-8-dodecyl-3,7-dihydroxyphenoxazine (1.3 mg/L final concentration) and 6-carboxy-2',7'-dichlorodihydrofluorescein diacetate (2 mg/L final concentration). The former assessed the cellular ROS formation in the lipid phase, and the latter in the aqueous phase. Fluorescence was measured by a plate-reader fluorimeter (PerkinElmer, Hungary) at excitation wavelengths of 578 and 495 nm and emission wavelengths of 597 and 522 nm for N-acetyl-8-dodecyl-resorufin and 6-carboxy-2',7'-dichlorofluorescein, respectively. The mitochondrial superoxide formation was assessed by MitoSOXTM Red (Thermo Fisher Scientific, Waltham, MA, USA). Cells were incubated for 30 min in 5  $\mu\text{M}$  of MitoSOXTM Red, then were rinsed and treated with 5 or 10  $\mu\text{M}$  of DEA or 5  $\mu\text{M}$  of taxol for 3 h. Fluorescence was recorded by the plate-reader fluorimeter at excitation wavelengths of 495 nm and emission wavelengths of 590 nm. Under these conditions, the fluorescence intensity is proportional to the mitochondrial superoxide level. The ROS levels were calculated from the slopes of the registration curves. These experiments were repeated five times.

#### **4.17 Measurement of mPT**

The B16F10 cells were seeded as described above for the viability assay and cultured in antibiotic-free medium overnight. Cells were washed with  $\text{Ca}^{2+}$  and  $\text{Mg}^{2+}$  free Hank's balanced salt solution (HBSS), and then treated with 250 nM of A23187, 90  $\mu\text{M}$  of  $\text{CoCl}_2$ , 1 g/L of glucose, 5 or 10  $\mu\text{M}$  of DEA or 1.5 mM of  $\text{CaCl}_2$  (positive control [52]), and/or 2.5  $\mu\text{M}$  of CsA in HBSS for 3 h. For the detection of mPT, acetoxymethylcalcein was added to the medium at a final concentration of 1  $\mu\text{M}$ . Fluorescence in wells resulting from unquenched de-esterified calcein in the mitochondria (cytoplasmic calcein is quenched by  $\text{Co}^{2+}$ ) was monitored using the ImageXpress Micro4 automated high-content imaging system (Molecular Devices LLC., San Jose, CA, USA) using a 4 $\times$  objective and epifluorescence illumination. The quantification of calcein fluorescent intensities was performed using the MetaXpress software. These experiments were repeated three times.



## 4.18 Statistical Analysis

Results are shown as means  $\pm$  standard deviation (SD). ANOVA using the post hoc Dunnett test (single way or two-ways) as well as Mann-Whitney U test were employed to calculate the concentration-dependent effects of DEA in each experiment. Statistical analyses were performed using IBM SPSS Statistics v20.0. Differences were regarded as significant at  $p \leq 0.05$ ,  $p \leq 0.01$ , and  $p \leq 0.001$ .



## 5 Results and Discussion 1.0

### 5.1 Results 1.0

#### 5.1.1 Effect of DEA on the Viability of B16F10 Melanoma Cells

To get an overview of DEA's effect on B16F10 cells, a short-term assay was performed. We treated the cells for 3–12 h with 5 or 10  $\mu\text{M}$  of DEA before determining their viability using the SRB assay. This assay is considered the most suitable for assessing the toxicity of substances in cultured cells, especially when the toxicity affects the mitochondria [53]. DEA had a statistically significant anti-proliferative and cell death-inducing effect on the cells in a time- and concentration-dependent manner. Therefore, the possible pathways contributing to DEA-induced cell death were further analyzed. Although at 5  $\mu\text{M}$  and for up to 6 h of incubation, this effect did not reach statistical significance (**Fig. 6**).

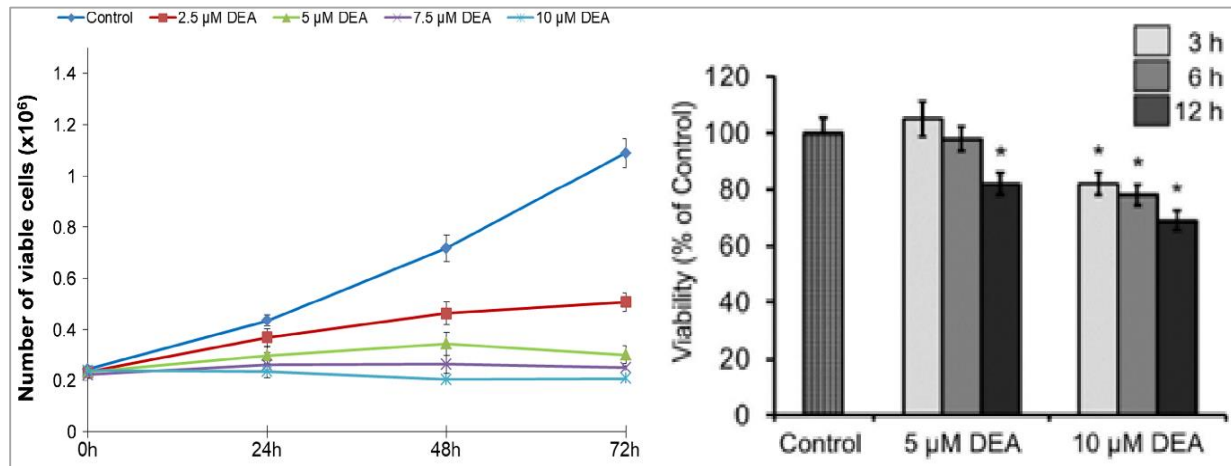


**Figure 6.** Effect of DEA on the viability of B16F10 melanoma cells. Cells were treated with 5-10  $\mu\text{M}$  of DEA for 3-72 h, and then the viability was determined using the SRB assay [53]. The results are expressed as the % viability of the control (means  $\pm$  SEM of five independent experiments). \* Indicates a significant difference relative to the control ( $p \leq 0.05$ ).

### 5.1.2 Effect of DEA on B16F10 Colony Formation

Colony formation assay utilizes lower drug concentrations and longer exposure times; therefore, it represents a situation more like the therapeutic one than the viability studies. Accordingly, we sought assess DEA's effect on colony forming ability of the B16F10 cells. We treated the cells with 0–3  $\mu\text{M}$  DEA for 7 days then colonies of  $> 0.5$  mm were counted. As we found, DEA significantly decreased number and size of the colonies even at the lowest concentration used (**Fig. 7**). These data indicate that DEA can induce cell death and can inhibit colony formation at low micromolar concentrations.

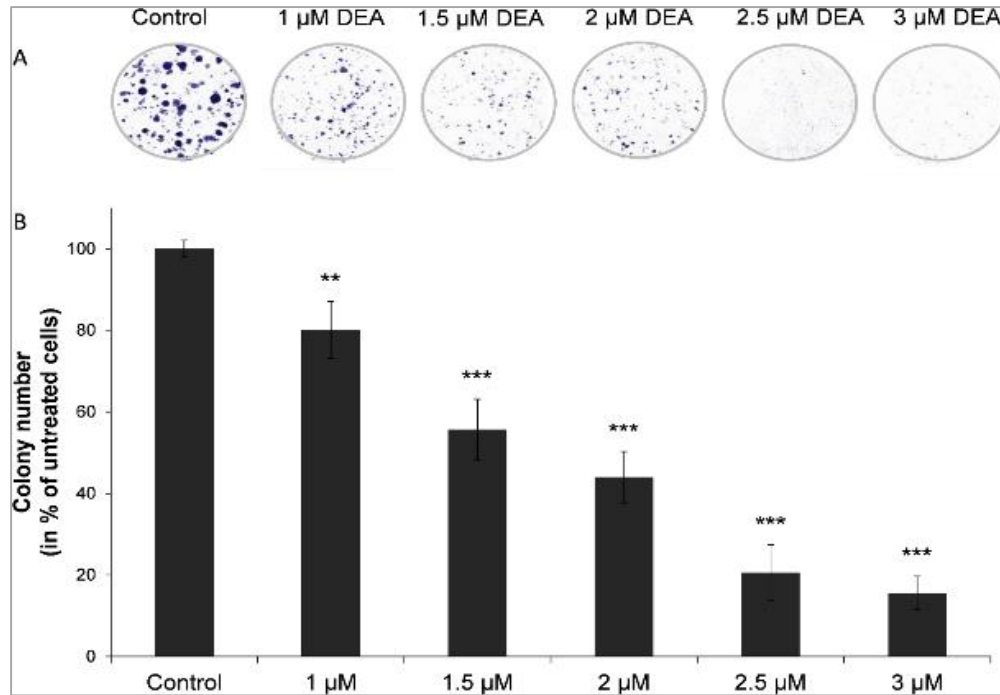


**Figure 7.** Effect of DEA on colony formation of B16F10 murine melanoma cells. For the assay the cells were exposed to increasing concentrations of DEA for 7 days. The results are presented as representative images (A) and as a bar diagram (B). Controls were treated with vehicle (0.2% DMSO). The results are mean  $\pm$  SD of three independent experiments performed in at least quadruplicate. Data were analyzed using ANOVA with Dunett post hoc test. The significant difference compared to the corresponding control group is described as the following: \*\*  $p \leq 0.01$  and \*\*\*  $p \leq 0.001$ .

### 5.1.3 Effect of DEA on Apoptosis Activation in B16F10 cell

Cell death could be of different mechanisms mainly necrosis or apoptosis [33], [34]. Since DEA induced cell death in B16F10 we were interested to investigate the mode of cell death induced by DEA. For that, flow cytometry with the Muse™ Annexin V & Dead Cell Assay was used. The assay utilizes cell surface annexin V binding that measures appearance of phosphatidylserine on the plasma membrane's external surface, a marker of apoptosis. We observed that DEA increased the total apoptosis rate in a dose-dependent manner. We found a total apoptosis rate of  $34.61 \pm 2.17\%$  for 5 and  $73.71 \pm 3.12\%$  for 10  $\mu\text{M}$  DEA in contrast to the control's  $10.11 \pm 1.97\%$  (Fig. 8). At the lower DEA concentration, rate of early apoptosis exceeded that of the late, however, at the higher concentration, late apoptosis predominated (Fig. 8).

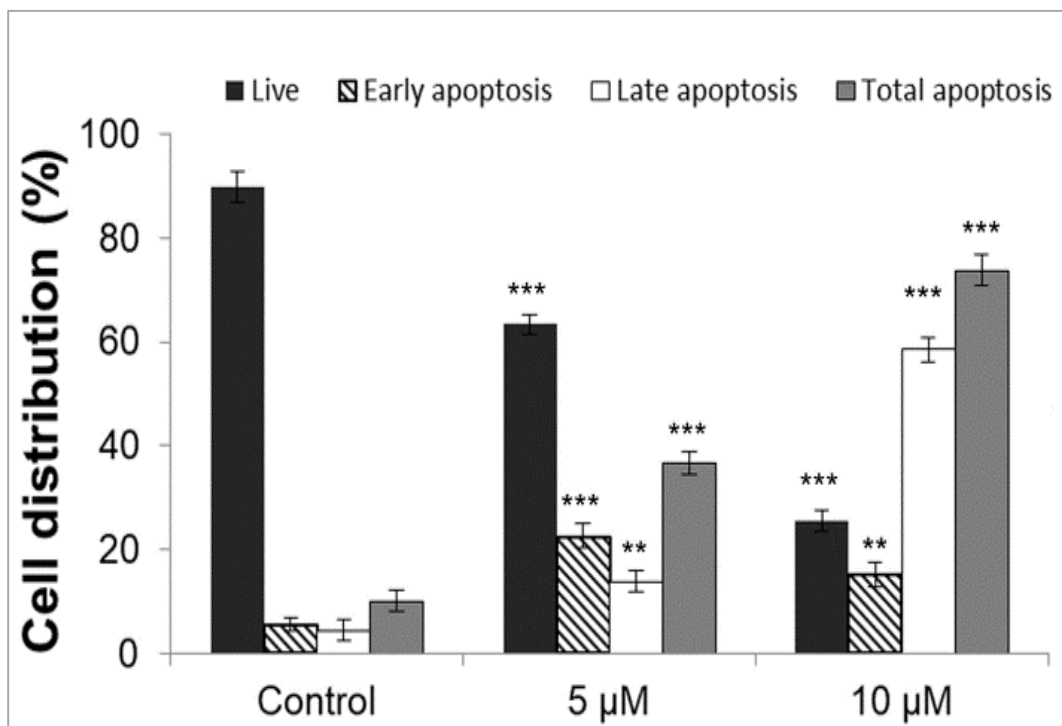


**Figure 8.** Effect of DEA on activation of apoptosis in B16F10 cells. After subjected to 24 hours' treatment with increasing concentrations of DEA the cells were stained with the Muse™ Annexin V & Dead Cell Reagent and measured on the Muse™ Cell Analyzer. (A) The bar chart shows the percent distribution of living (dark gray bars), early apoptotic (striped bars), late apoptotic (white bars) and total apoptotic cells (light gray bars). Controls were treated with vehicle (0.2% DMSO). The experiments were repeated three times in at least quadruplicate, and the results are expressed as the mean  $\pm$  SD. Data were analyzed using ANOVA with Dunnett post hoc test (A). The significant difference compared to the corresponding control groups is described as the following: \*\*  $p \leq 0.01$  and \*\*\*  $p \leq 0.001$ .

### 5.1.4 Effect of DEA on the Cell Cycle in B16F10 Cells

According to the data presented in Figure 8, DEA limits the proliferation of B16F10 cells through inducing predominantly apoptotic cell death. However, the net result of cell death and cell division is cell proliferation. Thus, we performed cell cycle analysis to study the other aspect of proliferation. We treated B16F10 cells with 5 and 10  $\mu\text{M}$  DEA for 24 hours and found that the percentage of cells in G0/G1 phase significantly increased from  $56.75 \pm 1.73\%$  (0  $\mu\text{M}$ ) stepwise to  $63.9 \pm 1.94\%$  (5  $\mu\text{M}$ ) and  $75.91 \pm 2.67\%$  (10  $\mu\text{M}$ ). At the same time there was a decrease in the percentage of S and G2/M phase cells (**Fig. 9**). These data indicate that DEA at both concentrations induced cell cycle arrest in the G0/G1 phase that may contribute to its overall inhibitory effect on B16F10 cell proliferation.

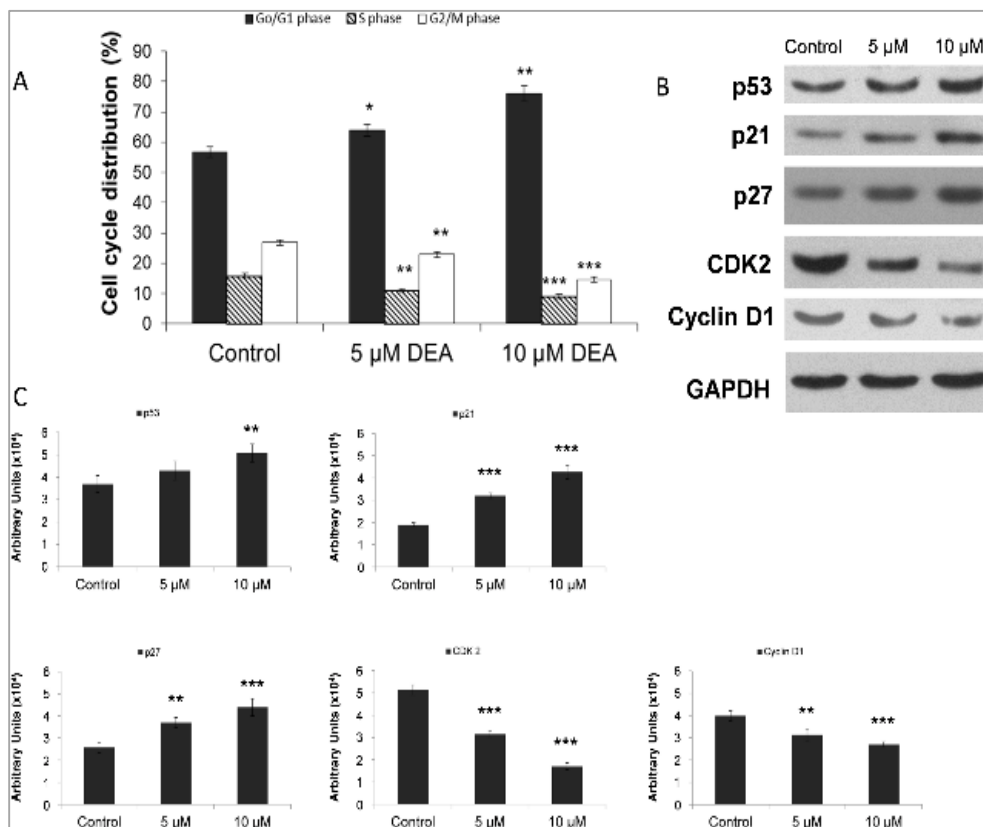


**Figure 9.** Effect of DEA on the cell cycle in B16F10 melanoma cells. The cells were treated with different concentrations of DEA (0, 5 and 10  $\mu\text{M}$ ) for 24 hours. Controls were treated with vehicle (0.2% DMSO). Then they were harvested, fixed with ethanol, and stained with propidium iodide. DNA content was determined by Muse™ Cell Analyzer. The results are presented as a bar diagram, percentage of cells in G0/G1 (dark grey bars), S (striped bars) and G2/M phases (white bars) of the cell cycle (A). Proteins from parallel cells were extracted for immunoblot analysis performed by using antibodies specific to p53, p21, p27, CDK2 and cyclin D1. GAPDH was used as a loading control. The results are presented as representative immunoblots (B) and densitometry analysis of immunoblots in bar diagrams (C). The results are mean  $\pm$  SD of three independent experiments performed in at least quadruplicate. Data were analyzed using ANOVA with Dunnett post hoc test (A) and with Mann-Whitney U test (C). The significant difference compared to the corresponding control group is described as the following: \*  $p \leq 0.05$ , \*\*  $p \leq 0.01$  and \*\*\*  $p \leq 0.001$ .



### 5.1.5 Effect of DEA on Outer Mitochondrial Membrane (OMM) Permeabilization

Accordingly, we assessed DEA's effect on OMM integrity by determining its effect on the expression, localization, and activation of Cyt c, Opa1, AIF, Bad, cleaved caspase-3, and Akt. To this end, we prepared whole-cell homogenate, and in parallel nuclear and cytoplasmic fractions from B16F10 melanoma cells treated with different concentrations of DEA for 6 h, and then subjected them to immunoblot analysis. To determine the phosphorylation states of Akt and Bad, we used phosphorylation-specific primary antibodies. At a concentration of 10  $\mu\text{M}$ , DEA increased the steady-state level of Bad and decreased Bad phosphorylation in a concentration-dependent manner (**Fig. 10**). Both effects shift the balance in the pro-apoptotic direction. Accordingly, DEA induces caspase-3 cleavage, as well as the release of Cyt c and Opa1 into the cytosol and nuclear translocation of AIF (**Fig. 10**). In addition, 10  $\mu\text{M}$  of DEA decreased Akt phosphorylation without affecting the steady-state level of the enzyme (**Fig. 10**). This latter effect of DEA was fully consistent with its effects on the other proteins studied. Together, these data indicated that DEA caused OMM permeabilization.

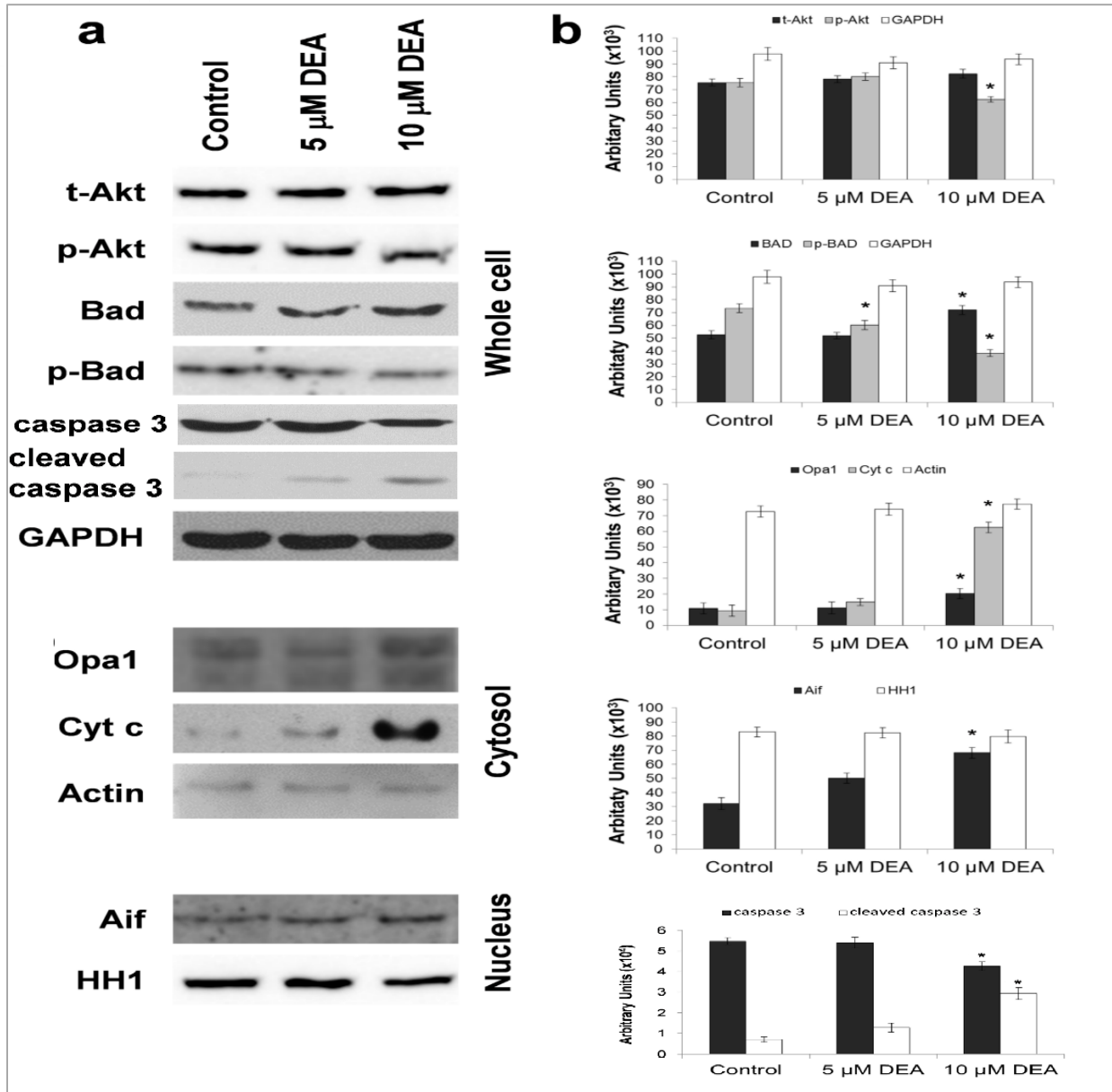


**Figure 10.** Effect of DEA on the OMM permeabilization in B16F10 melanoma cells. Cells were treated with 5 or 10  $\mu$ M of DEA for 6 h, harvested, and homogenized (Whole cell). Alternatively, nuclear and cytosolic fractions were prepared from the harvested cells. Steady-state levels and phosphorylation states of Akt and Bad were assessed in whole-cell homogenate. The steady-state levels of Cyt c, caspase-3, and Opa1 were determined in the cytosolic, whereas that of AIF was measured in the nuclear fraction by immunoblotting. In the whole-cell homogenate, the cytosolic fraction and the nuclear fraction, we used glyceraldehyde-3-phosphate dehydrogenase (GAPDH), actin and histone H1 (HH1), respectively, as loading controls. The proteins were visualized by enhanced chemiluminescence. (a) Representative blots. (b) Quantitative assessment of proteins in the subcellular fractions. Results are expressed as pixel density or chemiluminescence intensity of the bands, both expressed in arbitrary units (means  $\pm$  SEM of three independent experiments). \* Indicates a significant difference relative to the control ( $p \leq 0.05$ ).



### 5.1.6 Effect of DEA on the $\Delta\Psi_m$

Intact  $\Delta\Psi_m$  is pivotal for cellular survival due to its essential role in ATP synthesis, in providing the driving force for the transport of ions and proteins, and in mitochondrial quality control [33]. Accordingly, we were interested in how DEA treatment affects  $\Delta\Psi_m$  in B16F10 melanoma cells. For this purpose, we used a membrane potential-dependent fluorescent dye, JC-1, which accumulates in the mitochondria due to its positive charge. When  $\Delta\Psi_m$  is normal, the dye forms J-aggregates that emit red fluorescence upon excitation. Depolarization decreases the abundance of the dye in the mitochondria; consequently, the aggregates fall apart, and the monomer dye emits a green fluorescence when excited at 490 nm. When  $\Delta\Psi_m$  dissipates completely, the dye is not retained in the mitochondria, manifesting as a loss of fluorescence. Within 3 h, treatment with  $> 5 \mu\text{M}$  of DEA markedly depolarized the mitochondria in intact B16F10 melanoma cells (**Fig. 11**).

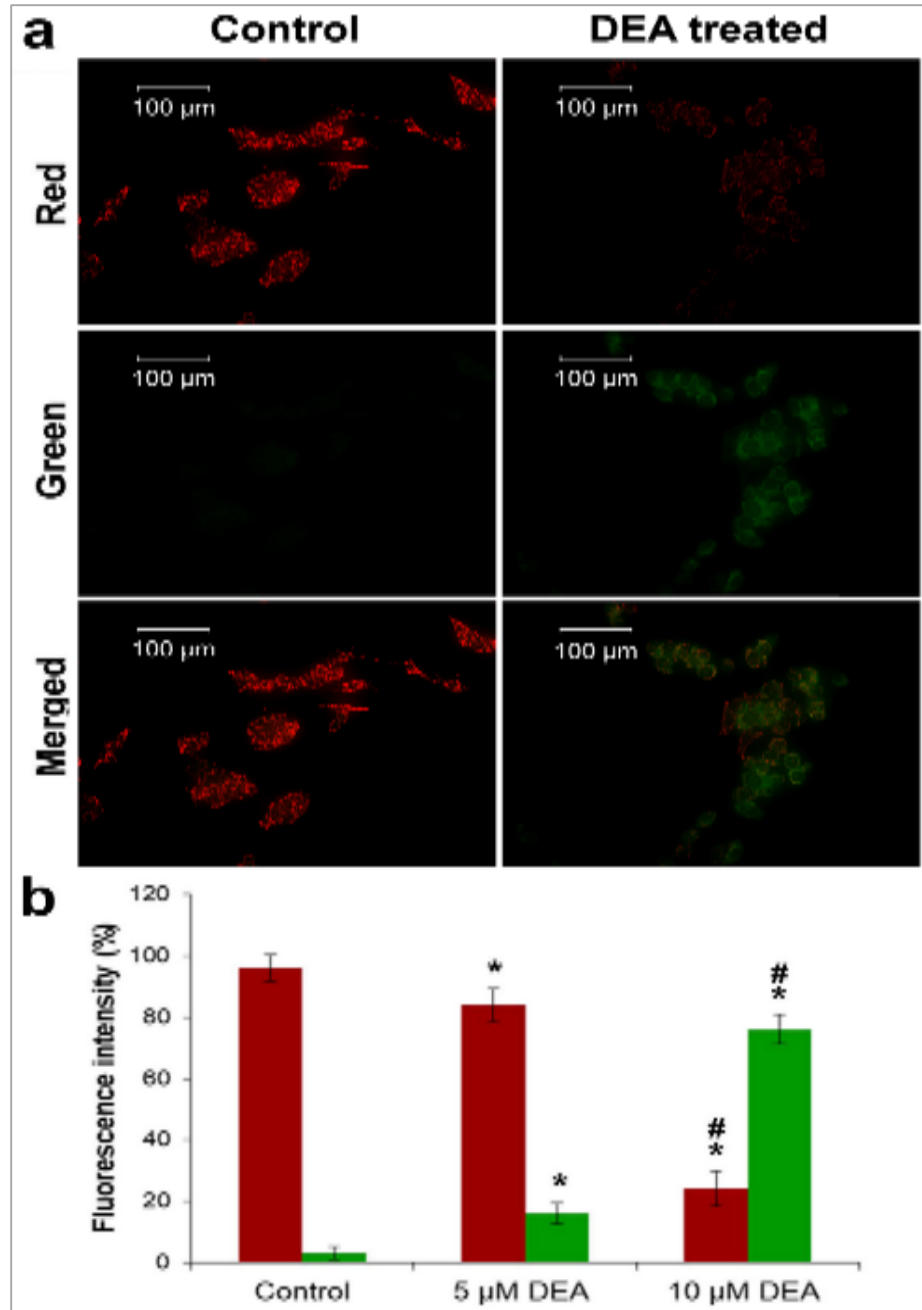


**Figure 11.** Effect of DEA on  $\Delta\Psi_m$  in B16F10 melanoma cells. Cells were treated with 5 or 10  $\mu$ M of DEA for 3 h.  $\Delta\Psi_m$  was assessed using the membrane potential-dependent fluorescent dye, JC-1. Red and green fluorescence indicates normal and depolarized  $\Delta\Psi_m$ , respectively. (a) Representative fluorescence images in the red, green, and merged channels of cells treated with 10  $\mu$ M of DEA. (b) Quantitative assessment of  $\Delta\Psi_m$ , expressed as the % of fluorescence intensity (means  $\pm$  SEM of three independent experiments). Quantitative comparisons are true within the same color only. Red and green bars denote red and green fluorescence, respectively. \* and # indicate a significant difference relative to the control and 5  $\mu$ M of DEA, respectively ( $p \leq 0.05$ ).



### 5.1.7 Effect of DEA on Mitochondrial Fragmentation

As mentioned in section 4.1.1.6, healthy  $\Delta\Psi_m$  is required for the mitochondrial fusion; therefore, compromised  $\Delta\Psi_m$  often results in mitochondrial fragmentation [35]. Therefore, compromised  $\Delta\Psi_m$  results in mitochondrial fragmentation, raising the possibility that DEA treatment causes such an effect. To test this possibility, we performed confocal fluorescence microscopy on DEA-treated B16F10 melanoma cells transiently transfected with mitochondria-targeted red fluorescent protein (mtRFP) expressing vector [54]. Under these conditions, the intensity of the mitochondrially localized fluorescence did not depend on  $\Delta\Psi_m$ . Treatment for 3 h with 10  $\mu\text{M}$  of DEA resulted in mitochondrial fragmentation comparable to that caused by 25  $\mu\text{M}$  of cisplatin (positive control [55]) (**Fig. 12**). Although treatment with 5  $\mu\text{M}$  of DEA tended to increase the mitochondrial fragmentation, the difference from the control did not reach the level of statistical significance (**Fig. 12**).

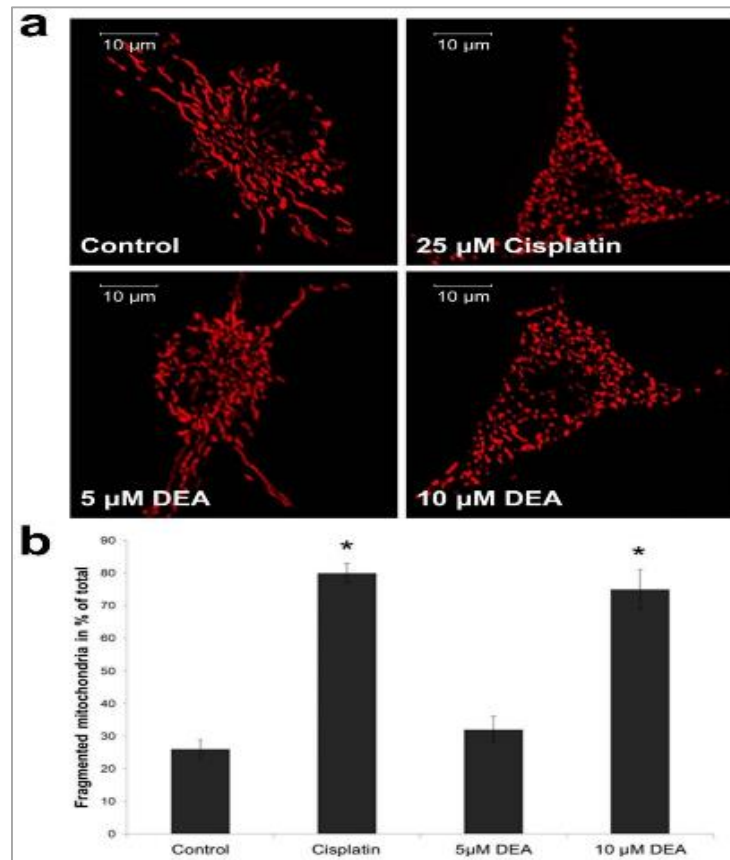


**Figure 12.** Effect of DEA on mitochondrial fragmentation. mtRFP-transfected cells were treated with 5 or 10  $\mu\text{M}$  of DEA, or 25  $\mu\text{M}$  of cisplatin, for 3 h. Mitochondrial fragmentation was determined based on confocal fluorescence images. (a) Representative fluorescence images for all the treatment groups. (b) Quantitative assessment of mitochondrial fragmentation expressed as % (means  $\pm$  SEM of three independent experiments). \* Indicates a significant difference relative to the control ( $p \leq 0.05$ ).

### 5.1.8 Effect of DEA on the Energy Metabolism of B16F10 Melanoma Cells

Given that the DEA treatment depolarized  $\Delta\Psi_m$  (**Fig. 11**), a major determinant of ATP synthesis, we next thought to determine the effect of DEA treatment on the energy metabolism of B16F10 cells. We used the Seahorse XF Cell Mito Stress Test to monitor the cellular oxygen consumption rate (OCR), an indicator of mitochondrial respiration, and the extracellular acidification rate (ECAR), an indicator of aerobic glycolysis in live B16F10 melanoma cells. We treated cells with 5 or 10  $\mu\text{M}$  of DEA for 3 h, and then monitored the OCR and ECAR for 75 min. After registering basal respiration (**Fig. 13a-1**) for 15 min, we added oligomycin, an inhibitor of FoF1 ATP synthase, to assess the ATP production (**Fig. 13a-4**). After 20 min of recording, we added carbonyl cyanide 4-(trifluoromethoxy) phenylhydrazone (FCCP), which uncouples respiration and ATP synthesis, to measure maximal respiration (**Fig. 13a-3**). After a further 20 min of recording, we inhibited mitochondrial respiration by adding the Complex I inhibitor rotenone and the Complex III inhibitor antimycin A to determine the proton leak and non-mitochondrial oxygen consumption (**Fig. 13a-2**, **Fig. 13a-5**). Simultaneously, we also monitored ECAR (**Fig. 13b**). From the original recordings, the instrument output multiple parameters of cellular energy metabolism (**Fig. 13c-k**). The DEA treatment did not significantly affect basal respiration (**Fig. 13c**) or proton leak (**Fig. 13d**), although 10  $\mu\text{M}$  of DEA tended to decrease the former and increase the latter. By contrast, 10  $\mu\text{M}$  of DEA did suppress the maximal respiration (**Fig. 13e**), ATP production (**Fig. 13f**), and coupling efficiency (**Fig. 13g**); the last of these indicates how tightly respiration is coupled to ATP synthesis. DEA decreased the non-mitochondrial oxygen consumption (**Fig. 13h**), and spare respiratory capacity, expressed either as the difference (**Fig. 13i**) or ratio (**Fig. 13j**) of maximal and basal respiration, in a concentration-dependent manner. Although it did not affect the basal fermentative ATP synthesis, DEA decreased lactate accumulation after oligomycin administration in a concentration-dependent manner (**Fig. 13b-k**), indicating that the drug interfered with the glycolytic machinery as well as the mitochondrial respiratory chain.

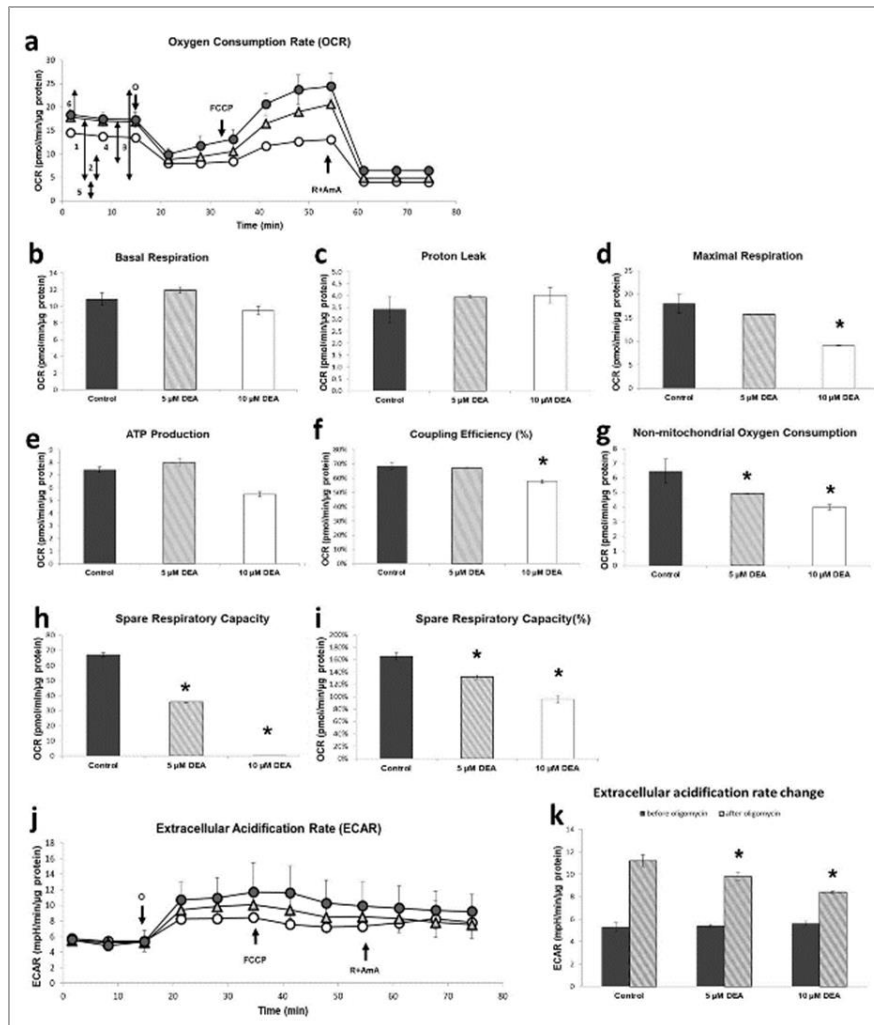


**Figure 13.** Effect of DEA on the energy metabolism of B16F10 melanoma cells. Cells were treated with 5 or 10  $\mu\text{M}$  of DEA for 3 h, and then the OCR and ECAR were monitored for 75 min. The FoF1 ATP synthase inhibitor oligomycin (o), the uncoupler FCCP, and the respiratory inhibitors rotenone and antimycin A (R+AmA) were added at the bold arrows. (a) OCR recordings for untreated (filled circles), 5  $\mu\text{M}$  of DEA-treated (triangles), and 10  $\mu\text{M}$  of DEA-treated (open circles) cells (means  $\pm$  SD of three independent experiments running in two replicates in each experiment). The double-headed arrows with numbers next to them indicate (1) basal respiration, (2) proton leak, (3) maximal respiration, (4) ATP production, (5) non-mitochondrial oxygen consumption, and (6) spare respiratory capacity. (b–i) Parameters derived from (a); for explanation, see the text and (a). Appropriate parts of the recordings were averaged and presented as the means  $\pm$  SEM of three independent experiments running in two replicates in each experiment. \* Indicates a significant difference relative to the control ( $p \leq 0.05$ ). (b) Basal respiration. (c) Proton leak. (d) Maximal respiration. (e) Mitochondrial ATP production. (f) Coupling efficiency; for explanation, see the text. (g) Non-mitochondrial oxygen consumption. (h,i) Spare respiratory capacity, presented as the difference (h) and ratio (i) of maximal and basal respiration. (j) ECAR recordings for untreated (filled circles), 5  $\mu\text{M}$  of DEA-treated (triangles), and 10  $\mu\text{M}$  of DEA-treated (open circles) cells (means  $\pm$  SD of three independent experiments running in two replicates in each experiment). All the labeling is the same as for (a). (k) Extracellular acidification rate before (dark bars) and after (light bars) the administration of oligomycin. OCR and ECAR data were normalized to mg of protein content.

### 5.1.9 Effect of DEA on Cellular Reactive Oxygen Species (ROS) Production

Cancer cells and tissues exist under persistent oxidative stress, which affects their survival and metastatic properties [30], [34]. Therefore, we were interested in whether DEA has any effect on ROS formation in the B16F10 melanoma line. To resolve this issue, we treated the cells with 5 and 10  $\mu\text{M}$  of DEA in the presence of the non-fluorescent reduced derivatives of fluorescent redox dyes and registered the increase in fluorescence resulting from the oxidizing effect of cellular ROS. We used two different fluorescent redox dyes to assess ROS formation separately in the aqueous and membranous compartments. Additionally, we used MitoSOXTM Red, a redox dye of red fluorescence targeted to the mitochondria, where it is oxidized selectively by superoxide [56]. Taxol, which generates ROS at low micromolar concentrations, was used as a positive control [51]. We did not detect significantly elevated ROS levels in either the aqueous or membranous compartments of B16F10 melanoma cells (**Fig. 14**). However, we found that 10  $\mu\text{M}$  of DEA did induce mitochondrial superoxide formation, which was much smaller in extent than the one caused by 5  $\mu\text{M}$  of Taxol (**Fig. 14**).

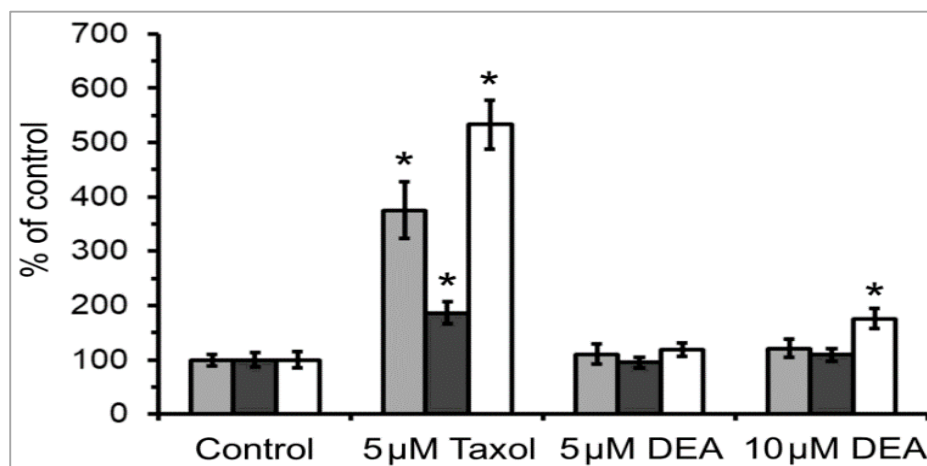


**Figure 14.** Effect of DEA on the cellular ROS formation in the B16F10 melanoma line. Cells were treated with 5 or 10  $\mu\text{M}$  of DEA or 5  $\mu\text{M}$  of taxol (positive control [51]). ROS formation in the lipid (light bars) and aqueous (dark bars) phase and mitochondrial superoxide production (empty bars) were calculated based on the rate of fluorescence intensity change vs. time; fluorescent dyes were generated by ROS-mediated oxidation from their respective non-fluorescent counterparts. The results are expressed as the % of ROS formation in the absence of agents (means  $\pm$  SEM of five independent experiments). \* Indicates a significant difference relative to the control ( $p \leq 0.05$ ).

### 5.1.10 Effect of DEA on mPT in Intact B16F10 Melanoma Cells

MOMP is usually followed with mPT pore opening, which leads to multiple mitochondrial disfunctions such as mitochondrial fission, swelling, loss of  $\Delta\Psi_m$ , and IMS proteins release. Therefore, we were interested in determining whether the drug influences mPT pore opening. Therefore, we measured mPT in intact live cells using a 96-well automated high-content fluorescence imaging system. The method is based on the quenching of calcein fluorescence by  $\text{Co}^{2+}$ . Non-fluorescent acetoxymethylcalcein is taken up by the cells and is converted intracellularly to fluorescent calcein by non-specific esterases.  $\text{Co}^{2+}$ , the cellular uptake of which is facilitated by the  $\text{Ca}^{2+}$  ionophore A23187, quenches the cytoplasmic calcein fluorescence; however, it cannot enter intact mitochondria, resulting in exclusively mitochondrial calcein fluorescence. When the mPT pore opens,  $\text{Co}^{2+}$  is free to enter the mitochondria and quench the calcein fluorescence there as well. Accordingly, we monitored the calcein fluorescence of melanoma cells treated with 5 or 10  $\mu\text{M}$  of DEA or 1.5 mM of  $\text{CaCl}_2$  (positive control [52]) in the presence of acetoxymethylcalcein,  $\text{CoCl}_2$ , and A23187 with or without CsA for 3 h. As expected, 10  $\mu\text{M}$  of DEA induced mPT that was CsA-independent (Fig. 15). Also, elevated  $\text{Ca}^{2+}$ , the cellular uptake of which is facilitated by A23187, caused a massive mPT that was fully CsA-dependent (Fig. 15).

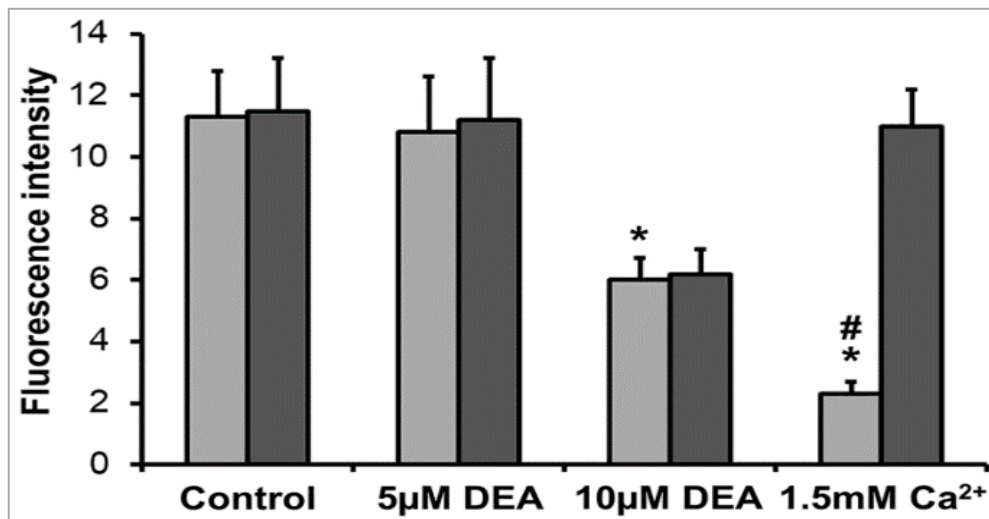


**Figure 15.** Effect of DEA on mPT in intact B16F10 melanoma cells. Cells were treated with 5 or 10  $\mu\text{M}$  of DEA or 1.5 mM of  $\text{Ca}^{2+}$  (positive control [52]) in the presence (dark bars) or absence (light bars) of the mPT inhibitor CsA for 3 h. mPT was assessed by monitoring the  $\text{Co}^{2+}$ -mediated quenching of mitochondrial calcein fluorescence. The results are expressed as fluorescence intensity (the means  $\pm$  SEM of three independent experiments). \* and # indicate a significant difference relative to control and CsA-treated cells of the same treatment group, respectively ( $p \leq 0.05$ ).

### 5.1.11 Effect of DEA on Lung Metastasis Formation in an In-Vivo Model

In-vivo study, the mid-ground between in-vitro and human trials, is of essential role in drug development and testing, since almost one-third of drug candidates have failed to proceed human trials due to the toxicity shown in the mid-stage [57]. To evaluate the effect of DEA on metastasis formation, we used an in-vivo lung metastasis model. Murine melanoma B16F10 cells were injected into the lateral tail vein of 6-weeks-old male C57BL/6 mice then they were divided into two groups (6 mice/group). Intraperitoneal administration of 25 mg/kg DEA or vehicle control was started 24 hours after tumor cell administration and was repeated every third day. At the 16th day of the experiment, the animals were sacrificed, and the lungs were removed for analysis. The lungs were weighted, and lung mass index was calculated (**Fig. 16A**). After the lungs were fixed in 4% formalin and photographed (**Fig. 16B**) and the number of tumor nodules on the lungs' surface was also determined (**Fig. 16C**). Accordingly, DEA treatment reduced lungs mass index and the number of tumor nodules (**Fig. 16A** and **16C**). Additionally, histopathological analysis was performed by an expert who was blind to the experiment on lung tissue sections after hematoxylin and eosin staining. There were melanoma cells with polyedric morphology with a great amount of melanin content as cytoplasm granules or in a perinuclear distribution. Additionally, aberrant nodular proliferation in broncho-alveolar regions characteristic of epithelial melanoma was observed in all sections (**Fig. 17A–17D**). However, there was a marked difference in tumor nodule pattern distribution and concentration between untreated and DEA treated animals. In the vehicle treated group, the nodules were of considerable size and were distributed in all part of the lung parenchyma (**Fig. 17A** and **17B**). In contrast, in the DEA group (**Fig. 17C** and **17D**), the tumor nodules were much smaller in size and were organized in a predominantly peripheral distribution (**Fig. 17C** and **17D**). To quantify the morphological observations, image analysis with the Panoramic Viewer Imaging System was performed on randomly selected sections (6 per lungs), and tumor area as the percentage of lung section area was calculated. As we found, the tumor area was significantly decreased in the lung tissue of DEA vs. vehicle treated animals (**Fig. 17E**). These results are in complete accordance with those of the macroscopic observations (**Fig. 16**) and indicate that DEA can inhibit melanoma tumor metastasis in-vivo.

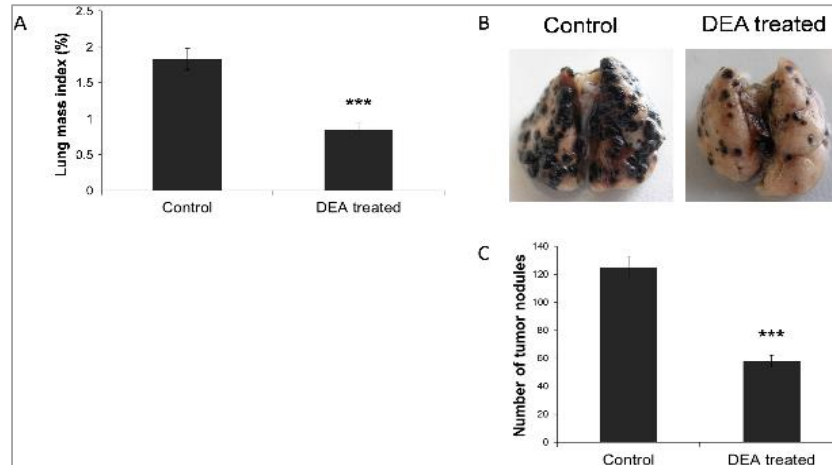


**Figure 16.** Effect of DEA on lung metastasis formation in-vivo. Lung metastasis in C57BL/6 mice was induced by injecting B16F10 cells into the lateral tail vein. Control animals received vehicle control (100  $\mu$ l 0.9% saline solution containing 10% ethanol) 24 hours after the administration of the B16 F10 cells, while the DEA group was treated with 25 mg/kg DEA intraperitoneally (6 mice/group). Treatment was repeated every third day. At the 16th day, the mice were sacrificed, the lungs were dissected, photographed and their mass was measured. Representative photos (B) of lungs of control and DEA treated animals are presented. Lung mass index (A) and the number of tumor nodules on the on lungs' surface (C) are presented as bar diagrams, mean  $\pm$  SD. Data were analyzed using Mann-Whitney U test. \*\*\* Indicates a significant difference relative to the control ( $p \leq 0.001$ ).

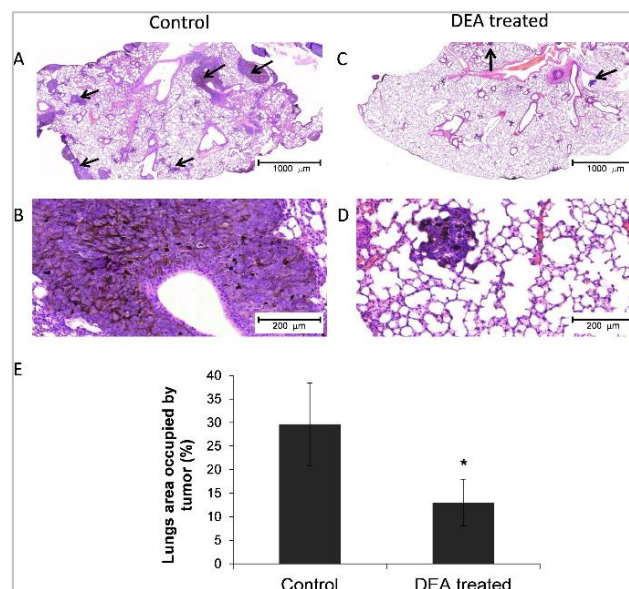


**Figure 17.** Histopathology analysis on lung tissue of mice injected with B16F10 melanoma cells. Lungs of B16F10 injected animals treated with vehicle control or 25mg/kg DEA every third day for 16 days were fixed in neutral buffered formalin, sectioned, and stained with hematoxylin and eosin. Representative sections (A-D) demonstrate darkly stained tumor nodules (arrows). Metastasis formation was quantitatively assessed by determining the tumor area (E) as percentage of the total lung section area, means  $\pm$  SD from 6 randomly selected section per lung by using the Panoramic Viewer Imaging System. Data were analyzed using MannWhitney U test. \* Indicates a significant difference relative to the control ( $p \leq 0.05$ )

## 5.2 Discussion 1.0


Melanoma (metastatic) is still the most lethal form of skin cancer and one of the top six most common cancer-related mortality worldwide. Unfortunately, melanoma is highly resistant to chemotherapy, most of chemotherapeutic agents have failed because of the patients' low response rates [58]. Consequently, a major cause of this resistance in melanoma is related to a defect in the apoptotic signaling pathway, BCL-2. However, according to the literature, cytostatic agents induce G1 arrest and down regulation of BCL-2. The latter effect is the typical function of p53, which is found to be non-mutated wild type expressed P53 by B16F10 melanoma cells [59]. In agreement with this view, DEA at low  $\mu\text{M}$  concentrations reduced the viability and proliferation of B16F10 cells (**Fig. 6, 7**) by acting as an apoptosis stimulating factor. First by detecting phosphatidylserine through annexin V positive staining (**Fig. 8**), upregulating P53, leading to cell cycle arrest in G0/G1 phase (**Fig. 9B**) and Bad, also downregulating p-Bad (**Fig. 10**). In a concentration- and time-dependent manner; DEA has significant anti-proliferative and pro-apoptotic effects on B16F10 cells *in-vitro*, which suggest its potentiality as an anti-cancer agent in melanoma treatment. Additionally, the resulting apoptosis likely involved mitochondrial mechanisms leading to Opa1, Cyt c, and AIF release from mitochondria (**Fig. 10**).

In melanomas, cell cycle's G1 phase regulators cyclins type D and E, CDK4/6, and CDK inhibitors are suggested to act as a therapeutic target [6], [9]. For this reason, we determined the effect of DEA on the cell cycle as well as on the metastasis inducer markers cyclin D1 and CDK2, the tumor suppressor p53, and the cell cycle inhibitors p21 and p27. As we observed, in a concentration dependent manner, DEA reduced cell proliferation by increasing number of cells in the G0/G1 phase that was accompanied by reduced steady state levels of cyclin D1 and CDK2, and increased levels of p21, p27 and p53 (**Fig. 9**). Due to the fact that p53 gene is not mutated in B16F10 cells, the observed G1 phase arrest by DEA was likely mediated through p21, in a p53-dependent manner.

The proliferation rate and lung metastasis formation of melanoma are relatively high [6], [9]. In this case, we performed colony formation and invasive growth experiments to test the effect of DEA on melanoma's migration and colony formation abilities. Our findings showed that DEA decreased colony formation below 50% of the control at 2  $\mu\text{M}$  DEA concentration during a seven-days exposure (**Fig. 7**). Also, DEA at 5  $\mu\text{M}$  concentration eliminated melanoma's invasive growth within 24 h treatment (**Fig. 6**).

The balance between cell proliferation and apoptosis determines the rate of tumor progression. Therefore, Constant activation of intracellular pro-survival signaling cascades such as the phosphatidylinositol 3-kinase/Akt pathway has been showed to significantly enhance cancer progression [60]. Akt, which is constitutively active in melanoma, stimulates cell proliferation and survival by repressing intrinsic apoptosis and increasing cell cycle advancement [60]. Progression and malignancy of various tumors is often associated with the constitutive activation of Akt, which



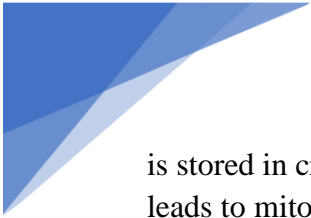


inactivates many proapoptotic proteins by phosphorylation such as Bad and caspase 9 at its Ser<sup>196</sup> [60]. The invasiveness of melanoma cells and their ability to form metastases may be related to the frequently observed high basal activity of Akt in these cells. Our results showed that the high basal levels of active, phosphorylated Akt (**Fig. 10**) was decreased dose dependently by DEA treatment in B16F10 cells, a highly invasive variant of B16 murine melanoma. This decrease in the activation of Akt may contribute to the effects of DEA on both the cell cycle (**Fig. 9**) and apoptosis (**Fig. 8**).

Mitochondria actively participate in all stages of cancer development including carcinogenesis, metastasis, survival, as well as therapy resistance [30], [34]. Importantly, OMMP is a significant factor in mitochondria-associated apoptosis, which is control by pro- and anti-apoptotic BCL-2 protein family. Typically, disrupting the balance between these proteins, downregulation of pro-apoptotic and upregulation of anti-apoptotic BCL-2, is the hallmark of cancer resistance to apoptosis [29], [30]. According to our findings (**Fig. 10**), 6h of DEA treatment was able to induce OMMP through elevating the steady-state activation of the pro-apoptotic BCL-2 family member Bad and inhibiting its phosphorylation. The permeabilization of OMM then results in the release of Cyt c to the cytosol activating caspases-dependent apoptosis though activating caspase-3 (**Fig. 10**), as well as the release of AIF from the mitochondria to the nucleus (**Fig. 10**), where it plays a role caspase-independent apoptosis by inducing chromatin condensation and DNA fragmentation. However, AIF release could be a result of mPT pore opening since AIF is an IMS protein.

mPT pore is located between the OMM and the IMM, upon opening it forms a non-specific passage to water and solutes of up to 1.5 kDa in size, which eventually leads to the release of IMS proteins such as EndoG, Cyt c, and AIF. In complete agreement with our results, AIF release was due to mPT pore opening (**Fig. 15**), 10  $\mu$ M of DEA results in CsA-independent mPT. Moreover, Ca<sup>2+</sup>, which is a main cause of mPT pore opening [34], [36] induced CsA-dependent mPT which was more than the one induced by 10  $\mu$ M of DEA (**Fig. 10**). Of note, continues opening of mPT pores results in disrupting different mitochondrial processes including the loss of  $\Delta\Psi_m$ .

$\Delta\Psi_m$  is essential for cell survival because its crucial role in ATP production, ROS generation, mitochondrial proteins transportation and network dynamics, and the regulation of apoptosis via IMS pro-apoptotic proteins release [34], [35]. Consequently, OMMP and mPT pore opening are indicator of  $\Delta\Psi_m$  depolarization. In this case, we showed that DEA treatment for 3 h was able to induce depolarization and partial loss of the  $\Delta\Psi_m$  (**Fig. 11**). Nonetheless, intact  $\Delta\Psi_m$  directly affects mitochondrial dynamics, mainly mitochondrial fusion [35], [37], [38]. Mitochondrial fusion and fission must be balanced, as below a certain  $\Delta\Psi_m$  threshold the fusion process will be disrupted. Accordingly, fusion of the IMM is controlled by L-OPA1 protein, when cleaved; it is released to the cytosol, in complete agreement with our findings, DEA treatment for 6 h was able to induce OPA1 cleavage and release to the cytosol (**Fig. 10**) indicating loss of fusion, which also contributes to the release of Cyt c from the mitochondrial, since huge amount of Cyt c




is stored in cristae junction which is also controlled by L-OPA1 [35]. Furthermore, loss of fusion leads to mitochondrial fragmentation, which is a hallmark of mitochondrial apoptosis and quality control since the fragmented mitochondria are eliminated by mitophagy. In context of therapy, cisplatin a chemotherapeutic drug used for different types of malignancies, it induces mitochondrial fragmentation, however, its use is still limited due to the nephrotoxicity side effect [55]. To complete our view of this process, we performed mitochondrial fragmentation experiment, and so within 3 h DEA treatment induced mitochondrial fragmentation that was almost the same effect as the two folds difference in concentration of the positive control cisplatin (**Fig. 12**). Considering that fusion requires intact  $\Delta\Psi_m$ , and DEA compromised  $\Delta\Psi_m$ , it seems that DEA promote mitochondrial fragmentation by impeding fusion, which needs further investigation to conclude whether its fission dependent or independent. The later effect might contribute to DEA's cytotoxic properties to limit *in-vivo* melanoma metastasis.

As mentioned above, intact  $\Delta\Psi_m$  plays a critical role in ATP production. Since cancer cells follow the Warburg effect, which explain the usage of glycolysis instead of OXPHOS for ATP production in tumor cells [30], [31], metastatic cells have elevated level of mitochondrial ATP synthesis. Indeed, 10  $\mu\text{M}$  concentration of DEA impeded both mitochondrial and glycolytic ATP synthesis pathways though reducing the fermentative glycolysis and non-mitochondrial oxygen consumption, as well as decreasing the maximal respiration and coupling efficiency (**Fig. 13**). Based on these effects on B16F10 cell's energy metabolism, DEA exhibits promise as a cancer therapy candidate.

Of note, the respiratory chain in mitochondrial is responsible for the majority of ATP production, as well as a massive source of ROS in cancers [61]. Notably, ROS signaling pathways were proposed to be oncologic targets, thus, different drugs were designed to increase cellular ROS production while inhibiting mitochondrial respiratory chain [62]. By using a mitochondria-targeted fluorescent redox dye, we found that DEA at a concentration of 10  $\mu\text{M}$  stimulates mitochondrial superoxide formation, which was less than 20% of that caused by 5  $\mu\text{M}$  of Taxol (**Fig. 14**). Although, ROS levels in the aqueous and membranous cellular compartments was not significantly affected by DEA treatment (**Fig. 14**), the same results were obtained in previous study [43]. Still, it is not clear whether DEA-ROS effect-related discrepancy was due to the insufficiency in elevating the overall cellular ROS by mitochondrial superoxide production, or due to technical issues.

Withal, *in-vitro* cell culture experiments translate very poorly to human studies; therefore, the therapeutic dose must be determined *in-vivo*. Since metastasis is fundamental property of malignant cancer cells, by which a certain tumor spreads from the location at which a tumor first arises to distant locations in the body [1], [5]. Cancer recurrence by metastasis is responsible for about 90% of mortality in neoplasm patients [63], which makes it a main target for anti-cancer therapy. Metastasizing proceeds in a series of sequential steps including invasion, intravasation, survival and translocation in the circulation system, extravasation, and survival in a new organ



[64]. Within its limitations, the B16F10 lung metastasis model mimics the majority of this process's steps. Through the period of 16 days, several large tumor loci in the lungs (**Fig. 16**) were formed upon B16F10 injection into the tail vein of the animals. These loci represent near 30% of tissue area in the lung's sections (**Fig. 17**). Both number and size of the tumor loci were reduced by DEA (**Figs. 16 and 17**) concluding that the drug has potentiality in reducing *in-vivo* metastasis formation. Of note, B16F10 have been selected for their metastasizing property, and therefore have low immunogenicity. Yet, the cells are of mouse tissue culture and not of human primary tumor origin. For that reason, further studies are needed preferably by using primary human melanomas to establish DEA's potentiality in the therapy of metastatic melanomas.

The data presented in this study provide *in-vitro* and *in-vivo* experimental evidence for DEA's potentiality in the therapy of metastatic melanomas. Based on the on the effects of DEA which indeed decreases  $\Delta\Psi$ ; induces mitochondrial fragmentation; decreases maximal respiration, ATP production, coupling efficiency, glycolysis, and non-mitochondrial oxygen consumption; and induces CsA-independent mPT and OMM permeabilization. All these effects may account for the rapid (3–12h) cytotoxicity of the drug and may account for DEA's long-term (24–72h) cytotoxicity and ability to suppress *in-vivo* metastasis.



## 6 Results and discussion 2.0

### 6.1 Results 2.0

#### 6.1.1 DEA Induced Apoptotic Cell Death in BC Cell Lines

DEA demonstrated signs of anti-neoplastic potentiality in therapy-resistant cancer cell line B16F10. Accordingly, we assessed its effect on the cell death process of the TN 4T1 BC line in comparison with the HR+ MCF-7 line of the less aggressive cancerous phenotype. We used flow cytometry with the Muse™ Annexin V & Dead Cell Assay kit to investigate the mode of DEA-induced cell death. The assay utilizes cell surface annexin V binding that measures the appearance of phosphatidylserine on the external surface of the plasma membrane, which is a marker of apoptosis. A dead cell marker, 7-aminoactinomycin D (7-AAD), was also used as an indicator of cell membrane structural integrity. Late apoptosis is demonstrated by double positivity. We treated the cells with 5 and 10  $\mu\text{M}$  DEA for 24 h before the flow cytometry analysis. In a concentration-dependent way, DEA induced early, then late apoptosis (**Fig. 18**). At the lower DEA concentration, the rate of early apoptosis exceeded that of the late; however, at the higher drug concentration, late apoptosis predominated in both BC cell lines (**Fig. 18**). However, we found a total apoptosis rate of  $28.18 \pm 6.34\%$  for 5 and  $56.05 \pm 5.12\%$  for 10  $\mu\text{M}$  DEA in the 4T1 cell line in contrast to the apoptosis rates of  $71.14 \pm 6.39\%$  for 5 and  $78.94 \pm 4.77\%$  for 10  $\mu\text{M}$  DEA observed in the MCF-7 cell line (**Fig. 18**), indicating that MCF-7 cells were more sensitive toward DEA treatment than the 4T1 cells.

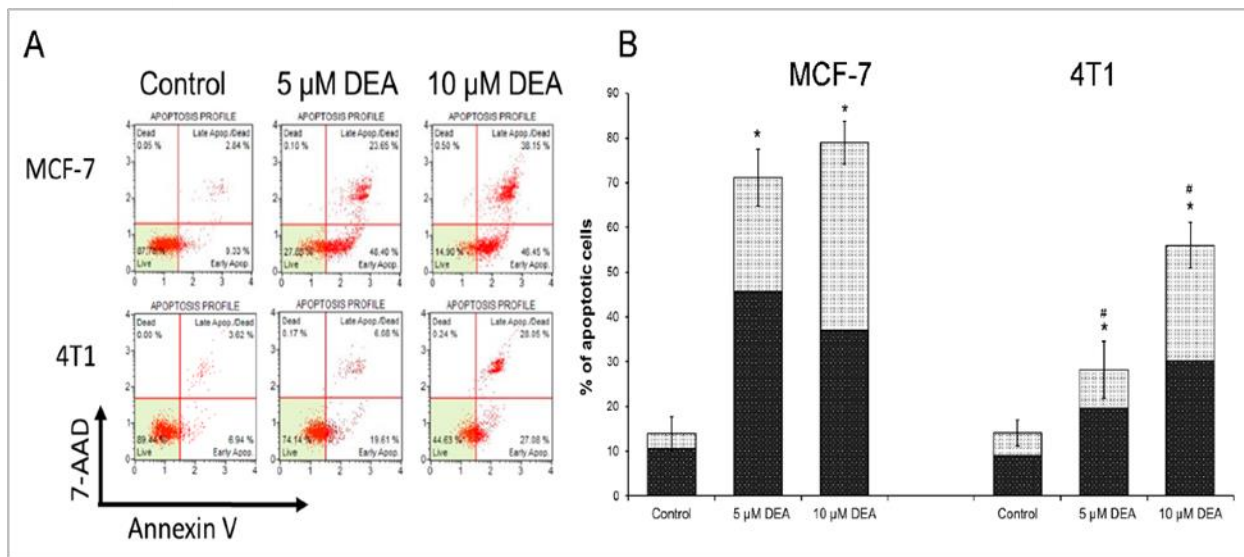


**Figure 18.** Effect of DEA on the apoptosis in BC cell lines. We treated MCF-7 and 4T1 cells with 5 or 10  $\mu\text{M}$  DEA for 24 h before determining the type of cell death by flow cytometry using the Muse™ Annexin V & Dead Cell Assay kit. The results are presented as representative dot plots (A) and bar diagrams (B) of three independent experiments. The bars (B) indicate the sum of early (dark bars) and late (light bars) apoptosis expressed as percentage of the total cell number, mean  $\pm$  SD of three independent experiments running in at least quadruplicate parallels. Controls were treated with vehicle (0.2% DMSO). \* Significant difference from the control ( $p \leq 0.05$ ). # Significant difference from the MCF-7 parallel ( $p \leq 0.05$ ).

### 6.1.2 DEA Mitigated Invasive Growth of BC Cell Lines

Cell migration, an important aspect of cancer invasiveness, is often assessed by means of the wound-healing assay [65]. Accordingly, we inflicted a wound into semi-confluent monolayers of MCF-7 and 4T1 cells and treated them by 0, 5, or 10  $\mu\text{M}$  DEA for 12 h. In accordance with its more malignant phenotype [66], cell migration of the TNBC cells was more intense, resulting in almost complete closing of the wound within 12 h, while the HR+ BC cell line achieved an about 40% healing during the same time. 10  $\mu\text{M}$  DEA treatment completely prevented wound healing in the 4T1 cell line, while it caused wound exacerbation due to killing cells at the wound edge in the MCF-7 cell line (Fig. 19). At the concentration of 5  $\mu\text{M}$ , DEA treatment induced a less pronounced effect on wound healing as it did at 10  $\mu\text{M}$  (Fig. 19). To supplement the wound-healing assay, we assessed the invasive growth of the MCF-7 and 4T1 cells using an xCelligence Real-Time Cell Analysis (RTCA) system. The cells were cultured in the presence of 0, 5, or 10  $\mu\text{M}$  DEA for 24 h and the cell index proportional to invasive growth of the cells was monitored in real time. DEA decreased invasive growth in a concentration-dependent manner in both MCF-7 and 4T1 cells (Fig. 20). Similarly to the results of the wound-healing experiment, MCF-7 was more sensitive to the drug than 4T1 (Fig. 20).

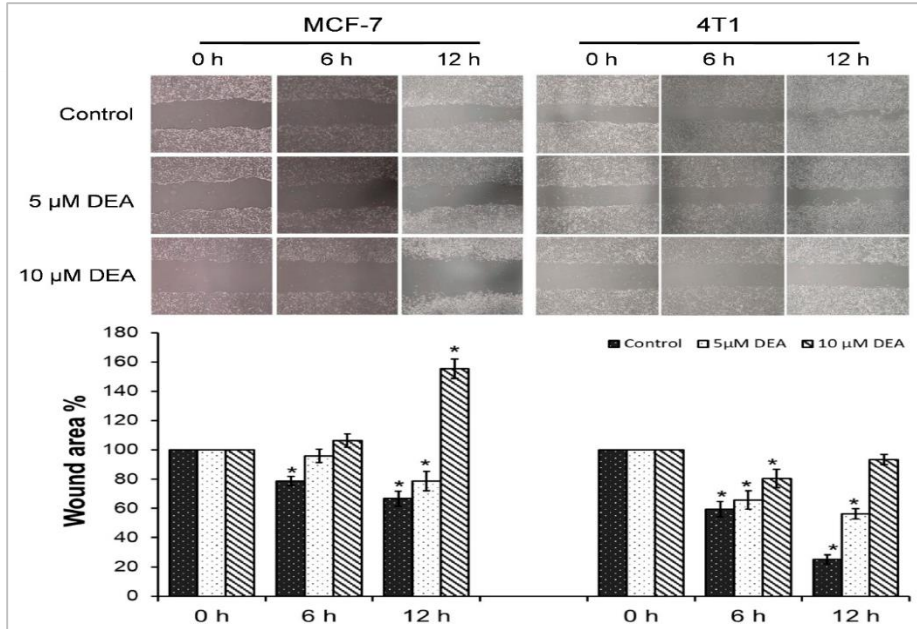


**Figure 19.** Effect of DEA on wound healing in BC cell lines. We inflicted a wound into semi-confluent cultures of MCF-7 and 4T1 cells, and treated them with 0, 5, or 10  $\mu\text{M}$  DEA for 12 h. The data are presented as representative images of the wounds taken at 0, 6, and 12 h and the wound area is the percentage of untreated plates at the 0 h time-point; results are the mean  $\pm$  SD of two independent experiments running in duplicates. \* Significant difference from the untreated control ( $p \leq 0.05$ ).

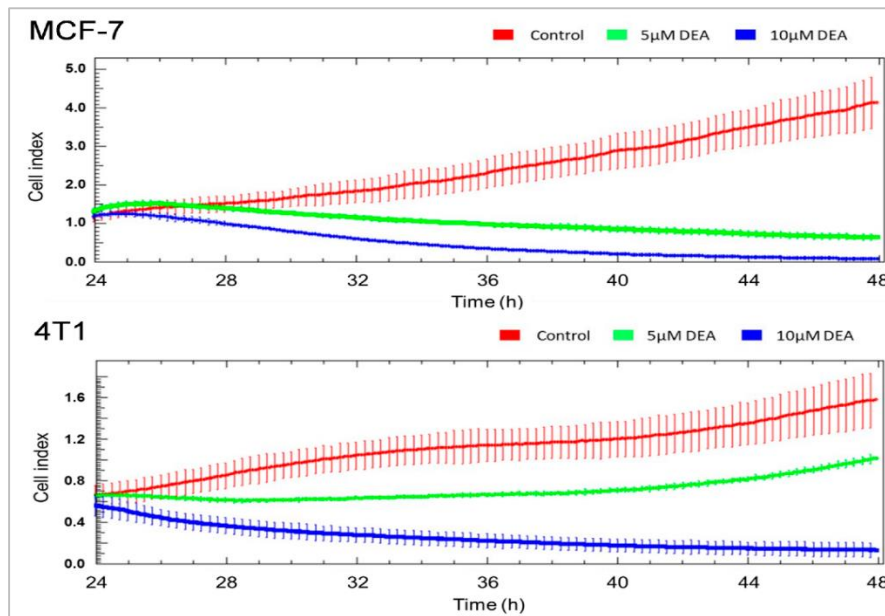


**Figure 20.** Effect of DEA on invasive growth of BC lines. MCF-7 and 4T1 cells were cultured in the presence of 0 (red line), 5  $\mu\text{M}$  (green line), or 10  $\mu\text{M}$  (blue line) DEA for 24 h, while the cell index was monitored by an RTCA system every 5 min. The results are presented as original recordings, mean  $\pm$  SD of two independent experiments running in triplicates.



### 6.1.3 DEA Differentially Modulated Regulators and Markers of the Cell Death Process in the BC Cell Lines

Previously, DEA showed an effect on anti-and-pro-apoptotic proteins in B16F10 melanoma cells (**Fig. 10**), which had a major impact on the pathways regarding intrinsic apoptosis. To gain greater insight into the apoptotic pathways induced by DEA in BC cell lines, we analyzed Akt activation, protein levels of BCL-2 family members including pro-apoptotic Bad and Bax and antiapoptotic BCL-2, and the caspase-3 cleavage and caspase-3-mediated cleavage of PARP, which are all reporters of the mitochondrial apoptotic pathway. As shown in Figure 21, the Akt phosphorylation at Ser<sup>473</sup> decreased in a concentration-dependent manner, while the total Akt remained constant. This was accompanied by a significant decrease in the phosphorylation level of Bad at Ser<sup>136</sup>, while the overall level of Bad protein remained constant in both cell lines. We also found that DEA indeed resulted in a dose-dependent increase in the amount of p53 protein in 4T1 cells (**Fig. 21**). We also measured a significant increase in Bax levels while BCL-2 levels decreased (**Fig. 21**). Furthermore, we found that DEA treatment led to an increase in the amount of a 19 kDa caspase-3 cleavage intermediate as well as cleaved poly (ADP-ribose) polymerase (PARP) (**Fig. 21**). Taken together, these data demonstrate that cytotoxic effects of DEA on MCF-7 and 4T1 cells are due to the activation, at least partially, of two apoptotic pathways, the PI3K/Akt pathway and the mitochondrial pathway.

A differential expression of the therapy-resistance- and metastasis-promoting COX-2 gene among BC cell lines of various phenotypes has been reported previously [67]. Accordingly, we studied DEA's effect on COX-2 protein levels in the 4T1 and MCF-7 cell lines. We detected considerable steady-state COX-2 levels in the TN BC cell line, while it was just above the detection limit in the HR+ one (**Fig. 20**). Additionally, DEA increased the COX-2 level in a concentration-dependent way in the TN 4T1 cell line only (**Fig. 21**).

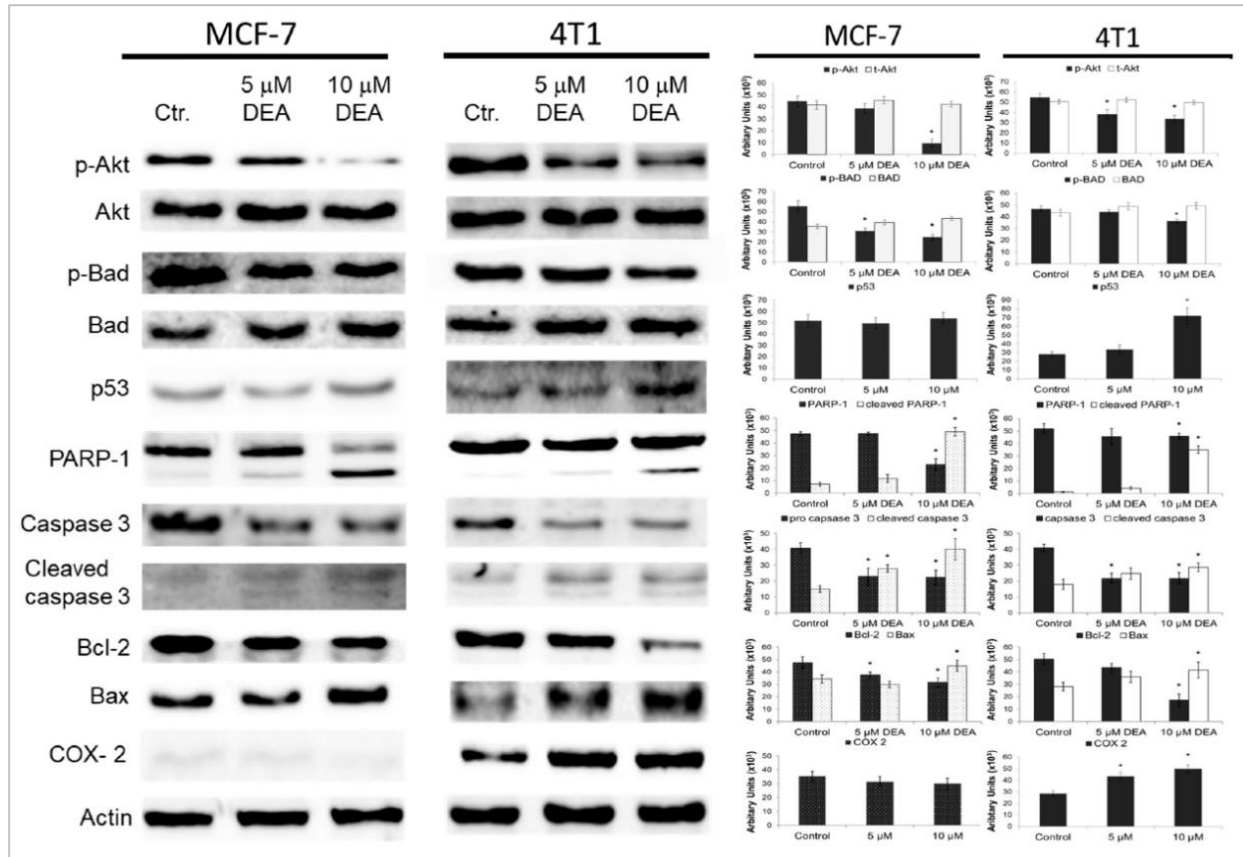


**Figure 21.** Effect of DEA on steady-state level of regulator and marker proteins of the cell death process in the BC cell lines. We evaluated the steady-state levels of p-Akt, Akt, p-Bad, Bad, BCL-2, Bax, p53, PARP-1, caspase 3, cleaved caspase 3, and COX-2 in the MCF-7 and 4T1 cells treated with 0, 5, or 10 μM DEA by immunoblot analysis. Results are presented as representative immunoblots and pixel densities of the bands, mean ± SD of three independent experiments. \* Significant difference from the control ( $p \leq 0.05$ ).



#### 6.1.4 DEA Caused the Loss of Mitochondrial Membrane Potential ( $\Delta\Psi_m$ )

$\Delta\Psi_m$  is a significant factor for mitochondrial processes such as, ATP synthesis and has several non-energetic functions essential for cell survival like mitochondrial dynamics especially mitochondrial fusion [33]. Therefore, we determined the effect of DEA on the  $\Delta\Psi_m$  of BC cells by using the positively charged fluorescent mitochondrial dye, JC-1. When the  $\Delta\Psi_m$  is normal, the dye accumulates in the mitochondria and forms J-aggregates that emit red fluorescence upon excitation. The aggregates disassemble, leaving green, fluorescent monomers as the  $\Delta\Psi_m$  decreases, and the fluorescence disappears upon complete mitochondrial depolarization. We treated the MCF-7 and 4T1 BC cell lines for 3 h with 0, 5, or 10  $\mu\text{M}$  DEA, before loading them with JC-1 and taking fluorescent microscopy images. At the concentration of 10  $\mu\text{M}$ , the drug significantly depolarized the mitochondria in both BC cell lines, while 5  $\mu\text{M}$  DEA did not have a considerable effect on the  $\Delta\Psi_m$  during the 3 h treatment (**Fig. 22**).

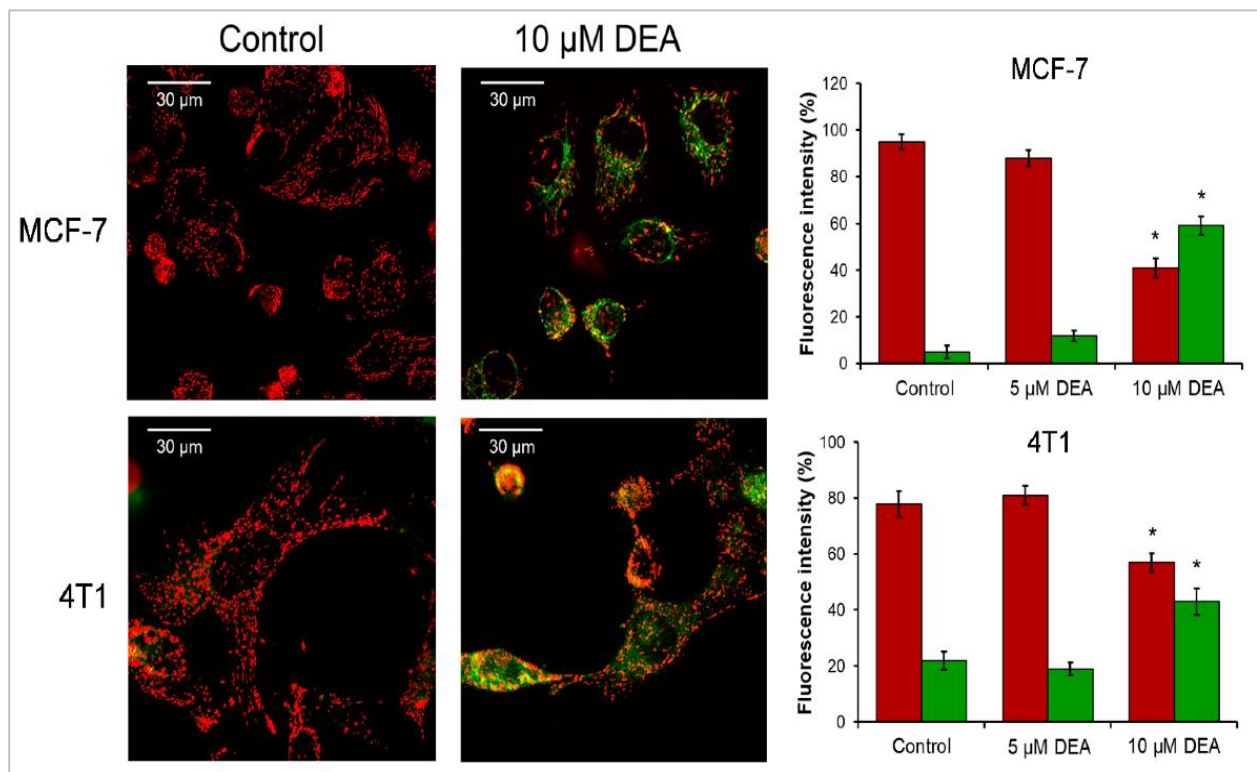


**Figure 22.** Effect of DEA on  $\Delta\Psi_m$  in BC cell lines. MCF-7 and 4T1 BC lines were treated with 0, 5, or 10  $\mu\text{M}$  DEA for 3 h before loading them with JC-1 dye and taking microscopy images. The data are presented as representative merged images of the control and 10  $\mu\text{M}$  DEA treated cells in the red and green channels, and as a percentage of the total fluorescence intensity in the bar diagram. Results are mean  $\pm$  SD of three independent experiments. \* Significant difference from the untreated control ( $p \leq 0.05$ ).




### 6.1.5 DEA Induced Mitochondrial Fragmentation in BC Cell Lines

Mitochondrial fusion requires healthy  $\Delta\Psi_m$ , which forms the basis of mitochondrial quality control [35]. Accordingly, we studied the effect of DEA on mitochondrial network dynamics by fluorescent microscopy after loading the cells with MitoTracker Red to visualize the mitochondria. The MCF-7 and 4T1 cells were treated with 0, 5, or 10  $\mu\text{M}$  of DEA for 3 h before the assessment of mitochondrial fragmentation [68]. Similarly, as it did in melanoma cells, DEA treatment caused mitochondrial fragmentation in both BC cell lines in a concentration-dependent manner (**Fig. 23A**). Recently, a link has been established between the proliferation of cancer cells and mitochondrial fragmentation. Accordingly, we performed immunoblot analysis of the proteins involved in the regulation of mitochondrial fusion and fission [35] from homogenates of BC cells treated identically to the fragmentation experiment in separate plates. In both BC cell lines, the DEA treatment increased the steady-state level of fusion-associated protein OPA1, but it decreased MFN 1 and 2 in 4T1 cells (**Fig. 23B**). However, it increased the steady-state level of fission-associated proteins such as DRP1 and Fis1 (**Fig. 23B**).

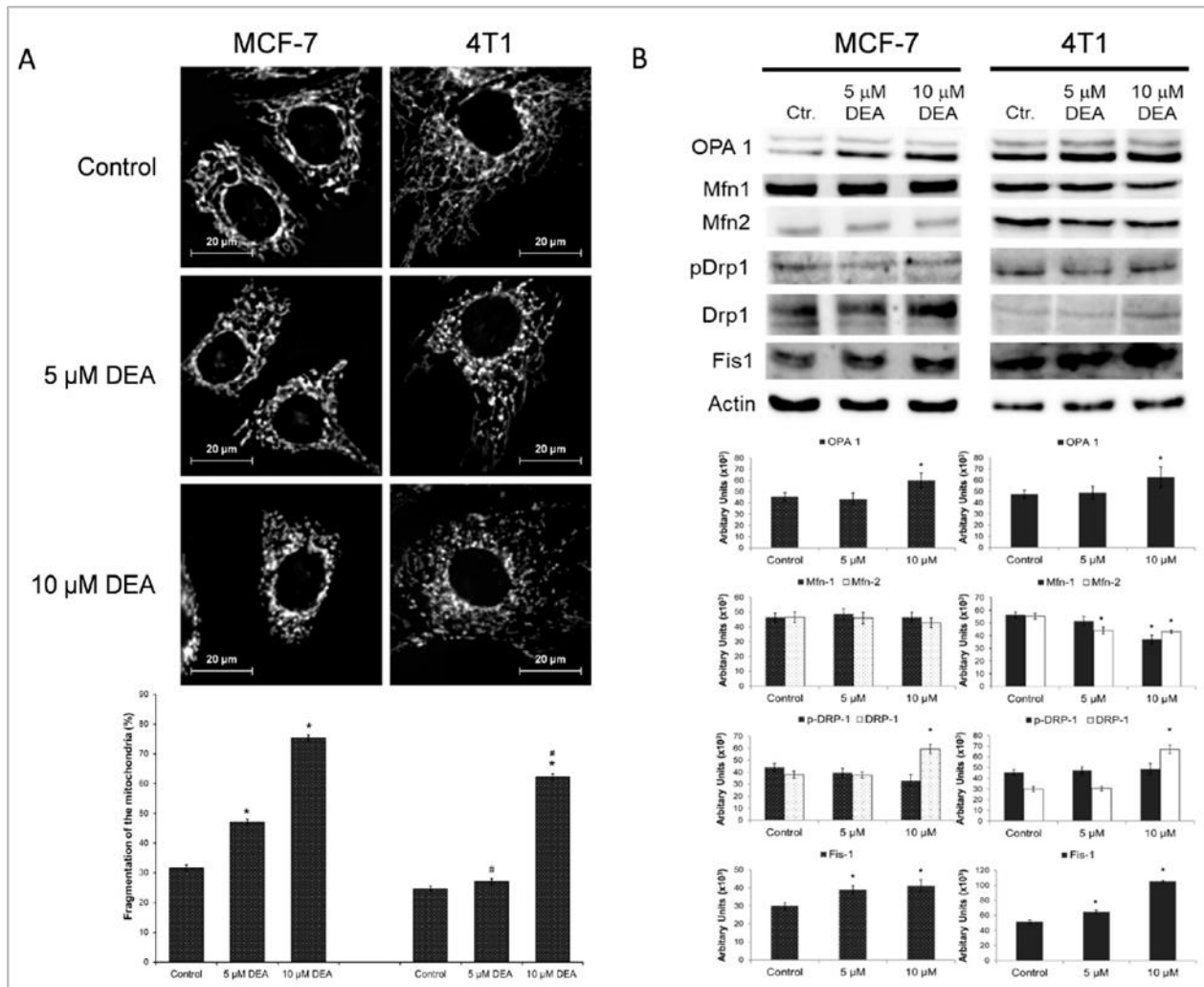


**Figure 23.** Effect of DEA on mitochondrial network dynamics in BC cell lines. MCF-7 and 4T1 cells were treated with 0, 5, or 10  $\mu$ M DEA for 3 h before loading them with MitoTracker Red dye and taking microscopy images. The data are presented as representative images and as percentage of fragmented mitochondria (A), mean  $\pm$  SD of three independent experiments. Separately, homogenates of identically treated cells were subjected to immunoblot analysis (B). The data are presented as representative immunoblots and as pixel densities of the bands, mean  $\pm$  SD of three independent experiments. \* Significant difference from the untreated control ( $p \leq 0.05$ ); # significant difference from the MCF-7 cells ( $p \leq 0.05$ ).



### 6.1.6 DEA Impeded Mitochondrial Energy Production in the BC Cell Lines

Given that the DEA treatment compromised  $\Delta\Psi_m$ , a major determinant of ATP synthesis as mentioned in section 4.2.1.4, we next sought to assess DEA's effect on energy metabolism of BC cells. We used a live cell respirometer to measure the cellular OCR and ECAR, which are indicators of oxidative and fermentative ATP production, respectively. We treated the MCF-7 and 4T1 cells with 0, 5, or 10  $\mu\text{M}$  DEA for 6 h before the bioenergetics assay. Parallel to OCR, ECAR was also monitored, and the instrument calculated multiple parameters of cellular energy metabolism from the original recordings (**Fig. 24**). At the concentration of 10  $\mu\text{M}$ , DEA significantly decreased basal respiration, maximal respiration, non-mitochondrial oxygen consumption, mitochondrial ATP production, coupling efficiency, and spare respiratory capacity in both BC cell lines (**Fig. 24**). Five  $\mu\text{M}$  DEA increased the proton leak in both cell lines (**Fig. 24**). On the other hand, DEA did not affect ECAR (**Fig. 24**), indicating that the drug did not interfere with the glycolytic machinery in either BC cell line.

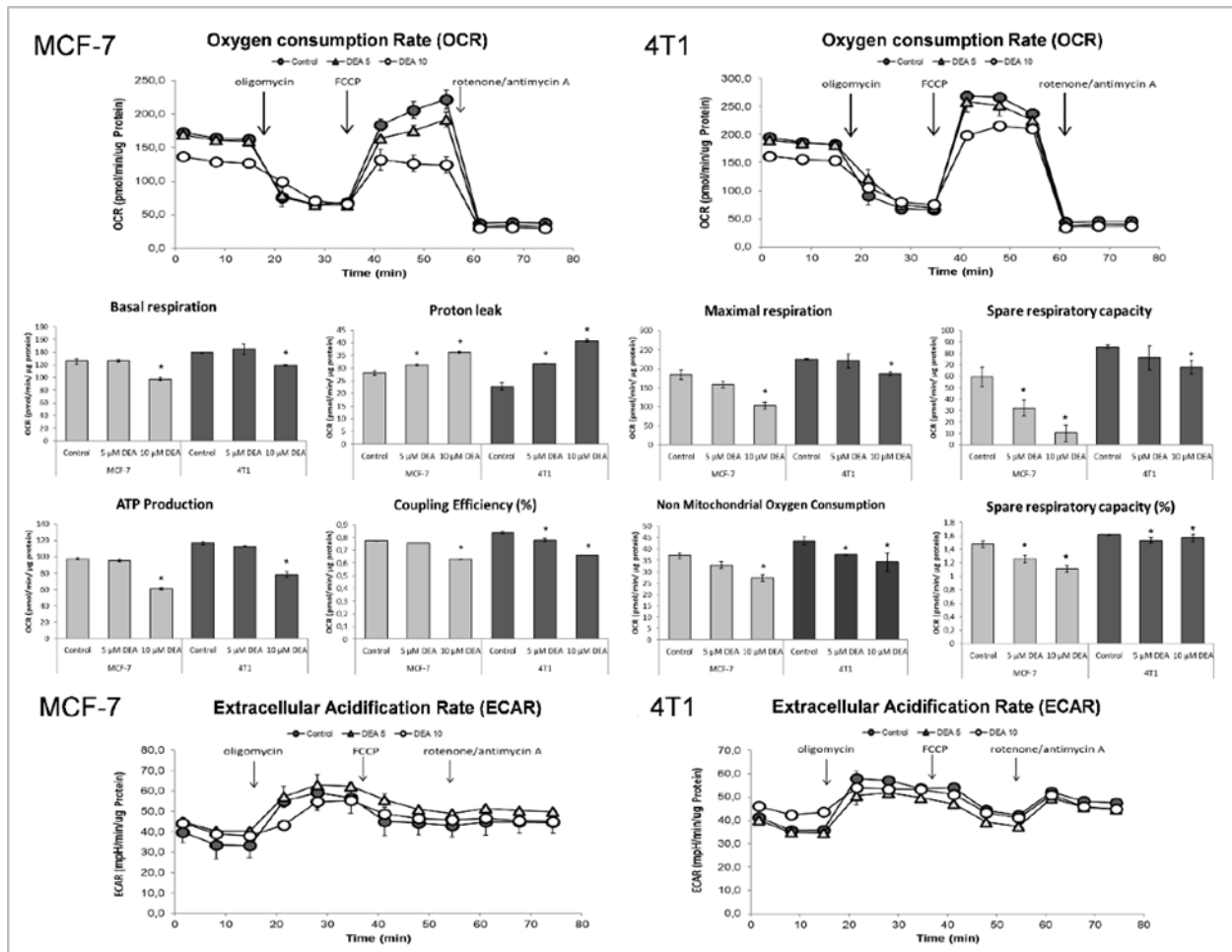


**Figure 24.** Effect of DEA on energy metabolism of the BC cell lines. MCF-7 (light bars) and 4T1 (dark bars) BC cells were treated with 0 (filled circles), 5 (triangles), or 10  $\mu\text{M}$  DEA (open circles) for 6 h before monitoring OCR and ECAR for 75 min. The  $\text{FoF}_1$  ATP synthase inhibitor oligomycin, the uncoupler FCCP, and the respiratory inhibitors rotenone and antimycin A were added at 15, 35, and 55 min of the respiratory measurement. OCR recordings. Data are presented as representative original recordings, and as parameters, means  $\pm$  SD of three independent experiments running in two replicates. OCR and ECAR data were normalized to mg protein content. \* Significant difference from the untreated control ( $p \leq 0.05$ ).

### 6.1.7 COX-2 Inhibition Potentiated DEA's Anti-Neoplastic Effect in the TN BC Cell Line

As shown in figure 21, elevated expression of COX-2, which might be associated with progressive tumor growth and resistance [26], [27], may have accounted for the increased resistance to DEA treatment of 4T1 TNBC cells compared to the HR+ MCF-7 cells. To test this possibility, we treated both cell lines with 0–15  $\mu\text{M}$  of DEA for 24 h in the presence and absence of 20  $\mu\text{M}$  of the COX-2 inhibitor celecoxib before measuring the viability of the cells using the SRB assay. The SRB assay is based on protein content rather than metabolic activity. Therefore, it is recommended for determining the cytotoxicity of substances that can have mitochondrial effects [53]. DEA reduced the viability of both BC lines in a time and concentration-dependent way (**Fig. 25A**). However, as expected, the viability loss caused by DEA treatment was higher for the MCF-7 than for the 4T1 cell line (**Fig. 25A**), indicating a higher treatment sensitivity for the former cell line. However, when COX-2 was inhibited by celecoxib, DEA's effect on the viability of 4T1 cells was significantly more pronounced (**Fig. 25B**) in contrast to MCF-7 cells (**Fig. 25C**), suggesting that COX-2 activation may have contributed to the resistance of 4T1 cells to DEA treatment.

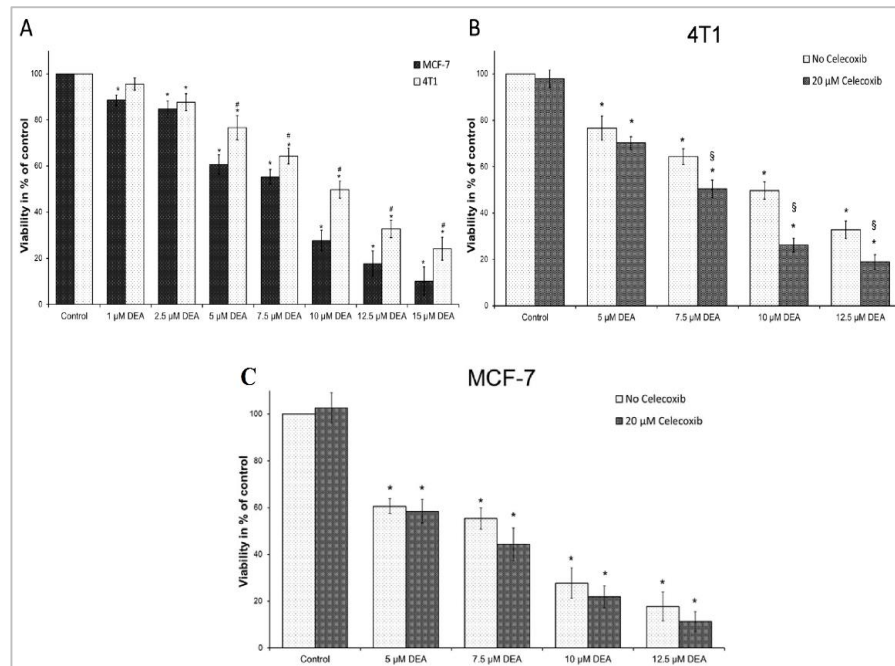


**Figure 25.** Effect of DEA on the viability of BC cell lines. (A): We treated MCF-7 (dark bars) and 4T1 (light bars) cells with 0 to 15  $\mu\text{M}$  DEA for 24 h. (B and C): We treated 4T1 and MCF-7 cells with 0 to 12.5  $\mu\text{M}$  DEA in the absence (light bars) or presence (dark bars) of 20  $\mu\text{M}$  celecoxib for 24 h. Viabilities were assessed using the SRB assay and were presented as percent of the untreated control, means  $\pm$  SD of three independent experiments performed in at least quadruplicates. \* Significant difference from the untreated control ( $p \leq 0.05$ ); # significant difference from the MCF-7 cells parallel ( $p \leq 0.05$ ); § significant difference from the no celecoxib parallel ( $p \leq 0.05$ ).

### 6.1.8 Effect of DEA on MCF-7 and 4T1 Colony Formation

To assess DEA's effect on colony forming ability of BC cell lines, a long-term assay was performed. Where the assay represents a situation more like the therapeutic one, through utilizing lower drug concentrations and longer exposure times. Accordingly, we tested the effect of COX-2 inhibition on DEA's anti-neoplastic effect using this method, too. We treated the MCF-7 and 4T1 cells with 0 to 2  $\mu\text{M}$  DEA in the presence or absence of 5  $\mu\text{M}$  celecoxib for 7 days before quantifying colony formation. Even at the concentration of 1  $\mu\text{M}$ , DEA significantly suppressed colony formation in both cell lines (**Fig. 26**). The TNBC line 4T1 demonstrated higher resistance against the treatment, since 2  $\mu\text{M}$  DEA almost eradicated MCF-7 colony formation while it induced about a 50% decrease only in the formation of 4T1 colonies (**Fig. 26**). However, as in the case of the viability study (**Fig. 25**), 5  $\mu\text{M}$  celecoxib augmented the effect of DEA on the 4T1 cells, and the combined treatment decreased colony formation in this cell line close to the level of the one observed in the MCF-7 line (**Fig. 26**). In contrast, celecoxib did not affect DEA's effect on MCF-7 colony formation (**Fig. 26**).

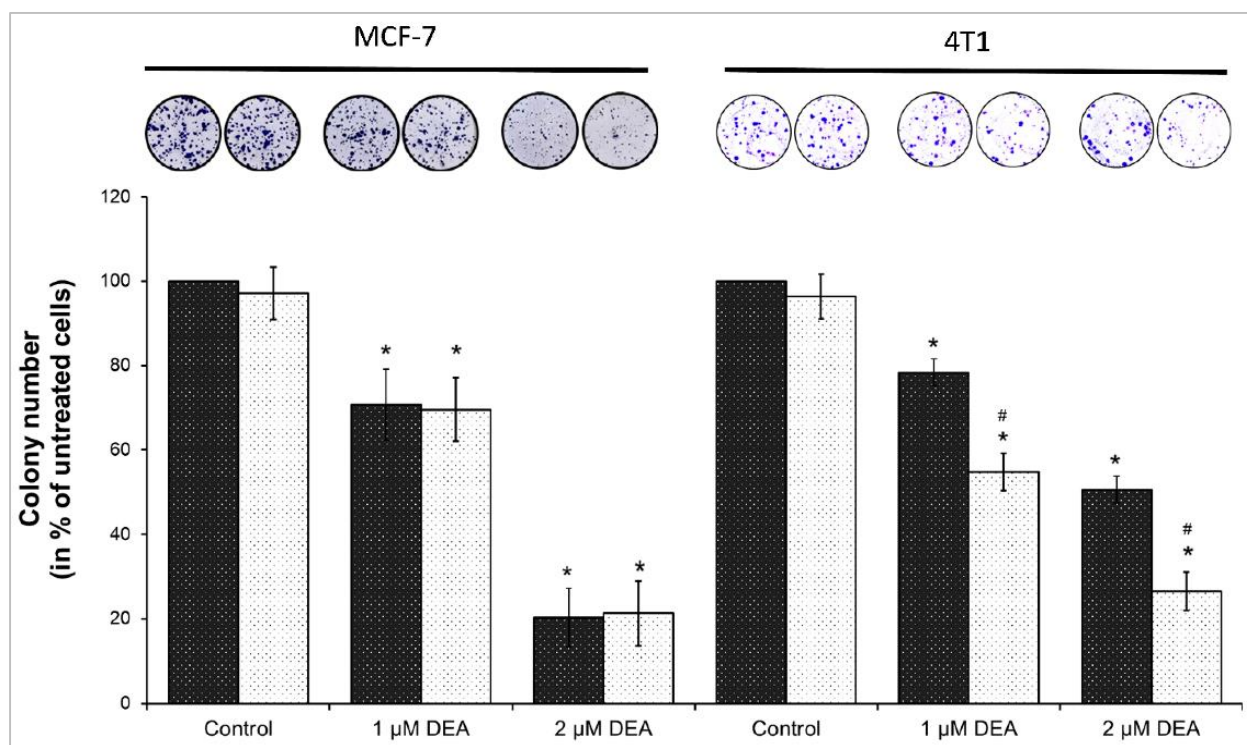


**Figure 26.** Effect of DEA and celecoxib on colony formation of BC lines. We treated MCF-7 and 4T1 cells with 0 to 2  $\mu\text{M}$  DEA in the absence (dark bars) or presence (light bars) of 5  $\mu\text{M}$  celecoxib for 7 days before determining colony formation. The data are presented as representative images of stained colonies in culturing plates and colony numbers are presented as the percentage of untreated plates, mean  $\pm$  SD of three independent experiments. \* Significant difference from the untreated control ( $p \leq 0.05$ ). # Significant difference from the no celecoxib parallel ( $p \leq 0.05$ ).


## 6.2 Discussion 2.0

Despite regular chemotherapy followed by a surgery, tumor cells frequently persist, and metastasis may develop [22]. New therapeutic strategies are needed to improve the prognosis of patients with aggressive tumors including breast tumor, especially TNBC, since this cancer type is characterized with metastatic patterns, aggressiveness and poor prognosis (5% of all cancer-related deaths) [15], [18]. This category of aggressive tumors has a balanced metabolism, where mitochondria is actively involved [69]. Mitochondria participate in neoplasm development starting from carcinogenesis via tumor survival and therapy resistance to metastasis formation and most of cancer types rely on mitochondrial ATP synthesis for energy production [30], [31], [69]. Therefore, drugs that significantly interfere with mitochondrial energy production and processes may have a therapeutic value in these tumors. DEA fulfill this principle based on its mitochondrial effects in B16F10 melanoma cells presented in part I. In the current study, we reported how low concentrations of DEA reduces the viability of the BC cell lines MCF-7 and 4T1 in a concentration- and time-dependent manner (**Fig. 25a**), through disrupting mitochondrial processes followed by apoptotic cell death (**Fig. 18**). Of note, the mouse 4T1 was used rather than the human MDA-MB-231 TNBC cell line, because the therapeutic dose of DEA must be determined in future animal experiments, since *in-vitro* cell culture experiments translate very poorly to human studies.

Mitochondria play a significant role in cellular survival through many mechanisms, most importantly ATP production and intrinsic apoptosis. The latter depends on ATP as an energy source, while energy shortage induces  $\Delta\Psi_m$  loss which enhances the release of pro-apoptotic IMS proteins to the cytosol resulting in apoptosis [33, 34]. Hence, DEA caused apoptotic cell death in both BC cell lines (**Fig. 18** and **Fig. 21**), which was determined by annexin V staining of the phosphatidylserine residues in the outer surface of the cell membrane (**Fig. 18**), decrease in the BCL-2/Bax ratio, activation of caspase 3 and cleavage of PARP-1 (**Fig. 21**); all are hallmarks of apoptosis [33], [34]. In agreement with its TN phenotype [15], [18], 4T1 cell line showed less sensitivity in response to DEA treatment than the HR+ MCF-7 cell line in these experiments (**Fig. 18-21** and **Fig. 25a**).

TNBC's proliferation and metastases formation in the liver, brain, and lungs are much higher than other BC types [18], [70]. Accordingly, we found that 4T1 cells were less sensitive against DEA treatment than the MCF-7 cells in colony formation (**Fig. 26**) and invasive growth (**Fig. 19** and **Fig. 20**) experiments as well. In addition, the results showed that DEA reduced colony formation below 50% of the control at a concentration of 2  $\mu\text{M}$  during a seven-day exposure (**Fig. 26**), and at 10  $\mu\text{M}$ , it eliminated invasive growth (**Fig. 19**) during a 12 h treatment, suggesting that DEA's therapeutic concentration may not exceed the DEA concentrations, which were observed previously [71] during human AM therapy.






One of the key roles in cellular survival is mitochondrial network dynamics regulation which requires a healthy  $\Delta\Psi_m$ . Since DEA decreased the  $\Delta\Psi_m$  in both BC cell lines (**Fig. 22**); mitochondrial dynamics would be disrupted and so mitochondrial biogenesis and quality control, which are essential for meeting the cellular energy and metabolic demands [34], [35]. Mitochondrial biogenesis is represented through mitochondrial fusion and fission processes that are mediated by large GTPases; MFN 1, 2 and OPA1 for the fusion and Drp1 for the fission [34], [38]. The latter is regulated by phosphorylation and recruited to the mitochondria by Fis1 [38]. Balance of the fusion and fission processes is maintained by intracellular signaling [35], [72], but the fusion is prevented when the  $\Delta\Psi_m$  is low [72]. Therefore, mitochondrial fragmentation is a common feature in many cancer types such as in breast, colon, and hepatocellular carcinomas, [73]. Fragmented mitochondria are more likely to be damaged and eliminated by mitophagy, leading for mitochondrial copy number reduction [37], [74]. Accordingly, DEA caused mitochondrial fragmentation in both BC cell lines (**Fig. 23a**) that might contribute to its anti-cancer properties. Since DEA depolarized the  $\Delta\Psi_m$  (**Fig. 22**), mitochondrial fragmentation caused by DEA treatment in BC cell lines seemed to be caused by promoting fission, as Drp1 expression increased accompanied by its decreased inhibitory phosphorylation (**Fig. 23b**). Compared to B16F10 melanoma cell line; it seems that mitochondrial fragmentation was caused by inhibiting fusion, which was supported by the release of OPA1 from mitochondria to the cytosol (**Fig. 10 and 12**). It seems that DEA interacted with a yet to be identified regulatory element related to the mitochondria that induced mitochondrial fragmentation by shifting the balance of fusion and fission. Thus, DEA's target has to be localized to the mitochondria, since DEA induced mitochondrial fission in isolated, Percoll gradient-purified mitochondria [43].

The effect of DEA on PI3K-AKT pathway was established earlier in B16F10 cells. It is well known that constant activation of PI3K-AKT signaling pathway is important for cancer progression through promoting cell survival and inhibiting apoptosis [60]. In TNBC, dysregulation of AKT signaling pathways is one of the most frequent oncogenic anomalies [75]. We showed that AKT activation was decreased by DEA in both BC cell lines (**Fig. 21**). Furthermore, phosphorylated AKT level, which is the baseline activation of AKT, in HR+ MCF-7 cell line was significantly lower than in TN 4T1 cell line (**Fig. 21**). Since AKT had strong mitochondria-protecting potential [76]; the decreased activation of AKT together with the abovementioned compromised mitochondrial functions may account for the differential apoptosis-promoting effect of DEA among the BC cell lines investigated (**Fig. 18**).

Inflammatory cells and factors are major components of the tumor microenvironment. COX-2 is one of the most significant immunomodulatory factors found in tumors, and the most studied anti-inflammatory target in cancer therapy since it is associated with large tumor size, lymph node metastasis, and poor differentiation [26], [27], [77]. The use of COX-2 inhibitor celecoxib in metastatic BC therapy as monotherapy and combination with aromatase inhibitors, proved to be effective through reducing the size and the area of the tumor. Currently, COX-2 overexpression is linked with anti-cancer drug resistance in BC. Of note, COX-2 is highly inducible and can be



rapidly upregulated in response to pro-inflammatory agents like cytokines, even though it is barely expressed in healthy tissues [26]–[28], [77]. Surprisingly, COX-2 was hardly detected in MCF-7 cell line and not affected by DEA treatment as well. However, in 4T1 TNBC cell line, COX-2 was expressed and even elevated when treated with different DEA concentrations (**Fig. 21**). While the upregulation of COX-2 has been implicated in cancer therapy resistance, the latter result raised the possibility that DEA reduced its own anti-cancer effects in the 4T1 cell line, thus creating the difference between the two BC cell lines in response to DEA treatment. Indeed, celecoxib enhanced DEA's effect on viability (**Fig. 25b and c**) and colony formation (**Fig. 26**) of the 4T1 cells only. Recently, studies have shown activation of caspase-3 during radiotherapy-induced apoptosis, which resulted in prostaglandin E<sub>2</sub> production by COX-2, that is linked with treatment resistance [78]. Accordingly, DEA treatment induced caspase-3 activation in both BC cell lines (**Fig. 21**) but upregulation of COX-2 expression in the 4T1 cell line only (**Fig. 21**). It seems that the DEA-induced caspase 3-assisted mitochondrial apoptosis (**Fig. 21**) resulted in COX-2-mediated resistance in 4T1 cells, which expressed it. Consequently, the difference in COX-2 expression accounted for, at least partially, the differential anti-neoplastic effects of DEA in several cell lines. These results also suggest that co-treatment with COX-2 inhibitors can increase the efficacy of DEA and significantly reduce therapy resistance.

Our results show the ability of DEA treatment to induce predominant apoptotic cell death by modulating mitochondrial functions in BC cells. Regardless the low efficacy compared to HR+ BC cells, DEA exerted anti-neoplastic effects in 4T1 TNBC cells, too. Besides, the upregulation of COX-2 in DEA-treated 4T1 cells, as a DEA-resistant mechanism, was counteracted by inhibiting COX-2 enzymatic activity.



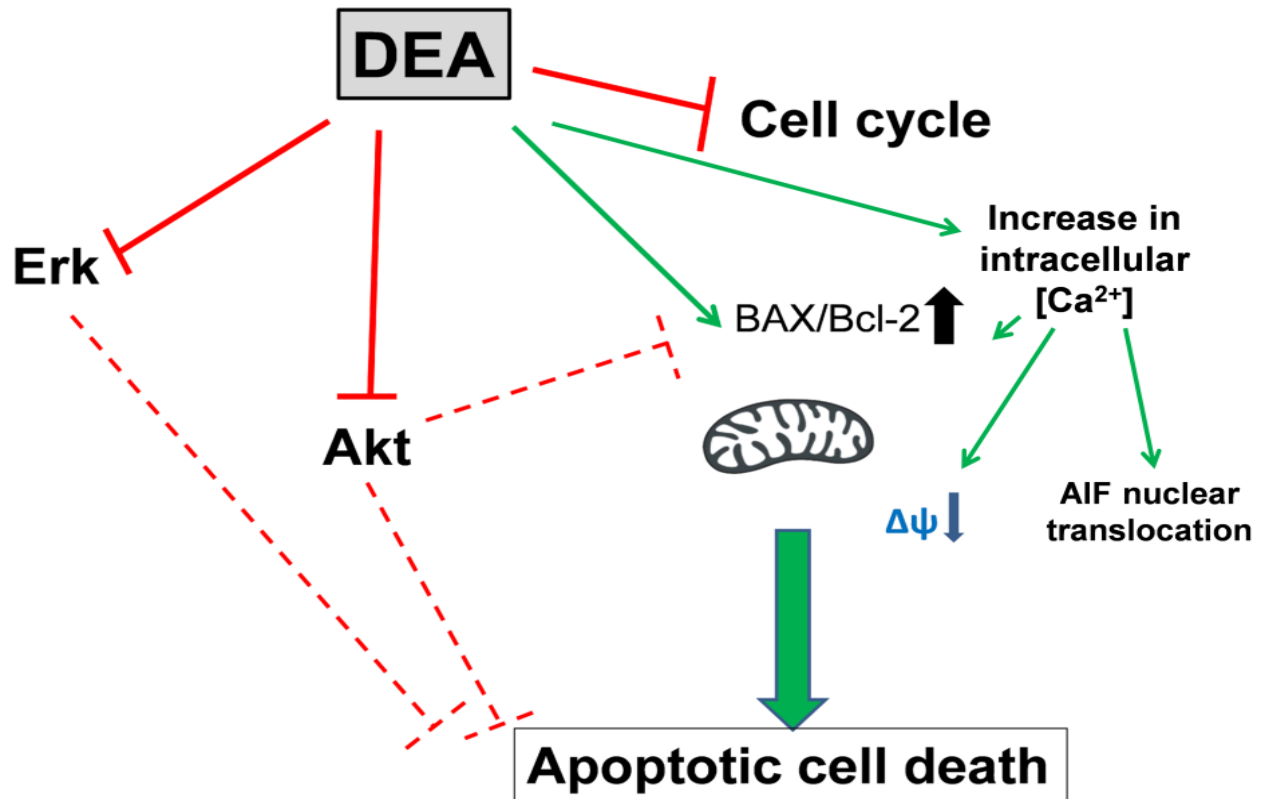
## 7 Conclusions

Cancer is the second leading cause of death worldwide, which makes it a major threat facing the humans. More than hundred types of cancer have been identified including skin and breast cancer. Accordingly, treatment choices are then considered based on the detected cancer type and stage. Designed anti-cancer treatments, for the majority of neoplasms especially the metastatic ones, are insufficient after the prolonged treatment period due to the resistance developed afterward. Other treatments were limited because of their toxic side effects. Here, Desethylamiodarone (DEA) is presented. DEA is the major metabolite of the well-known antiarrhythmic FDA approved drug, Amiodaron (AM).

In the first part of the study, a view of DEA's workflow was determined using *in-vitro* and *in-vivo* metastatic melanoma model. Since metastatic melanoma considered the most lethal form of skin cancer, and one of the top six most common cancer-related mortality worldwide. Consequently, DEA's main target was identified *in-vitro*, the mitochondrial mechanisms resulting in intrinsic apoptosis (**Fig. 27**), furthermore, melanoma growth and metastasis were inhibited by DEA's treatment *in-vivo*. Considering the therapeutic concentrations of anti-cancer drugs; DEA's treatment is much lower in both *in-vitro* and *in-vivo*, which elevate the chance of being a promising candidate for metastatic tumors therapy.

Regarding anti-cancer drug resistance, a highly resistant cancer type, TNBC, was used along with treatable type, HB<sup>+</sup> BC, under DEA's low treatment concentrations. By comparing the two types, TNBC showed less sensitivity as DEA's treatment increases through elevating the inflammatory COX-2 protein expression. Thus, a combination of DEA and COX-2 inhibitor celecoxib was used, which results in synergetic effect led to almost the same DEA's effect in both BC types. Concluding, DEA could be combined with specific inhibitors for resistant-cancer treatment.

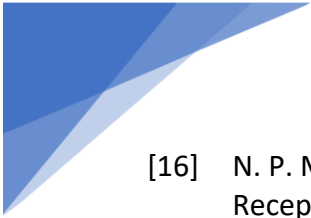
Since DEA is the major metabolite of AM, considering that within the suggested safety limits, the drug does not have therapy-restricting side effects, the safety concerns might not hinder the introduction of DEA into clinical studies.





*Figure 27. DEA induces tumor cell apoptosis through multiple pathways [47].*

## 8 References

- [1] S. Sarkar *et al.*, “Cancer Development, Progression, and Therapy: An Epigenetic Overview,” *Int J Mol Sci*, vol. 14, no. 10, pp. 21087–21113, Oct. 2013, doi: 10.3390/ijms141021087.
- [2] S. H. Hassanpour and M. Dehghani, “Review of cancer from perspective of molecular,” *Journal of Cancer Research and Practice*, vol. 4, no. 4, pp. 127–129, Dec. 2017, doi: 10.1016/j.jcrpr.2017.07.001.
- [3] R. L. Siegel, K. D. Miller, H. E. Fuchs, and A. Jemal, “Cancer statistics, 2022,” *CA Cancer J Clin*, vol. 72, no. 1, pp. 7–33, Jan. 2022, doi: 10.3322/caac.21708.
- [4] *EU Country Cancer Profile: Hungary 2023*. OECD, 2023. doi: 10.1787/ccaf0398-en.
- [5] G. Mathur, S. Nain, and P. K. Sharma, “Cancer: An Overview,” *Academic Journal of Cancer Research*, vol. 8, no. 1, pp. 1–09, 2015, doi: 10.5829/idosi.ajcr.2015.8.1.9336.
- [6] N. H. Khan *et al.*, “Skin cancer biology and barriers to treatment: Recent applications of polymeric micro/nanostructures,” *J Adv Res*, vol. 36, pp. 223–247, Feb. 2022, doi: 10.1016/j.jare.2021.06.014.
- [7] Z. Apalla, D. Nashan, R. B. Weller, and X. Castellsagué, “Skin Cancer: Epidemiology, Disease Burden, Pathophysiology, Diagnosis, and Therapeutic Approaches,” *Dermatol Ther (Heidelb)*, vol. 7, no. S1, pp. 5–19, Jan. 2017, doi: 10.1007/s13555-016-0165-y.
- [8] K. Orthaber, M. Pristovnik, K. Skok, B. Perić, and U. Maver, “Skin Cancer and Its Treatment: Novel Treatment Approaches with Emphasis on Nanotechnology,” *J Nanomater*, vol. 2017, pp. 1–20, 2017, doi: 10.1155/2017/2606271.
- [9] L. E. Davis, S. C. Shalin, and A. J. Tackett, “Current state of melanoma diagnosis and treatment,” *Cancer Biol Ther*, vol. 20, no. 11, pp. 1366–1379, Nov. 2019, doi: 10.1080/15384047.2019.1640032.
- [10] Z. Bognar *et al.*, “Amiodarone’s major metabolite, desethylamiodarone inhibits proliferation of B16-F10 melanoma cells and limits lung metastasis formation in an in vivo experimental model,” *PLoS One*, vol. 15, no. 9 September 2020, 2020, doi: 10.1371/journal.pone.0239088.
- [11] S. C. Naumann *et al.*, “Temozolomide- and fotemustine-induced apoptosis in human malignant melanoma cells: response related to MGMT, MMR, DSBs, and p53,” *Br J Cancer*, vol. 100, no. 2, pp. 322–333, Jan. 2009, doi: 10.1038/sj.bjc.6604856.
- [12] N. Harbeck *et al.*, “Breast cancer,” *Nat Rev Dis Primers*, vol. 5, no. 1, p. 66, Dec. 2019, doi: 10.1038/s41572-019-0111-2.
- [13] H. G. Kaplan, J. A. Malmgren, B. Guo, and M. K. Atwood, “Trastuzumab therapy duration in HER2-positive de novo metastatic breast cancer: 1999–2018,” *Breast Cancer Res Treat*, vol. 195, no. 2, pp. 171–180, Sep. 2022, doi: 10.1007/s10549-022-06678-1.
- [14] K. Won and C. Spruck, “Triple-negative breast cancer therapy: Current and future perspectives (Review),” *Int J Oncol*, vol. 57, no. 6, pp. 1245–1261, Oct. 2020, doi: 10.3892/ijo.2020.5135.
- [15] N. M. Almansour, “Triple-Negative Breast Cancer: A Brief Review About Epidemiology, Risk Factors, Signaling Pathways, Treatment and Role of Artificial Intelligence,” *Front Mol Biosci*, vol. 9, Jan. 2022, doi: 10.3389/fmolb.2022.836417.

- 
- [16] N. P. McAndrew and R. S. Finn, "Clinical Review on the Management of Hormone Receptor–Positive Metastatic Breast Cancer," *JCO Oncol Pract*, vol. 18, no. 5, pp. 319–327, May 2022, doi: 10.1200/OP.21.00384.
- [17] V. Scabia *et al.*, "Estrogen receptor positive breast cancers have patient specific hormone sensitivities and rely on progesterone receptor," *Nat Commun*, vol. 13, no. 1, p. 3127, Dec. 2022, doi: 10.1038/s41467-022-30898-0.
- [18] F. Gallyas *et al.*, "Involvement of Mitochondrial Mechanisms and Cyclooxygenase-2 Activation in the Effect of Desethylamiodarone on 4T1 Triple-Negative Breast Cancer Line," *Int J Mol Sci*, vol. 23, no. 3, 2022, doi: 10.3390/ijms23031544.
- [19] E. Bidram *et al.*, "A concise review on cancer treatment methods and delivery systems," *J Drug Deliv Sci Technol*, vol. 54, p. 101350, Dec. 2019, doi: 10.1016/j.jddst.2019.101350.
- [20] M. Shields, "Chemotherapeutics," in *Pharmacognosy*, Elsevier, 2017, pp. 295–313. doi: 10.1016/B978-0-12-802104-0.00014-7.
- [21] V. Schirrmacher, "From chemotherapy to biological therapy: A review of novel concepts to reduce the side effects of systemic cancer treatment (Review)," *Int J Oncol*, vol. 54, no. 2, pp. 407–419, Feb. 2019, doi: 10.3892/ijo.2018.4661.
- [22] N. Vasan, J. Baselga, and D. M. Hyman, "A view on drug resistance in cancer," *Nature*, vol. 575, no. 7782, pp. 299–309, Nov. 2019, doi: 10.1038/s41586-019-1730-1.
- [23] I. A. Cree and P. Charlton, "Molecular chess? Hallmarks of anti-cancer drug resistance," *BMC Cancer*, vol. 17, no. 1, p. 10, Dec. 2017, doi: 10.1186/s12885-016-2999-1.
- [24] S. Zhu *et al.*, "Ceramide kinase mediates intrinsic resistance and inferior response to chemotherapy in triple-negative breast cancer by upregulating Ras/ERK and PI3K/Akt pathways," *Cancer Cell Int*, vol. 21, no. 1, p. 42, Dec. 2021, doi: 10.1186/s12935-020-01735-5.
- [25] C. Holohan, S. van Schaeybroeck, D. B. Longley, and P. G. Johnston, "Cancer drug resistance: an evolving paradigm," *Nat Rev Cancer*, vol. 13, no. 10, pp. 714–726, Oct. 2013, doi: 10.1038/nrc3599.
- [26] H. Zhao *et al.*, "Inflammation and tumor progression: signaling pathways and targeted intervention," *Signal Transduct Target Ther*, vol. 6, no. 1, p. 263, Dec. 2021, doi: 10.1038/s41392-021-00658-5.
- [27] L. Y. Pang, E. A. Hurst, and D. J. Argyle, "Cyclooxygenase-2: A Role in Cancer Stem Cell Survival and Repopulation of Cancer Cells during Therapy," *Stem Cells Int*, vol. 2016, pp. 1–11, 2016, doi: 10.1155/2016/2048731.
- [28] C. R. Bell *et al.*, "Chemotherapy-induced COX-2 upregulation by cancer cells defines their inflammatory properties and limits the efficacy of chemoimmunotherapy combinations," *Nat Commun*, vol. 13, no. 1, p. 2063, Dec. 2022, doi: 10.1038/s41467-022-29606-9.
- [29] L. Dong, V. Gopalan, O. Holland, and J. Neuzil, "Mitocans Revisited: Mitochondrial Targeting as Efficient Anti-Cancer Therapy," *Int J Mol Sci*, vol. 21, no. 21, p. 7941, Oct. 2020, doi: 10.3390/ijms21217941.
- [30] L. Sainero-Alcolado, J. Liaño-Pons, M. V. Ruiz-Pérez, and M. Arsenian-Henriksson, "Targeting mitochondrial metabolism for precision medicine in cancer," *Cell Death Differ*, vol. 29, no. 7, pp. 1304–1317, Jul. 2022, doi: 10.1038/s41418-022-01022-y.

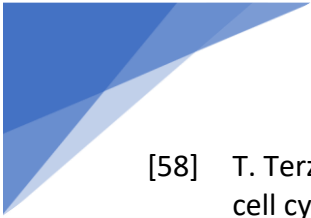
- 
- [31] L. Yu, X. Chen, X. Sun, L. Wang, and S. Chen, "The Glycolytic Switch in Tumors: How Many Players Are Involved?," *J Cancer*, vol. 8, no. 17, pp. 3430–3440, 2017, doi: 10.7150/jca.21125.
- [32] Y. Tsujimoto, L. R. Finger, J. Yunis, P. C. Nowell, and C. M. Croce, "Cloning of the Chromosome Breakpoint of Neoplastic B Cells with the t(14;18) Chromosome Translocation," *Science (1979)*, vol. 226, no. 4678, pp. 1097–1099, Nov. 1984, doi: 10.1126/science.6093263.
- [33] B. A. Carneiro and W. S. El-Deiry, "Targeting apoptosis in cancer therapy," *Nat Rev Clin Oncol*, vol. 17, no. 7, pp. 395–417, Jul. 2020, doi: 10.1038/s41571-020-0341-y.
- [34] C. Wang and R. J. Youle, "The Role of Mitochondria in Apoptosis," *Annu Rev Genet*, vol. 43, no. 1, pp. 95–118, Dec. 2009, doi: 10.1146/annurev-genet-102108-134850.
- [35] E. Zacharioudakis *et al.*, "Modulating mitofusins to control mitochondrial function and signaling," *Nat Commun*, vol. 13, no. 1, p. 3775, Dec. 2022, doi: 10.1038/s41467-022-31324-1.
- [36] F. H. J. Ramadan *et al.*, "Involvement of mitochondrial mechanisms in the cytostatic effect of desethylamiodarone in b16f10 melanoma cells," *Int J Mol Sci*, vol. 21, no. 19, 2020, doi: 10.3390/ijms21197346.
- [37] A. G. Gómez-Valadés *et al.*, "Mitochondrial cristae-remodeling protein OPA1 in POMC neurons couples Ca<sup>2+</sup> homeostasis with adipose tissue lipolysis," *Cell Metab*, vol. 33, no. 9, pp. 1820–1835.e9, Sep. 2021, doi: 10.1016/j.cmet.2021.07.008.
- [38] G. Edwards *et al.*, "Loss of AKAP1 triggers Drp1 dephosphorylation-mediated mitochondrial fission and loss in retinal ganglion cells," *Cell Death Dis*, vol. 11, no. 4, p. 254, Apr. 2020, doi: 10.1038/s41419-020-2456-6.
- [39] S. Herkenne *et al.*, "Developmental and Tumor Angiogenesis Requires the Mitochondria-Shaping Protein Opa1," *Cell Metab*, vol. 31, no. 5, pp. 987–1003.e8, May 2020, doi: 10.1016/j.cmet.2020.04.007.
- [40] L. Wang, R. Li, C. Song, Y. Chen, H. Long, and L. Yang, "Small-Molecule Anti-Cancer Drugs From 2016 to 2020: Synthesis and Clinical Application," *Nat Prod Commun*, vol. 16, no. 9, p. 1934578X2110403, Sep. 2021, doi: 10.1177/1934578X211040326.
- [41] L. Zhong *et al.*, "Small molecules in targeted cancer therapy: advances, challenges, and future perspectives," *Signal Transduct Target Ther*, vol. 6, no. 1, p. 201, Dec. 2021, doi: 10.1038/s41392-021-00572-w.
- [42] Dorian, "Amiodarone for the treatment and prevention of ventricular fibrillation and ventricular tachycardia," *Vasc Health Risk Manag*, p. 465, Jun. 2010, doi: 10.2147/VHRM.S6611.
- [43] G. Varbiro *et al.*, "Protective Effect of Amiodarone but Not N-Desethylamiodarone on Postischemic Hearts through the Inhibition of Mitochondrial Permeability Transition," *Journal of Pharmacology and Experimental Therapeutics*, vol. 307, no. 2, pp. 615–625, Nov. 2003, doi: 10.1124/jpet.103.053553.
- [44] F. Mehraein, "A Review on Amiodarone as an Antiarrhythmic Drug," in *Abnormal Heart Rhythms*, InTech, 2015. doi: 10.5772/60418.
- [45] K. Nobukuni, "Influence of Iodine-Containing Pharmaceuticals on Iodine Status and Thyroid Function: Iodine-Induced Hyperthyroidism and Hypothyroidism," in




*Comprehensive Handbook of Iodine: Nutritional, Biochemical, Pathological and Therapeutic Aspects*, Elsevier, 2009, pp. 927–935. doi: 10.1016/B978-0-12-374135-6.00096-0.

- [46] Z. Bognar *et al.*, “Desethylamiodarone—A metabolite of amiodarone—Induces apoptosis on T24 human bladder cancer cells via multiple pathways,” *PLoS One*, vol. 12, no. 12, p. e0189470, Dec. 2017, doi: 10.1371/journal.pone.0189470.
- [47] Z. Bognar, K. Fekete, R. Bognar, A. Szabo, R. A. Vass, and B. Sumegi, “Amiodarone’s major metabolite, desethylamiodarone, induces apoptosis in human cervical cancer cells,” *Can J Physiol Pharmacol*, vol. 96, no. 10, pp. 1004–1011, Oct. 2018, doi: 10.1139/cjpp-2018-0113.
- [48] W. W. Overwijk and N. P. Restifo, “B16 as a Mouse Model for Human Melanoma,” *Curr Protoc Immunol*, vol. 39, no. 1, Oct. 2000, doi: 10.1002/0471142735.im2001s39.
- [49] M. H. Ullman-Culleré and C. J. Foltz, “Body condition scoring: a rapid and accurate method for assessing health status in mice.,” *Lab Anim Sci*, vol. 49, no. 3, pp. 319–23, Jun. 1999.
- [50] C. R. DeWitt, N. Cleveland, R. C. Dart, and K. Heard, “The effect of amiodarone pretreatment on survival of mice with cocaine toxicity,” *Journal of Medical Toxicology*, vol. 1, no. 1, pp. 11–18, Dec. 2005, doi: 10.1007/BF03160899.
- [51] G. Varbiro, B. Veres, F. Gallyas, and B. Sumegi, “Direct effect of Taxol on free radical formation and mitochondrial permeability transition,” *Free Radic Biol Med*, vol. 31, no. 4, pp. 548–558, Aug. 2001, doi: 10.1016/S0891-5849(01)00616-5.
- [52] V. Petronilli *et al.*, “Transient and Long-Lasting Openings of the Mitochondrial Permeability Transition Pore Can Be Monitored Directly in Intact Cells by Changes in Mitochondrial Calcein Fluorescence,” *Biophys J*, vol. 76, no. 2, pp. 725–734, Feb. 1999, doi: 10.1016/S0006-3495(99)77239-5.
- [53] V. Vichai and K. Kirtikara, “Sulforhodamine B colorimetric assay for cytotoxicity screening,” *Nat Protoc*, vol. 1, no. 3, pp. 1112–1116, Aug. 2006, doi: 10.1038/nprot.2006.179.
- [54] K. Sumegi *et al.*, “BGP-15 Protects against Oxidative Stress- or Lipopolysaccharide-Induced Mitochondrial Destabilization and Reduces Mitochondrial Production of Reactive Oxygen Species,” *PLoS One*, vol. 12, no. 1, p. e0169372, Jan. 2017, doi: 10.1371/journal.pone.0169372.
- [55] L. Zhou *et al.*, “PINK1 Deficiency Ameliorates Cisplatin-Induced Acute Kidney Injury in Rats,” *Front Physiol*, vol. 10, Sep. 2019, doi: 10.3389/fphys.2019.01225.
- [56] D. Julian, K. L. April, S. Patel, J. R. Stein, and S. E. Wohlgemuth, “Mitochondrial depolarization following hydrogen sulfide exposure in erythrocytes from a sulfide-tolerant marine invertebrate,” *Journal of Experimental Biology*, vol. 208, no. 21, pp. 4109–4122, Nov. 2005, doi: 10.1242/jeb.01867.
- [57] D. A. Tagle, “The NIH microphysiological systems program: developing in vitro tools for safety and efficacy in drug development,” *Curr Opin Pharmacol*, vol. 48, pp. 146–154, Oct. 2019, doi: 10.1016/j.coph.2019.09.007.



- 
- [58] T. Terzian *et al.*, “p53 prevents progression of nevi to melanoma predominantly through cell cycle regulation,” *Pigment Cell Melanoma Res*, vol. 23, no. 6, pp. 781–794, Dec. 2010, doi: 10.1111/j.1755-148X.2010.00773.x.
- [59] B. Besztercei *et al.*, “Stress-Induced, p53-Mediated Tumor Growth Inhibition of Melanoma by Modulated Electrohyperthermia in Mouse Models without Major Immunogenic Effects,” *Int J Mol Sci*, vol. 20, no. 16, p. 4019, Aug. 2019, doi: 10.3390/ijms20164019.
- [60] F. Gallyas Jr and B. Sumegi, “Mitochondrial Protection by PARP Inhibition,” *Int J Mol Sci*, vol. 21, no. 8, p. 2767, Apr. 2020, doi: 10.3390/ijms21082767.
- [61] A. García-Sánchez, A. G. Miranda-Díaz, and E. G. Cardona-Muñoz, “The Role of Oxidative Stress in Physiopathology and Pharmacological Treatment with Pro- and Antioxidant Properties in Chronic Diseases,” *Oxid Med Cell Longev*, vol. 2020, pp. 1–16, Jul. 2020, doi: 10.1155/2020/2082145.
- [62] X. R. Chapa-Dubocq, K. M. Rodríguez-Graciani, R. A. Guzmán-Hernández, S. Jang, P. S. Brookes, and S. Javadov, “Cardiac Function is not Susceptible to Moderate Disassembly of Mitochondrial Respiratory Supercomplexes,” *Int J Mol Sci*, vol. 21, no. 5, p. 1555, Feb. 2020, doi: 10.3390/ijms21051555.
- [63] C. L. Chaffer and R. A. Weinberg, “A Perspective on Cancer Cell Metastasis,” *Science (1979)*, vol. 331, no. 6024, pp. 1559–1564, Mar. 2011, doi: 10.1126/science.1203543.
- [64] H. Hugo *et al.*, “Epithelial—mesenchymal and mesenchymal—epithelial transitions in carcinoma progression,” *J Cell Physiol*, vol. 213, no. 2, pp. 374–383, Nov. 2007, doi: 10.1002/jcp.21223.
- [65] S. Kauanova, A. Urazbayev, and I. Vorobjev, “The Frequent Sampling of Wound Scratch Assay Reveals the ‘Opportunity’ Window for Quantitative Evaluation of Cell Motility-Impeding Drugs,” *Front Cell Dev Biol*, vol. 9, Mar. 2021, doi: 10.3389/fcell.2021.640972.
- [66] K. Karamanou, M. Franchi, D. Vynios, and S. Brézillon, “Epithelial-to-mesenchymal transition and invadopodia markers in breast cancer: Lumican a key regulator,” *Semin Cancer Biol*, vol. 62, pp. 125–133, May 2020, doi: 10.1016/j.semcancer.2019.08.003.
- [67] J. Steenbrugge *et al.*, “Comparative Profiling of Metastatic 4T1- vs. Non-metastatic Py230-Based Mammary Tumors in an Intraductal Model for Triple-Negative Breast Cancer,” *Front Immunol*, vol. 10, Dec. 2019, doi: 10.3389/fimmu.2019.02928.
- [68] L. Zhan *et al.*, “Drp1-mediated mitochondrial fission promotes cell proliferation through crosstalk of p53 and NF-κB pathways in hepatocellular carcinoma,” *Oncotarget*, vol. 7, no. 40, pp. 65001–65011, Oct. 2016, doi: 10.18632/oncotarget.11339.
- [69] H. Moindjie, S. Rodrigues-Ferreira, and C. Nahmias, “Mitochondrial Metabolism in Carcinogenesis and Cancer Therapy,” *Cancers (Basel)*, vol. 13, no. 13, p. 3311, Jul. 2021, doi: 10.3390/cancers13133311.
- [70] W. Xiao *et al.*, “Breast cancer subtypes and the risk of distant metastasis at initial diagnosis: a population-based study,” *Cancer Manag Res*, vol. Volume 10, pp. 5329–5338, Nov. 2018, doi: 10.2147/CMAR.S176763.
- [71] J. F. Brien, S. Jimmo, F. J. Brennan, S. E. Ford, and P. W. Armstrong, “Distribution of amiodarone and its metabolite, desethylamiodarone, in human tissues,” *Can J Physiol Pharmacol*, vol. 65, no. 3, pp. 360–364, Mar. 1987, doi: 10.1139/y87-062.

- 
- [72] P. Mishra and D. C. Chan, "Metabolic regulation of mitochondrial dynamics," *Journal of Cell Biology*, vol. 212, no. 4, pp. 379–387, Feb. 2016, doi: 10.1083/jcb.201511036.
- [73] A. Inoue-Yamauchi and H. Oda, "Depletion of mitochondrial fission factor DRP1 causes increased apoptosis in human colon cancer cells," *Biochem Biophys Res Commun*, vol. 421, no. 1, pp. 81–85, Apr. 2012, doi: 10.1016/j.bbrc.2012.03.118.
- [74] M. L. Boland, A. H. Chourasia, and K. F. Macleod, "Mitochondrial Dysfunction in Cancer," *Front Oncol*, vol. 3, 2013, doi: 10.3389/fonc.2013.00292.
- [75] J. Pascual and N. C. Turner, "Targeting the PI3-kinase pathway in triple-negative breast cancer," *Annals of Oncology*, vol. 30, no. 7, pp. 1051–1060, Jul. 2019, doi: 10.1093/annonc/mdz133.
- [76] A. Tapodi *et al.*, "Pivotal Role of Akt Activation in Mitochondrial Protection and Cell Survival by Poly(ADP-ribose)polymerase-1 Inhibition in Oxidative Stress," *Journal of Biological Chemistry*, vol. 280, no. 42, pp. 35767–35775, Oct. 2005, doi: 10.1074/jbc.M507075200.
- [77] I. Sicking *et al.*, "Prognostic influence of cyclooxygenase-2 protein and mRNA expression in node-negative breast cancer patients," *BMC Cancer*, vol. 14, no. 1, p. 952, Dec. 2014, doi: 10.1186/1471-2407-14-952.
- [78] C. P. Allen *et al.*, "DNA Damage Response Proteins and Oxygen Modulate Prostaglandin E2 Growth Factor Release in Response to Low and High LET Ionizing Radiation," *Front Oncol*, vol. 5, Dec. 2015, doi: 10.3389/fonc.2015.00260.

## 9 List of Publication

### 9.1 First author publications connected to research topic:

- **Ramadan, Fadi H.J.**, et al. “Involvement of Mitochondrial Mechanisms in the Cytostatic Effect of Desethylamiodarone in B16F10 Melanoma Cells.” *International Journal of Molecular Sciences*, vol. 21, no. 19, 2020, p. 7346., doi:10.3390/ijms21197346. *Q1/D1. IF: 5,923*

### 9.2 Co-author publications connected to research topic:

- Bogнар, Zita, et al. “Amiodarone’s Major Metabolite, Desethylamiodarone Inhibits Proliferation of B16-F10 Melanoma Cells and Limits Lung Metastasis Formation in an In Vivo Experimental Model.” *PLOS ONE*, vol. 15, no. 9, 2020, doi:10.1371/journal.pone.0239088. *Q1. IF: 3.24*
- Gallyas, Ferenc, et al. “Involvement of Mitochondrial Mechanisms and Cyclooxygenase-2 Activation in the Effect of Desethylamiodarone on 4t1 Triple-Negative Breast Cancer Line.” *International Journal of Molecular Sciences*, vol. 23, no. 3, 2022, p. 1544., doi:10.3390/ijms23031544. *Q1/D1. IF: 6.208*

### 9.3 Co-author publications not connected to research topic:

- Szekeres, Zsolt, et al. “Clinical Study of Metabolic Parameters, Leptin and the SGLT2 Inhibitor Empagliflozin among Patients with Obesity and Type 2 Diabetes.” *International Journal of Molecular Sciences*, vol. 24, no. 5, Feb. 2023, p. 4405. *Crossref, https://doi.org/10.3390/ijms24054405. Q1/D1. IF: 6.208*

**Total IF: 21.579**

### 9.4 Participation in Conferences

#### 9.4.1 Oral presentations (first-author):

- **Fadi H. J. Ramadan**, Zita Bogнар, Anna Maria Cseh, Katalin Fekete, Csenge Antus, Rita Bogнар, Antal Tapodi, Balazs Sumegi, Ferenc Gallyas Jr. Amiodarone’s major metabolite, desethylamiodarone inhibits proliferation and in vivo metastasizing property of B16-F10 melanoma cells. 2020. Doctoral Student Association of the University of Pécs, Pecs, Hungary.
- **Fadi H. J. Ramadan**, Rita Bogнар, Aliz Szabo, Ferenc Gallyas Jr, Zita Bogнар. Involvement of mitochondrial mechanisms in the cytostatic effect of desethylamiodarone in B16F10 melanoma cells. 2021. Hungarian molecular life sciences, Eger, Hungary.

- **Fadi H. J. Ramadan**, Zita Bognar. Effect of Desethylamiodarone on Triple Negative Breast Cancer. 2021. Interdisciplinary doctoral conference, Pecs, Hungary.
- **Ramadan Fadi H J**, Hocsak Eniko, Bognár Rita, Fekete Katalin, Gallyas Ferenc, Bognár Zita. Effect of Desethylamiodarone on 4T1 triple negative breast cancer, 2022. Intelligens szakosodás stratégiai megvalósulása a Pécsi Tudományegyetemen. Pecs, Hungary.
- **Fadi H. J. Ramadan**, Rita Bognár, Aliz Szabo, Ferenc Gallyas Jr, Zita Bognár. Effect of Desethylamiodarone on Mitochondrial Mechanisms and Cyclooxygenase-2 in Breast Cancer Cell Lines. 2022. Annual Meeting of the Hungarian Biochemical Society, Pécs, Hungary.

#### 9.4.2 Oral presentations (Co-author):

- Bognár Zita, Bognár Rita, **Ramadan Fadi H J**, Sümegi Balázs. Egy ismert gyógyszermetabolit, a Desethylamiodarone potenciális szerepe az invazív hólyagdaganatok kezelésében. 2022. Intelligens szakosodás stratégiai megvalósulása a Pécsi Tudományegyetemen. Pecs, Hungary.

#### 9.4.3 Poster presentation (first-author):

- **F. H. J. Ramadan**, F. Gallyas Jr, Z. Bognar. Effect of Desethylamiodarone on Mitochondrial Mechanisms and Cyclooxygenase-2 in MCF-7 and 4T1 Breast Cancer Cell Lines. 2022. IUBMB-FEBS-PABMB Congress, The Biochemistry Summit Venue. Lisbon, Portugal.

#### 9.4.4 Poster presentation (Co-author):

- Zita Bognar, **Fadi H. J. Ramadan**, Rita Bognar, Eniko Hocsak, Kitti Andreidesz, Ferenc Gallyas Jr. Desethylamiodarone may have cytostatic potential on triple negative breast cancer. 2021. Hungarian molecular life sciences, Eger, Hungary.
- Zita Bognar; Fadi H.J Ramadan; Rita Bognar; Eniko Hocsak; Aliz Szabo, Kitti Andreidesz; Ferenc Gallyas Jr.: Amiodarone may have cytostatic potential on triple negative breast cancer, 2021; 50. Membrán Transzport Konferencia, Sümeg,



## *10 Acknowledgments*

First and foremost, I am extremely grateful to my supervisor Dr. Zita Bognar for sharing her knowledge and professional experience with me, and the assessment for achieving my Ph.D. My gratitude extends to the head of Biochemistry and Medical Chemistry department and the doctoral school of Interdisciplinary Medicine Prof. Ferenc Gallyas for the help, knowledge, and the support he gave before and during my Ph.D. Besides, I appreciate the help of my colleagues who were a part and helped in my research especially dr. Rita Bognar and Mr. Giran Laszlo for their technical support, along with staff of our Department, my PhD mates, and everyone who made my work smooth and comfortable. Also, I thank Tempus Public Foundation for awarding me Stipendium Hungaricum Scholarship. Finally, words won't be enough to express my gratitude to my family and friends; without their support I won't be at this point.

Fundings for research: Hungarian grants TKP2021-EGA-17, GINOP-2.3.3-15-2016-00025, GINOP-2.3.2-15-2016-00049 and EFOP-3.6.1-16-2016-00004. It was supported by the János Bolyai Research Scholarship of the Hungarian Academy of Sciences and by the ÚNKP-21-5, ÚNKP-22-5 New National Excellence Program of the Ministry for Innovation and Technology from the source of the National Research, Development and Innovation Fund and by the grants of Medical School of University of Pécs ÁOK KA.



*11 Appendix*



Article

# Involvement of Mitochondrial Mechanisms in the Cytostatic Effect of Desethylamiodarone in B16F10 Melanoma Cells

Fadi H. J. Ramadan <sup>1</sup> , Aliz Szabo <sup>1</sup>, Dominika Kovacs <sup>1</sup>, Aniko Takatsy <sup>1</sup>, Rita Bogнар <sup>1</sup>, Ferenc Gallyas Jr. <sup>1,2,3,\*</sup> and Zita Bogнар <sup>1</sup>

<sup>1</sup> Department of Biochemistry and Medical Chemistry, University of Pécs Medical School, 7624 Pécs, Hungary; fadi.ramadan@aok.pte.hu (F.H.J.R.); aliz.szabo@aok.pte.hu (A.S.); dominika.kovacs@aok.pte.hu (D.K.); Aniko.Takatsy@aok.pte.hu (A.T.); rita.bognar@aok.pte.hu (R.B.); zita.bognar@aok.pte.hu (Z.B.)

<sup>2</sup> Szentagothai Research Centre, University of Pécs, 7624 Pécs, Hungary

<sup>3</sup> HAS-UP Nuclear-Mitochondrial Interactions Research Group, 1245 Budapest, Hungary

\* Correspondence: ferenc.gallyas@aok.pte.hu; Tel.: +36-72-536-278

Received: 31 August 2020; Accepted: 1 October 2020; Published: 5 October 2020



**Abstract:** Previously, we showed that desethylamiodarone (DEA), a major metabolite of the widely used antiarrhythmic drug amiodarone, has direct mitochondrial effects. We hypothesized that these effects account for its observed cytotoxic properties and ability to limit *in vivo* metastasis. Accordingly, we examined DEA's rapid (3–12 h) cytotoxicity and its early (3–6 h) effects on various mitochondrial processes in B16F10 melanoma cells. DEA did not affect cellular oxygen radical formation, as determined using two fluorescent dyes. However, it did decrease the mitochondrial transmembrane potential, as assessed by JC-1 dye and fluorescence microscopy. It also induced mitochondrial fragmentation, as visualized by confocal fluorescence microscopy. DEA decreased maximal respiration, ATP production, coupling efficiency, glycolysis, and non-mitochondrial oxygen consumption measured by a Seahorse cellular energy metabolism analyzer. In addition, it induced a cyclosporine A-independent mitochondrial permeability transition, as determined by Co<sup>2+</sup>-mediated calcein fluorescence quenching measured using a high-content imaging system. DEA also caused outer mitochondrial membrane permeabilization, as assessed by the immunoblot analysis of cytochrome C, apoptosis inducing factor, Akt, phospho-Akt, Bad, and phospho-Bad. All of these data supported our initial hypothesis.

**Keywords:** amiodarone; apoptosis; metastatic melanoma; mitochondrial fusion-fission; mPT; Bad; Akt; Aif

## 1. Introduction

Mitochondrial processes are indispensable for most eukaryotic cells. As a metabolic compartment, mitochondria produce ~90% of cellular ATP and represent a hub in the catabolism and synthesis of essential intermediates and macromolecule precursors for cell growth and proliferation [1]. In addition, mitochondria participate in the maintenance of Ca<sup>2+</sup> homeostasis and redox balance, as well as the regulation of cell death [2]. Notably, mitochondria can regulate their functions according to the metabolic demands of the cell [3], and these functions are characteristically altered in cancer cells [4]. Accordingly, cancer is regarded as a mitochondrial metabolic disease [4–7], and intensive research efforts have been devoted to the identification of novel mitochondria-targeted therapeutic strategies [3,8].

Desethylamiodarone (DEA), the major metabolite of amiodarone (AM), accumulates rapidly in the extracardiac tissues of patients during AM antiarrhythmic therapy [9]. Although AM is one of the most

frequently prescribed antiarrhythmics in the United States and is widely used in various life-threatening ventricular tachyarrhythmias worldwide, AM therapy is often limited by the toxic side effects of both the parent molecule and DEA itself [10]. These side effects include thyroid, hepatic, pulmonary, cardiac, psychiatric, ocular, dermatologic, hematological, and neuromuscular symptoms [10], which in most cases appear when the AM plasma concentration exceeds the recommended therapeutic value of 5.7  $\mu\text{M}$  [11]. The tissue concentrations of AM and DEA can be 100–1000 times higher than the corresponding plasma concentration [11]. The accumulation of DEA in the myocardium, as well as in lung, liver, thyroid gland, pancreas, and skin, but not in adipose tissue, exceeds that of the parent molecule [9,12,13], and its mean elimination half-life is about 40 days [14]. Based on the tissue accumulation properties and toxic effects of DEA, we previously proposed that the compound has a potential use in cancer therapy and provided experimental evidence for its cytostatic and metastasis-limiting properties in the bladder, cervix, and melanoma cell lines [15–17].

In previous studies in isolated liver and heart mitochondria, we found that DEA at concentrations of 10–30  $\mu\text{M}$  inhibits the mitochondrial respiratory chain, collapses the mitochondrial membrane potential ( $\Delta\Psi_m$ ), and induces a mitochondrial permeability transition (mPT) [18]. We concluded that these effects could account for the toxic side effects of AM [18]. In light of the dependence of cancer cells on optimized mitochondrial metabolism, these effects of DEA may contribute to its observed cytotoxic and metastasis-limiting properties. To explore this possibility, in this study we examined the effects of DEA treatment on mitochondrial processes in B16F10 melanoma cells.

## 2. Results

### 2.1. Effect of DEA on Cellular Reactive Oxygen Species (ROS) Production

Cancer cells and tissues exist under persistent oxidative stress, which affects their survival and metastatic properties [19]. Therefore, we were interested in whether DEA has any effect on ROS formation in the B16F10 melanoma line. To resolve this issue, we treated the cells with 5 and 10  $\mu\text{M}$  of DEA in the presence of the non-fluorescent reduced derivatives of fluorescent redox dyes, and registered the increase in fluorescence resulting from the oxidizing effect of cellular ROS. We used two different fluorescent redox dyes to assess ROS formation separately in the aqueous and membranous compartments. Additionally, we used MitoSOX<sup>TM</sup> Red, a redox dye of red fluorescence targeted to the mitochondria, where it is oxidized selectively by superoxide [20]. Taxol, which generates ROS at low micromolar concentrations, was used as a positive control [21]. In agreement with our previous results obtained in isolated liver and heart mitochondria [18], we did not detect significantly elevated ROS levels in either the aqueous or membranous compartments of B16F10 melanoma cells (Figure 1). However, we found that 10  $\mu\text{M}$  of DEA did induce mitochondrial superoxide formation, which was much smaller in extent than the one caused by 5  $\mu\text{M}$  of Taxol (Figure 1).



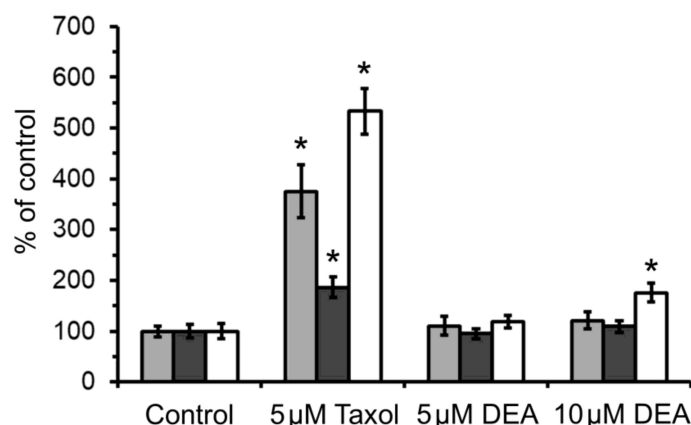


**Figure 1.** Effect of DEA on the cellular ROS formation in the B16F10 melanoma line. Cells were treated with 5 or 10  $\mu\text{M}$  of DEA or 5  $\mu\text{M}$  of taxol (positive control). ROS formation in the lipid (light bars) and aqueous (dark bars) phase and mitochondrial superoxide production (empty bars) were calculated based on the rate of fluorescence intensity change vs. time; fluorescent dyes were generated by ROS-mediated oxidation from their respective non-fluorescent counterparts. The results are expressed as the % of ROS formation in the absence of agents (means  $\pm$  SEM of five independent experiments). \* indicates a significant difference relative to the control ( $p < 0.05$ ).

## 2.2. Effect of DEA on the Mitochondrial Membrane Potential ( $\Delta\Psi_m$ )

$\Delta\Psi_m$  is a significant factor in ATP synthesis and has a number of non-energetic functions essential for cell survival [22]. Accordingly, we were interested in how DEA treatment affects  $\Delta\Psi_m$  in B16F10 melanoma cells. For this purpose, we used a membrane potential-dependent fluorescent dye, JC-1, which accumulates in the mitochondria due to its positive charge. When  $\Delta\Psi_m$  is normal, the dye forms J-aggregates that emit red fluorescence upon excitation. Depolarization decreases the abundance of the dye in the mitochondria; consequently, the aggregates fall apart, and the monomer dye emits a green fluorescence when excited at 490 nm. When  $\Delta\Psi_m$  dissipates completely, the dye is not retained in the mitochondria, manifesting as a loss of fluorescence. Within 3 h, treatment with  $> 5 \mu\text{M}$  of DEA markedly depolarized the mitochondria in intact B16F10 melanoma cells (Figure 2).

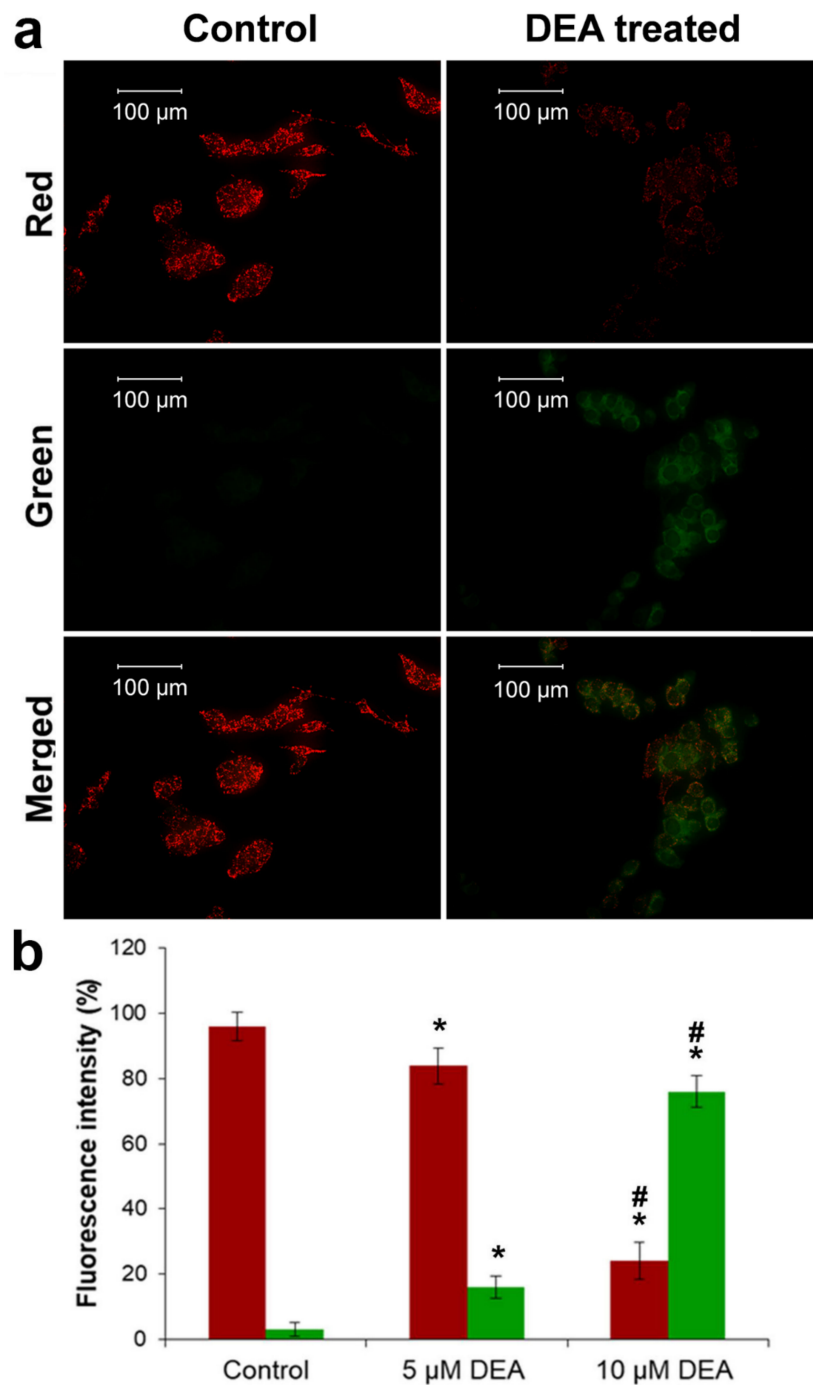


**Figure 2.** Effect of DEA on  $\Delta\Psi_m$  in B16F10 melanoma cells. Cells were treated with 5 or 10  $\mu\text{M}$  of DEA for 3 h.  $\Delta\Psi_m$  was assessed using the membrane potential-dependent fluorescent dye, JC-1. Red and green fluorescence indicates normal and depolarized  $\Delta\Psi_m$ , respectively. (a) Representative fluorescence images in the red, green, and merged channels of cells treated with 10  $\mu\text{M}$  of DEA. (b) Quantitative assessment of  $\Delta\Psi_m$ , expressed as the % of fluorescence intensity (means  $\pm$  SEM of three independent experiments). Quantitative comparisons are true within the same color only. Red and green bars denote red and green fluorescence, respectively. \* and # indicate a significant difference relative to the control and 5  $\mu\text{M}$  of DEA, respectively ( $p < 0.05$ ).

### 2.3. Effect of DEA on Mitochondrial Fragmentation in Intact B16F10 Melanoma Cells

Mitochondrial fusion requires healthy  $\Delta\Psi_m$ , which forms the basis of mitochondrial quality control [22]. Therefore, compromised  $\Delta\Psi_m$  results in mitochondrial fragmentation, raising the

possibility that DEA treatment causes such an effect. To test this possibility, we performed confocal fluorescence microscopy on DEA-treated B16F10 melanoma cells transiently transfected with mitochondria-targeted red fluorescent protein (mtRFP) expressing vector [23]. Under these conditions, the intensity of the mitochondrially localized fluorescence did not depend on  $\Delta\Psi_m$ . Treatment for 3 h with 10  $\mu\text{M}$  of DEA resulted in mitochondrial fragmentation comparable to that caused by 25  $\mu\text{M}$  of cisplatin (positive control [24]) (Figure 3). Although treatment with 5  $\mu\text{M}$  of DEA tended to increase the mitochondrial fragmentation, the difference from the control did not reach the level of statistical significance (Figure 3).

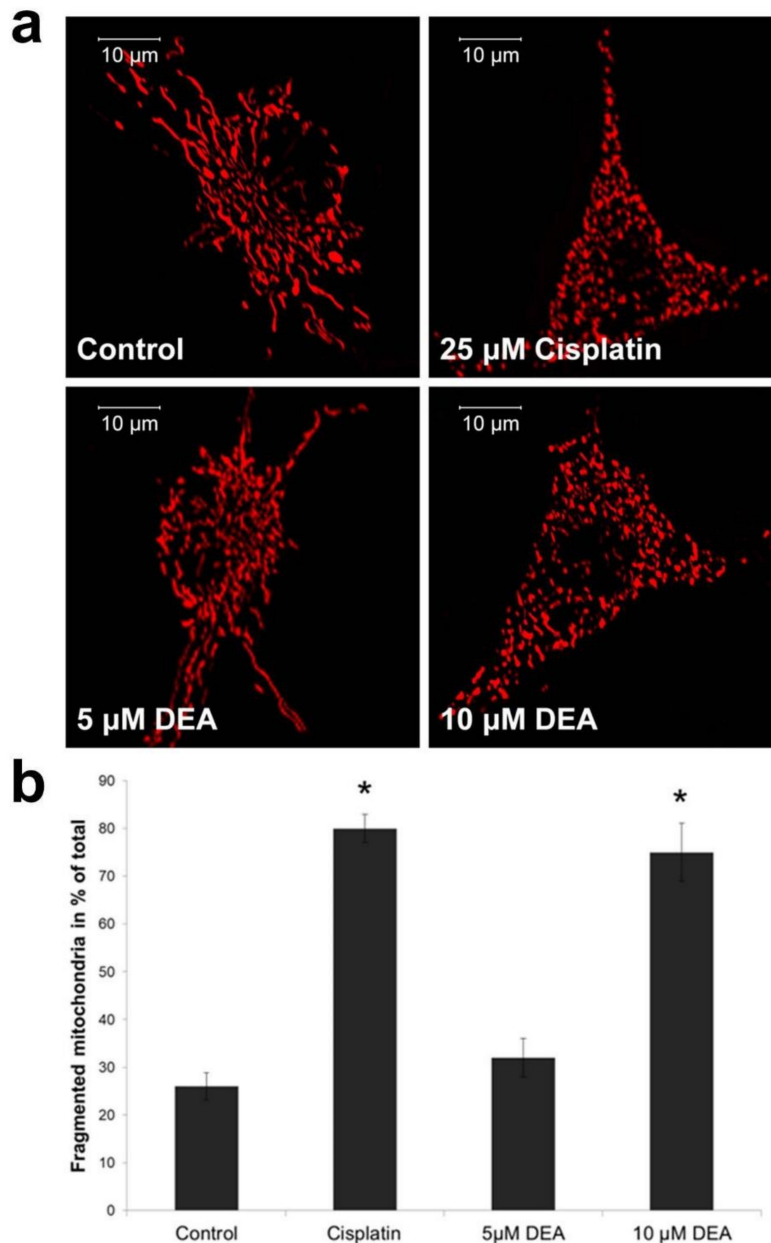


**Figure 3.** Effect of DEA on mitochondrial fragmentation. mtRFP-transfected cells were treated with 5 or 10  $\mu\text{M}$  of DEA, or 25  $\mu\text{M}$  of cisplatin (positive control [24]), for 3 h. Mitochondrial fragmentation was determined based on confocal fluorescence images, as described in [25]. (a) Representative fluorescence images for all the treatment groups. (b) Quantitative assessment of mitochondrial fragmentation expressed as % (means  $\pm$  SEM of three independent experiments). \* indicates a significant difference relative to the control ( $p < 0.05$ ).

#### 2.4. Effect of DEA on the Energy Metabolism of B16F10 Melanoma Cells

Given that the DEA treatment compromised  $\Delta\Psi_m$ , a major determinant of ATP synthesis [22], we next sought to assess DEA's effect on energy metabolism of B16F10 melanoma cells. We used the Seahorse XF Cell Mito Stress Test to monitor the cellular oxygen consumption rate (OCR), an indicator of mitochondrial respiration, and the extracellular acidification rate (ECAR), an indicator of aerobic glycolysis in live B16F10 melanoma cells. We treated cells with 5 or 10  $\mu\text{M}$  of DEA for 3 h, and then monitored the OCR and ECAR for 75 min. After registering basal respiration (Figure 4a-1) for 15 min, we added oligomycin, an inhibitor of  $F_0F_1$  ATP synthase, to assess the ATP production (Figure 4a-4). After 20 min of recording, we added carbonyl cyanide 4-(trifluoromethoxy) phenylhydrazone (FCCP), which uncouples respiration and ATP synthesis, to measure maximal respiration (Figure 4a-3). After a further 20 min of recording, we inhibited mitochondrial respiration by adding the Complex I inhibitor rotenone and the Complex III inhibitor antimycin A to determine the proton leak and non-mitochondrial oxygen consumption (Figure 4a-2, Figure 4a-5). Simultaneously, we also monitored ECAR (Figure 4b). From the original recordings, the instrument output multiple parameters of cellular energy metabolism (Figure 4c–k). The DEA treatment did not significantly affect basal respiration (Figure 4c) or proton leak (Figure 4d), although 10  $\mu\text{M}$  of DEA tended to decrease the former and increase the latter. By contrast, 10  $\mu\text{M}$  of DEA did suppress the maximal respiration (Figure 4e), ATP production (Figure 4f), and coupling efficiency (Figure 4g); the last of these indicates how tightly respiration is coupled to ATP synthesis. DEA decreased the non-mitochondrial oxygen consumption (Figure 4h), and spare respiratory capacity, expressed either as the difference (Figure 4i) or ratio (Figure 4j) of maximal and basal respiration, in a concentration-dependent manner. Although it did not affect the basal fermentative ATP synthesis, DEA decreased lactate accumulation after oligomycin administration in a concentration-dependent manner (Figure 4b–k), indicating that the drug interfered with the glycolytic machinery as well as the mitochondrial respiratory chain.

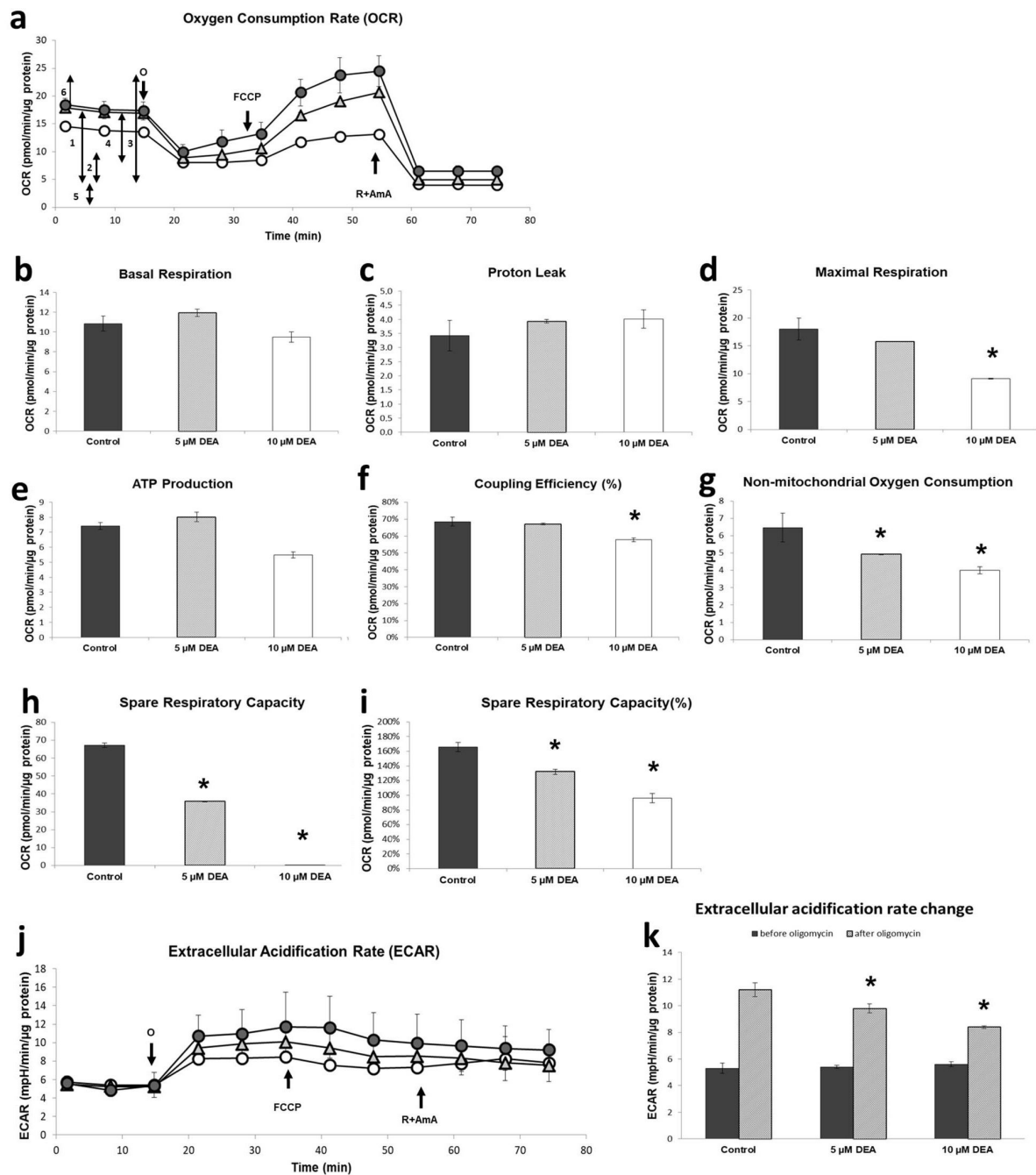


**Figure 4.** Effect of DEA on the energy metabolism of B16F10 melanoma cells. Cells were treated with 5 or 10  $\mu\text{M}$  of DEA for 3 h, and then the OCR and ECAR were monitored for 75 min. The  $F_0F_1$  ATP synthase inhibitor oligomycin (o), the uncoupler FCCP, and the respiratory inhibitors rotenone and antimycin A (R+AmA) were added at the bold arrows. (a) OCR recordings for untreated (filled circles), 5  $\mu\text{M}$  of DEA-treated (triangles), and 10  $\mu\text{M}$  of DEA-treated (open circles) cells (means  $\pm$  SD of three independent experiments running in two replicates in each experiment). The double-headed arrows with numbers next to them indicate (1) basal respiration, (2) proton leak, (3) maximal respiration, (4) ATP production, (5) non-mitochondrial oxygen consumption, and (6) spare respiratory capacity. (b–i) Parameters derived from (a); for explanation, see the text and (a). Appropriate parts of the recordings were averaged and presented as the means  $\pm$  SEM of three independent experiments running in two replicates in each experiment. \* indicates a significant difference relative to the control ( $p < 0.05$ ).

(b) Basal respiration. (c) Proton leak. (d) Maximal respiration. (e) Mitochondrial ATP production. (f) Coupling efficiency; for explanation, see the text. (g) Non-mitochondrial oxygen consumption. (h,i) Spare respiratory capacity, presented as the difference (h) and ratio (i) of maximal and basal respiration. (j) ECAR recordings for untreated (filled circles), 5  $\mu\text{M}$  of DEA-treated (triangles), and 10  $\mu\text{M}$  of DEA-treated (open circles) cells (means  $\pm$  SD of three independent experiments running in two replicates in each experiment). All the labeling is the same as for (a). (k) Extracellular acidification rate before (dark bars) and after (light bars) the administration of oligomycin. OCR and ECAR data were normalized to mg of protein content.

### 2.5. Effect of DEA on mPT in Intact B16F10 Melanoma Cells

According to our previous results, DEA induced mPT in isolated liver and heart mitochondria that was resistant to cyclosporine A, a specific inhibitor of mPT induced by elevated  $\text{Ca}^{2+}$  [26]. We were interested in determining whether the drug has the same effect in melanoma cells. Therefore, we adapted the method of Petronilli et al. [27] for measuring mPT in intact live cells using a 96-well automated high-content fluorescence imaging system. The method is based on the quenching of calcein fluorescence by  $\text{Co}^{2+}$ . Non-fluorescent acetoxymethylcalcein is taken up by the cells, and is converted intracellularly to fluorescent calcein by non-specific esterases.  $\text{Co}^{2+}$ , the cellular uptake of which is facilitated by the  $\text{Ca}^{2+}$  ionophore A23187, quenches the cytoplasmic calcein fluorescence; however, it cannot enter intact mitochondria, resulting in exclusively mitochondrial calcein fluorescence. When the mPT pore opens,  $\text{Co}^{2+}$  is free to enter the mitochondria and quench the calcein fluorescence there as well. Accordingly, we monitored the calcein fluorescence of melanoma cells treated with 5 or 10  $\mu\text{M}$  of DEA or 1.5 mM of  $\text{CaCl}_2$  (positive control [27]) in the presence of acetoxymethylcalcein,  $\text{CoCl}_2$ , and A23187 with or without CsA for 3 h. In complete agreement with our previous results obtained in isolated liver and heart mitochondria [18], 10  $\mu\text{M}$  of DEA induced mPT that was CsA-independent (Figure 5). As expected, elevated  $\text{Ca}^{2+}$ , the cellular uptake of which is facilitated by A23187, caused a massive mPT that was fully CsA-dependent (Figure 5).

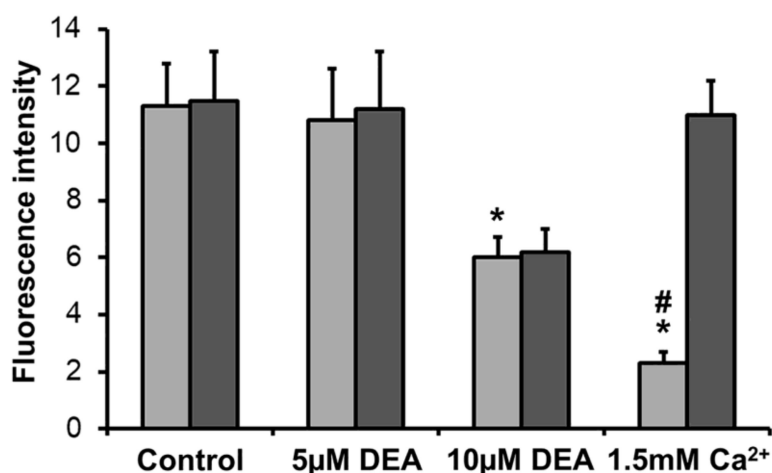


**Figure 5.** Effect of DEA on mPT in intact B16F10 melanoma cells. Cells were treated with 5 or 10  $\mu\text{M}$  of DEA or 1.5 mM of  $\text{Ca}^{2+}$  (positive control [27]) in the presence (dark bars) or absence (light bars) of the mPT inhibitor CsA for 3 h. mPT was assessed by monitoring the  $\text{Co}^{2+}$ -mediated quenching of mitochondrial calcein fluorescence [27]. The results are expressed as fluorescence intensity (the means  $\pm$  SEM of three independent experiments). \* and # indicate a significant difference relative to control and CsA-treated cells of the same treatment group, respectively ( $p < 0.05$ ).

### 2.6. Effect of DEA on Outer Mitochondrial Membrane (OMM) Permeabilization

OMM permeabilization can lead to apoptotic death [28]; therefore, we studied the effect of DEA on OMM integrity. When the OMM is intact, pro-apoptotic intermembrane proteins such as cytochrome C (Cyt c) and apoptosis-inducing factor (Aif) are retained in the mitochondria. Anti-apoptotic members

of the B-cell lymphoma 2 (Bcl2) family form heterodimers with pro-apoptotic members, thereby inactivating them. When the Bcl2-associated agonist of cell death (Bad) is dephosphorylated, it binds to anti-apoptotic Bcl2 family members, releasing the pro-apoptotic ones, which in turn dimerize with each other, translocate to the OMM, and permeabilize it. This leads to a release of the pro-apoptotic intermembrane proteins, eventually resulting in apoptotic cell death [28]. A major mechanism of protection against apoptosis is the phosphorylation of Bad by the cytoprotective kinase Akt [28]. Optic atrophy1 (Opa1) is an inner mitochondrial membrane (IMM)-associated large GTPase protein that is present in the mitochondria only [29]. Stimuli leading to OMM permeabilization and Cyt c release results also in release of Opa1 to the cytosol [30]. Accordingly, we assessed DEA's effect on OMM integrity by determining its effect on the expression, localization, and activation of Cyt c, Opa1, Aif, Bad, and Akt. To this end, we prepared whole-cell homogenate, and in parallel nuclear and cytoplasmic fractions from B16F10 melanoma cells treated with different concentrations of DEA for 6 h, and then subjected them to immunoblot analysis. To determine the phosphorylation states of Akt and Bad, we used phosphorylation-specific primary antibodies. At a concentration of 10  $\mu$ M, DEA increased the steady-state level of Bad and decreased Bad phosphorylation in a concentration-dependent manner (Figure 6). Both of these effects shift the balance in the pro-apoptotic direction. Accordingly, DEA induces the release of Cyt c and Opa1 into the cytosol and nuclear translocation of Aif (Figure 6). In addition, 10  $\mu$ M of DEA decreased Akt phosphorylation without affecting the steady-state level of the enzyme (Figure 6). This latter effect of DEA was fully consistent with its effects on the other proteins studied. Together, these data indicated that DEA caused OMM permeabilization.

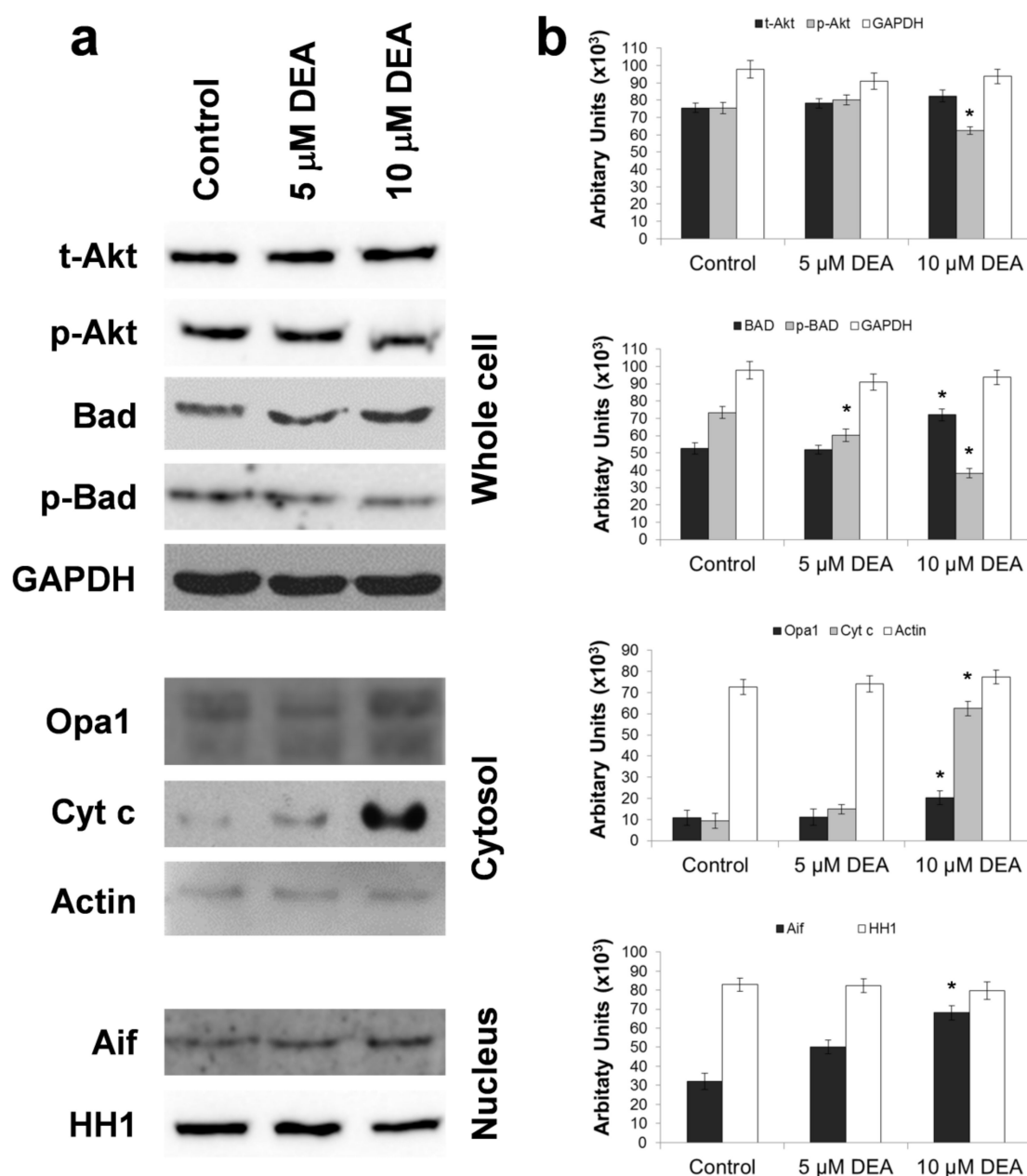


**Figure 6.** Effect of DEA on the OMM permeabilization in B16F10 melanoma cells. Cells were treated with 5 or 10  $\mu\text{M}$  of DEA for 6 h, harvested, and homogenized (Whole cell). Alternatively, nuclear and cytosolic fractions were prepared from the harvested cells. Steady-state levels and phosphorylation states of Akt and Bad were assessed in whole-cell homogenate. The steady-state levels of Cyt c and Opa1 were determined in the cytosolic, whereas that of Aif was measured in the nuclear fraction by immunoblotting. In the whole-cell homogenate, the cytosolic fraction and the nuclear fraction, we used glyceraldehyde-3-phosphate dehydrogenase (GAPDH), actin and histone H1 (HH1), respectively, as loading controls. The proteins were visualized by enhanced chemiluminescence. (a) Representative blots. (b) Quantitative assessment of proteins in the subcellular fractions. Results are expressed as pixel density or chemiluminescence intensity of the bands, both expressed in arbitrary units (means  $\pm$  SEM of three independent experiments). \* indicates a significant difference relative to the control ( $p < 0.05$ ).

### 2.7. Effect of DEA and Akt Inhibitors on the Viability of B16F10 Melanoma Cells

Because of the importance of mitochondrial processes in cancer [5], we were interested in determining whether the observed mitochondrial effects of DEA manifested as viability changes in



B16F10 melanoma cells. To this end, we treated the cells for 3–12 h with 5 or 10  $\mu\text{M}$  of DEA before determining their viability using the sulforhodamine B (SRB) assay. This assay is considered the most suitable for assessing the toxicity of substances in cultured cells, especially when the toxicity affects the mitochondria [31]. In complete agreement with our previous results [17], DEA decreased the viability of B16F10 melanoma cells in a time- and concentration-dependent manner, although at 5  $\mu\text{M}$  and for up to 6 h of incubation, this effect did not reach statistical significance (Figure 7).

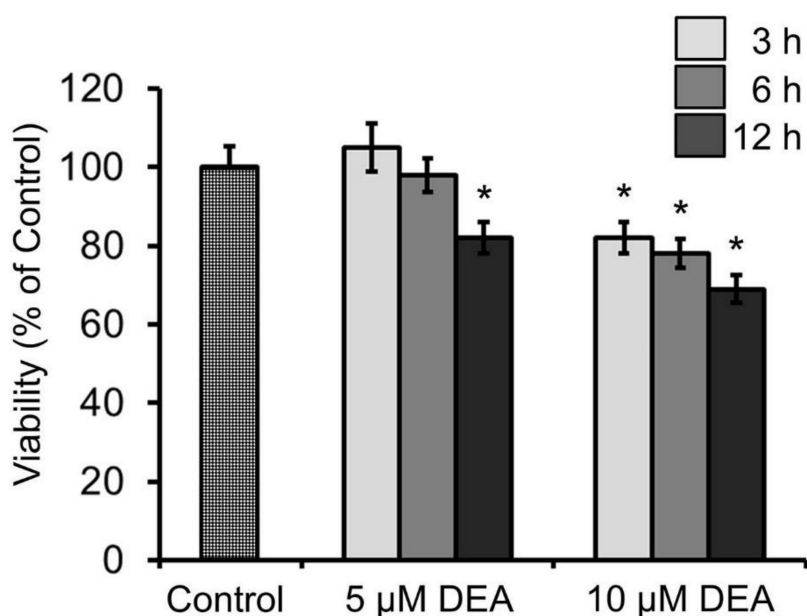


**Figure 7.** Effect of DEA on the viability of B16F10 melanoma cells. Cells were treated with 5 or 10  $\mu\text{M}$  of DEA for 3–12 h, and then the viability was determined using the SRB assay. The results are expressed as the % viability of the control (means  $\pm$  SEM of five independent experiments). \* indicates a significant difference relative to the control ( $p < 0.05$ ).

### 3. Discussion

Mitochondria contribute in multiple ways to carcinogenesis, tumor survival, and metastasis. The respiratory chain, situated in the inner mitochondrial membrane (IMM), is responsible for the majority of the ATP production under physiological conditions; moreover, it is a massive source of ROS formation in various maladies, including cancer [32,33]. Different ROS-associated signaling pathways have been proposed as oncologic therapeutic targets, particularly the nuclear factor erythroid 2-related factor 2 (Nrf2)–regulated anti-oxidant defense system [34,35]. A number of antineoplastic drugs and substances that inhibit the mitochondrial respiratory chain increase cellular ROS production [21,36–38]. Using a mitochondria-targeted fluorescent redox dye, we found that DEA at a concentration of 10  $\mu\text{M}$  but not at 5  $\mu\text{M}$  elicited mitochondrial superoxide formation (Figure 1). However, we failed to observe significantly elevated ROS levels either in the aqueous or membranous cellular compartments (Figure 1). The latter results are in accordance with our previous results obtained in isolated liver and heart mitochondria [18]. It is not clear whether this discrepancy was due to technical issues, or simply if the extent of mitochondrial superoxide production was insufficient to elevate the overall cellular ROS level. Indeed, oxidases—most notably, members of the NADPH oxidase family—are the major source of cellular ROS production besides the mitochondrial respiratory chain. Additionally, the latter is tightly controlled, and the superoxide produced by it is readily neutralized by antioxidant enzymes [39]. However, it is worth noting that the DEA-induced mitochondrial superoxide production was less than 20% of the one caused by 5  $\mu\text{M}$  of Taxol (Figure 1), and the Taxol-induced cellular ROS production was detectable by conventional fluorescent redox dyes [21], not only by MitoSOX<sup>TM</sup> Red.

In addition to its role in providing the driving force for ATP synthesis,  $\Delta\Psi_m$  plays essential roles in the transport of mitochondrial proteins encoded in the nucleus [40], as well as in cations such as  $K^+$ ,  $Ca^{2+}$ , and  $Mg^{2+}$  [22]; ROS generation [41] and mitochondrial network dynamics [42]; and the regulation of cell death via the release of pro-apoptotic intermembrane proteins [26,43,44]. The maintenance of  $\Delta\Psi_m$  is so important for cell survival that in ischemic situations, the  $F_0F_1$  ATPase can operate in reverse mode, consuming rather than synthesizing ATP to rescue the cell. Under such conditions, the substrate-level phosphorylation of non-glucose substrates supplies the ATP to be cleaved by the  $F_0F_1$  ATPase, providing a narrow survival window [45–47]. Cancer cells, especially those in solid tumors, exist in a permanent state of partial ischemia, to which their cytoplasmic and mitochondrial metabolic pathways must adapt [3,48]. Therefore, drugs that interfere with tumor cell metabolism could be of therapeutic value [3]. DEA is an example of such a candidate drug: it decreased  $\Delta\Psi_m$  in a concentration-dependent manner in B16F10 melanoma cells, and a 3 h treatment with 10  $\mu$ M of DEA massively decreased  $\Delta\Psi_m$  (Figure 2). This finding was in accord with our previous results obtained in isolated liver and rat mitochondria [18].

Mitochondrial network dynamics play important roles in mitochondrial biogenesis, the satisfaction of cellular energy and metabolic demands, retrograde signaling, and mitochondrial quality control [42,49]. To fulfill these tasks, continuous mitochondrial fusion and fission processes must be maintained in balance, and are mainly regulated by intracellular signaling [49]. However,  $\Delta\Psi_m$  plays a decisive role in this balance, as below a certain  $\Delta\Psi_m$  threshold the fusion process cannot take place [42,49]. Accordingly, excessive fission is a common feature of many tumors [50,51]. Although mitochondrial fission does not necessarily lead to apoptotic cell death, fragmented mitochondria are more susceptible to damage and are more apt to be eliminated by mitophagy, which forms the basis of mitochondrial quality control [52]. Excessive fission can lead to a significantly reduced mitochondrial DNA copy number, as observed in various malignancies including astrocytomas; prostate cancers; and breast, colon, and hepatocellular carcinomas [42]. Decreases in the mitochondrial copy number compromise normal mitochondrial function and promote cellular migration, thus contributing to tumor progression [53]. Accordingly, the fragmentation-inducing effect of DEA (Figure 3) may contribute to its cytotoxic properties and ability to limit in vivo metastasis, which we observed previously in cultured bladder and cervix carcinoma and melanoma cells [15–17]. Increased mitochondrial fragmentation results from increased fission or decreased fusion. Considering that fusion requires intact  $\Delta\Psi_m$  [29], and DEA-impaired  $\Delta\Psi_m$  (Figure 2), it seems likely that DEA caused mitochondrial fragmentation by impeding fusion. Opa1 is responsible for the fusion of the IMM, and maintains its cristae morphology [29]. Short and long isoforms of the protein are in balance, and normally they are associated with the IMM. However, their balance is disrupted, and the protein is released to the cytosol when stimuli disturb the  $\Delta\Psi_m$  and/or permeabilize the OMM [30]. DEA at a concentration of 10  $\mu$ M evoked Opa1 release to the cytosol (Figure 6), indicating that its mitochondrial fragmentation-inducing effect was indeed caused by impeding fusion rather than by promoting fission.

Cancer cells change their metabolism in characteristic ways to adapt to the predominantly hypoxic conditions of their environment [54]. For energy production, many cancer types prefer glycolysis over mitochondrial oxidative phosphorylation, even in the presence of sufficient oxygen. The importance of this switch in ATP production, known as the Warburg effect [55], is validated by the diagnostic value of  $^{18}F$ -deoxyglucose positron emission tomography in identifying tumors based on their increased glucose uptake [56,57]. However, the most malignant cancer types, including cancer stem cells, metastatic tumor cells, and therapy-resistant tumor cells, have elevated levels of mitochondrial ATP synthesis [58,59]. Moreover, oxidative phosphorylation is essential for the survival, proliferation, and metastasis of these cells and forms the basis of their resistance to chemotherapy and radiotherapy [60,61]. Accordingly, oxidative phosphorylation is considered as an emerging therapeutic target, especially for the most malignant cancer types [62]. Based on its effects on energy metabolism in B16F10 melanoma cells, DEA exhibits promise as a candidate cancer therapy. At a concentration of 10  $\mu$ M, DEA diminished maximal respiration, ATP production, and coupling efficiency (Figure 4). These findings are in line with our

previous results obtained in isolated liver and heart mitochondria [18]. Additionally, DEA decreased fermentative glycolysis and non-mitochondrial oxygen consumption in a concentration-dependent manner (Figure 4). This latter effect might contribute to the drug's cytotoxic and anti-metastatic properties. Impeding both the mitochondrial and glycolytic ATP producing pathways (Figure 4) seems an attractive mechanism for DEA's cytotoxic property. However, this remains to be proven in future studies aimed at identifying the targets of DEA both in the respiratory chain and the glycolytic pathway.

Adverse environmental conditions such as hypoxia, low nutrient availability, and growth factor withdrawal can induce mitochondria-associated cell death, most often in the form of mPT or OMM permeabilization. When opened, the mPT pore forms a nonspecific channel, allowing the unrestricted passage of water and solutes of up to 1.5 kDa in size across the IMM [26]. The physiological role of transient channel opening remains unknown; however, prolonged opening results in the complete loss of  $\Delta\Psi_m$ , the termination of ATP synthesis, mitochondrial swelling, and the rupture of the IMM due to water influx driven by the high osmolarity of the mitochondrial matrix [26,63]. Outflowing  $\text{Ca}^{2+}$  triggers mPT in the neighboring mitochondria, resulting in eventual necrotic cell death [26]. However, cancer cells are often relatively resistant to mPT induction [64]. In complete agreement with our previous results obtained in isolated liver and heart mitochondria [18], 10  $\mu\text{M}$  of DEA induced a CsA-independent mPT (Figure 5). This likely contributes to DEA's cytotoxicity in cultured bladder carcinoma, cervical carcinoma, and melanoma cells [15–17]. Furthermore, DEA definitely compromised IMM integrity, as calcein fluorescence was not quenched in the absence of DEA or  $\text{Ca}^{2+}$  stimulation (data not shown). In addition,  $\text{Ca}^{2+}$  evoked a CsA-dependent mPT that was more pronounced than the mPT induced by 10  $\mu\text{M}$  of DEA (Figure 5). The identity and composition of the mPT pore remains controversial [63], and CsA-independent mPT induction has been reported by others [65]. Therefore, we will refer to this effect of DEA as “mPT-inducing” until a clearer definition of mPT can be established.

The other major form of mitochondria-associated cell death is OMM permeabilization-mediated apoptosis. However, resistance to apoptosis is a hallmark of cancer that is achieved by disrupting the balance between pro- and anti-apoptotic Bcl2 proteins [66]. Resistance arises due to a multitude of mechanisms, including the downregulation of pro-apoptotic, up-regulation of anti-apoptotic Bcl-2 genes [67], and upregulation of protein inhibitors of apoptosis [68]. Although only preliminary data are available regarding how DEA interferes with these mechanisms, some trends have emerged. Firstly, even a relatively short DEA treatment (6 h) elevates the steady-state level of the pro-apoptotic Bcl-2 family member Bad (Figure 6). Future studies should investigate whether Bad levels rise due to the upregulation of expression or the inhibition of degradation. Second, the Akt, which is constitutively active in melanomas [69], was inactivated by 10  $\mu\text{M}$  of DEA (Figure 6). In this case, the duration was more than adequate for the observed effect, as the covalent regulation of a kinase activity could be achieved within minutes. The observed decrease in Bad phosphorylation and increase in Cyt c and Aif release (Figure 6) could be explained by the previous two findings.

However, the data in Figure 6 also indicate that several elements of the signaling network underlying DEA's OMM-permeabilizing effect were not examined in this study. Although it is difficult to compare blots using different primary antibodies, it seems unlikely that the observed Akt inhibition can fully account for the reduction in Bad phosphorylation (Figure 6). Additionally, the extent of Cyt c release seems disproportional with the other observed changes (Figure 6). Future studies should seek to identify missing mechanisms. On the other hand, all the aforementioned data are in line with our previous findings on DEA [15–18], and they account for the time- and concentration-dependent cytostatic effect of DEA treatment (Figure 7). Based on the data presented in this study, it is difficult to propose a mechanism that can explain the said multiple effects on several mitochondrial processes. Considering the central role of  $\text{Ca}^{2+}$  in regulating apoptosis and thereby the survival and therapy resistance of cancer cells [70], it is a limitation of this study that it cannot account for DEA's effect on intracellular calcium.

On the other hand, we presented experimental evidence that DEA decreases  $\Delta\Psi$ ; induces mitochondrial fragmentation; decreases maximal respiration, ATP production, coupling efficiency, glycolysis, and non-mitochondrial oxygen consumption; and induces CsA-independent mPT and OMM permeabilization. All of these effects may account for the rapid (3–12 h) cytotoxicity of the drug. Furthermore, these results are in agreement with our previous findings obtained in isolated liver and heart mitochondria, and may account for DEA's long-term (24–72 h) cytotoxicity and ability to suppress *in vivo* metastasis by bladder carcinoma, cervical carcinoma, and melanoma cell lines [15–18].

## 4. Materials and Methods

### 4.1. Materials

Protease inhibitor cocktail and all chemicals for cell culture were purchased from Sigma-Aldrich Kft (Budapest, Hungary). DEA was a gift from Professor Andras Varro (Department of Pharmacology and Pharmacotherapy, University of Szeged, Szeged, Hungary). The following primary antibodies were used: anti-Bad, anti-phospho-Bad (Ser136), anti-Akt, anti-phospho-Akt (Ser473), anti-AIF, anti-histonH1, anti-cytochrome C, anti-Opa1 (1:500 dilution), anti-GAPDH (1:2000, clone 6C5), and anti-actin (1:2000). All the antibodies were purchased from Cell Signaling Technology (Beverly, MA, USA), but GAPDH that was from EMD Millipore Bioscience (Darmstadt, Germany).

### 4.2. Cell Culture

B16F10 mouse metastatic melanoma cells were obtained from the American Type Culture Collection (LGC Standards, Wesel, Germany). B16F10 cells were split twice a week for 4 months and maintained as monolayer adherent cultures under standard conditions (5% CO<sub>2</sub>, 37 °C) in RPMI 1640 media supplemented with 10% fetal calf serum (FCS) and 1% penicillin–streptomycin mixture (Life Technologies, Darmstadt, Germany).

### 4.3. Cell Viability Assay

B16F10 cells were seeded in 96-well plates at a starting density of  $5 \times 10^3$  cells/well in quintuplicate (five replicate wells per sample) overnight. The cells were treated with 0, 5, or 10  $\mu\text{M}$  of DEA for 3–12 h. After treatment, the cells were washed in phosphate-buffered saline (PBS) and fixed in 100  $\mu\text{L}$  of cold 10% trichloroacetic acid solution. The plates were incubated for 30 min at 4 °C, washed five times with distilled water, and dried overnight at room temperature. The cellular protein content in the wells was determined by the SRB assay. Briefly, 70  $\mu\text{L}$  of 0.4% SRB (Sigma-Aldrich Co., Budapest, Hungary) prepared in 1% acetic acid were added to each well and incubated for 30 min at room temperature. The SRB reagent was discarded, and the plates were washed five times with 1% acetic acid and dried at room temperature for a few hours. Then, 200  $\mu\text{L}$  of a 10 mM Tris base was added to each well, and the samples were incubated at room temperature on a plate shaker for 30 min to solubilize the bound SRB. Absorbance was measured at 560 and 600 nm in parallel on a plate reader. OD<sub>600</sub> was subtracted as a background from the OD<sub>560</sub>. These experiments were repeated five times.

### 4.4. Bioenergetic Analysis

To determine the balance of oxidative vs. fermentative energy production in B16F10 cells, OCR and ECAR were measured using a Seahorse XFp Analyzer (Agilent, Santa Clara, CA, USA). Cells were seeded into XFp cell culture 8-well miniplates at a starting density of  $4 \times 10^4$  cell/well in duplicate and cultured under standard conditions overnight. Then, the cells were treated with 0, 5, or 10  $\mu\text{M}$  of DEA for 3 h. Prior to the measurement, the medium was replaced with Seahorse XF Assay Media (Agilent, Santa Clara, CA, USA) pH 7.4 supplemented with 10 mM of glucose, 2 mM of L-glutamine, and 1 mM of pyruvate. Mitochondrial stress test was performed using the following inhibitors at the indicated final concentrations: 1  $\mu\text{M}$  of oligomycin, 1  $\mu\text{M}$  of FCCP, and 1  $\mu\text{M}$  of rotenone–antimycin A. In each experiment, two wells without cells were running to assess the non-cellular oxygen consumption,

which was subtracted from the corresponding OCR value. The OCR and ECAR data were normalized to the mg protein content using the Micro BCA Protein Assay kit (Thermo Fisher Scientific, Waltham, MA, USA) for the measurement of protein concentrations. No other data correction was applied. These experiments were repeated three times.

#### 4.5. $\Delta\Psi_m$ Assay

Changes in  $\Delta\Psi_m$  were assayed using the mitochondrial fluorescent dye JC-1. B16F10 cells were seeded at a starting density of  $2.5 \times 10^4$  cells/well in 6-well plates containing coverslips and cultured at least overnight before the experiment. After subjecting the cells to different concentrations of DEA for 3 h, the coverslips were rinsed twice in PBS and placed upside down on top of a small chamber formed by a microscope slide filled with PBS supplemented with 10% FCS and 1  $\mu\text{g}/\text{mL}$  of JC-1 dye (Molecular Probes, Eugene, OR, USA). The cells were imaged with a Nikon Eclipse Ti-U fluorescent microscope (Auro-Science Consulting Ltd., Budapest, Hungary) equipped with a Spot RT3 camera, using a 20 $\times$  objective lens with epifluorescence illumination. After the cells were loaded with dye for 15 min, the same microscopic field was imaged with a 490 nm bandpass excitation and > 590 nm (red) and < 546 nm (green) emission filters. Under these conditions, we did not observe considerable bleed-through between the red and green channels. The quantification of JC-1 fluorescence intensities in each sample was performed in 15 randomly chosen microscopic fields containing 20–30 cells using the MetaXpress image analyzer software (Molecular Devices LLC., San Jose, CA, USA). These experiments were repeated three times.

#### 4.6. Analysis of Mitochondrial Network Dynamics

For confocal imaging, B16F10 cells were seeded onto 25 mm round glass coverslip medium at a starting density of  $2.5 \times 10^4$  cells/coverslip, and cultured in antibiotic-free culture for 24 h. The transient transfection of B16F10 cells with mtRFP was performed using TransFectin Lipid Reagent (Bio-Rad, Hercules, CA, USA). On the following day, the cells were treated for 3 h, as indicated in the text; washed twice in PBS; and fixed in 4% formalin. Fluorescence was visualized on an Olympus FluoView 1000 (Olympus, Hamburg, Germany) confocal laser scanning microscope. For excitation, a multiline argon-ion laser at 488 nm and a green helium-neon laser at 543 nm were used (10  $\mu\text{s}/\text{pixel}$ ) in the photon-counting and sequential mode. The field of interest was scanned in XYZ mode, scanning the total thickness of the cells with a 1.5  $\mu\text{m}$  layer distance and taking 1024  $\times$  1024 pixel images of each layer. The quantitative determination of mitochondrial fragmentation was performed as described [25]; we considered mitochondria shorter than 2  $\mu\text{m}$  to be fragmented and those longer than 5  $\mu\text{m}$  as filamentous. These experiments were repeated three times.

#### 4.7. Subcellular Fractionation

Three semi-confluent 10 cm plates of B16F10 cells were harvested, washed twice with PBS, and resuspended in 1 mL of fractionation buffer (250 mM of sucrose, 20 mM of 2-[4-(2-hydroxyethyl)piperazin-1-yl]ethanesulfonic acid (HEPES), pH 7.4, 10 mM of KCl, 1.5 mM of  $\text{MgCl}_2$ , 1 mM of ethylenediamine-tetraacetic acid (EDTA), 1 mM of ethyleneglycol-tetraacetic acid (EGTA), 1 mM of dithiothreitol (DTT), and proteinase inhibitor cocktail (Sigma, #P2714)). The cell lysate was manually homogenized in a Teflon–glass homogenizer, chilled on ice, and centrifuged for 7 min at 720 $\times$  g at 4  $^\circ\text{C}$ . The nuclear pellet was resuspended in 700  $\mu\text{L}$  of fractionation buffer, re-homogenized, and centrifuged for 10 min at 600 $\times$  g. This procedure was repeated one more time, and the pellet was resuspended in lysis buffer (10% glycerol, 25 mM of NaCl, 50 mM of NaF, 10 mM of Na-pyrophosphate, 2 nM of EGTA, 2 nM of DTT, 20 nM of p-nitrophenyl-phosphate, 25 mM of Tris-HCl, pH 7.4, 50 nM of beta-glycerophosphate, and 0.1% Triton X-100) to yield the nuclear fraction. The supernatant of the 7 min, 720 $\times$  g centrifugation step was subjected to centrifugation at 10,000 $\times$  g for 5 min at 4  $^\circ\text{C}$ . The supernatant and pellet of this step yielded the cytoplasmic and mitochondrial fractions, respectively; the latter was not used in this study.

#### 4.8. Immunoblot Analysis

B16F10 cells were seeded in 10 cm plates at  $10^6$  cells/plate and treated as described above for the cell viability assay. The cells were harvested at intervals in chilled lysis buffer containing 0.5 mM of sodium-metavanadate, 1 mM of EDTA, and protease inhibitor cocktail (1:200). The cell lysates were boiled and subjected to 10% sodium dodecyl sulfate polyacrylamide gel electrophoresis before being transferred to nitrocellulose membranes. The membranes were blocked in 5% low-fat milk for 1.5 h at room temperature, and then exposed to primary antibodies at 4 °C overnight in blocking solution. Appropriate horseradish peroxidase-conjugated secondary antibodies were used at a dilution of 1:5000. Signals were visualized by using enhanced chemiluminescence and captured on X-ray film. The films were scanned, and the pixel densities of the bands were determined using the NIH ImageJ software. Alternatively, chemiluminescence was measured on an Azure 300 (Azure Biosystems) imaging system that digitized the bands' chemiluminescence intensities using its inbuilt software. For stripping and reprobing, the membranes were washed in stripping buffer (0.1 M glycine, 5 M  $MgCl_2$ , pH 2.8) for 1 h at room temperature. After washing and blocking, the membranes were incubated with primary antibodies against non-phosphorylated or loading control proteins. These experiments were repeated three times.

#### 4.9. Determination of Cellular ROS Formation

B16F10 cells were seeded as described above for the viability assay and treated with 5 or 10  $\mu M$  of DEA or 5  $\mu M$  of taxol (positive control [21]). The cellular ROS levels were determined based on the formation of N-acetyl-8-dodecyl-resorufin and 6-carboxy-2',7'-dichlorofluorescein from their nonfluorescent reduced counterparts, N-acetyl-8-dodecyl-3,7-dihydroxyphenoxazine (1.3 mg/L final concentration) and 6-carboxy-2',7'-dichlorodihydrofluorescein diacetate (2 mg/L final concentration), as described previously [21,71]. The former assessed the cellular ROS formation in the lipid phase, and the latter in the aqueous phase. Fluorescence was measured by a plate-reader fluorimeter (PerkinElmer, Hungary) at excitation wavelengths of 578 and 495 nm and emission wavelengths of 597 and 522 nm for N-acetyl-8-dodecyl-resorufin and 6-carboxy-2',7'-dichlorofluorescein, respectively. The mitochondrial superoxide formation was assessed by MitoSOX<sup>TM</sup> Red (Thermo Fisher Scientific, Waltham, MA, USA). Cells were incubated for 30 min in 5  $\mu M$  of MitoSOX<sup>TM</sup> Red, then were rinsed and treated with 5 or 10  $\mu M$  of DEA or 5  $\mu M$  of taxol for 3 h. Fluorescence was recorded by the plate-reader fluorimeter at excitation wavelengths of 495 nm and emission wavelengths of 590 nm. Under these conditions, the fluorescence intensity is proportional to the mitochondrial superoxide level [20]. The ROS levels were calculated from the slopes of the registration curves. These experiments were repeated five times.

#### 4.10. Measurement of mPT in Intact B16F10 Cells

The B16F10 cells were seeded as described above for the viability assay and cultured in antibiotic-free medium overnight. Cells were washed with  $Ca^{2+}$ - and  $Mg^{2+}$ -free Hank's balanced salt solution (HBSS), and then treated with 250 nM of A23187, 90  $\mu M$  of  $CoCl_2$ , 1 g/L of glucose, 5 or 10  $\mu M$  of DEA or 1.5 mM of  $CaCl_2$  (positive control [27]), and/or 2.5  $\mu M$  of CsA in HBSS for 3 h. For the detection of mPT, acetoxymethylcalcein was added to the medium at a final concentration of 1  $\mu M$ . Fluorescence in wells resulting from unquenched de-esterified calcein in the mitochondria [27] (cytoplasmic calcein is quenched by  $Co^{2+}$ ) was monitored using the ImageXpress Micro4 automated high-content imaging system (Molecular Devices LLC., San Jose, CA, USA) using a 4 $\times$  objective and epifluorescence illumination. The quantification of calcein fluorescent intensities was performed using the MetaXpress software. These experiments were repeated three times.

#### 4.11. Data Analysis

All the data are expressed as means  $\pm$  standard deviation (SD). The concentration-dependent effects of DEA in each experiment were tested with ANOVA using the post hoc Dunnett test. Differences

were considered significant at  $p < 0.05$ . Statistical analyses were performed using IBM SPSS Statistics v20.0.

**Author Contributions:** Conceptualization, Z.B. and F.G.; methodology, Z.B.; investigation, F.H.J.R., A.S., D.K., R.B., and A.T.; writing—original draft preparation, F.H.J.R., A.S., Z.B., and F.G.; writing—review and editing, Z.B. and F.G.; visualization, Z.B.; A.S., D.K., R.B. funding acquisition, F.G. All authors have read and agreed to the published version of the manuscript.

**Funding:** This research was funded by Hungarian grants GINOP-2.3.3-15-2016-00025, GINOP-2.3.2-15-2016-00049, EFOP-3.6.1-16-2016-00004, and the Higher Education Institutional Excellence Program.

**Acknowledgments:** The authors thank Laszlo Giran for technical help with the preparation of the figures. We apologize to any authors of relevant studies that we have failed to cite.

**Conflicts of Interest:** The authors declare no conflict of interest. The funders had no role in the design of the study; the collection, analysis, or interpretation of data; the writing of the manuscript; or the decision to publish the results.

## Abbreviations

AIF	Apoptosis inducing factor
AM	Amiodarone
Bad	Bcl2 associated agonist of cell death
Bcl2	B-cell lymphoma2
CsA	Cyclosporine A
Cyt c	Cytochrome C
DEA	Desethylamiodarone
$\Delta\Psi_m$	Mitochondrial membrane potential
DTT	Dithiothreitol
ECAR	Extracellular acidification rate
EDTA	Ethylenediamine-tetraacetic acid
EGTA	Ethyleneglycol-tetraacetic acid
FCCP	Carbonyl cyanide 4-(trifluoromethoxy) phenylhydrazone
FCS	Fetal calf serum
GAPDH	Glyceraldehyde-3-phosphate dehydrogenase
HBSS	Hank's balanced salt solution
HEPES	2-[4-(2-hydroxyethyl)piperazin-1-yl]ethanesulfonic acid
HH1	Histone H1
IMM	Inner mitochondrial membrane
mPT	Mitochondrial permeability transition
mtRFP	mitochondria-targeted red fluorescent protein
Nrf2	Nuclear factor erythroid 2-related factor 2
OCR	Oxygen consumption rate
OD	Optical density
OMM	Outer mitochondrial membrane
Opa1	Optic atrophy1
PBS	Phosphate-buffered saline
ROS	Reactive oxygen species
SD	Standard deviation
SEM	Standard error of the mean
SRB	Sulforhodamine B
Tris	2-Amino-2-hydroxymethyl-propane-1,3-diol

## References

1. Vasan, K.; Werner, M.; Chandel, N.S. Mitochondrial Metabolism as a Target for Cancer Therapy. *Cell Metab.* **2020**, *32*, 341–352. [[CrossRef](#)]

2. Zhou, D.R.; Eid, R.; Boucher, E.; Miller, K.A.; Mandato, C.A.; Greenwood, M.T. Stress is an agonist for the induction of programmed cell death: A review. *Biochim. Biophys. Acta Mol. Cell Res.* **2019**, *1866*, 699–712. [[CrossRef](#)]
3. Weinberg, S.E.; Chandel, N.S. Targeting mitochondria metabolism for cancer therapy. *Nat. Chem. Biol.* **2015**, *11*, 9–15. [[CrossRef](#)]
4. Giampazolias, E.; Tait, S.W. Mitochondria and the hallmarks of cancer. *FEBS J.* **2016**, *283*, 803–814. [[CrossRef](#)] [[PubMed](#)]
5. Vyas, S.; Zaganjor, E.; Haigis, M.C. Mitochondria and Cancer. *Cell* **2016**, *166*, 555–566. [[CrossRef](#)] [[PubMed](#)]
6. Martinez-Outschoorn, U.E.; Peiris-Pages, M.; Pestell, R.G.; Sotgia, F.; Lisanti, M.P. Cancer metabolism: A therapeutic perspective. *Nat. Rev. Clin. Oncol.* **2017**, *14*, 11–31. [[CrossRef](#)] [[PubMed](#)]
7. Porporato, P.E.; Filigheddu, N.; Pedro, J.M.B.; Kroemer, G.; Galluzzi, L. Mitochondrial metabolism and cancer. *Cell Res.* **2018**, *28*, 265–280. [[CrossRef](#)] [[PubMed](#)]
8. Ghosh, P.; Vidal, C.; Dey, S.; Zhang, L. Mitochondria Targeting as an Effective Strategy for Cancer Therapy. *Int. J. Mol. Sci.* **2020**, *21*. [[CrossRef](#)]
9. Brien, J.F.; Jimmo, S.; Brennan, F.J.; Ford, S.E.; Armstrong, P.W. Distribution of amiodarone and its metabolite, desethylamiodarone, in human tissues. *Can. J. Physiol. Pharm.* **1987**, *65*, 360–364. [[CrossRef](#)]
10. Colunga Biancatelli, R.M.; Congedo, V.; Calvosa, L.; Ciacciarelli, M.; Polidoro, A.; Iuliano, L. Adverse reactions of Amiodarone. *J. Geriatr. Cardiol.* **2019**, *16*, 552–566.
11. Holt, D.W.; Tucker, G.T.; Jackson, P.R.; Storey, G.C. Amiodarone pharmacokinetics. *Am. Heart J.* **1983**, *106*, 840–847. [[CrossRef](#)]
12. Daniels, J.M.; Brien, J.F.; Massey, T.E. Pulmonary fibrosis induced in the hamster by amiodarone and desethylamiodarone. *Toxicol. Appl. Pharm.* **1989**, *100*, 350–359. [[CrossRef](#)]
13. Honegger, U.E.; Zuehlke, R.D.; Scuntaro, I.; Schaefer, M.H.; Toplak, H.; Wiesmann, U.N. Cellular accumulation of amiodarone and desethylamiodarone in cultured human cells. Consequences of drug accumulation on cellular lipid metabolism and plasma membrane properties of chronically exposed cells. *Biochem. Pharm.* **1993**, *45*, 349–356. [[CrossRef](#)]
14. Singh, B.N.; Nademane, K.; Josephson, M.A.; Ikeda, N.; Venkatesh, N.; Kannan, R. The electrophysiology and pharmacology of verapamil, flecainide, and amiodarone: Correlations with clinical effects and antiarrhythmic actions. *Ann. NY Acad. Sci.* **1984**, *432*, 210–235. [[CrossRef](#)] [[PubMed](#)]
15. Bogнар, Z.; Fekete, K.; Antus, C.; Hocsak, E.; Bogнар, R.; Tapodi, A.; Boronkai, A.; Farkas, N.; Gallyas, F.J.; Sumegi, B.; et al. Desethylamiodarone-A metabolite of amiodarone-Induces apoptosis on T24 human bladder cancer cells via multiple pathways. *PLoS ONE* **2017**, *12*, e0189470. [[CrossRef](#)] [[PubMed](#)]
16. Bogнар, Z.; Fekete, K.; Bogнар, R.; Szabo, A.; Vass, R.A.; Sumegi, B. Amiodarone’s major metabolite, desethylamiodarone, induces apoptosis in human cervical cancer cells. *Can. J. Physiol. Pharm.* **2018**, *96*, 1004–1011. [[CrossRef](#)] [[PubMed](#)]
17. Bogнар, Z.; Cseh, A.M.; Fekete, K.; Antus, C.; Bogнар, R.; Tapodi, A.; Ramadan, F.H.J.; Sumegi, B.; Gallyas, F.J. Amiodarone’s major metabolite, desethylamiodarone inhibits proliferation of B16-F10 melanoma cells and limits lung metastasis formation in an *in vivo* experimental model. *PLoS ONE* **2020**, *15*, e0239088. [[CrossRef](#)]
18. Varbiro, G.; Toth, A.; Tapodi, A.; Bogнар, Z.; Veres, B.; Sumegi, B.; Gallyas, F.J. Protective effect of amiodarone but not N-desethylamiodarone on postischemic hearts through the inhibition of mitochondrial permeability transition. *J. Pharm. Exp.* **2003**, *307*, 615–625. [[CrossRef](#)]
19. Hayes, J.D.; Dinkova-Kostova, A.T.; Tew, K.D. Oxidative Stress in Cancer. *Cancer Cell* **2020**, *38*, 167–197. [[CrossRef](#)]
20. Julian, D.; April, K.L.; Patel, S.; Stein, J.R.; Wohlgemuth, S.E. Mitochondrial depolarization following hydrogen sulfide exposure in erythrocytes from a sulfide-tolerant marine invertebrate. *J. Exp. Biol.* **2005**, *208*, 4109–4122. [[CrossRef](#)]
21. Varbiro, G.; Veres, B.; Gallyas, F.; Sumegi, B. Direct effect of taxol on free radical formation and mitochondrial permeability transition. *Free Radic. BioMed.* **2001**, *31*, 548–558. [[CrossRef](#)]
22. Zorova, L.D.; Popkov, V.A.; Plotnikov, E.Y.; Silachev, D.N.; Pevzner, I.B.; Jankauskas, S.S.; Babenko, V.A.; Zorov, S.D.; Balakireva, A.V.; Juhaszova, M.; et al. Mitochondrial membrane potential. *Anal. Biochem.* **2018**, *552*, 50–59. [[CrossRef](#)] [[PubMed](#)]



23. Sumegi, K.; Fekete, K.; Antus, C.; Debreceni, B.; Hocsak, E.; Gallyas, F.J.; Sumegi, B.; Szabo, A. BGP-15 Protects against Oxidative Stress-or Lipopolysaccharide-Induced Mitochondrial Destabilization and Reduces Mitochondrial Production of Reactive Oxygen Species. *PLoS ONE* **2017**, *12*, e0169372. [[CrossRef](#)] [[PubMed](#)]
24. Zhou, L.; Zhang, L.; Zhang, Y.; Yu, X.; Sun, X.; Zhu, T.; Li, X.; Liang, W.; Han, Y.; Qin, C. PINK1 Deficiency Ameliorates Cisplatin-Induced Acute Kidney Injury in Rats. *Front. Physiol.* **2019**, *10*, 1225. [[CrossRef](#)] [[PubMed](#)]
25. del Campo, A.; Parra, V.; Vasquez-Trincado, C.; Gutierrez, T.; Morales, P.E.; Lopez-Crisosto, C.; Bravo-Sagua, R.; Navarro-Marquez, M.F.; Verdejo, H.E.; Contreras-Ferrat, A.; et al. Mitochondrial fragmentation impairs insulin-dependent glucose uptake by modulating Akt activity through mitochondrial Ca<sup>2+</sup> uptake. *Am. J. Physiol. Endoc. M* **2014**, *306*, E1–E13. [[CrossRef](#)]
26. Green, D.R.; Reed, J.C. Mitochondria and apoptosis. *Science* **1998**, *281*, 1309–1312. [[CrossRef](#)]
27. Petronilli, V.; Miotto, G.; Canton, M.; Brini, M.; Colonna, R.; Bernardi, P.; Di Lisa, F. Transient and long-lasting openings of the mitochondrial permeability transition pore can be monitored directly in intact cells by changes in mitochondrial calcein fluorescence. *Biophys. J.* **1999**, *76*, 725–734. [[CrossRef](#)]
28. Edlich, F. BCL-2 proteins and apoptosis: Recent insights and unknowns. *Biochem. Biophys. Res. Commun.* **2018**, *500*, 26–34. [[CrossRef](#)]
29. Panek, T.; Elias, M.; Vancova, M.; Lukes, J.; Hashimi, H. Returning to the Fold for Lessons in Mitochondrial Crista Diversity and Evolution. *Curr. Biol.* **2020**, *30*, R575–R588. [[CrossRef](#)]
30. Sanderson, T.H.; Raghunayakula, S.; Kumar, R. Release of mitochondrial Opa1 following oxidative stress in HT22 cells. *Mol. Cell Neurosci.* **2015**, *64*, 116–122. [[CrossRef](#)]
31. Vichai, V.; Kirtikara, K. Sulforhodamine B colorimetric assay for cytotoxicity screening. *Nat. Protoc.* **2006**, *1*, 1112–1116. [[CrossRef](#)]
32. Toyokuni, S.; Okamoto, K.; Yodoi, J.; Hiai, H. Persistent oxidative stress in cancer. *FEBS Lett.* **1995**, *358*, 1–3. [[CrossRef](#)]
33. Garcia-Sanchez, A.; Miranda-Diaz, A.G.; Cardona-Munoz, E.G. The Role of Oxidative Stress in Physiopathology and Pharmacological Treatment with Pro- and Antioxidant Properties in Chronic Diseases. *Oxid. Med. Cell Longev.* **2020**, *2020*, 2082145. [[CrossRef](#)]
34. Liu, Y.; Lang, F.; Yang, C. NRF2 in human neoplasm: Cancer biology and potential therapeutic target. *Pharmacology* **2020**, 107664. [[CrossRef](#)]
35. Moldogazieva, N.T.; Lutsenko, S.V.; Terentiev, A.A. Reactive Oxygen and Nitrogen Species-Induced Protein Modifications: Implication in Carcinogenesis and Anticancer Therapy. *Cancer Res.* **2018**, *78*, 6040–6047. [[CrossRef](#)] [[PubMed](#)]
36. Ferroni, P.; Della-Morte, D.; Palmirotta, R.; McClendon, M.; Testa, G.; Abete, P.; Rengo, F.; Rundek, T.; Guadagni, F.; Roselli, M. Platinum-based compounds and risk for cardiovascular toxicity in the elderly: Role of the antioxidants in chemoprevention. *Rejuvenation Res.* **2011**, *14*, 293–308. [[CrossRef](#)] [[PubMed](#)]
37. Tan, N.; Liu, J.; Li, P.; Sun, Z.; Pan, J.; Zhao, W. Reactive oxygen species metabolism-based prediction model and drug for patients with recurrent glioblastoma. *Aging (Albany Ny)* **2019**, *11*, 11010–11029. [[CrossRef](#)]
38. Chapa-Dubocq, X.R.; Rodriguez-Graciani, K.M.; Guzman-Hernandez, R.A.; Jang, S.; Brookes, P.S.; Javadov, S. Cardiac Function is not Susceptible to Moderate Disassembly of Mitochondrial Respiratory Supercomplexes. *Int. J. Mol. Sci.* **2020**, *21*. [[CrossRef](#)] [[PubMed](#)]
39. Moloney, J.N.; Cotter, T.G. ROS signalling in the biology of cancer. *Semin. Cell Dev. Biol.* **2018**, *80*, 50–64. [[CrossRef](#)]
40. Neupert, W.; Herrmann, J.M. Translocation of proteins into mitochondria. *Annu. Rev. Biochem.* **2007**, *76*, 723–749. [[CrossRef](#)]
41. Korshunov, S.S.; Skulachev, V.P.; Starkov, A.A. High protonic potential actuates a mechanism of production of reactive oxygen species in mitochondria. *FEBS Lett.* **1997**, *416*, 15–18. [[CrossRef](#)]
42. Srinivasan, S.; Guha, M.; Kashina, A.; Avadhani, N.G. Mitochondrial dysfunction and mitochondrial dynamics-The cancer connection. *Biochim. Biophys. Acta Bioenerg.* **2017**, *1858*, 602–614. [[CrossRef](#)] [[PubMed](#)]
43. Tait, S.W.; Green, D.R. Mitochondrial regulation of cell death. *Cold Spring Harb. Perspect. Biol.* **2013**, *5*. [[CrossRef](#)]
44. Fatokun, A.A.; Dawson, V.L.; Dawson, T.M. Parthanatos: Mitochondrial-linked mechanisms and therapeutic opportunities. *Br. J. Pharm.* **2014**, *171*, 2000–2016. [[CrossRef](#)]

45. Baxter, P.; Chen, Y.; Xu, Y.; Swanson, R.A. Mitochondrial dysfunction induced by nuclear poly(ADP-ribose) polymerase-1: A treatable cause of cell death in stroke. *Transl. Stroke Res.* **2014**, *5*, 136–144. [[CrossRef](#)] [[PubMed](#)]
46. Chinopoulos, C.; Seyfried, T.N. Mitochondrial Substrate-Level Phosphorylation as Energy Source for Glioblastoma: Review and Hypothesis. *ASN Neuro* **2018**, *10*, 1759091418818261. [[CrossRef](#)]
47. Chinopoulos, C. Acute sources of mitochondrial NAD(+) during respiratory chain dysfunction. *Exp. Neurol.* **2020**, *327*, 113218. [[CrossRef](#)]
48. Ashley, N.; Poulton, J. Mitochondrial DNA is a direct target of anti-cancer anthracycline drugs. *Biochem. Biophys. Res. Commun.* **2009**, *378*, 450–455. [[CrossRef](#)]
49. Mishra, P.; Chan, D.C. Metabolic regulation of mitochondrial dynamics. *J. Cell Biol.* **2016**, *212*, 379–387. [[CrossRef](#)]
50. Rehman, J.; Zhang, H.J.; Toth, P.T.; Zhang, Y.; Marsboom, G.; Hong, Z.; Salgia, R.; Husain, A.N.; Wietholt, C.; Archer, S.L. Inhibition of mitochondrial fission prevents cell cycle progression in lung cancer. *FASEB J.* **2012**, *26*, 2175–2186. [[CrossRef](#)]
51. Inoue-Yamauchi, A.; Oda, H. Depletion of mitochondrial fission factor DRP1 causes increased apoptosis in human colon cancer cells. *Biochem. Biophys. Res. Commun.* **2012**, *421*, 81–85. [[CrossRef](#)] [[PubMed](#)]
52. Pickles, S.; Vigie, P.; Youle, R.J. Mitophagy and Quality Control Mechanisms in Mitochondrial Maintenance. *Curr. Biol.* **2018**, *28*, R170–R185. [[CrossRef](#)] [[PubMed](#)]
53. Boland, M.L.; Chourasia, A.H.; Macleod, K.F. Mitochondrial dysfunction in cancer. *Front. Oncol.* **2013**, *3*, 292. [[CrossRef](#)]
54. Bennett, N.K.; Nguyen, M.K.; Darch, M.A.; Nakaoka, H.J.; Cousineau, D.; Ten Hoeve, J.; Graeber, T.G.; Schuelke, M.; Maltepe, E.; Kampmann, M.; et al. Defining the ATPome reveals cross-optimization of metabolic pathways. *Nat. Commun.* **2020**, *11*, 4319. [[CrossRef](#)] [[PubMed](#)]
55. Warburg, O. On respiratory impairment in cancer cells. *Science* **1956**, *124*, 269–270.
56. Gatenby, R.A.; Gillies, R.J. Why do cancers have high aerobic glycolysis? *Nat. Rev. Cancer* **2004**, *4*, 891–899. [[CrossRef](#)]
57. Kroemer, G.; Pouyssegur, J. Tumor cell metabolism: Cancer’s Achilles’ heel. *Cancer Cell* **2008**, *13*, 472–482. [[CrossRef](#)]
58. LeBleu, V.S.; O’Connell, J.T.; Gonzalez Herrera, K.N.; Wikman, H.; Pantel, K.; Haigis, M.C.; de Carvalho, F.M.; Damascena, A.; Domingos Chinen, L.T.; Rocha, R.M.; et al. PGC-1 $\alpha$  mediates mitochondrial biogenesis and oxidative phosphorylation in cancer cells to promote metastasis. *Nat. Cell Biol.* **2014**, *16*, 992–1003. [[CrossRef](#)]
59. Lin, C.S.; Liu, L.T.; Ou, L.H.; Pan, S.C.; Lin, C.I.; Wei, Y.H. Role of mitochondrial function in the invasiveness of human colon cancer cells. *Oncol. Rep.* **2018**, *39*, 316–330. [[CrossRef](#)]
60. Hirpara, J.; Eu, J.Q.; Tan, J.K.M.; Wong, A.L.; Clement, M.V.; Kong, L.R.; Ohi, N.; Tsunoda, T.; Qu, J.; Goh, B.C.; et al. Metabolic reprogramming of oncogene-addicted cancer cells to OXPHOS as a mechanism of drug resistance. *Redox. Biol.* **2019**, *25*, 101076. [[CrossRef](#)]
61. Zhang, G.; Frederick, D.T.; Wu, L.; Wei, Z.; Krepler, C.; Srinivasan, S.; Chae, Y.C.; Xu, X.; Choi, H.; Dimwamwa, E.; et al. Targeting mitochondrial biogenesis to overcome drug resistance to MAPK inhibitors. *J. Clin. Invest.* **2016**, *126*, 1834–1856. [[CrossRef](#)] [[PubMed](#)]
62. Ashton, T.M.; McKenna, W.G.; Kunz-Schughart, L.A.; Higgins, G.S. Oxidative Phosphorylation as an Emerging Target in Cancer Therapy. *Clin. Cancer Res.* **2018**, *24*, 2482–2490. [[CrossRef](#)] [[PubMed](#)]
63. Sileikyte, J.; Forte, M. The Mitochondrial Permeability Transition in Mitochondrial Disorders. *Oxid. Med. Cell Longev.* **2019**, *2019*, 3403075. [[CrossRef](#)] [[PubMed](#)]
64. Bonora, M.; Wieckowski, M.R.; Chinopoulos, C.; Kepp, O.; Kroemer, G.; Galluzzi, L.; Pinton, P. Molecular mechanisms of cell death: Central implication of ATP synthase in mitochondrial permeability transition. *Oncogene* **2015**, *34*, 1475–1486. [[CrossRef](#)] [[PubMed](#)]
65. Kanno, T.; Fujita, H.; Muranaka, S.; Yano, H.; Utsumi, T.; Yoshioka, T.; Inoue, M.; Utsumi, K. Mitochondrial swelling and cytochrome c release: Sensitivity to cyclosporin A and calcium. *Physiol. Chem. Phys. Med. NMR.* **2002**, *34*, 91–102.
66. Danese, A.; Patergnani, S.; Bonora, M.; Wieckowski, M.R.; Previati, M.; Giorgi, C.; Pinton, P. Calcium regulates cell death in cancer: Roles of the mitochondria and mitochondria-associated membranes (MAMs). *Biochim. Biophys. Acta Bioenerg.* **2017**, *1858*, 615–627. [[CrossRef](#)]

67. Lopez, J.; Tait, S.W. Mitochondrial apoptosis: Killing cancer using the enemy within. *Br. J. Cancer* **2015**, *112*, 957–962. [[CrossRef](#)]
68. Nguyen, C.; Pandey, S. Exploiting Mitochondrial Vulnerabilities to Trigger Apoptosis Selectively in Cancer Cells. *Cancers (Basel)* **2019**, *11*. [[CrossRef](#)]
69. Rathore, R.; McCallum, J.E.; Varghese, E.; Florea, A.M.; Busselberg, D. Overcoming chemotherapy drug resistance by targeting inhibitors of apoptosis proteins (IAPs). *Apoptosis* **2017**, *22*, 898–919. [[CrossRef](#)]
70. Chamcheu, J.C.; Roy, T.; Uddin, M.B.; Banang-Mbeumi, S.; Chamcheu, R.N.; Walker, A.L.; Liu, Y.Y.; Huang, S. Role and Therapeutic Targeting of the PI3K/Akt/mTOR Signaling Pathway in Skin Cancer: A Review of Current Status and Future Trends on Natural and Synthetic Agents Therapy. *Cells* **2019**, *8*. [[CrossRef](#)]
71. Priber, J.; Fonai, F.; Jakus, P.B.; Racz, B.; Chinopoulos, C.; Tretter, L.; Gallyas, F.J.; Sumegi, B.; Veres, B. Cyclophilin D disruption attenuates lipopolysaccharide-induced inflammatory response in primary mouse macrophages. *Biochem. Cell Biol.* **2015**, *93*, 241–250. [[CrossRef](#)] [[PubMed](#)]



© 2020 by the authors. Licensee MDPI, Basel, Switzerland. This article is an open access article distributed under the terms and conditions of the Creative Commons Attribution (CC BY) license (<http://creativecommons.org/licenses/by/4.0/>).

## RESEARCH ARTICLE

# Amiodarone's major metabolite, desethylamiodarone inhibits proliferation of B16-F10 melanoma cells and limits lung metastasis formation in an *in vivo* experimental model

Zita Bogнар<sup>1\*</sup>, Anna Maria Cseh<sup>1</sup>, Katalin Fekete<sup>1</sup>, Csenge Antus<sup>1</sup>, Rita Bogнар<sup>1</sup>, Antal Tapodi<sup>1</sup>, Fadi H. J. Ramadan<sup>1</sup>, Balazs Sumegi<sup>1,2,3†</sup>, Ferenc Gallyas, Jr.<sup>1,2,3</sup>

**1** Department of Biochemistry and Medical Chemistry, University of Pecs, Medical School, Pecs, Hungary, **2** MTA-PTE Nuclear-Mitochondrial Interactions Research Group, Pecs, Hungary, **3** Szentagotthai Research Center, University of Pecs, Medical School, Pecs, Hungary

† Deceased.

\* [zita.bognar@aok.pte.hu](mailto:zita.bognar@aok.pte.hu)



## OPEN ACCESS

**Citation:** Bogнар Z, Cseh AM, Fekete K, Antus C, Bogнар R, Tapodi A, et al. (2020) Amiodarone's major metabolite, desethylamiodarone inhibits proliferation of B16-F10 melanoma cells and limits lung metastasis formation in an *in vivo* experimental model. PLoS ONE 15(9): e0239088. <https://doi.org/10.1371/journal.pone.0239088>

**Editor:** Salvatore V. Pizzo, Duke University School of Medicine, UNITED STATES

**Received:** March 13, 2020

**Accepted:** August 30, 2020

**Published:** September 25, 2020

**Copyright:** © 2020 Bogнар et al. This is an open access article distributed under the terms of the [Creative Commons Attribution License](https://creativecommons.org/licenses/by/4.0/), which permits unrestricted use, distribution, and reproduction in any medium, provided the original author and source are credited.

**Data Availability Statement:** All relevant data are within the manuscript.

**Funding:** This research was funded by Hungarian grants GINOP-2.3.3-15-2016-00025, GINOP-2.3.2-15-2016-00049, EFOP-3.6.1-16-2016-00004, and Higher Education Institutional Excellence Program. Grants were received by authors BS and FGJ. The funders had no role in study design, data collection and decision to publish, or preparation of the manuscript.

## Abstract

Previously, we demonstrated the *in vitro* anti-tumor effects of desethylamiodarone (DEA) in bladder and cervix cancer cell lines. In the present study, we intended to establish its potentiality in B16-F10 metastatic melanoma cells *in vitro* and *in vivo*. We assessed cell proliferation, apoptosis and cell cycle by using sulforhodamine B assay, Muse™ Annexin V & Dead Cell and Muse® Cell Cycle assays, respectively. We determined colony formation after crystal violet staining. For studying mechanistic aspects, immunoblotting analysis was performed. We used a C57BL/6 experimental lung metastasis model for demonstrating *in vivo* anti-metastatic potential of DEA. DEA inhibited *in vitro* proliferation and colony formation, and *in vivo* lung metastasizing properties of B16-F10 cells. It arrested the cells in G0/G1 phase of their cycle likely via p21 in a p53-dependent fashion, and induced caspase mediated apoptosis likely via inversely regulating Bcl-2 and Bax levels, and reducing Akt and ERK1/2 activation. In this study, we provided *in vitro* and *in vivo* experimental evidences for DEA's potentiality in the therapy of metastatic melanomas. Since DEA is the major metabolite of amiodarone, a worldwide used antiarrhythmic drug, safety concerns could be resolved more easily for it than for a novel pharmacological agent.

## Introduction

Desethylamiodarone (DEA), the major metabolite of the widely used antiarrhythmic drug amiodarone (AM) also has antiarrhythmic activity [1]. Both AM and DEA are strongly bound to plasma proteins [2]. During AM treatment, DEA rapidly accumulates in extracardiac tissues; sometimes in higher concentrations than AM itself does [3–5]. Tissue concentrations of

**Competing interests:** The authors have declared that no competing interests exist.

AM and of DEA are hundred to more than thousand times higher than the corresponding plasma concentrations of 1.6–5.3  $\mu\text{M}$  for AM, and 1.7–4.5  $\mu\text{M}$  for AM plus DEA [6]. The most affected are adipose, liver and lung tissues, but skin, pancreas, myocardium and thyroid gland also massively accumulate these drugs. Except for the adipose tissue, concentration of the metabolite are usually higher than that of the parent molecule following chronic administration of AM [7]. Repetitive exposures of cell cultures to AM and DEA resulted in a cumulative and partially saturable uptake. Under all conditions tested, DEA accumulation was higher than that of AM [8]. The mean elimination half-life was found to be about 40 days and varies considerably between individuals [9].

The therapeutic concentration of AM has been recommended to be  $< 5.7 \mu\text{M}$  [10]. However, antiarrhythmic AM therapy is limited by the toxic side effects of both the parent molecule and DEA [11]. These side effects manifest in cardiac, ocular, pulmonary, hepatic, dermatologic, hematological, psychiatric, thyroid and neuromuscular adverse reactions, and chronic AM treatment even can cause epididymitis and syndrome of inappropriate antidiuretic hormone secretion [11]. Based on its tissue accumulation properties and toxic effects, we proposed its potentiality in cancer therapy [12, 13]. In this study, we investigated DEA's therapeutic potentiality in metastatic melanoma since new effective and safe treatments for this type of cancer are urgently needed.

Clarifying melanocyte biology, relevant oncogenic mutations as well as involved molecular signaling pathways on melanomagenesis have expanded our knowledge about melanoma remarkably in the past three decades [14]. However, melanoma is still the most lethal form of skin cancer accounting for approximately 132,000 new cases each year [15]. Despite the inflation of therapeutically approaches, metastatic melanoma still has a very poor prognosis, with a five-year survival rate of 15.1% [15, 16]. The prognosis even worse when the tumor has disseminated to distant sites and visceral organs [17]; the median survival time is only 6–9 months and the 3-year survival rate is about 10–15% [18]. Additionally, metastatic melanoma is highly resistant to chemotherapy. Most conventional chemotherapy agents have failed because of the patients' low response rates [19] and significant toxicity of the agents [20, 21] emphasizing the importance of finding novel therapeutic tools. Accordingly, in this study we investigated the effect of DEA on growth, apoptosis of B16-F10 melanoma cells, and on lung metastasis formation in an *in vivo* experimental model.

## Materials and methods

### Materials

Protease inhibitor cocktail and all chemicals for cell culture were purchased from Sigma-Aldrich Co. (Budapest, Hungary). DEA was a gift from Professor Andras Varro (Department of Pharmacology and Pharmacotherapy, University of Szeged, Szeged, Hungary). The following primary antibodies were used: anti-Bcl-2, anti-Bax, anti-caspase 3 (clone H-277), anti-poly (ADP-ribose) polymerase 1 (PARP-1), anti-Akt, anti-phospho-Akt (Ser<sup>473</sup>), anti-extracellular signal-regulated kinase (ERK1/2) (Thr<sup>202</sup>/Tyr<sup>204</sup>), anti-phospho-ERK1/2 (Thr<sup>202</sup>/Tyr<sup>204</sup>), anti-p53, anti-p21, anti-p27, anti-cyclin dependent kinase (CDK)2, anti-cyclin D1 each 1:500 dilution and anti-glyceraldehyde-3-phosphate dehydrogenase (GAPDH) (1:2000, clone 6C5). Antibodies were purchased from Cell Signaling Technology (Beverly, MA, USA) except caspase 3, PARP-1, which were bought from Santa Cruz Biotechnology (Wembley, UK), while anti-GAPDH antibody was obtained from EMD Millipore Bioscience (Darmstadt, Germany).

### Cell culture

Metastatic melanotic B16-F10 mouse melanoma cell line was purchased from the American Type Culture Collection (LGC Standards, Wesel, Germany). Cells were cultured in Dulbecco's

modified Eagle's medium supplemented with 10% fetal bovine serum and an antibiotic solution (1% penicillin and streptomycin mixture) (Life Technologies, Darmstadt, Germany). Cells were maintained in a humidified environment at 37°C with 5% CO<sub>2</sub>. They were split twice weekly for up to a maximum of 10 weeks. Cells were tested by MycoAlert™ Plus Mycoplasma detection kit monthly.

### Cell proliferation assay

B16-F10 cells (10<sup>5</sup>/well) were cultured in 96-well cell culture plates overnight and treated with different concentrations (2.5–10 μM) of DEA. The attached cells were fixed in situ with addition of cold 10% trichloroacetic acid solution at 0, 24, 48 and 72 hours after treatment. Cell number (absorbance) was then estimated by the sulforhodamine B (SRB) assay, as previously described [22]. Proliferation was assessed by comparing light absorbance measured at the first time and was presented as fold values. The measurements were performed in quadruplicates and repeated three times.

### Cell viability assay

B16-F10 cells (3 × 10<sup>5</sup>/well) were plated in 24-well plates, cultured overnight and treated with the indicated concentration of DEA for 24, 48 or 72 hours. Cell viability after DEA treatment was quantified using the Muse™ Cell Count & Viability Assay, and the flow cytometry-based Muse™ Cell Analyzer (EMD Millipore Bioscience) according to the instructions provided by the manufacturer. Cell viability was expressed as the relative percentage of living cells of the control samples. The experiments were performed in quadruplicate and repeated three times.

### Colony formation assay

B16-F10 cells were plated in triplicates into 6-well plates at a starting density of 500 cells/well, before treating them with different concentrations of DEA. After 7 days of incubation, the cells were washed and stained with crystal violet and the colonies with diameter of > 0.5 mm were counted. The number of colonies was determined and normalized to the number of colonies in the controls. All experiments were repeated three times.

### Detection of apoptosis

For quantitative analysis of apoptosis, we used the Muse™ Annexin V & Dead Cell Assay on a Muse™ Cell Analyzer. The assay utilizes annexin V to detect phosphatidylserine on the external membrane of apoptotic cells. B16-F10 cells at a starting density of 1 × 10<sup>6</sup> cells were seeded onto regular plates and treated for 24 hours without or with the indicated concentrations of DEA. The cells were harvested, and 100 μL of cell suspension was added to 100 μL of the Muse™ Annexin V & Dead Cell reagent. After 20 minutes of incubation at room temperature in the dark, the samples were analyzed according to the manufacturer's protocol. All experiments were repeated three times.

### Cell cycle assay

After treatment with DEA (10 μM) for 24 hours, B16-F10 cells were collected by centrifugation at 300 × g for 5 minutes, washed with ice-cold phosphate buffered saline (PBS), fixed with 70% ethanol, stained with a premixed reagent composed of the nuclear DNA intercalating stain propidium iodide (PI) and RNase A in a proprietary formulation, and analyzed according to the manufacturer's protocol. PI discriminates cells at different stages of the cell cycle, based on differential DNA content in the presence of RNase to increase the specificity of DNA staining.

The Muse Cell Cycle Software Module performs calculations automatically. All experiments were repeated three times.

### Immunoblot analysis

B16-F10 cells at a starting density of  $1 \times 10^6$  cells were seeded into regular plates and treated as for the cell viability assay. Cells were harvested at intervals in a chilled lysis buffer containing 0.5 mM sodium-metavanadate, 1 mM EDTA and protease and phosphatase inhibitor cocktails (1:200), all purchased from Sigma–Aldrich Co. Cell lysates were boiled and subjected to 10% sodium dodecyl sulfate polyacrylamide gel electrophoresis before being transferred to nitrocellulose membranes. The membranes were blocked in 5% low-fat milk for 1.5 hours at room temperature before being exposed to primary antibodies at 4°C overnight in a blocking solution. Appropriate horseradish peroxidase-conjugated secondary antibodies were used at a dilution of 1:5000 (anti-mouse and anti-rabbit IgGs; Sigma–Aldrich Co.) and visualized by enhanced chemiluminescence (Amersham Biosciences, Piscataway, New Jersey, USA). The films were scanned, and the pixel volumes of the bands were determined using NIH Image J software (Bethesda, Maryland, USA). For membrane stripping and reprobing, the membranes were washed in a stripping buffer (0.1 M glycine, 5 M MgCl<sub>2</sub>, pH 2.8) for an hour at room temperature. After washing and blocking, the membranes were incubated with primary antibodies for nonphosphorylated or loading control proteins. All experiments were repeated three times.

### Ethics

Animal experiments were conducted in strict accordance with the recommendations in the Guide for the Care and Use of Laboratory Animals of the National Institutes of Health. The experimental protocol was approved by the Animal Research Review Committee of the University of Pécs, Hungary (Permit number: BA02/2000-5/2017).

### Mouse pulmonary metastasis model

Six weeks old male C57BL/6 mice were bred and maintained at the Department of Biochemistry and Medical Chemistry, University of Pécs, Medical School. All animals were housed 3 or 4 per cage, under controlled laboratory conditions ( $22 \pm 1^\circ\text{C}$ , 50 – 60% relative humidity and 12/12 hour light-dark cycles) with free access to water and standard rodent chow. Paper tunnels were used for environmental enrichment.

We used the pulmonary metastasis model that is widely used as an *in vivo* test for assessing antitumor efficacy of medications [23]. B16-F10 cells ( $5 \times 10^5/0.1$  ml) were injected into the lateral tail vein of mice using 30G 1/2 needle and 1-ml syringe. There were no changes observed in motility or food intake in tumor bearing animals during the experiment. All animals were checked at least once daily for aspects of general health including activity, posture and fur grooming, body condition score was also assessed as previously described [24].

The mode of DEA administration and dosage were determined based on the study by DeWitt et al. [25]. Prior to the study, safety of DEA treatment was confirmed by administration of 25 mg/kg DEA to 5 mice for two weeks. Mice were randomly divided into 2 groups of 6 mice each. Each mouse was given a daily intraperitoneal injection of either 100  $\mu$ l 0.9% saline solution containing 10% ethanol as the vehicle control or 25 mg/kg DEA. Treatment was started one day after cell injection and was given every third day, lasted for consecutive 16 days after injection when the animals were weighed and sacrificed by cervical dislocation under isoflurane (AbbVie Ltd., Budapest, Hungary) anesthesia. The lungs were removed, rinsed in PBS, and weighed. The lung mass index was calculated as the ratio of lung weight to body weight. The harvested lungs were fixed in 4% formalin. Tumor nodules on the surfaces of the lungs

were counted under a stereomicroscope. Then, the whole lung was embedded in optimum cutting temperature compound (Sakura Finetek, USA), sectioned (12  $\mu\text{m}$  thickness), and stained with hematoxylin and eosin. Histological observations were performed under a microscope (BX51, Olympus, Japan) by an expert blind to the experiment. Percentage of the total area occupied by tumor was measured using the Panoramic viewer 1.15.4 (3DHISTECH, Hungary).

## Data analysis

All data are expressed as mean  $\pm$  standard deviation (SD). The concentration-dependent effects of DEA in each experiment were tested with ANOVA using the post hoc Dunnett test. We used the Mann-Whitney U test to compare the treated example to the vehicle-treated control. Differences were considered significant at values of  $p \leq 0.05$ . Statistical analyses were performed using IBM SPSS Statistics v20.0 (IBM Corporation, New York, USA).

## Result

### Effects of DEA on cell viability

B16-F10 murine melanoma cells in monolayer culture were treated with increasing concentrations of DEA for 24, 48 and 72 hours. DEA had a statistically significant antiproliferative and cell death-inducing effect on the cells determined by using the SRB assay (Fig 1A) and the Muse™ Cell Count & Viability Assay (Fig 1B). The vehicle-treated cells served as negative controls. These data indicate that DEA induces cell death in a dose- and time-dependent manner; therefore, the possible pathways contributing to DEA-induced cell death were further analyzed.

### Effect of DEA on colony formation

To assess DEA's effect on colony forming ability of the B16-F10 cells, a long-term assay was performed. We treated the cells with 0–3  $\mu\text{M}$  DEA for 7 days then colonies of  $> 0.5$  mm were counted. As we found, DEA significantly decreased number and size of the colonies even at the lowest concentration used (Fig 2). These data indicate that DEA can induce cell death and can inhibit colony formation at low micromolar concentrations.

### Effect of DEA on activation of apoptosis in B16-F10 cells

Flow cytometry with the Muse™ Annexin V & Dead Cell Assay was used to investigate the mode of DEA induced cell death. The assay utilizes cell surface annexin V binding that measures appearance of phosphatidylserine on the plasma membrane's external surface, a marker of apoptosis. We observed that DEA increased the total apoptosis rate in a dose-dependent manner. We found a total apoptosis rate of  $34.61 \pm 2.17\%$  for 5 and  $73.71 \pm 3.12\%$  for 10  $\mu\text{M}$  DEA in contrast to the control's  $10.11 \pm 1.97\%$  (Fig 3A). At the lower DEA concentration, rate of early apoptosis exceeded that of the late, however, at the higher concentration, late apoptosis predominated (Fig 3A).

### Effect of DEA on apoptosis related proteins in B16-F10 cells

To examine how treatment with DEA affects the steady-state levels of apoptosis related proteins, B16-F10 cells were treated with 5 and 10  $\mu\text{M}$  of DEA for 24 hours, then the cells were lysed, and immunoblot analyses were performed on the extracted proteins. We found that the expression of Bcl-2 was significantly decreased as compared with control while the expression of Bax was significantly increased (Fig 3B and 3C). Additionally, DEA dose-dependently



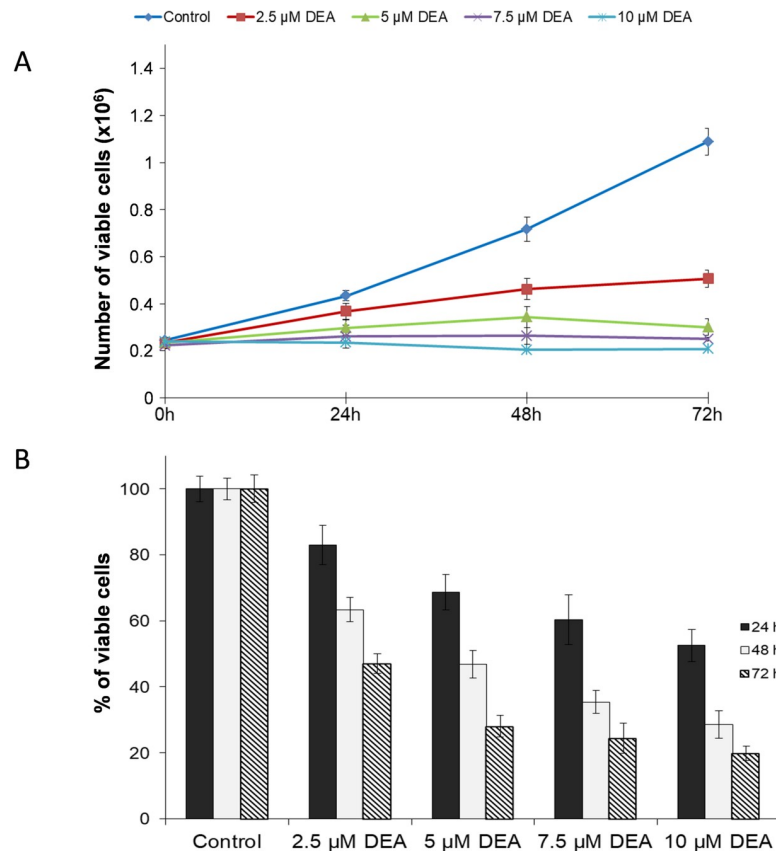


**Fig 1. Effect of DEA on cell proliferation and viability of B16-F10 murine melanoma cells.** The cells were incubated with the indicated concentrations of DEA for 24, 48 and 72 hours. Controls were treated with vehicle (0.2% DMSO). Cell proliferation and viability were assessed by using the SRB assay (A) and the Muse™ Cell Count & Viability Assay (B). Data represent means  $\pm$  SD of three independent experiments performed in at least quadruplicate. Data were analyzed using ANOVA with Dunett post hoc test. \*\*  $p \leq 0.01$  and \*\*\*  $p \leq 0.001$  compared to the corresponding control group.

<https://doi.org/10.1371/journal.pone.0239088.g001>

activated the effector caspase, caspase 3, which activation was confirmed by corresponding cleavage of PARP-1, a target of caspase 3 (Fig 3B and 3C). These data indicate that DEA predominantly activates apoptotic cell death via several pathways that can be an advantage in cancer therapy, where apoptotic pathways can be inactivated during the development of cytostatic resistance.

### Effect of DEA on the cell cycle in B16-F10 cells

Cell proliferation is the net result of cell division and cell death. Although the data presented in Fig 3 suggest that DEA limits proliferation of B16-F10 by inducing predominantly apoptotic cell death, we performed cell cycle analysis to study the other aforementioned aspect of proliferation. We treated B16-F10 cells with 5 and 10  $\mu$ M DEA for 24 hours, and found that the percentage of cells in G0/G1 phase significantly increased from  $56.75 \pm 1.73\%$  (0  $\mu$ M) stepwise to  $63.9 \pm 1.94\%$  (5  $\mu$ M) and  $75.91 \pm 2.67\%$  (10  $\mu$ M). At the same time there was a decrease in the percentage of S and G2/M phase cells (Fig 4A). These data indicate that DEA at both concentrations induced cell cycle arrest in the G0/G1 phase that may contribute to its overall inhibitory effect on B16-F10 cell proliferation.

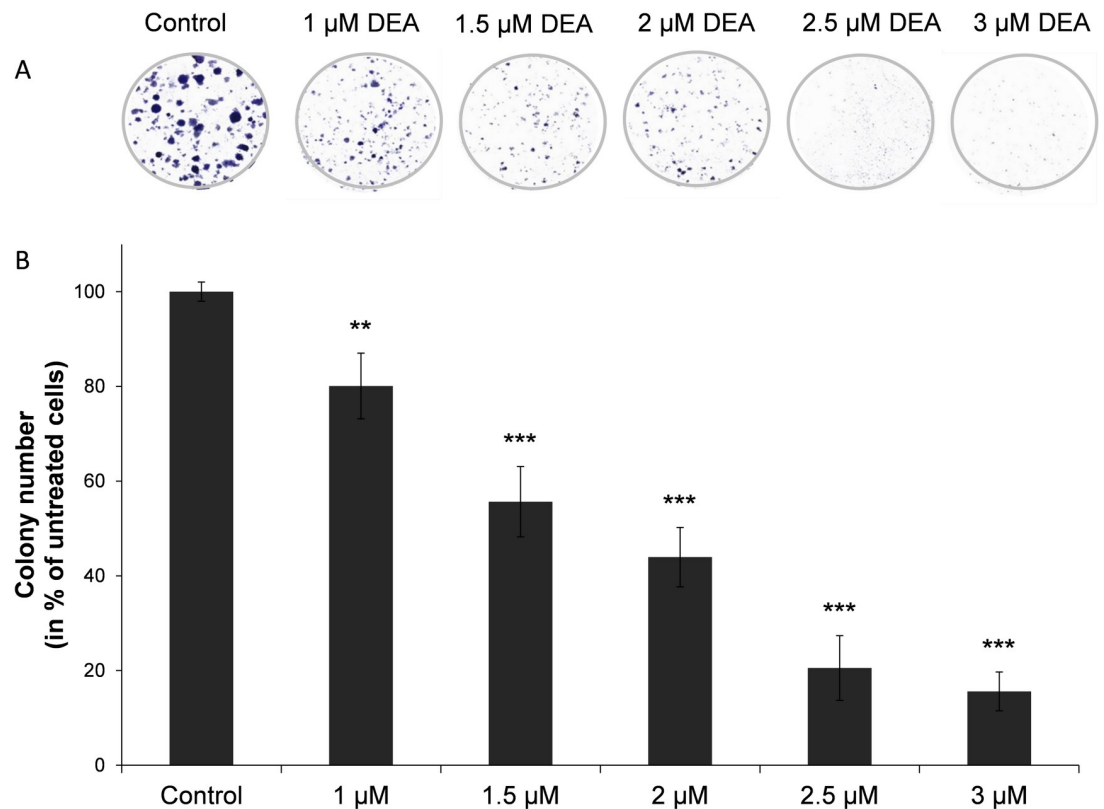


**Fig 2. Effect of DEA on colony formation of B16-F10 murine melanoma cells.** For the assay the cells were exposed to increasing concentrations of DEA for 7 days. The results are presented as representative images (A) and as a bar diagram (B). Controls were treated with vehicle (0.2% DMSO). The results are mean  $\pm$  SD of three independent experiments performed in at least quadruplicate. Data were analyzed using ANOVA with Dunett post hoc test. \*\*  $p \leq 0.01$  and \*\*\*  $p \leq 0.001$  compared to the control group.

<https://doi.org/10.1371/journal.pone.0239088.g002>

To investigate the mechanisms of DEA-induced cell cycle arrest, we examined the expression of cell cycle-related proteins by immunoblotting. DEA treatment (10  $\mu$ M) for 24 hours, significantly increased p53, p21 and p27 while decreased CDK2 and cyclin D1 steady-state protein levels (Fig 4B and 4C).

### Effect of DEA on cytoprotective kinase signaling pathways

ERK promotes cell proliferation, differentiation and survival, while Akt is considered as a major cell and tissue protecting pathway. Therefore, we wanted to know whether DEA affected activation of these kinases. To this end, we determined phosphorylation status of Akt, ERK1/2 in B16-F10 cells treated with 0–10  $\mu$ M DEA by using phosphorylation specific primary antibodies and immunoblotting. As we found, DEA did not affect Akt or ERK1/2 steady-state protein level at either concentration used. However, there was a concentration-dependent down-regulation of Akt Ser<sup>473</sup> phosphorylation upon DEA treatment (Fig 5A and 5B). Basically, identical results were found for ERK1/2 (Fig 5A and 5B).

### Effect of DEA on lung metastasis formation in an *in vivo* experimental model

To evaluate the effect of DEA on metastasis formation, we used an *in vivo* lung metastasis model. Murine melanoma B16-F10 cells were injected into the lateral tail vein of 6-weeks-old

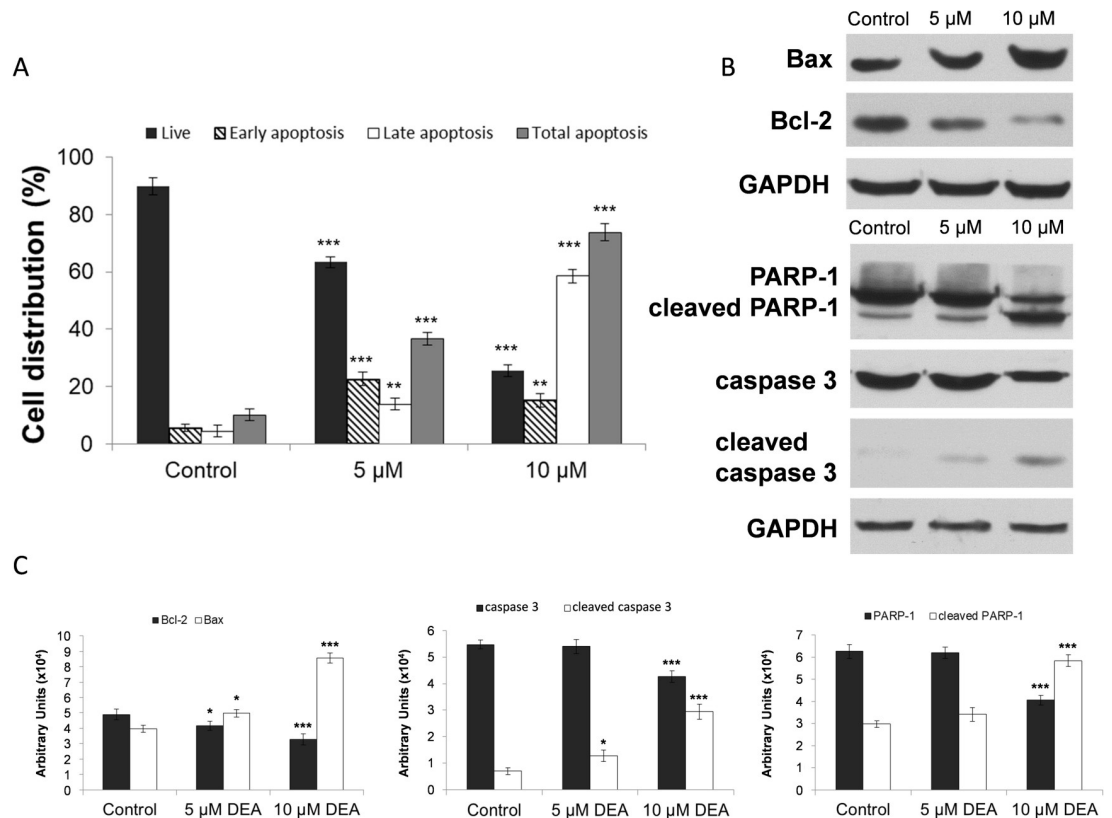


**Fig 3. Effect of DEA on activation of apoptosis in B16-F10 cells.** After subjected to 24 hours treatment with increasing concentrations of DEA the cells were stained with the Muse™ Annexin V & Dead Cell Reagent and measured on the Muse™ Cell Analyzer. (A) The bar chart shows the percent distribution of living (dark gray bars), early apoptotic (striped bars), late apoptotic (white bars) and total apoptotic cells (light gray bars). Controls were treated with vehicle (0.2% DMSO). (B) Immunoblot analysis on total cell lysates was performed using antibodies against Bax, Bcl-2, PARP-1, caspase 3 and cleaved caspase 3. The results of the immunoblot analysis and the densitometric analysis of the immunoblots are presented in panels B and C. The experiments were repeated three times in at least quadruplicate, and the results are expressed as the mean  $\pm$  SD. Data were analyzed using ANOVA with Dunnett post hoc test (A) and with Mann-Whitney U test (C). \*  $p \leq 0.05$ , \*\*  $p \leq 0.01$  and \*\*\*  $p \leq 0.001$  compared to the corresponding control group.

<https://doi.org/10.1371/journal.pone.0239088.g003>

male C57BL/6 mice then they were divided into two groups (6 mice/group). Intraperitoneal administration of 25 mg/kg DEA or vehicle control was started 24 hours after tumor cell administration, and was repeated every third day. At the 16<sup>th</sup> day of the experiment, the animals were sacrificed and the lungs were removed for analysis. The lungs were weighted and lung mass index was calculated (Fig 6A). After the lungs were fixed in 4% formalin and photographed (Fig 6B) and the number of tumor nodules on the lungs' surface was also determined (Fig 6C). Accordingly, DEA treatment diminished lungs mass index and the number of tumor nodules (Fig 6A and 6C).

Additionally, histopathological analysis was performed by an expert who was blind to the experiment on lung tissue sections after hematoxylin and eosin staining. There were melanoma cells with polyedric morphology with a great amount of melanin content as cytoplasm granules or in a perinuclear distribution. Additionally, aberrant nodular proliferation in broncho-alveolar regions characteristic of epithelial melanoma was observed in all sections (Fig 7A–7D). However, there was a marked difference in tumor nodule pattern distribution and concentration between untreated and DEA treated animals. In the vehicle treated group, the nodules were of considerable size and were distributed in all part of the lung parenchyma (Fig

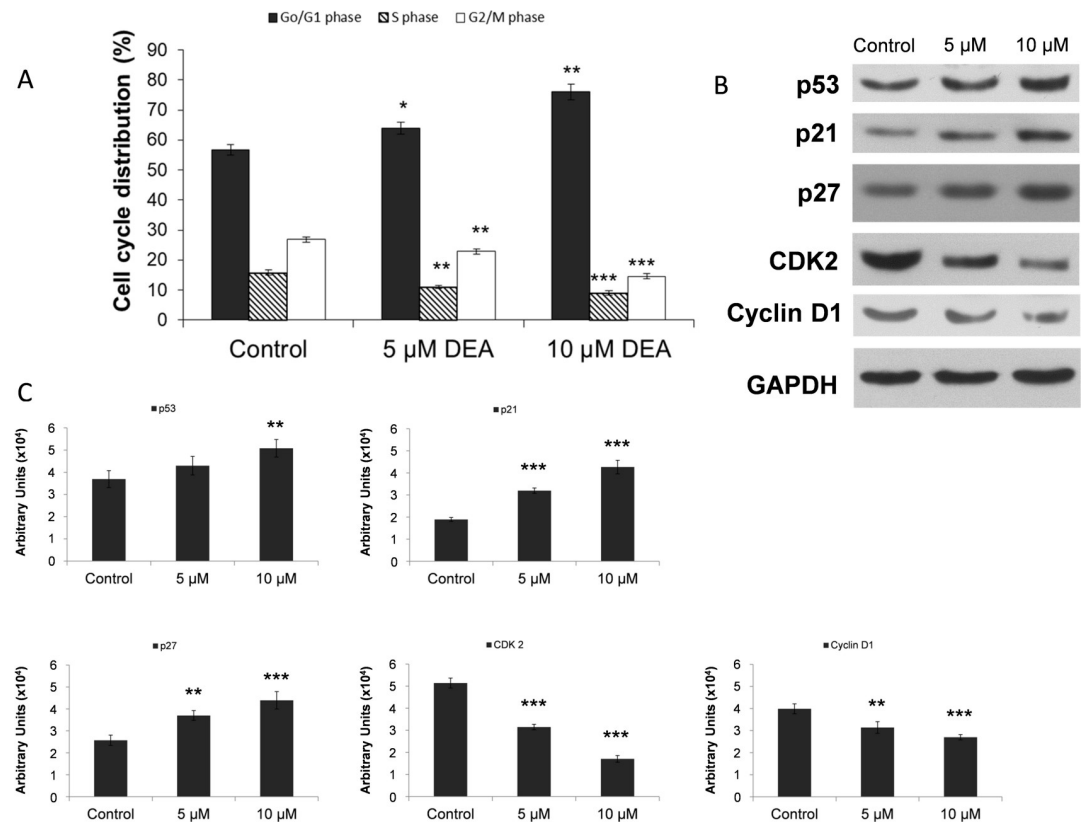


**Fig 4. Effect of DEA on the cell cycle in B16-F10 melanoma cells.** The cells were treated with different concentrations of DEA (0, 5 and 10  $\mu$ M) for 24 hours. Controls were treated with vehicle (0.2% DMSO). Then they were harvested, fixed with ethanol and stained with propidium iodide. DNA content was determined by Muse™ Cell Analyzer. The results are presented as a bar diagram, percentage of cells in G0/G1 (dark grey bars), S (striped bars) and G2/M phases (white bars) of the cell cycle (A). Proteins from parallel cells were extracted for immunoblot analysis performed by using antibodies specific to p53, p21, p27, CDK2 and cyclin D1. GAPDH was used as a loading control. The results are presented as representative immunoblots (B) and densitometric analysis of immunoblots in bar diagrams (C). The results are mean  $\pm$  SD of three independent experiments performed in at least quadruplicate. Data were analyzed using ANOVA with Dunnett post hoc test (A) and with Mann-Whitney U test (C). \*  $p \leq 0.05$ , \*\*  $p \leq 0.01$  and \*\*\*  $p \leq 0.001$  compared to the corresponding control group.

<https://doi.org/10.1371/journal.pone.0239088.g004>

7A and 7B). In contrast, in the DEA group (Fig 7C and 7D), the tumor nodules were much smaller in size and were organized in a predominantly peripheral distribution (Fig 7C and 7D). To quantify the morphological observations, image analysis with the Panoramic Viewer Imaging System was performed on randomly selected sections (6 per lungs), and tumor area as the percentage of lung section area was calculated. As we found, the tumor area was significantly decreased in the lung tissue of DEA vs. vehicle treated animals (Fig 7E). These results are in complete accordance with those of the macroscopic observations (Fig 6) and indicate that DEA can inhibit melanoma tumor metastasis *in vivo*.

## Discussion

Previously, we demonstrated that DEA significantly inhibited the proliferation and viability of T24 human transitional cell bladder carcinoma and HeLa human cervical cancer cell lines [12, 13]. It mitigated colony formation *in vitro*, as well as it induced apoptosis and G0/G1 phase cell cycle arrest in a dose-dependent manner [12, 13], exactly as it did in the present study in mouse B16-F10 melanoma cells (Figs 1–4). *In vitro* antiproliferative and apoptosis-promoting properties of a drug represent a rather poor translational value for its potentiality in human

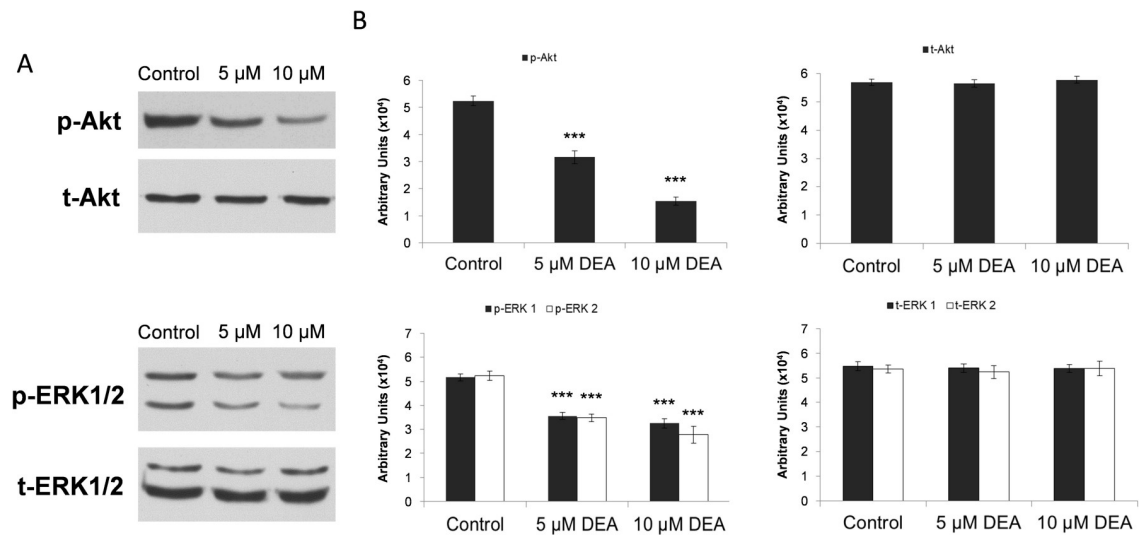


**Fig 5. Effect of various DEA concentrations on the activation of cytoprotective signaling kinases in B16-F10 cells.** Total cell extracts were analyzed by immunoblotting 24 hours after the DEA treatments. Activation of Akt and ERK1/2 as well as equal protein loading was confirmed by kinase specific primary antibodies: anti-Akt (t-Akt), anti-phospho-Akt (p-Akt), anti-ERK1/2 (t-ERK1/2) and anti-phospho-ERK1/2 (p-ERK1/2). The figure shows the results of the immunoblots (A) and the densitometric analysis (B) of three independent experiments. Data are expressed as the mean  $\pm$  SD, and presented as arbitrary unit. Data were analyzed using Mann-Whitney U test. \*\*\*  $p \leq 0.001$  compared to the control group.

<https://doi.org/10.1371/journal.pone.0239088.g005>

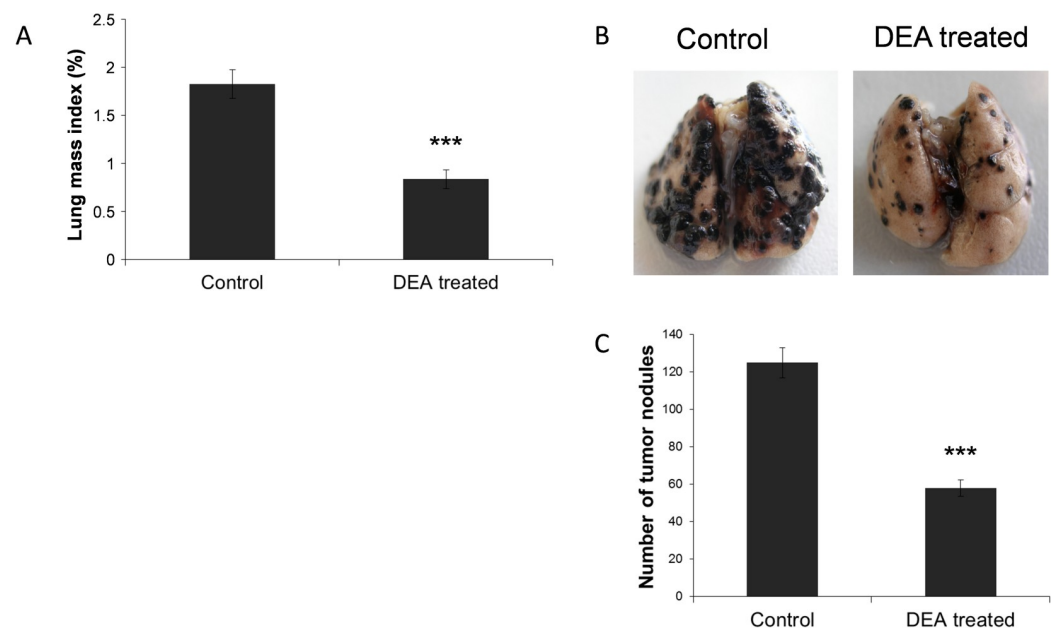


**Fig 6. Effect of DEA on lung metastasis formation in vivo.** Lung metastasis in C57BL/6 mice was induced by injecting B16-F10 cells into the lateral tail vein. Control animals received vehicle control (100  $\mu$ l 0.9% saline solution containing 10% ethanol) 24 hours after the administration of the B16 F10 cells, while the DEA group was treated with 25 mg/kg DEA intraperitoneally (6 mice/group). Treatment was repeated every third day. At the 16<sup>th</sup> day, the mice were sacrificed, the lungs were dissected, photographed and their mass was measured. Representative photos (A) of lungs of control and DEA treated animals are presented. Lung mass index (B) and the number of tumor nodules on the on lungs' surface (C) are presented as bar diagrams, mean  $\pm$  SD. Data were analyzed using Mann-Whitney U test. \*\*\*  $p \leq 0.001$  compared to control group.

<https://doi.org/10.1371/journal.pone.0239088.g006>

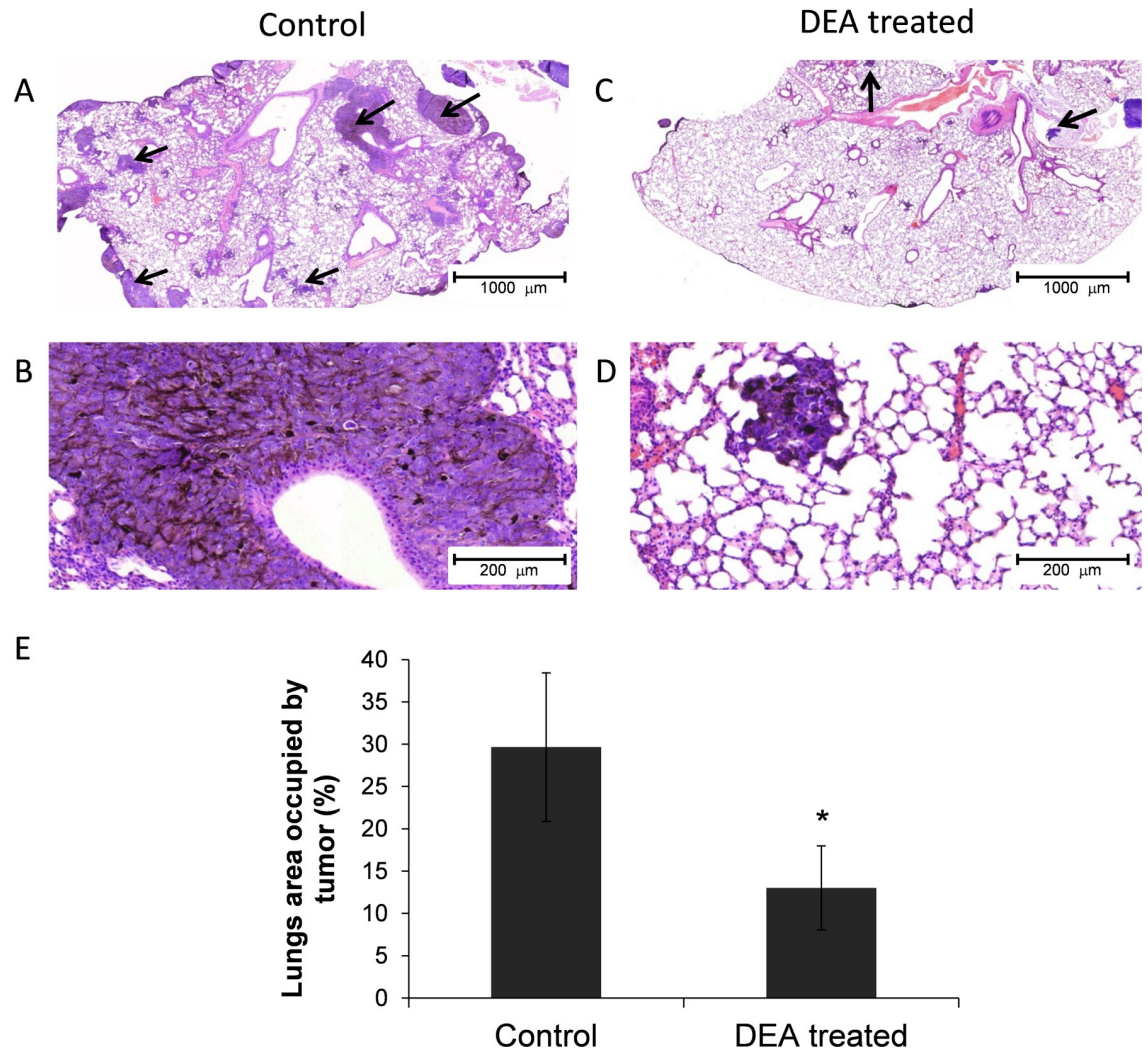


**Fig 7. Histopathology analysis on lung tissue of mice injected with B16-F10 melanoma cells.** Lungs of B16-F10 injected animals treated with vehicle control or 25mg/kg DEA every third day for 16 days were fixed in neutral buffered formalin, sectioned and stained with hematoxylin and eosin. Representative sections (A-D) demonstrate darkly stained tumor nodules (arrows). Metastasis formation was quantitatively assessed by determining the tumor area (E) as percentage of the total lung section area, means  $\pm$  SD from 6 randomly selected section per lung by using the Panoramic Viewer Imaging System. Data were analyzed using Mann-Whitney U test. \*  $p \leq 0.05$  compared to control.

<https://doi.org/10.1371/journal.pone.0239088.g007>

cancer therapy. On the other hand, a uniform effect on three very different, highly proliferative cell lines indicate that DEA interferes with fundamental survival promoting processes likely present in most cancer cell lines of different tissue and species origin.

A defective apoptosis signaling pathway has been considered a major cause of chemoresistance in melanoma. High expression of Bcl-2 is correlated with resistance to chemotherapy in human melanomas and other tumors [26]. Furthermore, in wild-type p53 expressing melanoma cell lines such as B16-F10, cytostatic agents induce G1 arrest and down-regulation of Bcl-2 [27–29]. In a complete agreement with this view, we found DEA to act as an apoptosis-stimulating factor for the melanoma cells presumably via upregulation of p53 and Bax, and downregulation of Bcl-2 (Figs 3 and 4). The resulting apoptosis likely involved mitochondrial mechanisms leading to caspase 3 activation as it was evidenced by cleavage of caspase 3 and its downstream target PARP-1 (Fig 3).

A number of evidence indicates that G1/G0 arrest occurs during the early steps of apoptosis in different cancer types following cytostatic treatment [30, 31]. For melanomas, regulators of the cell cycle's G1 phase transition such as D and E type cyclins, CDK4/6, CDK inhibitors including p16 and p14, and retinoblastoma protein were suggested as diagnostic tools or therapeutic targets [13, 32–34]. Accordingly, we determined DEA's effect on the cell cycle as well as on the metastasis inducer markers cyclin D1 and CDK2 [13, 35], the tumor suppressor p53 [36], and the cell cycle inhibitors p21 and p27 [37]. As we found, in a concentration dependent manner, DEA increased number of cells in the G0/G1 phase that was accompanied by reduced steady state levels of cyclin D1 and CDK2, and increased levels of p21, p27 and p53 (Fig 4). Because the p53 gene is not mutated in B16-F10 cells [27, 28], the observed induction of G1 phase arrest by DEA was likely mediated through p21, in a p53-dependent fashion.

Sustained activation of intracellular prosurvival signaling cascades such as the phosphatidylinositol 3-kinase/Akt pathway has been showed to significantly enhance cancer progression. Akt promotes cell survival and proliferation by suppressing apoptosis and stimulating cell cycle advancement [38, 39]. Progression and malignancy of various tumors is often associated with the constitutive activation of Akt [38, 40], which inactivates many proapoptotic proteins by phosphorylation [39]. The invasiveness of melanoma cells and their ability to form metastases may be related to the frequently observed high basal activity of Akt in these cells [41]. Our group showed that the high basal levels of active, phosphorylated Akt [38, 42] was decreased dose dependently by DEA treatment in B16-F10 cells (Fig 5), a highly invasive variant of B16 murine melanoma. This decrease in the activation of Akt may contribute to the effects of DEA on the cell cycle (Fig 4) and apoptosis (Fig 3).

The ERK pathway participates in the phosphorylation over 250 cellular substrates [43] thereby regulating various cellular processes such as cell adhesion, cell cycle progression, migration, survival, differentiation, metabolism, proliferation, and transcription [44]. Its activation was reported to induce cell cycle entry and G1 progression by upregulating proliferative transcription factors [45] and downregulating antiproliferative genes [46]. Accordingly, in melanomas, apoptotic resistance and metastatic property was reported to be associated with ERK pathway activation [47, 48]. Similarly to Akt, we observed a high basal level of activated ERK1/2 in the B16-F10 melanoma cell line that was diminished by DEA treatment in a dose dependent manner again without affecting total ERK1/2 steady-state level (Fig 5). Like in the case of Akt, attenuation of ERK1/2 activation could likely contribute to DEA's effect on cell cycle (Fig 4) and apoptosis (Fig 3).

Metastasis is fundamental property of malignant cancer cells by which a certain cancer spreads from the location at which a tumor first arises to distant locations in the body [49, 50]. Cancer recurrence by metastasis is responsible for about 90% of mortality in cancer patients [51] and is currently a main target for cancer therapy. Metastasizing proceeds in a series of sequential steps including invasion, intravasation, survival and translocation in the circulation system, extravasation and survival in a new organ [52]. Within its limitations, the B16-F10 lung metastasis model [53] mimics all but the first two steps of this process. During the period of 16 days, the B16-F10 injected into tail vein of the animals formed a number of large tumor loci in the lungs (Fig 6) that occupied about 30% of tissue area in the lungs sections (Fig 7). Both number and size of the tumor loci were reduced by DEA (Figs 6 and 7) indicating that the drug has potentiality in reducing *in vivo* metastasis formation. However, the B16-F10 cells are of mouse tissue culture and not of human primary tumor origin. Additionally, they have been selected for their metastasizing property, and therefore have low immunogenicity [54]. Accordingly, further studies are needed preferably by using primary human melanomas to establish DEA's potentiality in the therapy of metastatic melanomas.

## Conclusion

In this study, we provided *in vitro* and *in vivo* experimental evidences for DEA's potentiality in the therapy of metastatic melanomas. Since DEA is the major metabolite of amiodarone, a worldwide used antiarrhythmic drug, safety concerns could be resolved more easily for it than for a novel pharmacological agent.

## Supporting information

**S1 File.**  
(ZIP)

## Author Contributions

**Conceptualization:** Zita Bogнар, Katalin Fekete, Rita Bogнар, Balazs Sumegi, Ferenc Gallyas, Jr.

**Data curation:** Anna Maria Cseh, Rita Bogнар.

**Formal analysis:** Rita Bogнар, Antal Tapodi, Fadi H. J. Ramadan, Ferenc Gallyas, Jr.

**Investigation:** Zita Bogнар, Anna Maria Cseh, Katalin Fekete, Csenge Antus, Antal Tapodi, Fadi H. J. Ramadan.

**Methodology:** Zita Bogнар, Anna Maria Cseh, Katalin Fekete, Rita Bogнар, Antal Tapodi, Balazs Sumegi, Ferenc Gallyas, Jr.

**Project administration:** Rita Bogнар, Antal Tapodi.

**Supervision:** Balazs Sumegi, Ferenc Gallyas, Jr.

**Visualization:** Katalin Fekete, Csenge Antus, Antal Tapodi, Fadi H. J. Ramadan.

**Writing – original draft:** Zita Bogнар, Katalin Fekete, Balazs Sumegi, Ferenc Gallyas, Jr.

**Writing – review & editing:** Zita Bogнар, Anna Maria Cseh, Katalin Fekete, Csenge Antus, Rita Bogнар, Antal Tapodi, Fadi H. J. Ramadan, Ferenc Gallyas, Jr.

## References

1. Pallandi RT, Campbell TJ. Resting, and rate-dependent depression of Vmax of guinea-pig ventricular action potentials by amiodarone and desethylamiodarone. *Br J Pharmacol.* 1987; 92: 97–103. <https://doi.org/10.1111/j.1476-5381.1987.tb11300.x> PMID: 3664094
2. Lalloz MR, Byfield PG, Greenwood RM, Himsworth RL. Binding of amiodarone by serum proteins and the effects of drugs, hormones and other interacting ligands. *J Pharm Pharmacol.* 1984; 36: 366–372. <https://doi.org/10.1111/j.2042-7158.1984.tb04400.x> PMID: 6146666
3. Daniels JM, Brien JF, Massey TE. Pulmonary fibrosis induced in the hamster by amiodarone and desethylamiodarone. *Toxicol Appl Pharmacol.* 1989; 100: 350–359. [https://doi.org/10.1016/0041-008x\(89\)90321-9](https://doi.org/10.1016/0041-008x(89)90321-9) PMID: 2781562
4. Nokin P, Jungbluth L, Mouton J. Protective effects of amiodarone pretreatment on mitochondrial function and high energy phosphates in ischaemic rat heart. *J Mol Cell Cardiol.* 1987; 19: 603–614. [https://doi.org/10.1016/s0022-2828\(87\)80366-8](https://doi.org/10.1016/s0022-2828(87)80366-8) PMID: 3625789
5. Vander Elst L, Goudemant JF, Mouton J, Chatelain P, Van Haverbeke Y, Muller RN. Amiodarone pretreatment effects on ischemic isovolumic rat hearts: a P-31 nuclear magnetic resonance study of intracellular pH and high-energy phosphates contents evolutions. *J Cardiovasc Pharmacol.* 1990; 15: 377–385. PMID: 1691360
6. Holt DW, Tucker GT, Jackson PR, Storey GC. Amiodarone pharmacokinetics. *Am Heart J.* 1983; 106: 840–847. [https://doi.org/10.1016/0002-8703\(83\)90006-6](https://doi.org/10.1016/0002-8703(83)90006-6) PMID: 6613830



7. Brien JF, Jimmo S, Brennan FJ, Ford SE, Armstrong PW. Distribution of amiodarone and its metabolite, desethylamiodarone, in human tissues. *Can J Physiol Pharmacol*. 1987; 65: 360–364. <https://doi.org/10.1139/y87-062> PMID: 3580958
8. Honegger UE, Zuehlke RD, Scuntaro I, Schaefer MH, Toplak H, Wiesmann UN. Cellular accumulation of amiodarone and desethylamiodarone in cultured human cells. Consequences of drug accumulation on cellular lipid metabolism and plasma membrane properties of chronically exposed cells. *Biochem Pharmacol*. 1993; 45: 349–356. [https://doi.org/10.1016/0006-2952\(93\)90070-d](https://doi.org/10.1016/0006-2952(93)90070-d) PMID: 8382061
9. Singh BN, Nademane K, Josephson MA, Ikeda N, Venkatesh N, Kannan R. The electrophysiology and pharmacology of verapamil, flecainide, and amiodarone: correlations with clinical effects and antiarrhythmic actions. *Ann N Y Acad Sci*. 1984; 432: 210–235. <https://doi.org/10.1111/j.1749-6632.1984.tb14522.x> PMID: 6395762
10. Staubli M, Bircher J, Galeazzi RL, Remund H, Studer H. Serum concentrations of amiodarone during long term therapy. Relation to dose, efficacy and toxicity. *Eur J Clin Pharmacol*. 1983; 24: 485–494. <https://doi.org/10.1007/BF00609891> PMID: 6861863
11. Colunga Biancatelli RM, Congedo V, Calvosa L, Ciacciarelli M, Polidoro A, Iuliano L. Adverse reactions of Amiodarone. *J Geriatr Cardiol*. 2019; 16: 552–566. <https://doi.org/10.11909/j.issn.1671-5411.2019.07.004> PMID: 31447894
12. Bogнар Z, Fekete K, Antus C, Hocsak E, Bogнар R, Tapodi A, et al. Desethylamiodarone-A metabolite of amiodarone-Induces apoptosis on T24 human bladder cancer cells via multiple pathways. *PLoS One*. 2017; 12: e0189470. <https://doi.org/10.1371/journal.pone.0189470> PMID: 29220397
13. Bogнар Z, Fekete K, Bogнар R, Szabo A, Vass RA, Sumegi B. Amiodarone's major metabolite, desethylamiodarone, induces apoptosis in human cervical cancer cells. *Can J Physiol Pharmacol*. 2018; 96: 1004–1011. <https://doi.org/10.1139/cjpp-2018-0113> PMID: 29847733
14. Sullivan RJ, Fisher DE. Understanding the biology of melanoma and therapeutic implications. *Hematol Oncol Clin North Am*. 2014; 28: 437–453. <https://doi.org/10.1016/j.hoc.2014.02.007> PMID: 24880940
15. de Vries E, Coebergh JW. Melanoma incidence has risen in Europe. *BMJ*. 2005; 331: 698.
16. Boissy RE, Nordlund JJ. Molecular basis of congenital hypopigmentary disorders in humans: a review. *Pigment Cell Res*. 1997; 10: 12–24. <https://doi.org/10.1111/j.1600-0749.1997.tb00461.x> PMID: 9170158
17. Sandru A, Voinea S, Panaitescu E, Blidaru A. Survival rates of patients with metastatic malignant melanoma. *J Med Life*. 2014; 7: 572–576. PMID: 25713625
18. Balch CM, Gershenwald JE, Soong SJ, Thompson JF, Atkins MB, Byrd DR, et al. Final version of 2009 AJCC melanoma staging and classification. *J Clin Oncol*. 2009; 27: 6199–6206. <https://doi.org/10.1200/JCO.2009.23.4799> PMID: 19917835
19. Terzian T, Torchia EC, Dai D, Robinson SE, Muraio K, Stiegmann RA, et al. p53 prevents progression of nevi to melanoma predominantly through cell cycle regulation. *Pigment Cell Melanoma Res*. 2010; 23: 781–794. <https://doi.org/10.1111/j.1755-148X.2010.00773.x> PMID: 20849464
20. Dzwierzynski WW. Managing malignant melanoma. *Plast Reconstr Surg*. 2013; 132: 446e–460e. <https://doi.org/10.1097/PRS.0b013e31829ad411> PMID: 23985656
21. Weinstock MA. Early detection of melanoma. *JAMA*. 2000; 284: 886–889. <https://doi.org/10.1001/jama.284.7.886> PMID: 10938181
22. Wang X, Yue P, Chan CB, Ye K, Ueda T, Watanabe-Fukunaga R, et al. Inhibition of mammalian target of rapamycin induces phosphatidylinositol 3-kinase-dependent and Mnk-mediated eukaryotic translation initiation factor 4E phosphorylation. *Mol Cell Biol*. 2007; 27: 7405–7413. <https://doi.org/10.1128/MCB.00760-07> PMID: 17724079
23. Overwijk WW, Restifo NP. B16 as a mouse model for human melanoma. *Curr Protoc Immunol*. 2001; Chapter 20: Unit 20 21.
24. Ullman-Cullere MH, Foltz CJ. Body condition scoring: a rapid and accurate method for assessing health status in mice. *Lab Anim Sci*. 1999; 49: 319–323. PMID: 10403450
25. DeWitt CR, Cleveland N, Dart RC, Heard K. The effect of amiodarone pretreatment on survival of mice with cocaine toxicity. *J Med Toxicol*. 2005; 1: 11–18. <https://doi.org/10.1007/BF03160899> PMID: 18072097
26. Selzer E, Schlagbauer-Wadl H, Okamoto I, Pehamberger H, Potter R, Jansen B. Expression of Bcl-2 family members in human melanocytes, in melanoma metastases and in melanoma cell lines. *Melanoma Res*. 1998; 8: 197–203. <https://doi.org/10.1097/00008390-199806000-00001> PMID: 9664140
27. Li G, Bush JA, Ho VC. p53-dependent apoptosis in melanoma cells after treatment with camptothecin. *J Invest Dermatol*. 2000; 114: 514–519. <https://doi.org/10.1046/j.1523-1747.2000.00867.x> PMID: 10692111

28. Li G, Tang L, Zhou X, Tron V, Ho V. Chemotherapy-induced apoptosis in melanoma cells is p53 dependent. *Melanoma Res.* 1998; 8: 17–23. <https://doi.org/10.1097/00008390-199802000-00004> PMID: 9508372
29. Melnikova VO, Bolshakov SV, Walker C, Ananthaswamy HN. Genomic alterations in spontaneous and carcinogen-induced murine melanoma cell lines. *Oncogene.* 2004; 23: 2347–2356. <https://doi.org/10.1038/sj.onc.1207405> PMID: 14743208
30. Park HS, Hwang HJ, Kim GY, Cha HJ, Kim WJ, Kim ND, et al. Induction of apoptosis by fucoidan in human leukemia U937 cells through activation of p38 MAPK and modulation of Bcl-2 family. *Mar Drugs.* 2013; 11: 2347–2364. <https://doi.org/10.3390/md11072347> PMID: 23880928
31. Park HS, Kim GY, Nam TJ, Deuk Kim N, Hyun Choi Y. Antiproliferative activity of fucoidan was associated with the induction of apoptosis and autophagy in AGS human gastric cancer cells. *J Food Sci.* 2011; 76: T77–83. <https://doi.org/10.1111/j.1750-3841.2011.02099.x> PMID: 21535865
32. Dobashi Y, Takehana T, Ooi A. Perspectives on cancer therapy: cell cycle blockers and perturbators. *Curr Med Chem.* 2003; 10: 2549–2558. <https://doi.org/10.2174/0929867033456495> PMID: 14529470
33. Paternot S, Bockstaele L, Bisteau X, Kooken H, Coulonval K, Roger PP. Rb inactivation in cell cycle and cancer: the puzzle of highly regulated activating phosphorylation of CDK4 versus constitutively active CDK-activating kinase. *Cell Cycle.* 2010; 9: 689–699. <https://doi.org/10.4161/cc.9.4.10611> PMID: 20107323
34. Shapiro GI, Harper JW. Anticancer drug targets: cell cycle and checkpoint control. *J Clin Invest.* 1999; 104: 1645–1653. <https://doi.org/10.1172/JCI9054> PMID: 10606615
35. Gould Rothberg BE, Bracken MB, Rimm DL. Tissue biomarkers for prognosis in cutaneous melanoma: a systematic review and meta-analysis. *J Natl Cancer Inst.* 2009; 101: 452–474. <https://doi.org/10.1093/jnci/djp038> PMID: 19318635
36. Baker SJ, Fearon ER, Nigro JM, Hamilton SR, Preisinger AC, Jessup JM, et al. Chromosome 17 deletions and p53 gene mutations in colorectal carcinomas. *Science.* 1989; 244: 217–221. <https://doi.org/10.1126/science.2649981> PMID: 2649981
37. Murray AW. Recycling the cell cycle: cyclins revisited. *Cell.* 2004; 116: 221–234. [https://doi.org/10.1016/s0092-8674\(03\)01080-8](https://doi.org/10.1016/s0092-8674(03)01080-8) PMID: 14744433
38. Grabacka M, Plonka PM, Urbanska K, Reiss K. Peroxisome proliferator-activated receptor alpha activation decreases metastatic potential of melanoma cells in vitro via down-regulation of Akt. *Clin Cancer Res.* 2006; 12: 3028–3036. <https://doi.org/10.1158/1078-0432.CCR-05-2556> PMID: 16707598
39. Vivanco I, Sawyers CL. The phosphatidylinositol 3-Kinase AKT pathway in human cancer. *Nat Rev Cancer.* 2002; 2: 489–501. <https://doi.org/10.1038/nrc839> PMID: 12094235
40. Nicholson KM, Anderson NG. The protein kinase B/Akt signalling pathway in human malignancy. *Cell Signal.* 2002; 14: 381–395. [https://doi.org/10.1016/s0898-6568\(01\)00271-6](https://doi.org/10.1016/s0898-6568(01)00271-6) PMID: 11882383
41. Li G, Kalabis J, Xu X, Meier F, Oka M, Bogenrieder T, et al. Reciprocal regulation of MelCAM and AKT in human melanoma. *Oncogene.* 2003; 22: 6891–6899. <https://doi.org/10.1038/sj.onc.1206819> PMID: 14534536
42. Fidler IJ. Selection of successive tumour lines for metastasis. *Nat New Biol.* 1973; 242: 148–149. <https://doi.org/10.1038/newbio242148a0> PMID: 4512654
43. Unal EB, Uhlitz F, Bluthgen N. A compendium of ERK targets. *FEBS Lett.* 2017; 591: 2607–2615. <https://doi.org/10.1002/1873-3468.12740> PMID: 28675784
44. Wortzel I, Seger R. The ERK Cascade: Distinct Functions within Various Subcellular Organelles. *Genes Cancer.* 2011; 2: 195–209. <https://doi.org/10.1177/1947601911407328> PMID: 21779493
45. Murphy LO, Smith S, Chen RH, Fingar DC, Blenis J. Molecular interpretation of ERK signal duration by immediate early gene products. *Nat Cell Biol.* 2002; 4: 556–564. <https://doi.org/10.1038/ncb822> PMID: 12134156
46. Yamamoto T, Ebisuya M, Ashida F, Okamoto K, Yonehara S, Nishida E. Continuous ERK activation downregulates antiproliferative genes throughout G1 phase to allow cell-cycle progression. *Curr Biol.* 2006; 16: 1171–1182. <https://doi.org/10.1016/j.cub.2006.04.044> PMID: 16782007
47. Sang B, Zhang YY, Guo ST, Kong LF, Cheng Q, Liu GZ, et al. Dual functions for OVAAL in initiation of RAF/MEK/ERK prosurvival signals and evasion of p27-mediated cellular senescence. *Proc Natl Acad Sci U S A.* 2018; 115: E11661–E11670. <https://doi.org/10.1073/pnas.1805950115> PMID: 30478051
48. Li CY, Wang Q, Wang XM, Li GX, Shen S, Wei XL. Gambogic acid exhibits anti-metastatic activity on malignant melanoma mainly through inhibition of PI3K/Akt and ERK signaling pathways. *Eur J Pharmacol.* 2019; 864: 172719. <https://doi.org/10.1016/j.ejphar.2019.172719> PMID: 31586634
49. Tarin D. Cell and tissue interactions in carcinogenesis and metastasis and their clinical significance. *Semin Cancer Biol.* 2011; 21: 72–82. <https://doi.org/10.1016/j.semcancer.2010.12.006> PMID: 21147229

50. Chambers AF, Groom AC, MacDonald IC. Dissemination and growth of cancer cells in metastatic sites. *Nat Rev Cancer*. 2002; 2: 563–572. <https://doi.org/10.1038/nrc865> PMID: [12154349](https://pubmed.ncbi.nlm.nih.gov/12154349/)
51. Chaffer CL, Weinberg RA. A perspective on cancer cell metastasis. *Science*. 2011; 331: 1559–1564. <https://doi.org/10.1126/science.1203543> PMID: [21436443](https://pubmed.ncbi.nlm.nih.gov/21436443/)
52. Hugo H, Ackland ML, Blick T, Lawrence MG, Clements JA, Williams ED, et al. Epithelial—mesenchymal and mesenchymal—epithelial transitions in carcinoma progression. *J Cell Physiol*. 2007; 213: 374–383. <https://doi.org/10.1002/jcp.21223> PMID: [17680632](https://pubmed.ncbi.nlm.nih.gov/17680632/)
53. Fidler IJ, Kripke ML. Metastasis results from preexisting variant cells within a malignant tumor. *Science*. 1977; 197: 893–895. <https://doi.org/10.1126/science.887927> PMID: [887927](https://pubmed.ncbi.nlm.nih.gov/887927/)
54. Akiyama Y, Watanabe M, Maruyama K, Ruscetti FW, Wiltout RH, Yamaguchi K. Enhancement of anti-tumor immunity against B16 melanoma tumor using genetically modified dendritic cells to produce cytokines. *Gene Ther*. 2000; 7: 2113–2121. <https://doi.org/10.1038/sj.gt.3301353> PMID: [11223993](https://pubmed.ncbi.nlm.nih.gov/11223993/)



Article

# Involvement of Mitochondrial Mechanisms and Cyclooxygenase-2 Activation in the Effect of Desethylamiodarone on 4T1 Triple-Negative Breast Cancer Line

Ferenc Gallyas, Jr. <sup>1,2,3</sup> , Fadi H. J. Ramadan <sup>1</sup> , Kitti Andreidesz <sup>1</sup>, Eniko Hocsak <sup>1</sup>, Aliz Szabo <sup>1</sup>, Antal Tapodi <sup>1</sup>, Gyongyi N. Kiss <sup>1</sup>, Katalin Fekete <sup>1</sup>, Rita Bogнар <sup>1</sup>, Arpad Szanto <sup>4</sup> and Zita Bogнар <sup>1,\*</sup>

- <sup>1</sup> Department of Biochemistry and Medical Chemistry, University of Pecs Medical School, 7624 Pecs, Hungary; ferenc.gallyas@aok.pte.hu (F.G.J.); fadi.ramadan@aok.pte.hu (F.H.J.R.); andreidesz.kitti@pte.hu (K.A.); Eniko.hocsak@aok.pte.hu (E.H.); aliz.szabo@aok.pte.hu (A.S.); antal.tapodi@aok.pte.hu (A.T.); gyongyi.nagyne@aok.pte.hu (G.N.K.); Katalin.fekete@aok.pte.hu (K.F.); rita.bognar@aok.pte.hu (R.B.)
- <sup>2</sup> Szentagotai Research Centre, University of Pecs, 7624 Pecs, Hungary
- <sup>3</sup> LERN-UP Nuclear-Mitochondrial Interactions Research Group, 1245 Budapest, Hungary
- <sup>4</sup> Urology Clinic, UP Medical Center, University of Pecs Medical School, 7624 Pecs, Hungary; szanto.arpad@pte.hu
- \* Correspondence: zita.bognar@aok.pte.hu; Tel.: +36-72-536-276



**Citation:** Gallyas, F., Jr.; Ramadan, F.H.J.; Andreidesz, K.; Hocsak, E.; Szabo, A.; Tapodi, A.; Kiss, G.N.; Fekete, K.; Bogнар, R.; Szanto, A.; et al. Involvement of Mitochondrial Mechanisms and Cyclooxygenase-2 Activation in the Effect of Desethylamiodarone on 4T1 Triple-Negative Breast Cancer Line. *Int. J. Mol. Sci.* **2022**, *23*, 1544. <https://doi.org/10.3390/ijms23031544>

Academic Editor: Antonella Zannetti

Received: 30 November 2021

Accepted: 26 January 2022

Published: 28 January 2022

**Publisher's Note:** MDPI stays neutral with regard to jurisdictional claims in published maps and institutional affiliations.



**Copyright:** © 2022 by the authors. Licensee MDPI, Basel, Switzerland. This article is an open access article distributed under the terms and conditions of the Creative Commons Attribution (CC BY) license (<https://creativecommons.org/licenses/by/4.0/>).

**Abstract:** Novel compounds significantly interfering with the mitochondrial energy production may have therapeutic value in triple-negative breast cancer (TNBC). This criterion is clearly fulfilled by desethylamiodarone (DEA), which is a major metabolite of amiodarone, a widely used antiarrhythmic drug, since the DEA previously demonstrated anti-neoplastic, anti-metastasizing, and direct mitochondrial effects in B16F10 melanoma cells. Additionally, the more than fifty years of clinical experience with amiodarone should answer most of the safety concerns about DEA. Accordingly, in the present study, we investigated DEA's potential in TNBC by using a TN and a hormone receptor positive (HR+) BC cell line. DEA reduced the viability, colony formation, and invasive growth of the 4T1 cell line and led to a higher extent of the MCF-7 cell line. It lowered mitochondrial transmembrane potential and induced mitochondrial fragmentation. On the other hand, DEA failed to significantly affect various parameters of the cellular energy metabolism as determined by a Seahorse live cell respirometer. Cyclooxygenase 2 (COX-2), which was upregulated by DEA in the TNBC cell line only, accounted for most of 4T1's DEA resistance, which was counteracted by the selective COX-2 inhibitor celecoxib. All these data indicate that DEA may have potentiality in the therapy of TNBC.

**Keywords:** amiodarone; apoptosis; colony formation; invasive growth; Akt pathway;  $\Delta\Psi_m$ ; therapy resistance; mitochondrial fragmentation; Seahorse

## 1. Introduction

Breast cancer (BC) is the most frequent cancer type in women and the second primary cause of cancer-related death worldwide. Triple-negative (TN) form of the disease represents about 10–20% of all BC cases. Although of heterogeneous phenotype, TNBC is characterized by the lack of estrogen receptor (ER), progesterone receptor (PR), and human epidermal growth factor receptor (HER)2/neu gene amplification. TNBC patients typically present at a younger age a larger average tumor size, higher grade, and higher rates of lymph node positivity compared to patients with ER/PR-positive tumors [1]. Due to these features, TNBCs do not respond or became resistant to targeted therapies and, accordingly, have poor prognosis [2]. Furthermore, a progressive drug resistance leading to the formation of non-responding metastases often limits the systemic therapy [3,4]. Taxane- and anthracycline-based treatment represent the mainstream of TNBC chemotherapy, although optimization of the protocols is yet to be accomplished [4]. Previous studies suggest that

there is a correlation between inflammation and tumor formation [5], and intensive research is trying to uncover the complex interaction between breast cancer and the immune system [6,7].

Cyclooxygenase-2 (COX-2) is an inducible form of the enzyme that catalyzes the synthesis of prostanoids, including prostaglandin E2 (PGE2), a major mediator of inflammation and angiogenesis. COX-2 is overexpressed in cancer cells and is associated with progressive tumor growth and resistance of cancer cells to conventional chemotherapy and radiation [8]. Furthermore, elevated expression of the COX-2 gene and activation of the COX-2/matrix metalloproteinase 1 pathway was implicated in brain metastasis formation of BC [9,10]. According to the current view, conventional chemotherapy and radiotherapy selects resistant cancer cells that are able to reinitiate tumor growth. There is compelling evidence of an active proliferative response, driven by increased COX-2 expression and PGE2 release, which contributes to the repopulation of the tumor and the resulting poor outcome for the patients [8]. Recent *in vitro* and *in vivo* pre-clinical studies have demonstrated that COX-2 overexpression plays a key role in tumor resistance by stimulating epithelial cell proliferation and angiogenesis, increasing multidrug resistance, and enhancing cell motility and invasion [8,11–14]. In TNBC, elevated COX-2 expression promotes stemness, indicating COX-2 as a potential therapeutic target [15]. However, clinical studies utilizing selective COX-2 inhibitors such as celecoxib in BC patients provided conflicting results indicating that molecular mechanisms associated with tumor development influenced the resistance to COX-2 inhibitors [16].

Based on their central role in metabolism and cell death regulation, mitochondria have emerged as novel anti-cancer therapeutic targets [17]. Mitochondria constitute a central hub in intermediary metabolism, are responsible for the majority of ATP synthesis, and regulate cell death via signaling molecules and the release of pro-apoptotic intermembrane proteins [18,19]. Cancer cells tend to use glycolysis for energy production even in the presence of sufficient oxygen supply to preserve intermediates for biosynthetic purpose [20]. However, cancers of the most aggressive phenotype such as drug-resistant and stem cancer cells rely on oxidative phosphorylation for energy production and reprogram their metabolism to meet the challenges of fast proliferation [17,20]. Accordingly, drugs that interfere with the mitochondrial functions disrupt this delicately balanced reprogrammed metabolism to an extent that is incompatible with survival and thus have strong potential in anti-cancer therapy [17,21].

Recent clinical trials combine immunotherapy with the traditional chemotherapy to combat therapy resistance [22]; however, effective management of TNBC patients remains a challenge in the clinical practice. On the other hand, the introduction of new drugs into the clinical practice is much delayed by the very lengthy safety protocols, which can be significantly shortened by repositioning a drug already approved for human therapy [23]. Desethylamidarone (DEA) is the major metabolite of amiodarone (AM), an antiarrhythmic agent widely used in various life-threatening ventricular tachyarrhythmias. During antiarrhythmic therapy, AM accumulates rapidly in the lipophilic tissues, together with DEA [24], which is generated from the mother compound by the liver. Therapeutic AM plasma concentration is limited to 5.7  $\mu\text{M}$  [25], since therapy-restricting side effects [26] develop in most cases at higher plasma concentrations. However, the accumulation of AM and DEA in tissues can result in concentrations exceeding the plasma concentration 100 to 1000 times [25]. Unlike AM, DEA is quite stable in the body, and it is eliminated with a half-life of about 40 days [27]. Except for the adipose tissue, its tissue accumulation exceeds that of AM [24,28,29]. However, at concentrations observable at therapeutic AM doses [24], DEA does not have therapy restricting side effects [30], which may hinder its introduction into clinical studies.

DEA's accumulative and toxic properties suggested that it might have an anti-neoplastic potentiality. Furthermore, there is a vast clinical experience with the safety features of DEA gathered during the more than 50 years of AM's therapeutic use [26]. That is, if DEA exerted a sufficiently effective anti-neoplastic effect at concentrations not exceeding

those existing during AM therapy, it could be a readily available tool in cancer therapy. Previously, we reported DEA's cytotoxicity in the bladder, cervix, and melanoma cell lines and its metastasis-limiting properties in a rodent lung metastasis model [31–33]. Furthermore, by using the B16F10 melanoma cell line, we demonstrated that DEA affected mitochondrial processes in live cells [34] similarly as it did previously in isolated liver and heart mitochondria [35]. A uniform anti-neoplastic effect on three very different, highly proliferative cell lines indicated that DEA interferes with fundamental survival-promoting processes likely present in most cancer cell lines of different tissue and species of origin. In the present report, we studied the anti-neoplastic and mitochondrial effects of DEA and combined the cytotoxic effect of DEA and the selective COX-2 inhibitor celecoxib on a TN line in comparison with a hormone receptor positive (HR+) BC line to identify potential differences in DEA's molecular mechanisms in these two cancer types.

## 2. Results

### 2.1. DEA Induced Apoptotic Cell Death in BC Cell Lines

Previously, DEA demonstrated signs of anti-neoplastic potentiality in various cancer cell lines [31–33], including therapy-resistant lines such as T24 [32] and B16F10 [33]. Accordingly, we assessed its effect on the cell death process of the TN 4T1 BC line in comparison with the HR+ MCF-7 line of the less aggressive cancerous phenotype [36]. We used flow cytometry with the Muse™ Annexin V & Dead Cell Assay kit to investigate the mode of DEA-induced cell death. The assay utilizes cell surface annexin V binding that measures the appearance of phosphatidylserine on the external surface of the plasma membrane, which is a marker of apoptosis. A dead cell marker, 7-aminoactinomycin D (7-AAD), was also used as an indicator of cell membrane structural integrity. Late apoptosis is demonstrated by double positivity. We treated the cells with 5 and 10  $\mu\text{M}$  DEA for 24 h before the flow cytometry analysis. In a concentration-dependent way, DEA induced early, then late apoptosis (Figure 1). At the lower DEA concentration, the rate of early apoptosis exceeded that of the late; however, at the higher drug concentration, late apoptosis predominated in both BC cell lines (Figure 1). However, we found a total apoptosis rate of  $28.18 \pm 6.34\%$  for 5 and  $56.05 \pm 5.12\%$  for 10  $\mu\text{M}$  DEA in the 4T1 cell line in contrast to the apoptosis rates of  $71.14 \pm 6.39\%$  for 5 and  $78.94 \pm 4.77\%$  for 10  $\mu\text{M}$  DEA observed in the MCF-7 cell line (Figure 1), indicating that MCF-7 cells were more sensitive toward DEA treatment than the 4T1 cells.

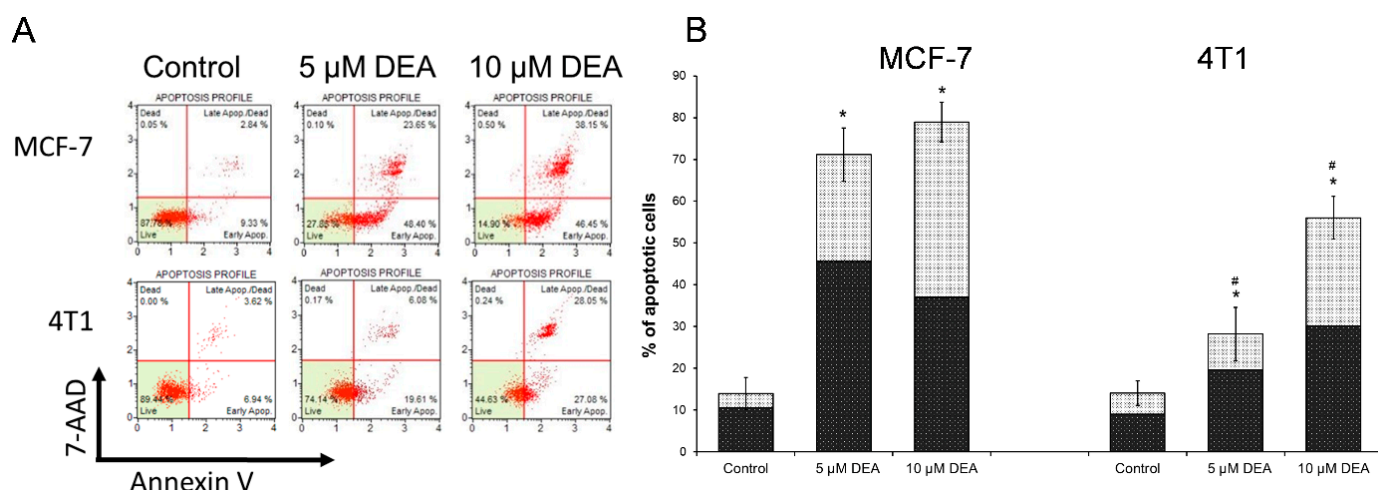


**Figure 1.** Effect of DEA on the apoptosis in BC cell lines. We treated MCF-7 and 4T1 cells with 5 or 10  $\mu\text{M}$  DEA for 24 h before determining the type of cell death by flow cytometry using the Muse™ Annexin V & Dead Cell Assay kit. The results are presented as representative dot plots (A) and bar diagrams (B) of three independent experiments. The bars (B) indicate the sum of early (dark bars) and late (light bars) apoptosis expressed as percentage of the total cell number, mean  $\pm$  SD of three independent experiments running in at least quadruplicate parallels. Controls were treated with vehicle (0.2% DMSO). \* significant difference from the control ( $p < 0.05$ ). # significant difference from the MCF-7 parallel ( $p < 0.05$ ).

## 2.2. DEA Mitigated Invasive Growth of BC Cell Lines

Cell migration, an important aspect of cancer invasiveness, is often assessed by means of the wound-healing assay [37]. Accordingly, we inflicted a wound into semi-confluent monolayers of MCF-7 and 4T1 cells and treated them by 0, 5, or 10  $\mu\text{M}$  DEA for 12 h. In accordance with its more malignant phenotype [38], cell migration of the TNBC cells was more intense, resulting in almost complete closing of the wound within 12 h, while the HR+ BC cell line achieved an about 40% healing during the same time. Ten  $\mu\text{M}$  DEA treatment completely prevented wound healing in the 4T1 cell line, while it caused wound exacerbation due to killing cells at the wound edge in the MCF-7 cell line (Figure 2). At the concentration of 5  $\mu\text{M}$ , DEA treatment induced a less pronounced effect on wound healing as it did at 10  $\mu\text{M}$  (Figure 2).

To supplement the wound-healing assay, we assessed the invasive growth of the MCF-7 and 4T1 cells using an xCelligence Real-Time Cell Analysis (RTCA) system. The cells were cultured in the presence of 0, 5, or 10  $\mu\text{M}$  DEA for 24 h and the cell index proportional to invasive growth of the cells was monitored in real time. DEA decreased invasive growth in a concentration-dependent manner in both MCF-7 and 4T1 cells (Figure 3). Similarly to the results of the wound-healing experiment, MCF-7 was more sensitive to the drug than 4T1 (Figure 3).

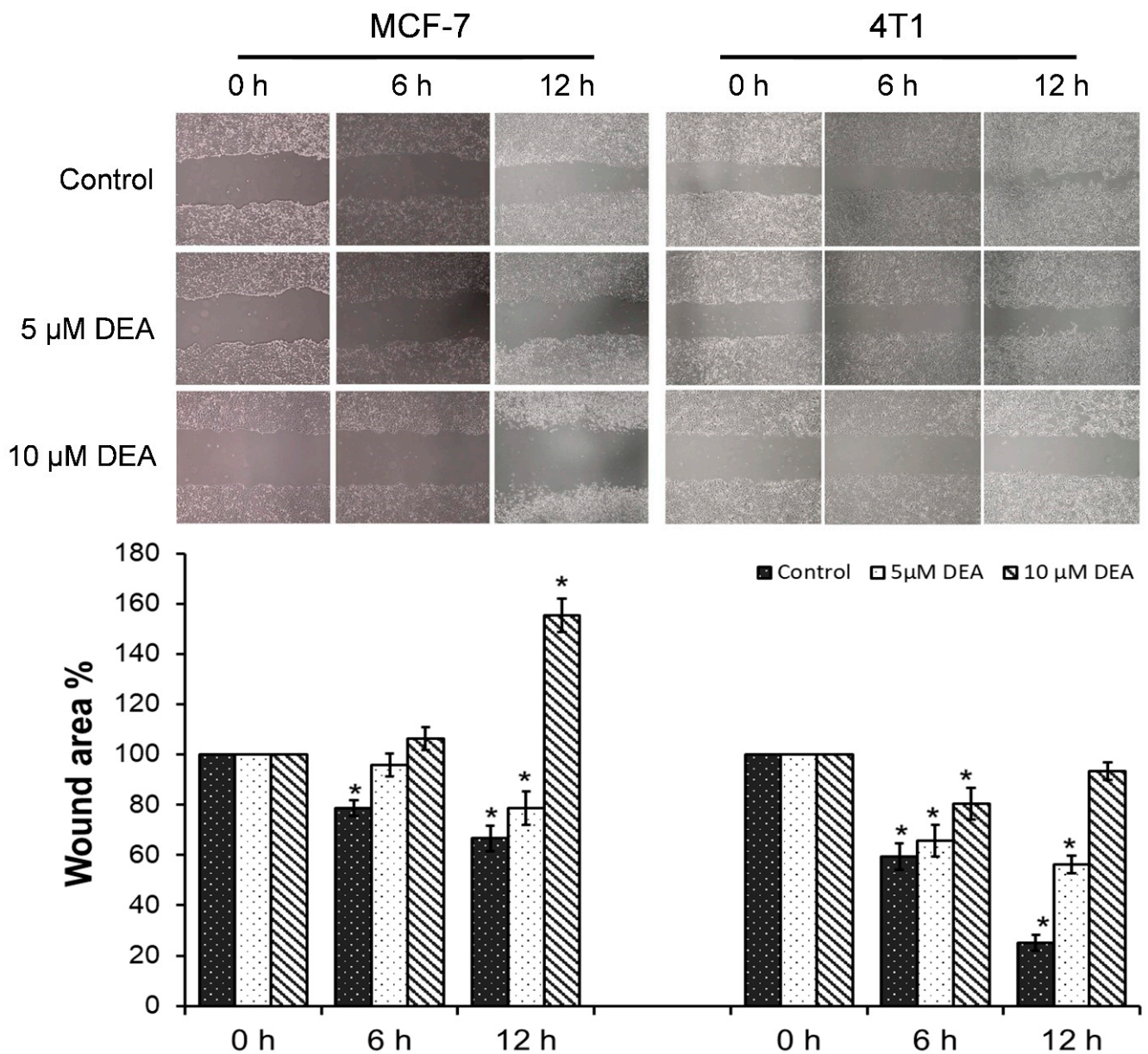


**Figure 2.** Effect of DEA on wound healing in BC cell lines. We inflicted a wound into semi-confluent cultures of MCF-7 and 4T1 cells, and treated them with 0, 5, or 10 μM DEA for 12 h. The data are presented as representative images of the wounds taken at 0, 6, and 12 h and the wound area is the percentage of untreated plates at the 0 h time-point; results are the mean ± SD of two independent experiments running in duplicates. \* significant difference from the untreated control ( $p < 0.05$ ).



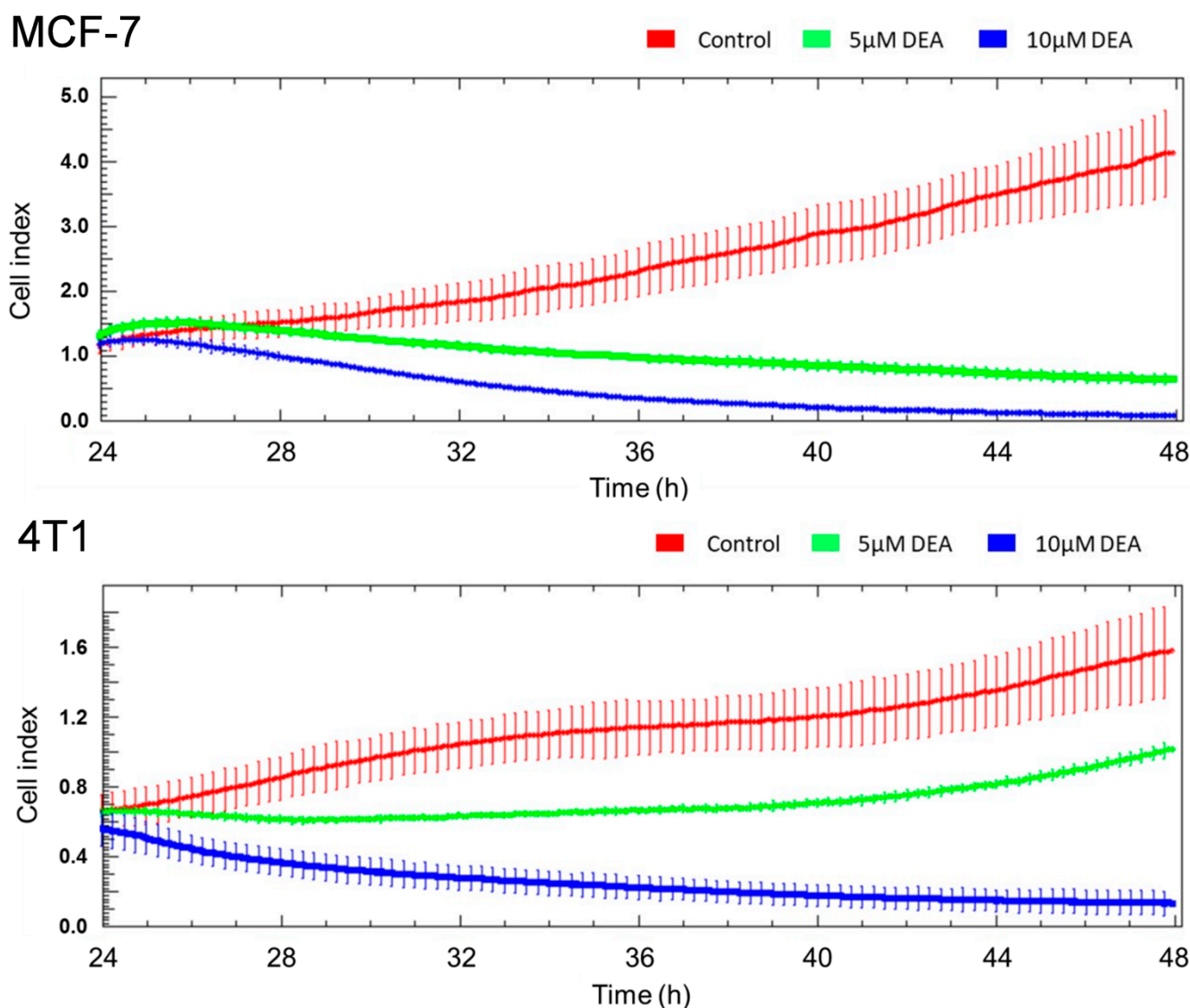


**Figure 3.** Effect of DEA on invasive growth of BC lines. MCF-7 and 4T1 cells were cultured in the presence of 0 (red line), 5 µM (green line), or 10 µM (blue line) DEA for 24 h, while the cell index was monitored by an RTCA system every 5 min. The results are presented as original recordings, mean ± SD of two independent experiments running in triplicates.

### 2.3. DEA Differentially Modulated Regulators and Markers of the Cell Death Process in the BC Cell Lines

To gain greater insight into the apoptosis pathway induced by DEA, we analyzed Akt activation, protein levels of Bcl-2 family members including pro-apoptotic Bad and Bax and antiapoptotic Bcl-2, and the caspase-3 cleavage and caspase-3-mediated cleavage of PARP, which are all reporters of the mitochondrial apoptotic pathway. As shown in Figure 4, the Akt phosphorylation at Ser<sup>473</sup> decreased in a concentration-dependent manner, while the total Akt remained constant. This was accompanied by a significant decrease in the phosphorylation level of Bad at Ser<sup>136</sup>, while the overall level of Bad protein remained constant in both cell lines. We also found that DEA indeed resulted in a dose-dependent increase in the amount of p53 protein in 4T1 cells (Figure 4). We also measured a significant increase in Bax levels while Bcl-2 levels decreased (Figure 4). Furthermore, we found that DEA treatment led to an increase in the amount of a 19 kDa caspase-3 cleavage intermediate as well as cleaved poly (ADP-ribose) polymerase (PARP) (Figure 4). Taken together, these data demonstrate that cytotoxic effects of DEA on MCF-7 and 4T1 cells are due to the

activation, at least partially, of two apoptotic pathways, the PI3K/Akt pathway and the mitochondrial pathway.

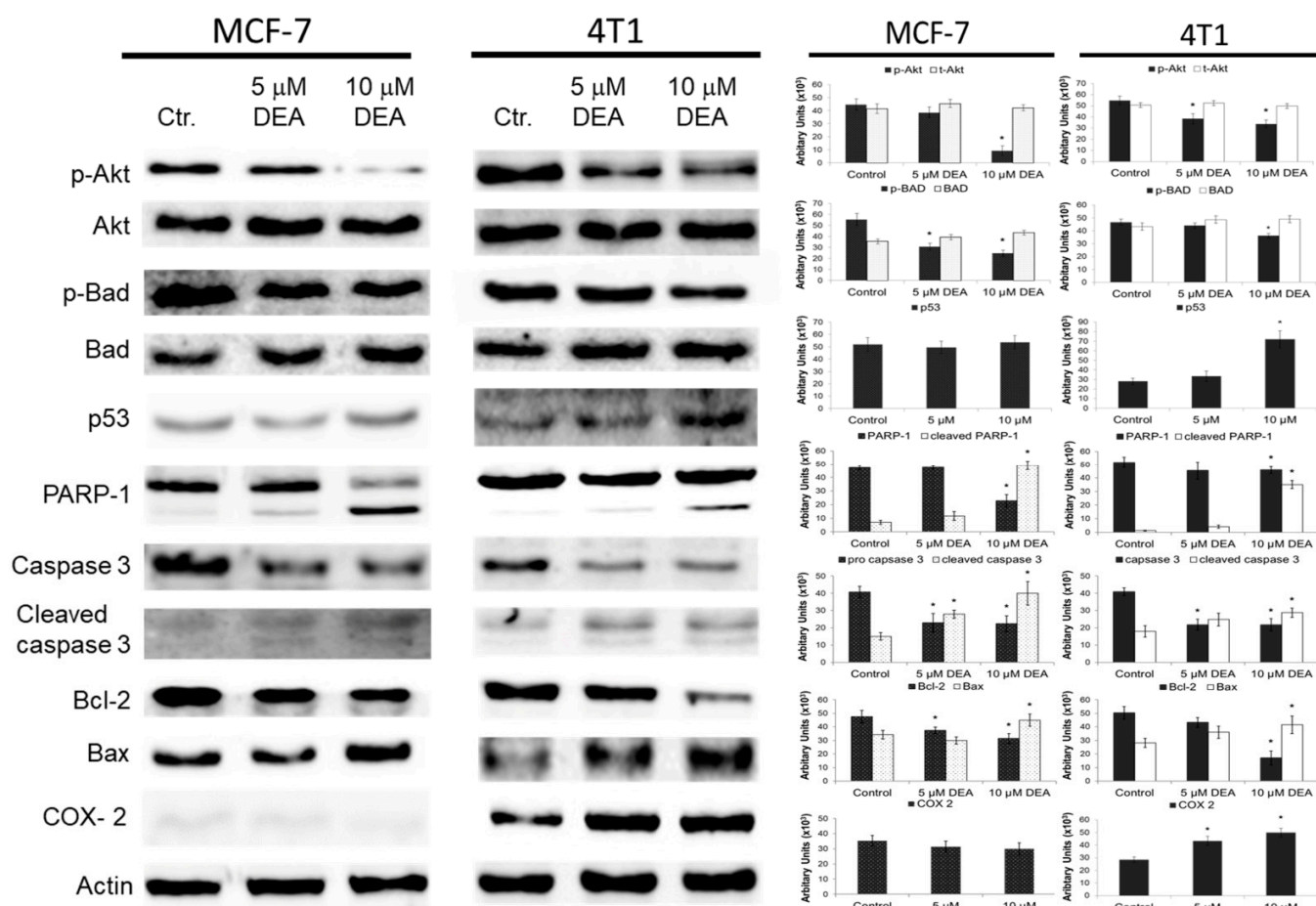


**Figure 4.** Effect of DEA on steady-state level of regulator and marker proteins of the cell death process in the BC cell lines. We evaluated the steady-state levels of p-Akt, Akt, p-Bad, Bad, Bcl-2, Bax, p53, PARP-1, caspase 3, cleaved caspase 3, and COX-2 in the MCF-7 and 4T1 cells treated with 0, 5, or 10  $\mu$ M DEA by immunoblot analysis. Results are presented as representative immunoblots and pixel densities of the bands, mean  $\pm$  SD of three independent experiments. \* Significant difference from the control ( $p < 0.05$ ). Additional representative immunoblots for p-Akt, Akt, p-Bad, Bad, Bcl-2, Bax, PARP-1, and COX-2 are presented in Supplementary Figure S1.

A differential expression of the therapy-resistance- and metastasis-promoting COX-2 gene among BC cell lines of various phenotypes has been reported previously [39]. Accordingly, we studied DEA's effect on COX-2 protein levels in the 4T1 and MCF-7 cell lines. In agreement with previous data [39], we detected considerable steady-state COX-2 levels in the TN BC cell line, while it was just above the detection limit in the HR+ one (Figure 3). Additionally, DEA increased the COX-2 level in a concentration-dependent way in the TN 4T1 cell line only (Figure 4).

#### 2.4. DEA Caused the Loss of Mitochondrial Membrane Potential ( $\Delta\Psi_m$ )

Intact  $\Delta\Psi_m$  is pivotal for cellular survival due to its essential role in ATP synthesis, in providing the driving force for the transport of ions and proteins, and in mitochondrial quality control [40]. Therefore, we determined the effect of DEA on the  $\Delta\Psi_m$  of BC cells by using the positively charged fluorescent mitochondrial dye, JC-1. When the  $\Delta\Psi_m$  is normal, the dye accumulates in the mitochondria and forms J-aggregates that emit red fluorescence upon excitation. The aggregates disassemble, leaving green fluorescent monomers as the

$\Delta\Psi_m$  decreases, and the fluorescence disappears upon complete mitochondrial depolarization. We treated the MCF-7 and 4T1 BC cell lines for 3 h with 0, 5, or 10  $\mu\text{M}$  DEA, before loading them with JC-1 and taking fluorescent microscopy images. At the concentration of 10  $\mu\text{M}$ , the drug significantly depolarized the mitochondria in both BC cell lines, while 5  $\mu\text{M}$  DEA did not have a considerable effect on the  $\Delta\Psi_m$  during the 3 h treatment (Figure 5).

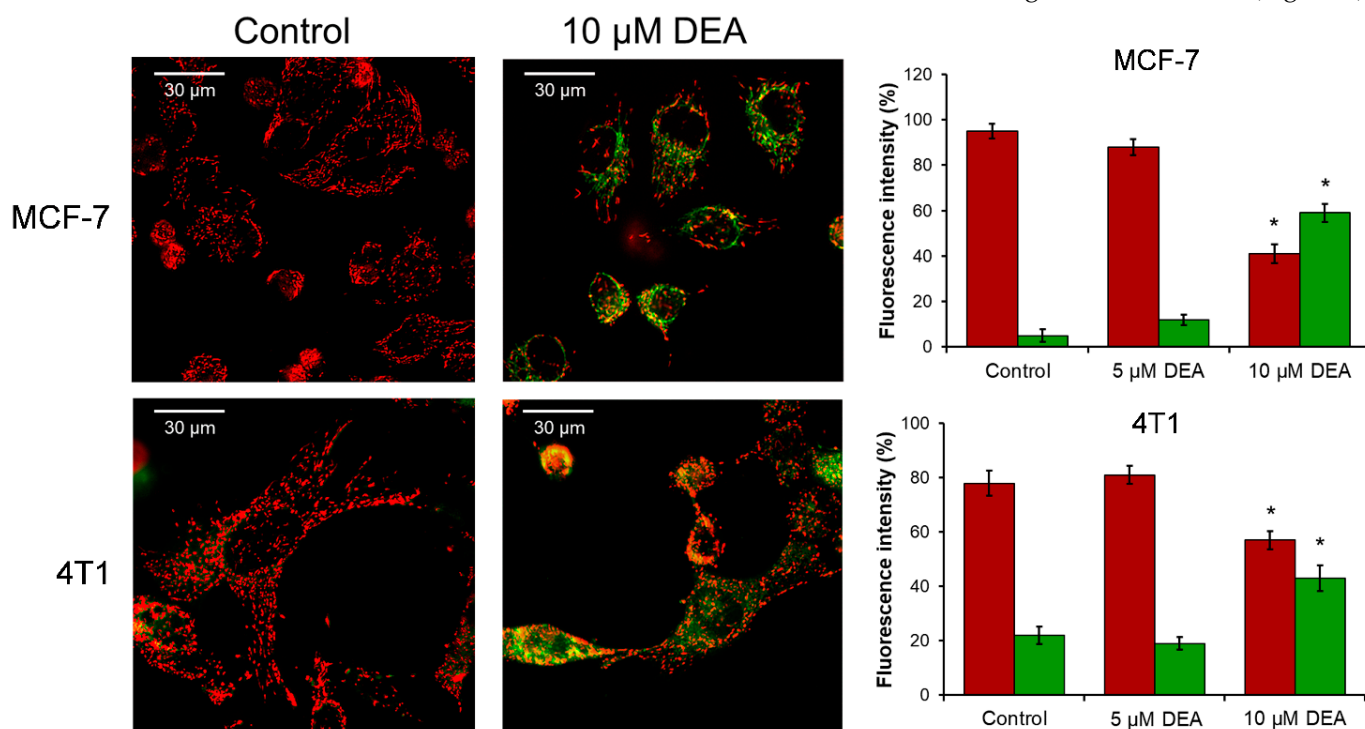


**Figure 5.** Effect of DEA on  $\Delta\Psi_m$  in BC cell lines. MCF-7 and 4T1 BC lines were treated with 0, 5, or 10  $\mu\text{M}$  DEA for 3 h before loading them with JC-1 dye and taking microscopy images. The data are presented as representative merged images of the control and 10  $\mu\text{M}$  DEA treated cells in the red and green channels, and as a percentage of the total fluorescence intensity in the bar diagram. Results are mean  $\pm$  SD of three independent experiments. \* significant difference from the untreated control ( $p < 0.05$ ).

### 2.5. DEA Induced Mitochondrial Fragmentation in BC Cell Lines

Healthy  $\Delta\Psi_m$  is required for the mitochondrial fusion; therefore, compromised  $\Delta\Psi_m$  often results in mitochondrial fragmentation. We studied the effect of DEA on mitochondrial network dynamics by fluorescent microscopy after loading the cells with MitoTracker Red to visualize the mitochondria. The MCF-7 and 4T1 cells were treated with 0, 5, or 10  $\mu\text{M}$  of DEA for 3 h before the assessment of mitochondrial fragmentation. Similarly, as it did in melanoma cells previously [34], DEA treatment caused mitochondrial fragmentation in both BC cell lines in a concentration-dependent manner (Figure 6A).

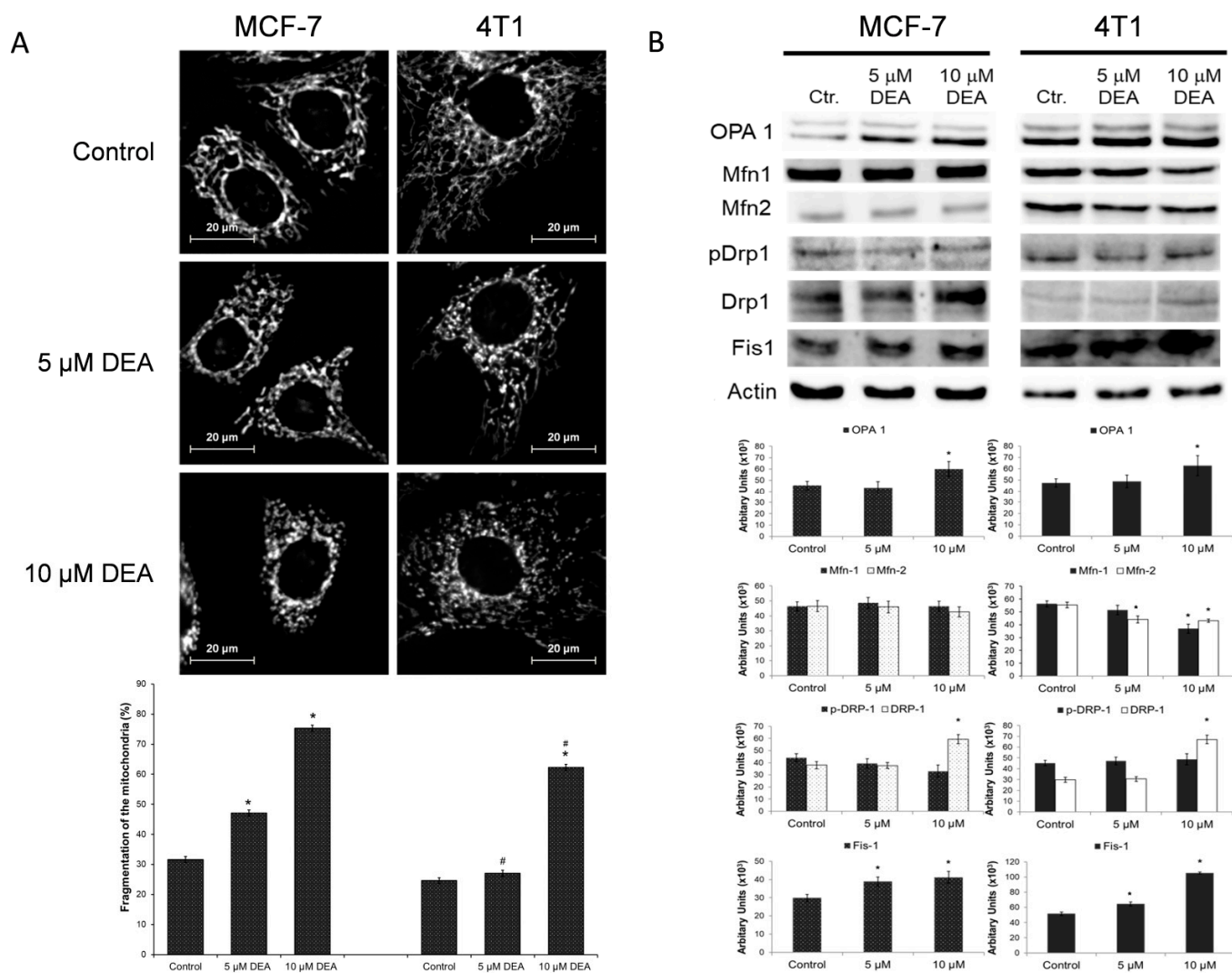


**Figure 6.** Effect of DEA on mitochondrial network dynamics in BC cell lines. MCF-7 and 4T1 cells were treated with 0, 5, or 10  $\mu$ M DEA for 3 h before loading them with MitoTracker Red dye and taking microscopy images. Mitochondrial fragmentation was determined as described in [41]. The data are presented as representative images and as percentage of fragmented mitochondria (A), mean  $\pm$  SD of three independent experiments. Additional representative images are presented in Supplementary Figure S2. Separately, homogenates of identically treated cells were subjected to immunoblot analysis (B). The data are presented as representative immunoblots and as pixel densities of the bands, mean  $\pm$  SD of three independent experiments. \* significant difference from the untreated control ( $p < 0.05$ ); # significant difference from the MCF-7 cells ( $p < 0.05$ ).

Recently, a link has been established between the proliferation of cancer cells and mitochondrial fragmentation [42]. Accordingly, we performed immunoblot analysis of the proteins involved in the regulation of mitochondrial fusion and fission [43] from homogenates of BC cells treated identically to the fragmentation experiment in separate plates. In both BC cell lines, the DEA treatment increased the steady-state level of fusion-associated protein optic atrophy 1 (OPA1), but it decreased mitofusin (Mfn) 1 and 2 in 4T1 cells (Figure 6B). However, it increased the steady-state level of fission-associated proteins such as dynamin-related protein 1 (DRP1) and mitochondrial fission 1 protein (Fis1) (Figure 6B).

## 2.6. DEA Impeded Mitochondrial Energy Production in the BC Cell Lines

To determine the effect of DEA treatment on the energy metabolism of the BC cell lines, we used a live cell respirometer to measure the cellular oxygen consumption rate (OCR) and extracellular acidification rate (ECAR), which are indicators of oxidative and fermentative ATP production, respectively. We treated the MCF-7 and 4T1 cells with 0, 5, or 10  $\mu\text{M}$  DEA for 6 h before the bioenergetics assay. Parallel to OCR, ECAR was also monitored, and the instrument calculated multiple parameters of cellular energy metabolism from the original recordings (Figure 7). At the concentration of 10  $\mu\text{M}$ , DEA significantly decreased basal respiration, maximal respiration, non-mitochondrial oxygen consumption, mitochondrial ATP production, coupling efficiency, and spare respiratory capacity in both BC cell lines (Figure 6). Five  $\mu\text{M}$  DEA increased the proton leak in both cell lines (Figure 7). On the other hand, DEA did not affect ECAR (Figure 7), indicating that the drug did not interfere with the glycolytic machinery in either BC cell line.

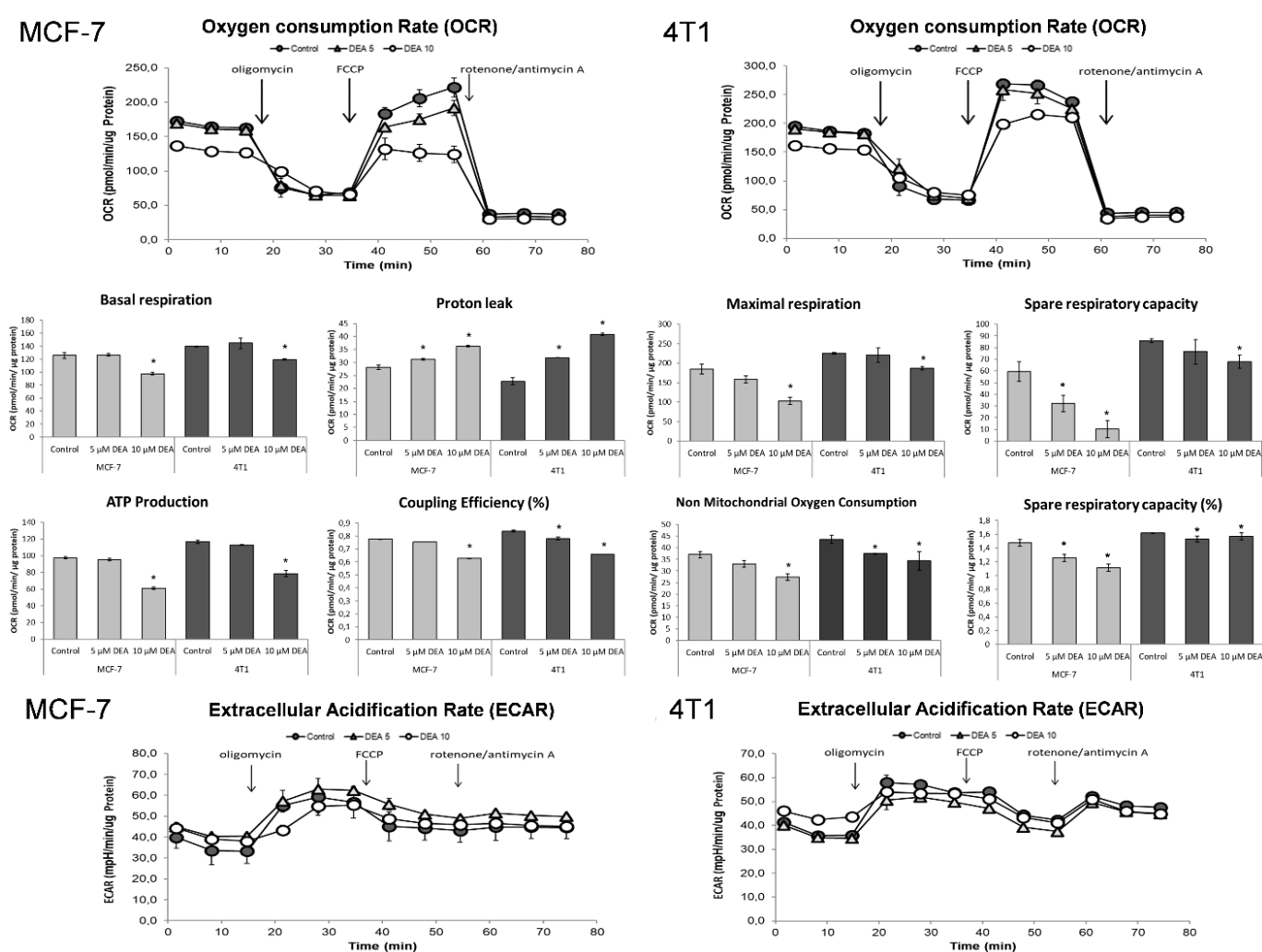


**Figure 7.** Effect of DEA on energy metabolism of the BC cell lines. MCF-7 (light bars) and 4T1 (dark bars) BC cells were treated with 0 (filled circles), 5 (triangles), or 10  $\mu\text{M}$  DEA (open circles) for 6 h before monitoring OCR and ECAR for 75 min. The FoF<sub>1</sub> ATP synthase inhibitor oligomycin, the uncoupler FCCP, and the respiratory inhibitors rotenone and antimycin A were added at 15, 35, and 55 min of the respiratory measurement. OCR recordings. Data are presented as representative original recordings, and as parameters, means  $\pm$  SD of three independent experiments running in two replicates. OCR and ECAR data were normalized to mg protein content. \* significant difference from the untreated control ( $p < 0.05$ ).

### 2.7. COX-2 Inhibition Potentiated DEA's Anti-Neoplastic Effect in the TN BC Cell Line

Elevated expression of COX-2—associated with progressive tumor growth and resistance [8]—may have accounted for the increased resistance to DEA treatment of 4T1 TNBC cells compared to the HR+ MCF-7 cells. To test this possibility, we treated both cell lines with 0–15  $\mu\text{M}$  of DEA for 24 h in the presence and absence of 20  $\mu\text{M}$  of the COX-2 inhibitor celecoxib before measuring the viability of the cells using the sulforhodamine B (SRB) assay. The SRB assay is based on protein content rather than metabolic activity. Therefore, it is recommended for determining the cytotoxicity of substances that can have mitochondrial effects [44]. DEA reduced the viability of both BC lines in a time and concentration-dependent way (Figure 8A). However, as expected, the viability loss caused by DEA treatment was higher for the MCF-7 than for the 4T1 cell line (Figure 7A), indicating a higher treatment sensitivity for the former cell line. However, when COX-2 was inhibited by celecoxib, DEA's effect on the viability of 4T1 cells was significantly more pronounced (Figure 8B) in contrast to MCF-7 cells (Supplementary Figure S3), suggesting that COX-2 activation may have contributed to the resistance of 4T1 cells to DEA treatment.

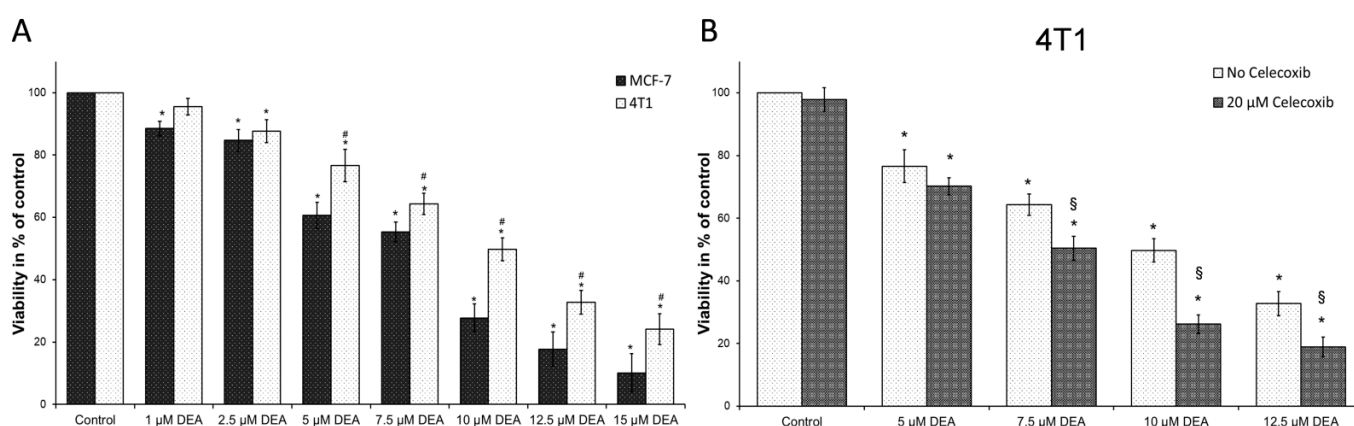


**Figure 8.** Effect of DEA on the viability of BC cell lines. (A): We treated MCF-7 (dark bars) and 4T1 (light bars) cells with 0 to 15  $\mu\text{M}$  DEA for 24 h. (B): We treated 4T1 cells with 0 to 12.5  $\mu\text{M}$  DEA in the absence (light bars) or presence (dark bars) of 20  $\mu\text{M}$  celecoxib for 24 h. Viabilities were assessed using the SRB assay and were presented as percent of the untreated control, means  $\pm$  SD of three independent experiments performed in at least quadruplicates. \* significant difference from the untreated control ( $p < 0.05$ ); # significant difference from the MCF-7 cells parallel ( $p < 0.05$ ); § significant difference from the no celecoxib parallel ( $p < 0.05$ ).

Colony formation assay utilizes lower drug concentrations and longer exposure times; therefore, it represents a situation more similar to the therapeutic one than the viability studies. Accordingly, we tested the effect of COX-2 inhibition on DEA's anti-neoplastic effect using this method, too. We treated the MCF-7 and 4T1 cells with 0 to 2  $\mu\text{M}$  DEA in the presence or absence of 5  $\mu\text{M}$  celecoxib for 7 days before quantifying colony formation. Even at the concentration of 1  $\mu\text{M}$ , DEA significantly suppressed colony formation in both cell lines (Figure 9). The TNBC line 4T1 demonstrated higher resistance against the treatment, since 2  $\mu\text{M}$  DEA almost eradicated MCF-7 colony formation while it induced about a 50% decrease only in the formation of 4T1 colonies (Figure 9). However, as in the case of the viability study (Figure 8), 5  $\mu\text{M}$  celecoxib augmented the effect of DEA on the 4T1 cells, and the combined treatment decreased colony formation in this cell line close to the level of the one observed in the MCF-7 line (Figure 9). In contrast, celecoxib did not affect DEA's effect on MCF-7 colony formation (Figure 9).

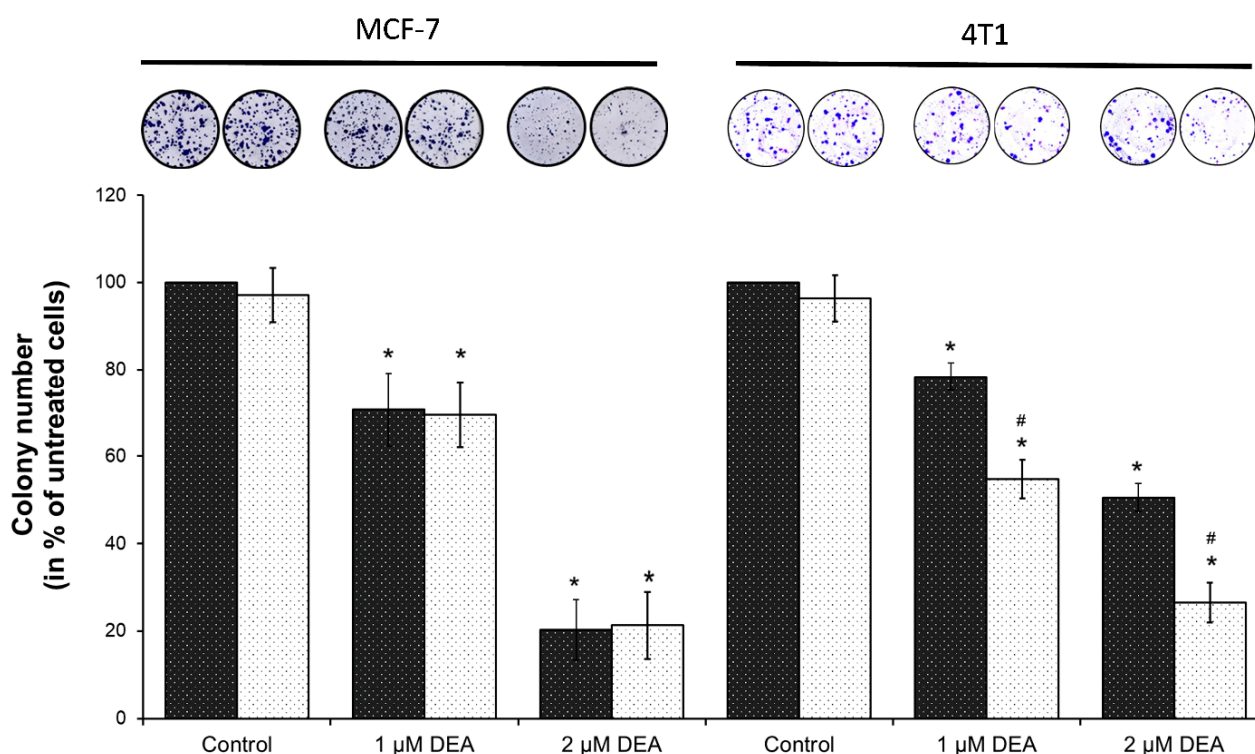


**Figure 9.** Effect of DEA and celecoxib on colony formation of BC lines. We treated MCF-7 and 4T1 cells with 0 to 2  $\mu\text{M}$  DEA in the absence (dark bars) or presence (light bars) of 5  $\mu\text{M}$  celecoxib for 7 days before determining colony formation. The data are presented as representative images of stained colonies in culturing plates and colony numbers are presented as the percentage of untreated plates, mean  $\pm$  SD of three independent experiments. \* significant difference from the untreated control ( $p < 0.05$ ). # significant difference from the no celecoxib parallel ( $p < 0.05$ ).

### 3. Discussion

Targeting tumor metabolism seems an evident possibility, since aggressive cancers have a delicately balanced metabolism, which answers the seemingly impossible challenge of rapid proliferation in an environment of low oxygen and nutrient availability [45]. Mitochondria actively participate in all stages of cancer development from carcinogenesis via tumor survival and therapy resistance to metastasis formation [46,47], and most cancer types of high clinical grade rely on mitochondrial ATP synthesis for energy production [48,49]. Accordingly, drugs that significantly interfere with mitochondrial energy production may have therapeutic value in these tumors [50]. Based on its mitochondrial effects in B16F10 melanoma cells [34], DEA fulfills this criterion. Furthermore, and in agreement with our previous results on T24 bladder and HeLa cervix carcinomas and B16F10 melanoma [31–33], DEA at low  $\mu\text{M}$  concentrations reduced the viability of the BC cell lines MCF-7 and 4T1 in a concentration- and time-dependent manner (Figure 8A). However, *in vitro* cell culture experiments translate very poorly to human studies; therefore, the therapeutic dose of DEA should be determined in future animal experiments. Accordingly, the mouse 4T1 rather than the human MDA-MB-231 TNBC cell line was used in the present study.

Mitochondria regulate cellular survival via ATP production, reactive oxygen species (ROS) generation, and the intrinsic apoptotic pathway [51]. These pathways mutually regulate each other. The oxidative phosphorylation produces most of the cellular ATP, and it is one of the major source of ROS [52]. On the other hand, apoptosis depends on ATP as an energy source, while the energy shortage results in  $\Delta\Psi_m$  loss, which initiates apoptosis via the release of pro-apoptotic intermembrane proteins, such as cytochrome c, apoptosis-inducing factor, and endonuclease G [53]. DEA induced predominantly apoptotic cell death in both BC cell lines (Figures 1 and 4), which was demonstrated by fluorescent staining of

the phosphatidylserine residues in the outer face of the cell membrane (Figure 1), decrease in the Bcl-2/Bax ratio, activation of caspase 3, and cleavage of PARP-1 (Figure 4); all of them are hallmarks of apoptosis [54]. In agreement with its TN phenotype [36], the 4T1 cell line demonstrated higher resistance against DEA treatment than the HR+ MCF-7 cell line in these experiments (Figures 1–4 and Figure 8A).

The proliferation rate and formation of brain, liver, and lungs metastases are much higher in the TN than in other types of BC [55]. In full agreement with these data, we found that 4T1 cells were more resistant toward DEA treatment than the MCF-7 cells in colony formation (Figure 9) and invasive growth (Figures 2 and 3) experiments, too. Additionally, the findings showed that DEA decreased colony formation below 50% of the control at a concentration of 2  $\mu$ M during a seven-day exposure (Figure 9), and at 10  $\mu$ M, it abolished invasive growth (Figure 2) during a 12 h treatment, indicating that DEA's therapeutic concentration (to be determined in vivo) may not exceed the DEA concentrations, which were observed during human AM therapy [24].

Constant proliferation under chronic ischemic conditions put an extra metabolic burden on cancer cells. They have to fine-tune their metabolism to meet this challenge [52,56], which makes them vulnerable against drugs that interfere with their metabolism [52]. DEA may represent such a drug candidate, since it decreased the  $\Delta\Psi_m$  in a concentration-dependent manner in both BC cell lines (Figure 5) similarly as it did in isolated liver and rat mitochondria [35] and in the B16F10 melanoma line [34].

One of the essential roles of the  $\Delta\Psi_m$  in cellular survival is the regulation of mitochondrial network dynamics that have a role in mitochondrial biogenesis and quality control, retrograde signaling, and meeting cellular energy and metabolic demands [57,58]. Mitochondrial fusion and fission processes are mediated by large GTPases; Mfn 1 and 2 and OPA1 for the fusion and Drp1 for the fission [21]. The latter is regulated by phosphorylation and recruited to the mitochondria by Fis1 [21]. Balance of the fusion and fission processes is maintained by intracellular signaling [58], but the fusion is prevented when the  $\Delta\Psi_m$  is too low [57,58]. Therefore, in many cancer types such as in astrocytomas, prostate cancers, and breast, colon, and hepatocellular carcinomas, mitochondrial fragmentation is a common feature [59,60]. Fragmented mitochondria are more prone to damage and readily eliminated by mitophagy, leading to a reduced mitochondrial copy number [21]. DEA induced fragmentation of the mitochondria in both BC cell lines (Figure 6) that could contribute to its anti-neoplastic properties. Since DEA depolarized the  $\Delta\Psi_m$  (Figure 5), it seems logical that the DEA-induced mitochondrial fragmentation was caused by inhibiting fusion that was supported by the release of OPA1 in the case of B16F10 melanoma previously [34]. In contrast, in the BC cell lines, mitochondrial fragmentation seemed to be caused by promoting fission, as it was supported by the increased Drp1 expression that was accompanied by its decreased inhibitory phosphorylation (Figure 6). It seems likely that DEA interacted with a yet to be identified regulatory element located to the mitochondria and induced mitochondrial fragmentation by shifting the balance of fusion and fission. DEA's target has to be localized to the mitochondria, since DEA induced mitochondrial fission in isolated, Percoll gradient-purified mitochondria [35].

Prolonged activation of intracellular pro-survival signaling cascades, such as the phosphatidylinositol 3-kinase–Akt pathway, has been shown to significantly enhance cancer progression. Akt promotes cell survival and proliferation by suppressing apoptosis and stimulating cell cycle advancement [61,62]. The poor prognosis of various tumors is often associated with the constitutive activation of Akt [61,63], which phosphorylates and thereby inactivates pro-apoptotic proteins such as Bad [62]. Accordingly, dysregulation of the Akt signaling pathway is one of the most frequent oncogenic aberrations of TNBC too [64]. We demonstrated that Akt activation [61,65] was reduced dose dependently by DEA treatment in both BC cell lines. Additionally, in the HR+ MCF-7 cell line, the level of phosphorylated Akt that is the baseline activation of Akt was significantly lower than in the TN 4T1 cell line (Figure 4). The decreased Akt activation together with the



forementioned compromised mitochondrial functions may account for the differential apoptosis-promoting effect of DEA among the BC cell lines investigated (Figure 1).

Inflammatory cells and inflammatory cell mediators are prominent components of the microenvironment of tumors [14]. One of the most important immunomodulatory agents found in tumors is COX-2. It is associated with indicators of poor prognosis such as lymph node metastasis, poor differentiation, and large tumor size [66–68], making COX-2 the most commonly studied anti-inflammatory target in cancer therapy. The selective COX-2 inhibitor celecoxib in monotherapy and in combination with aromatase inhibitors proved to be effective in metastatic breast cancer by reducing breast tumor size and area [16,69]. In recent decades, COX-2 overexpression has been implicated in therapy resistance of various human cancers, including breast cancer [70–73]. Although hardly expressed in healthy tissues, COX-2 is highly inducible and can be rapidly upregulated in response to various pro-inflammatory agents, including cytokines, mitogens, and tumor promoters [74]. In agreement with these findings, COX-2 level was hardly detectable in the MCF-7 cells, and it was not affected by DEA treatment, while the metastatic 4T1 cell line expressed COX-2, which was elevated by DEA treatment in a concentration-dependent manner (Figure 4). Since the upregulation of COX-2 has been implicated in cancer therapy resistance [8], the latter result raised the possibility that DEA decreased its own anti-neoplastic effects in the 4T1 cell line, thereby creating the difference between the two BC cell lines in response to DEA treatment. Indeed, celecoxib potentiated DEA's effect on viability (Figure 8B) and colony formation (Figure 9) of the 4T1 cells only. Recent studies demonstrated that during radiotherapy-induced apoptosis, caspase 3 activation led to COX-2-mediated production of prostaglandin E<sub>2</sub>, eventually resulting in treatment resistance [75]. DEA treatment led to caspase 3 activation in both BC cell lines (Figure 4) but upregulation of COX-2 expression in the 4T1 cell line only (Figure 4). It is likely that the DEA-induced caspase 3-assisted mitochondrial apoptosis (Figure 4) resulted in COX-2-mediated resistance in the 4T1 cell line, which expressed it. Accordingly, the difference in COX-2 expression accounted for, at least partially, the differential anti-neoplastic effects of DEA. These results also suggest that co-treatment with COX-2 inhibitors can increase the efficacy of DEA and significantly reduce therapy resistance.

#### 4. Conclusions

Regardless of the mechanism, the available data indicate that DEA by interacting with a mitochondrially localized target or targets can modulate mitochondrial functions and definitely can induce the predominantly apoptotic cell death of BC cells. Although less effectively than in the HR+ BC line, DEA at low micromolar concentrations exerted effective anti-neoplastic effects in the highly treatment-resistant 4T1 TNBC cells line. Furthermore, COX-2 upregulation accounted for most of the DEA resistance by the 4T1 line that was counteracted by inhibiting COX-2's enzymatic activity. Accordingly, considering that within the suggested safety limits, the drug does not have therapy-restricting side effects, the safety concerns might not hinder the introduction of DEA into clinical studies.

#### 5. Materials and Methods

##### 5.1. Materials

DEA was kindly donated by Professor Andras Varro (Department of Pharmacology and Pharmacotherapy, University of Szeged, Szeged, Hungary). All other materials if not indicated otherwise were from Sigma-Aldrich (St. Louis, MI, USA). All antibodies were from Cell Signaling Technology (Beverly, MA, USA). The following primary antibodies were used: anti-OPA1, anti-Mfn1, anti-Mfn2, anti-Drp1, anti-phospho-Drp1(Ser637), anti-Fis1, anti-Akt, anti-p-Akt, anti-Bad, anti-p-Bad, anti-Bax, anti-Bcl-2, anti-PARP, anti-caspase-3, anti-p53, anti-COX-2 (1:500 dilution), anti-actin (1:2000 dilution).

## 5.2. Cell Cultures

MCF-7 and 4T1 cell lines were from the American Type Culture Collection (Manassas, VA, USA). Both cell lines were split twice a week and were maintained as monolayer adherent cultures under standard conditions (5% CO<sub>2</sub>, 37 °C). MCF-7 cells were cultured in RPMI 1640 media supplemented with 10% (*v/v*) fetal bovine serum (FBS) and 1% penicillin–streptomycin mixture (Life Technologies, Darmstadt, Germany). 4T1 cells were cultured in RPMI 1640 media supplemented with 10% FBS, 1% penicillin–streptomycin mixture, glucose, pyruvate, and sodium bicarbonate.

## 5.3. Cell Viability Assay

MCF-7 and 4T1 cells were seeded in 96-well plates in quintuplicates at a density of 10<sup>4</sup> cells, respectively. After an overnight acclimation, the cells were treated with 0 to 15 μM DEA for 24 or 48 h; then, the cells were rinsed with phosphate-buffered saline (PBS) and were fixed in 100 μL of chilled 10% trichloroacetic acid solution. Following 30 min incubation at 4 °C, the plates were rinsed five times with distilled water and then were dried overnight at room temperature. Then, 70 μL of 0.4% SRB (Sigma-Aldrich, St. Louis, MI, USA) prepared in 1% acetic acid were added to each well for 30 min at room temperature. Afterwards, the solution was discarded, and the plates were washed five times with 1% acetic acid and were dried at room temperature for 3 h. Then, 200 μL of a 10 mM tris(hydroxymethyl)aminomethane base was added to each well, and the plates were agitated at room temperature on a plate shaker for 30 min to solubilize the bound SRB. Absorbance was measured simultaneously at 560 and 600 nm with a GloMax<sup>®</sup>-Multi Instrument (Promega, Madison, WI, USA). Optical density (OD)<sub>600</sub> was subtracted as a background from the OD<sub>560</sub>. The experiments were repeated five times.

## 5.4. Apoptosis Assay

To detect live, early apoptotic, late apoptotic, and dead cells, a MUSE Annexin V & Dead Cell Kit (Luminex Corporation, Austin, TX, USA) was used. The experiments were carried out according to the manufacturer's protocol. MCF-7 and 4T1 cells were plated at a starting density of 10<sup>5</sup> cells/well into 6-well plates and were treated for 24 h with 0, 5, or 10 μM DEA. After the treatment, the cells were harvested and were diluted in their medium. Then, 100 μL Annexin V reagent was added to the samples (100 μL), which was followed by 20 min incubation in a dark room at room temperature. Five thousand single-cell events were measured per sample using a MUSE Cell Analyzer device.

## 5.5. Bioenergetics Assay

OCR and ECAR were monitored by an Agilent Seahorse XFp Analyzer (Agilent, Santa Clara, CA, USA). MCF-7 and 4T1 cells were seeded into XFp cell culture 8-well miniplates at a starting density of 3 × 10<sup>4</sup> cells/well. After overnight incubation, the cells were treated with 0, 5, or 10 μM DEA for 6 h. After the treatment, the medium was replaced to Seahorse XF assay Medium (Agilent, Santa Clara, CA, USA) pH 7.4 supplemented with 10 mM glucose, 1 mM pyruvate, and 2 mM glutamine. For the measurement, we used the following inhibitors: 1 μM of oligomycin, 1 μM of FCCP, and 1 μM of rotenone/antimycin A. After monitoring 15 min of basal respiration, the FoF1 ATPase inhibitor oligomycin was added to the system to assess ATP production. After another 20 min of recording, carbonyl cyanide 4-(trifluoromethoxy) phenylhydrazone (FCCP) was added that uncouples respiration and ATP synthesis, allowing the assessment of maximal respiration. After 20 min of further recording, the Complex I and Complex III inhibitor rotenone and antimycin A were administered to inhibit mitochondrial respiration completely for calculating proton leak and non-mitochondrial oxygen consumption. Non-cellular oxygen consumption was assessed in 2 wells running without cells and was subtracted from the corresponding OCR value. The OCR and ECAR data were normalized to the mg protein content determined by using a DC Protein Assay kit (Bio-Rad, Hercules, CA, USA). No other data correction was applied.

### 5.6. Immunoblot Analysis

MCF-7 and 4T1 cells were seeded in 10 cm plates at a starting density of  $10^6$  cells/plate, were cultured overnight, and then were treated with 0, 5, or 10  $\mu\text{M}$  DEA for 24 h. The cells were harvested in a chilled lysis buffer containing 0.5 mM sodium–metavanadate, 1 mM ethylenediamine–tetraacetic acid, and protease and phosphatase inhibitor cocktails (1:200). After boiling, the cell lysates were subjected to 10% sodium dodecyl sulfate polyacrylamide gel electrophoresis; then, the proteins were transferred to nitrocellulose membranes. After blocking the membranes in 5% bovine serum albumin (BSA) for 1.5 h at room temperature, they were exposed to primary antibodies diluted in blocking solution at 4 °C overnight. Appropriate horseradish peroxidase-conjugated secondary antibodies were used at a dilution of 1:5000 (anti-mouse and anti-rabbit IgGs; Sigma-Aldrich, St. Louis, MI, USA). Chemiluminescence generated by applying the WesternBright ECL HRP substrate (Advansta, San Jose, CA, USA) was measured using an Azure 300 (Azure Biosystems, Dublin, CA, USA) high-resolution imaging system. Pixel volumes of the bands were determined using ImageJ software. For membrane stripping and re-probing, the membranes were washed in a stripping buffer containing 0.1 M glycine and 5 M  $\text{MgCl}_2$  (pH 2.8) for 30 min at room temperature. After washing and blocking, the membranes were re-probed.

### 5.7. Colony Formation Assay

MCF-7 and 4T1 cells were plated at a starting density of 500 cells/well into 6-well plates. After culturing overnight, the cells were treated with 0–2  $\mu\text{M}$  DEA for 7 days. Then, the cells were washed with PBS (Biowest, Nuaille, France) and stained with 0.1% Coomassie Brilliant blue R 250 (Merck KGaA, Darmstadt, Germany) in 30% methanol and 10% acetic acid. Using ImageJ software, scanned colonies were quantified.

### 5.8. Migration Assay

To assess cell motility, we used the wound-healing assay. MCF-7 and 4T1 cells were seeded into flat-bottom 6-well plates, and they were cultured to form a sub-confluent monolayer. Then, a wound was inflicted into the cell layer by using a sterile 200  $\mu\text{L}$  pipette tip, and the cells were treated with 0, 5, or 10  $\mu\text{M}$  DEA for up to 12 h. The wounds were imaged at 0, 6, and 12 h by an EVOS microscope (Thermo Scientific Hungary, Budapest, Hungary) at 4 $\times$  magnification. The distance differences were measured using ImageJ software. The experiment was repeated twice in duplicates.

### 5.9. Measurement of Invasive Growth

MCF7 and 4T1 cells were seeded at a starting density of  $9 \times 10^3$ /well and  $5 \times 10^3$ /well, respectively, in an electronic microtiter plate (E-Plate<sup>®</sup>) (ACEA Biosciences, San Diego, CA, USA). The cells were cultured for 24 h before they were treated with 0, 5, or 10  $\mu\text{M}$  DEA for 24 h, during which the impedance was measured every 5 min. The xCELLigence Real-Time Cell Analysis (RTCA) device (ACEA Biosciences, San Diego, CA, USA) was used according to the manufacturer's protocol. The instrument was placed in a humidified incubator at 37 °C and 5%  $\text{CO}_2$ . These experiments were repeated twice running in three parallels.

### 5.10. $\Delta\Psi_m$ Assay

We used the membrane potential-dependent fluorescent dye, JC-1 (Sigma-Aldrich) at the final concentration of 1  $\mu\text{M}$  for determining the  $\Delta\Psi_m$ . MCF-7 and 4T1 cells were seeded on glass coverslips and cultured at least overnight before experiments. After subjecting the cells to the appropriate treatment (as indicated in the figure legend), coverslips were rinsed twice in PBS, and cells were incubated in phosphate-buffer containing JC-1 (5 mg/mL) stain for 30 min in a  $\text{CO}_2$  incubator at 37 °C. Images were taken with a Nikon microscope (Inverted Microscope Eclipse Ti-U Instruction, Auro-Science Ltd., Budapest, Hungary) equipped with a SPOT RT3 2Mp Monochrome camera including SPOT Advanced software, using a 20 $\times$  objective. The same microscopic field was first imaged using the red channel followed by the green channels, and the resulting images were merged by Adobe Photoshop

7.0. In control experiments, we did not observe considerable bleed-through between the red and green channels. The same calibration parameters were applied for the batch of images obtained from the same experiment. For quantification, the ImageJ software was used after converting the images to grayscale. All experiments were performed in triplicate.

#### 5.11. Analysis of Mitochondrial Network Dynamics

MCF-7 and 4T1 cells were seeded in ultrathin-bottomed 96-well plates and were cultured overnight. The cells were treated as indicated in the figure legends, were rinsed twice in PBS, and were incubated in PBS containing 20 nM of MitoTracker Red for 30 min in a CO<sub>2</sub> incubator at 37 °C. Fluorescence images were taken via a 60× Plan Apo Lambda objective of an ImageXpress Micro 4 High-Content Imaging System (Bioscience Ltd., Budapest, Hungary). Image analysis for mitochondrial fragmentation was performed by MetaXpress High-Content Image Acquisition and Analysis Software as described [41]. Mitochondria shorter than 2 μm were considered as fragmented, while those longer than 5 μm were considered as filamentous. All experiments were performed in triplicates.

#### 5.12. Statistical Analysis

Results are shown as means ± standard deviation (SD). ANOVA using the post hoc Dunnett test (single way or two-ways) was employed to calculate the concentration-dependent effects of DEA in each experiment. Statistical analyses were performed using IBM SPSS Statistics v20.0. Differences were regarded as significant at  $p < 0.05$ .

**Supplementary Materials:** The following supporting information can be downloaded at: <https://www.mdpi.com/article/10.3390/ijms23031544/s1>.

**Author Contributions:** Conceptualization, Z.B. and F.G.J.; methodology, Z.B.; investigation, F.H.J.R., K.A., E.H., A.S. (Aliz Szabo), R.B., G.N.K. and A.T.; writing—original draft preparation Z.B., A.S. (Arpad Szanto) and F.G.J.; writing—review and editing, Z.B., A.S. (Arpad Szanto) and F.G.J.; visualization, Z.B., K.F. and R.B.; funding acquisition, Z.B., E.H. and F.G.J. All authors have read and agreed to the published version of the manuscript.

**Funding:** This research was funded by Hungarian grants GINOP-2.3.3-15-2016-00025, GINOP-2.3.2-15-2016-00049, EFOP-3.6.1-16-2016-00004, and the Ministry for Innovation and Technology: TKP2021-EGA-17. This paper was supported by the János Bolyai Research Scholarship of the Hungarian Academy of Sciences and by the ÚNKP-21-5 New National Excellence Program of the Ministry for Innovation and Technology from the source of the National Research, Development and Innovation Fund and by the grants ÁOK KA-2021-04 and ÁOK KA-2021-11.

**Institutional Review Board Statement:** Not applicable.

**Informed Consent Statement:** Not applicable.

**Data Availability Statement:** Data is contained within the article or Supplementary Material.

**Acknowledgments:** The authors thank Laszlo Giran for technical help with preparation of the figures. We apologize to any authors of relevant studies that we have failed to cite.

**Conflicts of Interest:** The authors declare no conflict of interest. The funders had no role in the design of the study; the collection, analyses, or interpretation of data; the writing of the manuscript, or the decision to publish the results.

## References

1. Perou, C.M.; Sorlie, T.; Eisen, M.B.; van de Rijn, M.; Jeffrey, S.S.; Rees, C.A.; Pollack, J.R.; Ross, D.T.; Johnsen, H.; Akslén, L.A.; et al. Molecular portraits of human breast tumours. *Nature* **2000**, *406*, 747–752. [[CrossRef](#)] [[PubMed](#)]
2. Masoud, V.; Pages, G. Targeted therapies in breast cancer: New challenges to fight against resistance. *World J. Clin. Oncol* **2017**, *8*, 120–134. [[CrossRef](#)] [[PubMed](#)]
3. Chakrabarty, A.; Chakraborty, S.; Bhattacharya, R.; Chowdhury, G. Senescence-Induced Chemoresistance in Triple Negative Breast Cancer and Evolution-Based Treatment Strategies. *Front. Oncol.* **2021**, *11*, 674354. [[CrossRef](#)] [[PubMed](#)]
4. Lebert, J.M.; Lester, R.; Powell, E.; Seal, M.; McCarthy, J. Advances in the systemic treatment of triple-negative breast cancer. *Curr. Oncol.* **2018**, *25* (Suppl. 1), S142–S150. [[CrossRef](#)] [[PubMed](#)]

5. Coussens, L.M.; Werb, Z. Inflammation and cancer. *Nature* **2002**, *420*, 860–867. [[CrossRef](#)] [[PubMed](#)]
6. Edechi, C.A.; Ikeogu, N.; Uzonna, J.E.; Myal, Y. Regulation of Immunity in Breast Cancer. *Cancers* **2019**, *11*, 1080. [[CrossRef](#)] [[PubMed](#)]
7. Hiam-Galvez, K.J.; Allen, B.M.; Spitzer, M.H. Systemic immunity in cancer. *Nat. Rev. Cancer* **2021**, *21*, 345–359. [[CrossRef](#)] [[PubMed](#)]
8. Pang, L.Y.; Hurst, E.A.; Argyle, D.J. Cyclooxygenase-2: A Role in Cancer Stem Cell Survival and Repopulation of Cancer Cells during Therapy. *Stem Cells Int.* **2016**, *2016*, 2048731. [[CrossRef](#)] [[PubMed](#)]
9. Bos, P.D.; Zhang, X.H.; Nadal, C.; Shu, W.; Gomis, R.R.; Nguyen, D.X.; Minn, A.J.; van de Vijver, M.J.; Gerald, W.L.; Foekens, J.A.; et al. Genes that mediate breast cancer metastasis to the brain. *Nature* **2009**, *459*, 1005–1009. [[CrossRef](#)] [[PubMed](#)]
10. Wu, K.; Fukuda, K.; Xing, F.; Zhang, Y.; Sharma, S.; Liu, Y.; Chan, M.D.; Zhou, X.; Qasem, S.A.; Pochampally, R.; et al. Roles of the cyclooxygenase 2 matrix metalloproteinase 1 pathway in brain metastasis of breast cancer. *J. Biol. Chem.* **2015**, *290*, 9842–9854. [[CrossRef](#)]
11. Bao, S.; Wu, Q.; McLendon, R.E.; Hao, Y.; Shi, Q.; Hjelmeland, A.B.; Dewhirst, M.W.; Bigner, D.D.; Rich, J.N. Glioma stem cells promote radioresistance by preferential activation of the DNA damage response. *Nature* **2006**, *444*, 756–760. [[CrossRef](#)] [[PubMed](#)]
12. Calabrese, C.; Poppleton, H.; Kocak, M.; Hogg, T.L.; Fuller, C.; Hamner, B.; Oh, E.Y.; Gaber, M.W.; Finklestein, D.; Allen, M.; et al. A perivascular niche for brain tumor stem cells. *Cancer Cell* **2007**, *11*, 69–82. [[CrossRef](#)] [[PubMed](#)]
13. Jones, D.L.; Wagers, A.J. No place like home: Anatomy and function of the stem cell niche. *Nat. Rev. Mol. Cell. Biol.* **2008**, *9*, 11–21. [[CrossRef](#)] [[PubMed](#)]
14. Mantovani, A.; Allavena, P.; Sica, A.; Balkwill, F. Cancer-related inflammation. *Nature* **2008**, *454*, 436–444. [[CrossRef](#)]
15. Tian, J.; Hachim, M.Y.; Hachim, I.Y.; Dai, M.; Lo, C.; Raffa, F.A.; Ali, S.; Lebrun, J.J. Cyclooxygenase-2 regulates TGFbeta-induced cancer stemness in triple-negative breast cancer. *Sci. Rep.* **2017**, *7*, 40258. [[CrossRef](#)]
16. Tian, J.; Wang, V.; Wang, N.; Khadang, B.; Boudreault, J.; Bakdounes, K.; Ali, S.; Lebrun, J.J. Identification of MFGE8 and KLK5/7 as mediators of breast tumorigenesis and resistance to COX-2 inhibition. *Breast Cancer Res.* **2021**, *23*, 23. [[CrossRef](#)]
17. Dong, L.; Neuzil, J. Targeting mitochondria as an anticancer strategy. *Cancer Commun.* **2019**, *39*, 63. [[CrossRef](#)]
18. Fontana, F.; Limonta, P. The multifaceted roles of mitochondria at the crossroads of cell life and death in cancer. *Free Radic. Biol. Med.* **2021**, *176*, 203–221. [[CrossRef](#)]
19. Hamilton, C.; Fox, J.P.; Longley, D.B.; Higgins, C.A. Therapeutics Targeting the Core Apoptotic Machinery. *Cancers* **2021**, *13*, 2618. [[CrossRef](#)]
20. Patra, S.; Elahi, N.; Armorer, A.; Arunachalam, S.; Omala, J.; Hamid, I.; Ashton, A.W.; Joyce, D.; Jiao, X.; Pestell, R.G. Mechanisms Governing Metabolic Heterogeneity in Breast Cancer and Other Tumors. *Front. Oncol.* **2021**, *11*, 700629. [[CrossRef](#)]
21. Boland, M.L.; Chourasia, A.H.; Macleod, K.F. Mitochondrial dysfunction in cancer. *Front. Oncol.* **2013**, *3*, 292. [[CrossRef](#)] [[PubMed](#)]
22. Zheng, H.; Siddharth, S.; Parida, S.; Wu, X.; Sharma, D. Tumor Microenvironment: Key Players in Triple Negative Breast Cancer Immunomodulation. *Cancers* **2021**, *13*, 3357. [[CrossRef](#)] [[PubMed](#)]
23. Ashburn, T.T.; Thor, K.B. Drug repositioning: Identifying and developing new uses for existing drugs. *Nat. Rev. Drug Discov.* **2004**, *3*, 673–683. [[CrossRef](#)]
24. Brien, J.F.; Jimmo, S.; Brennan, F.J.; Ford, S.E.; Armstrong, P.W. Distribution of amiodarone and its metabolite, desethylamiodarone, in human tissues. *Can. J. Physiol. Pharmacol.* **1987**, *65*, 360–364. [[CrossRef](#)] [[PubMed](#)]
25. Holt, D.W.; Tucker, G.T.; Jackson, P.R.; Storey, G.C. Amiodarone pharmacokinetics. *Am. Heart J.* **1983**, *106 Pt 2*, 840–847. [[CrossRef](#)]
26. Colunga Biancatelli, R.M.; Congedo, V.; Calvosa, L.; Ciacciarelli, M.; Polidoro, A.; Iuliano, L. Adverse reactions of Amiodarone. *J. Geriatr. Cardiol.* **2019**, *16*, 552–566. [[PubMed](#)]
27. Singh, B.N.; Nademane, K.; Josephson, M.A.; Ikeda, N.; Venkatesh, N.; Kannan, R. The electrophysiology and pharmacology of verapamil, flecainide, and amiodarone: Correlations with clinical effects and antiarrhythmic actions. *Ann. N. Y. Acad. Sci.* **1984**, *432*, 210–235. [[CrossRef](#)] [[PubMed](#)]
28. Daniels, J.M.; Brien, J.F.; Massey, T.E. Pulmonary fibrosis induced in the hamster by amiodarone and desethylamiodarone. *Toxicol. Appl. Pharmacol.* **1989**, *100*, 350–359. [[CrossRef](#)]
29. Honegger, U.E.; Zuehlke, R.D.; Scuntaro, I.; Schaefer, M.H.; Toplak, H.; Wiesmann, U.N. Cellular accumulation of amiodarone and desethylamiodarone in cultured human cells. Consequences of drug accumulation on cellular lipid metabolism and plasma membrane properties of chronically exposed cells. *Biochem. Pharmacol.* **1993**, *45*, 349–356. [[CrossRef](#)]
30. Morvay, N.; Baczkó, I.; Sztojokov-Ivanov, A.; Falkay, G.; Papp, J.G.; Varro, A.; Lepran, I. Long-term pretreatment with desethylamiodarone (DEA) or amiodarone (AMIO) protects against coronary artery occlusion induced ventricular arrhythmias in conscious rats. *Can. J. Physiol. Pharmacol.* **2015**, *93*, 773–777. [[CrossRef](#)]
31. Bogнар, Z.; Fekete, K.; Antus, C.; Hocsak, E.; Bogнар, R.; Tapodi, A.; Boronkai, A.; Farkas, N.; Gallyas, F., Jr.; Sumegi, B.; et al. Desethylamiodarone-A metabolite of amiodarone-Induces apoptosis on T24 human bladder cancer cells via multiple pathways. *PLoS ONE* **2017**, *12*, e0189470. [[CrossRef](#)] [[PubMed](#)]
32. Bogнар, Z.; Fekete, K.; Bogнар, R.; Szabo, A.; Vass, R.A.; Sumegi, B. Amiodarone’s major metabolite, desethylamiodarone, induces apoptosis in human cervical cancer cells. *Can. J. Physiol. Pharmacol.* **2018**, *96*, 1004–1011. [[CrossRef](#)] [[PubMed](#)]

33. Bogнар, Z.; Cseh, A.M.; Fekete, K.; Antus, C.; Bogнар, R.; Tapodi, A.; Ramadan, F.H.J.; Sumegi, B.; Gallyas, F., Jr. Amiodarone's major metabolite, desethylamiodarone inhibits proliferation of B16-F10 melanoma cells and limits lung metastasis formation in an in vivo experimental model. *PLoS ONE* **2020**, *15*, e0239088. [[CrossRef](#)] [[PubMed](#)]
34. Ramadan, F.H.J.; Szabo, A.; Kovacs, D.; Takatsy, A.; Bogнар, R.; Gallyas, F., Jr.; Bogнар, Z. Involvement of Mitochondrial Mechanisms in the Cytostatic Effect of Desethylamiodarone in B16F10 Melanoma Cells. *Int. J. Mol. Sci.* **2020**, *21*, 7346. [[CrossRef](#)] [[PubMed](#)]
35. Varbiro, G.; Toth, A.; Tapodi, A.; Bogнар, Z.; Veres, B.; Sumegi, B.; Gallyas, F., Jr. Protective effect of amiodarone but not N-desethylamiodarone on postischemic hearts through the inhibition of mitochondrial permeability transition. *J. Pharmacol. Exp. Ther.* **2003**, *307*, 615–625. [[CrossRef](#)] [[PubMed](#)]
36. Ensenyat-Mendez, M.; Llinas-Arias, P.; Orozco, J.I.J.; Iniguez-Munoz, S.; Salomon, M.P.; Sese, B.; DiNome, M.L.; Marzese, D.M. Current Triple-Negative Breast Cancer Subtypes: Dissecting the Most Aggressive Form of Breast Cancer. *Front. Oncol.* **2021**, *11*, 681476. [[CrossRef](#)] [[PubMed](#)]
37. Schafer, M.; Werner, S. Cancer as an overhealing wound: An old hypothesis revisited. *Nat. Rev. Mol. Cell. Biol.* **2008**, *9*, 628–638. [[CrossRef](#)]
38. Karamanou, K.; Franchi, M.; Vynios, D.; Brezillon, S. Epithelial-to-mesenchymal transition and invadopodia markers in breast cancer: Louican a key regulator. *Semin. Cancer Biol.* **2020**, *62*, 125–133. [[CrossRef](#)]
39. Steenbrugge, J.; Vander Elst, N.; Demeyere, K.; De Wever, O.; Sanders, N.N.; Van Den Broeck, W.; Dirix, L.; Van Laere, S.; Meyer, E. Comparative Profiling of Metastatic 4T1- vs. Non-metastatic Py230-Based Mammary Tumors in an Intraductal Model for Triple-Negative Breast Cancer. *Front. Immunol.* **2019**, *10*, 2928. [[CrossRef](#)]
40. Zorova, L.D.; Popkov, V.A.; Plotnikov, E.Y.; Silachev, D.N.; Pevzner, I.B.; Jankauskas, S.S.; Babenko, V.A.; Zorov, S.D.; Balakireva, A.V.; Juhaszova, M.; et al. Mitochondrial membrane potential. *Anal. Biochem.* **2018**, *552*, 50–59. [[CrossRef](#)]
41. Del Campo, A.; Parra, V.; Vasquez-Trincado, C.; Gutierrez, T.; Morales, P.E.; Lopez-Crisosto, C.; Bravo-Sagua, R.; Navarro-Marquez, M.F.; Verdejo, H.E.; Contreras-Ferrat, A.; et al. Mitochondrial fragmentation impairs insulin-dependent glucose uptake by modulating Akt activity through mitochondrial Ca<sup>2+</sup> uptake. *Am. J. Physiol. Endocrinol. Metab.* **2014**, *306*, E1–E13. [[CrossRef](#)] [[PubMed](#)]
42. Zhan, L.; Cao, H.; Wang, G.; Lyu, Y.; Sun, X.; An, J.; Wu, Z.; Huang, Q.; Liu, B.; Xing, J. Drp1-mediated mitochondrial fission promotes cell proliferation through crosstalk of p53 and NF-kappaB pathways in hepatocellular carcinoma. *Oncotarget* **2016**, *7*, 65001–65011. [[CrossRef](#)] [[PubMed](#)]
43. Adebayo, M.; Singh, S.; Singh, A.P.; Dasgupta, S. Mitochondrial fusion and fission: The fine-tune balance for cellular homeostasis. *FASEB J.* **2021**, *35*, e21620. [[CrossRef](#)] [[PubMed](#)]
44. Vichai, V.; Kirtikara, K. Sulforhodamine B colorimetric assay for cytotoxicity screening. *Nat. Protoc.* **2006**, *1*, 1112–1116. [[CrossRef](#)] [[PubMed](#)]
45. Moindjie, H.; Rodrigues-Ferreira, S.; Nahmias, C. Mitochondrial Metabolism in Carcinogenesis and Cancer Therapy. *Cancers* **2021**, *13*, 3311. [[CrossRef](#)]
46. Hirpara, J.; Eu, J.Q.; Tan, J.K.M.; Wong, A.L.; Clement, M.V.; Kong, L.R.; Ohi, N.; Tsunoda, T.; Qu, J.; Goh, B.C.; et al. Metabolic reprogramming of oncogene-addicted cancer cells to OXPHOS as a mechanism of drug resistance. *Redox Biol.* **2019**, *25*, 101076. [[CrossRef](#)]
47. Zhang, G.; Frederick, D.T.; Wu, L.; Wei, Z.; Krepler, C.; Srinivasan, S.; Chae, Y.C.; Xu, X.; Choi, H.; Dimwamwa, E.; et al. Targeting mitochondrial biogenesis to overcome drug resistance to MAPK inhibitors. *J. Clin. Invest.* **2016**, *126*, 1834–1856. [[CrossRef](#)]
48. LeBleu, V.S.; O'Connell, J.T.; Gonzalez Herrera, K.N.; Wikman, H.; Pantel, K.; Haigis, M.C.; de Carvalho, F.M.; Damascena, A.; Domingos Chinen, L.T.; Rocha, R.M.; et al. PGC-1alpha mediates mitochondrial biogenesis and oxidative phosphorylation in cancer cells to promote metastasis. *Nat. Cell. Biol.* **2014**, *16*, 992–1003. [[CrossRef](#)]
49. Lin, C.S.; Liu, L.T.; Ou, L.H.; Pan, S.C.; Lin, C.I.; Wei, Y.H. Role of mitochondrial function in the invasiveness of human colon cancer cells. *Oncol. Rep.* **2018**, *39*, 316–330. [[CrossRef](#)]
50. Ashton, T.M.; McKenna, W.G.; Kunz-Schughart, L.A.; Higgins, G.S. Oxidative Phosphorylation as an Emerging Target in Cancer Therapy. *Clin. Cancer Res.* **2018**, *24*, 2482–2490. [[CrossRef](#)]
51. Guerra, F.; Arbini, A.A.; Moro, L. Mitochondria and cancer chemoresistance. *Biochim. Biophys. Acta Bioenerg.* **2017**, *1858*, 686–699. [[CrossRef](#)] [[PubMed](#)]
52. Weinberg, S.E.; Chandel, N.S. Targeting mitochondria metabolism for cancer therapy. *Nat. Chem. Biol.* **2015**, *11*, 9–15. [[CrossRef](#)] [[PubMed](#)]
53. Burke, P.J. Mitochondria, Bioenergetics and Apoptosis in Cancer. *Trends Cancer* **2017**, *3*, 857–870. [[CrossRef](#)] [[PubMed](#)]
54. Green, D.R.; Reed, J.C. Mitochondria and apoptosis. *Science* **1998**, *281*, 1309–1312. [[CrossRef](#)] [[PubMed](#)]
55. Xiao, W.; Zheng, S.; Yang, A.; Zhang, X.; Zou, Y.; Tang, H.; Xie, X. Breast cancer subtypes and the risk of distant metastasis at initial diagnosis: A population-based study. *Cancer Manag. Res.* **2018**, *10*, 5329–5338. [[CrossRef](#)] [[PubMed](#)]
56. Ashley, N.; Poulton, J. Mitochondrial DNA is a direct target of anti-cancer anthracycline drugs. *Biochem. Biophys. Res. Commun.* **2009**, *378*, 450–455. [[CrossRef](#)]
57. Srinivasan, S.; Guha, M.; Kashina, A.; Avadhani, N.G. Mitochondrial dysfunction and mitochondrial dynamics-The cancer connection. *Biochim. Biophys. Acta Bioenerg.* **2017**, *1858*, 602–614. [[CrossRef](#)]
58. Mishra, P.; Chan, D.C. Metabolic regulation of mitochondrial dynamics. *J. Cell Biol.* **2016**, *212*, 379–387. [[CrossRef](#)]

59. Rehman, J.; Zhang, H.J.; Toth, P.T.; Zhang, Y.; Marsboom, G.; Hong, Z.; Salgia, R.; Husain, A.N.; Wietholt, C.; Archer, S.L. Inhibition of mitochondrial fission prevents cell cycle progression in lung cancer. *FASEB J.* **2012**, *26*, 2175–2186. [[CrossRef](#)]
60. Inoue-Yamauchi, A.; Oda, H. Depletion of mitochondrial fission factor DRP1 causes increased apoptosis in human colon cancer cells. *Biochem. Biophys. Res. Commun.* **2012**, *421*, 81–85. [[CrossRef](#)]
61. Grabacka, M.; Plonka, P.M.; Urbanska, K.; Reiss, K. Peroxisome proliferator-activated receptor alpha activation decreases metastatic potential of melanoma cells in vitro via down-regulation of Akt. *Clin. Cancer Res.* **2006**, *12*, 3028–3036. [[CrossRef](#)] [[PubMed](#)]
62. Vivanco, I.; Sawyers, C.L. The phosphatidylinositol 3-Kinase AKT pathway in human cancer. *Nat. Rev. Cancer* **2002**, *2*, 489–501. [[CrossRef](#)] [[PubMed](#)]
63. Nicholson, K.M.; Anderson, N.G. The protein kinase B/Akt signalling pathway in human malignancy. *Cell. Signal.* **2002**, *14*, 381–395. [[CrossRef](#)]
64. Pascual, J.; Turner, N.C. Targeting the PI3-kinase pathway in triple-negative breast cancer. *Ann. Oncol* **2019**, *30*, 1051–1060. [[CrossRef](#)]
65. Fidler, I.J. Selection of successive tumour lines for metastasis. *Nat. New Biol.* **1973**, *242*, 148–149. [[CrossRef](#)]
66. Gallo, O.; Masini, E.; Bianchi, B.; Bruschini, L.; Paglierani, M.; Franchi, A. Prognostic significance of cyclooxygenase-2 pathway and angiogenesis in head and neck squamous cell carcinoma. *Hum. Pathol.* **2002**, *33*, 708–714. [[CrossRef](#)]
67. Jiao, G.; Ren, T.; Lu, Q.; Sun, Y.; Lou, Z.; Peng, X.; Liang, W.; Guo, W. Prognostic significance of cyclooxygenase-2 in osteosarcoma: A meta-analysis. *Tumour Biol.* **2013**, *34*, 2489–2495. [[CrossRef](#)]
68. Sicking, I.; Rommens, K.; Battista, M.J.; Bohm, D.; Gebhard, S.; Lebrecht, A.; Cotarelo, C.; Hoffmann, G.; Hengstler, J.G.; Schmidt, M. Prognostic influence of cyclooxygenase-2 protein and mRNA expression in node-negative breast cancer patients. *BMC Cancer* **2014**, *14*, 952. [[CrossRef](#)]
69. Falandry, C.; Canney, P.A.; Freyer, G.; Dirix, L.Y. Role of combination therapy with aromatase and cyclooxygenase-2 inhibitors in patients with metastatic breast cancer. *Ann. Oncol.* **2009**, *20*, 615–620. [[CrossRef](#)]
70. Hida, T.; Yatabe, Y.; Achiwa, H.; Muramatsu, H.; Kozaki, K.; Nakamura, S.; Ogawa, M.; Mitsudomi, T.; Sugiura, T.; Takahashi, T. Increased expression of cyclooxygenase 2 occurs frequently in human lung cancers, specifically in adenocarcinomas. *Cancer Res.* **1998**, *58*, 3761–3764.
71. Hwang, D.; Scollard, D.; Byrne, J.; Levine, E. Expression of cyclooxygenase-1 and cyclooxygenase-2 in human breast cancer. *J. Natl. Cancer Inst.* **1998**, *90*, 455–460. [[CrossRef](#)] [[PubMed](#)]
72. Soslow, R.A.; Dannenberg, A.J.; Rush, D.; Woerner, B.M.; Khan, K.N.; Masferrer, J.; Koki, A.T. COX-2 is expressed in human pulmonary, colonic, and mammary tumors. *Cancer* **2000**, *89*, 2637–2645. [[CrossRef](#)]
73. Subbaramaiah, K.; Telang, N.; Ramonetti, J.T.; Araki, R.; DeVito, B.; Weksler, B.B.; Dannenberg, A.J. Transcription of cyclooxygenase-2 is enhanced in transformed mammary epithelial cells. *Cancer Res.* **1996**, *56*, 4424–4429. [[PubMed](#)]
74. Claria, J. Cyclooxygenase-2 biology. *Curr. Pharm. Des.* **2003**, *9*, 2177–2190. [[CrossRef](#)]
75. Allen, C.P.; Tinganelli, W.; Sharma, N.; Nie, J.; Sicard, C.; Natale, F.; King, M., 3rd; Keysar, S.B.; Jimeno, A.; Furusawa, Y.; et al. DNA Damage Response Proteins and Oxygen Modulate Prostaglandin E2 Growth Factor Release in Response to Low and High LET Ionizing Radiation. *Front. Oncol.* **2015**, *5*, 260. [[CrossRef](#)] [[PubMed](#)]